UNIVERSITEIT VAN PRETORIA
UNIVERSITY OF PRETORIA
YUNIBESITHI YA PRETORIA

The development of quantum dot thin films for sensing organic pollutants in water

By

Wilmé Putter

Submitted in partial fulfilment of the requirements for the degree

Master of Science (Chemistry)

In the Department of Chemistry, Faculty of Natural and Agricultural Sciences

University of Pretoria

March 2023

Supervisor: Professor Patricia B. C. Forbes

Co-supervisor: Dr Sifiso A. Nsibande

Declaration of Authorship

I, Wilmé Putter, declare that this dissertation, which I submit for the degree of Masters in Science at the University of Pretoria, is my own work and has not been previously submitted by me for a degree at this or any other tertiary institution.

Signed: _____ Date: _____

Acknowledgements

I would like to thank and show my gratitude to the best supervisor, Professor Patricia B. C. Forbes, thank you for your motivation, support and for guiding me in this journey and always going above and beyond for me and my colleagues. I could truly not have asked for a better supervisor. I would also like to thank my co-supervisor Dr Sifiso A. Nsibande, for your help and friendliness. I would like to thank the two of you jointly for all the lessons I learnt from you and for helping me grow in this field.

Gratitude and thankfulness go to SASOL (South African Coal, Oil and Gas Company) for financially supporting me throughout my studies and giving me mentorship and leadership where needed. I am thankful for all the opportunities you have given me, and for employing me where I am learning many skills to advance my career. Then I would also like to thank Rand Water for financially supporting my study through the professorial chair of Prof Forbes and investing in research to improve the quality of our drinking water in South Africa. I would also like to thank the University of Pretoria for the funding provided to me throughout this project and in my undergraduate studies.

I would like to thank Erna, Charity and Coenraad from the Microscopy Unit for all their help and guidance with SEM and TEM. Thank you to all the colleagues and friends in the student's office. I will miss you all and I am thankful to have met such a great group of excellent young scientists and to have made lifelong friends. Finally, I want to thank God, my parents and friends for encouraging me in all my years of education and always loving and supporting me.

Output

A manuscript entitled “CdSeTe/ZnS quantum dots immobilized into polydimethylsiloxane thin films for sensing phenanthrene in water” has been prepared for submission to the *South African Journal of Chemistry*.

Abstract

Organic pollutants in water are a significant environmental problem, as they can have harmful effects on both human health and the ecosystem. Atrazine and phenanthrene are two common organic pollutants that are often found in water sources. In this study, the aim was to develop a fluorescence sensor that could detect these pollutants in water using a combination of quantum dots (QDs) and polydimethylsiloxane (PDMS) polymer. The study involved the synthesis of quantum dots, which were then interacted with the target organic molecules in solution to confirm proof of concept. The QDs were then immobilized into PDMS, and the thin film synthesis methodology was optimized. The films were then interacted with the target analytes in synthetic standard solutions as well as an inlet water sample obtained from Rand Water.

Hydrophobic QDs were successfully synthesized by the organometallic hot-injection method. The hydrophobic nature of the QDs was maintained to facilitate their optimal interaction with the PDMS. The QDs were synthesized twice and the second batch resulting in CdSeTe core QDs and CdSeTe/ZnS core/shell (C/S) QDs were used further in the study. The maximum emission wavelength peak of the core QDs was 588 nm and upon the addition of the shell this red-shifted to 594 nm after 60 min of the reaction.

The size of the QDs was determined using transmission electron microscopy (TEM) and it was found that core and C/S QDs had average particle diameters of 3.06 and 4.02 nm, respectively. A size increase was observed as the shell layer had been coated over the QD core. There was also a slightly larger size distribution for the C/S QDs than what was observed with the core QDs with full width half maximum (FWHM) values of 31.0 and 49.5 nm respectively.

The optimal excitation wavelength for the QDs in chloroform solution was 420 nm and an emission range of 430-800 nm was used to measure changes in fluorescence with 4 nm slit widths. When the QDs in chloroform solution were interacted with atrazine for 1 min, quenching was observed. This correlated to literature and served as proof of concept for the rest of the experiments.

The photoluminescence quantum yield (PLQY) of the QDs was measured by comparison to Rhodamine 6G in ethanol and was calculated to be 47%. The calculated PLQY of the QDs was lower than expected as the fluorescence of the C/S QDs was very bright even when they were immobilized in the PDMS to produce QD@PDMS thin films. Various film preparation parameters were tested and optimised, including those

relating to the spin coater, the QD concentration in the film, film curing temperatures, as well as fluorescence measurement parameters. It was found that spin coating the PDMS at a speed of 500 rpm (300 rpm/s) for 10 s and then curing the films on a hot plate at a temperature of 80 ^{o}C for 15 min produced the best quality films with optimal, evenly distributed QDs and no bubbles within the material or striations over the surface. These were the optimized film spin coating parameters used further in the study. The QD concentration within the films was also varied where two different concentrations were tested. Films with low QD concentration (LQD) and high QD concentration (HQD) were prepared by dissolving QDs in chloroform to form solutions with concentrations of 0.004 g/mL and 0.008 g/mL, respectively. In each case, the QD@chloroform solution was then sonicated for 30 min to fully disperse the QDs, whereafter the curing agent and PDMS were added using a ratio of 1 mL QD@chloroform solution: 1 g curing agent: 10 g PDMS. The excitation wavelength was optimized for the QD@PDMS films, and a wavelength of 400 nm was used with an emission range of 410-700 nm and slit widths of 2 nm.

The film thicknesses were measured by breaking the films under liquid nitrogen and examining them with a scanning electron microscope (SEM). The thicknesses ranged from 250.44 µm for HQD films to 437.68 µm for a film with no QDs. These values, along with the film masses, were used to calculate the concentration of QDs within the films. The concentrations were determined to be 0.28 and 0.51 mg/mL for LQD and HQD films, respectively.

The thin films were then interacted with atrazine. Atrazine is a widely used herbicide that belongs to the class of triazine herbicides. It is an organic, polar compound which is highly soluble in water and other polar solvents. The interaction between QD@PDMS films and various concentrations of atrazine in ethanol for 1 min was tested. The LQD films exhibited quenching (as expected from literature based on measurements in solution), while the HQD films showed enhancement.

The effect of various solvents on the fluorescence of the films was tested, by immersing the films in various solvents (100% H_2O, 100% ethanol and a mixture of the two, H_2O: ethanol (2:1)) for 24 hours. Enhancement was seen for both LQD and HQD films with 100% H_2O and 100% ethanol, whilst slight quenching was seen with H_2O: ethanol (2:1). It was found that the solvents used did not have a significant effect on the fluorescence properties of the films, therefore any changes observed in fluorescence were attributed to the interaction of an organic molecule with the films.

The LQD and HQD thin films were then interacted with phenanthrene (Phe), which is a polycyclic aromatic hydrocarbon (PAH) that is composed of three fused benzene rings and is non-polar. It therefore has a strong affinity for non-polar PDMS surfaces, due to the intermolecular van der Waals forces that exist between the two non-polar entities. Three films each of optimized LQD and HQD were immersed in 4 mL phenanthrene solutions containing H_2O: ethanol (2:1) solvent at concentrations of 0, 5.61×10^{-6}, and 5.61×10^{-5} M for a duration of 24 hours. The fluorescence of the films was measured before and after the interaction with the solutions, and again after 21 days of standing on the laboratory bench. Enhancement was observed for LQD and HQD films that were interacted with Phe, where films tested with solvent blanks showed quenching. For LQD films, the F/F_0 value increased as the Phe concentration increased, which correlated to literature where it was previously seen that L-cysteine capped CdSeTe/ZnSe/ZnS QDs conjugated to graphene oxide (GO) showed fluorescence enhancement with increasing concentrations of phenanthrene (Adegoke & Forbes, 2016).

The LQD and HQD films were then tested with a water sample obtained from Rand Water (RW) from the inlet to a water treatment plant. No significant results were observed with unconcentrated, filtered water sample. The pre-concentration of 400 mL inlet water was achieved through solid-phase extraction (SPE). When the films were immersed and interacted with a 3 mL concentrated extract in ethanol and deionized water for 24 hours, quenching was observed for both LQD and HQD films with F/F_0 values of 0.75 and 0.83 respectively, which likely indicated the presence of organic pollutants in the water sample.

It was observed that when the films were exposed to ambient light over time, there was enhanced fluorescence, whereafter storing films in complete darkness reduced the enhanced illumination of the films close to the original values before exposure to ambient light. Thus, it was found that the films are very sensitive to ultraviolet and ambient light, and the effect that light has on the QD fluorescence emission should thus be investigated further. It is thus recommended that the films be stored in the dark after synthesis and prior to use. Additional research into the influence of variations in exposure to light on the fluorescence emission of QD@PDMS is crucial for future development of this material as a fluorescence sensor. This study has shown the potential of the QD@PDMS thin films in the sensing of non-polar organic pollutants (specifically PAHs) in water and has successfully developed a facile means to reproducibly produce thin films for fluorescence sensing.

Table of Contents

List of Figures

List of Tables

List of Abbreviations

2D	two-dimensional
A/W	air-water
ACHe	acetylcholinesterase
AES	Auger electron spectroscopy
AFM	atomic force microscopy
AO	atomic orbital
BAM	Brewster angle microscopy
C-bDs	carbon-based dots
CD	carbon dot
CE	capillary electrophoresis
C/S	core/shell
CP	conjugated polymer
CPS	counts per second
CSS	core/shell/shell
ECP	emerging chemical pollutant
EDS	energy-dispersive X-ray spectroscopy
ELISA	enzyme-linked immunosorbent assay
FIA	fluorescence immunoassay
FRET	fluorescence resonance energy transfer
FT-IR	Fourier transform infrared
FWHM	full width half maximum
GC	gas chromatography
GC-MS	gas chromatography- mass spectrometry
GC-TOFMS	gas chromatography- time of flight mass spectrometry
GQD	graphene quantum dot
HPLC	high-performance liquid chromatography
HOMO	highest occupied molecular orbital
HQD	high concentration quantum dot
IC	ion chromatography

IR	infrared
LB	Langmuir-Blodgett
LED	light-emitting diode
LIF	laser induced fluorescence
LC-MS/MS	liquid chromatography-tandem mass spectrometry
LCAO	linear combination of atomic orbitals
LOD	limit of detection
LQD	low concentration quantum dot
LS	Langmuir-Schaefer
LUMO	lowest unoccupied molecular orbital
MCL	maximum contaminant level
MIP	molecularly imprinted polymer
MMA	methyl methacrylate
MO	molecular orbital
mSGP	magnetic silica beads/graphene quantum dots/ molecularly imprinted polypyrrole
NC	nanocrystal
NP	nanoparticle
OA	oleic acid
ODA	octadecylamine
ODE	1-octadecene
OP	oligomer phosphine
OTS	octadecyltrichlorosilane
PAA	polyacrylic acid
PAD	pulsed-amperometric detector
PAH	polycyclic aromatic hydrocarbon
PD	polymer dot
PDMS	polydimethylsiloxane
PDSA	polydisubstituted acetylene
PEG	polyethylene glycol
Phe	phenanthrene
PL	photoluminescence

PLQY	photoluminescence quantum yield
PMMA	polymethyl methacrylate
POP	persistent organic pollutant
ppb	parts per billion
ppm	parts per million
PSMA	polystyrene-co-maleic anhydride
PSMS	polystyrene microspheres
PVA	polyvinyl alcohol
PVP	polyvinylpyrrolidone
PXRD	powder X-ray diffraction
QD	quantum dot
QDQW	quantum dot quantum well
QY	quantum yield
RGB	red green blue
Rh6G	rhodamine 6G
RPM	revolutions per minute
SAM	self-assembled monolayer
SEM	scanning electron microscopy
SERS	surface enhanced Raman spectroscopy
S-GQD	sulphur-doped graphene quantum dot
SIMS	secondary ion mass spectrometry
SPR	surface plasmon resonance
TDA	tridodecylamine
TDPA	tetradecylphosphonic acid
TEM	transmission electron microscopy
TGA	thioglycolic acid
TOP	trioctylphosphine
TOPO	trioctylphosphine oxide
TP	toxicity potential
USA	United States of America
US EPA	United States Environmental Protection Agency

UPLC	ultra-performance liquid chromatography
UV	ultraviolet
UV-Vis	ultraviolet-visible spectroscopy
VSF	vibrational sum frequency spectroscopy
W	wurtzite
WHO	World Health Organization
WHP	weighted hazard potential
XPS	X-ray photoelectron spectroscopy
XRD	X-ray diffraction
ZB	zinc blende

Chapter 1: Introduction

1.1. Introduction to organic water pollutants

An extremely diverse range of toxic and potentially toxic organic pollutants have been released into the environment by anthropogenic activities (Wang et al., 2022). The quantities and types of pollutants that have been detected in rivers, lakes, and drinking water treatment plants have notably increased (Feng et al., 2003; Zhou et al., 2006), thus posing a threat to the aquatic ecosystem. Even at low concentrations, some of these pollutants may have biological activity in water, which could cause harm to the environment and to human health through toxicity, carcinogenesis, and interfering with organism functions (Samia et al., 2018; Barrón Cuenca et al., 2019; Silvia et al., 2019). Furthermore, when these organic pollutants are present in water, they may produce toxic by-products when they undergo degradation or humification reactions (Wang et al., 2022).

Organic chemical contaminants in water include several compound classes like dyes, petroleum, pesticides, pharmaceuticals, polycyclic aromatic hydrocarbons (PAHs), polychlorinated biphenyls (PCBs) and surfactants (Chowdhury et al., 2016; Samia et al., 2018). The target organic pollutants included in this study were a pesticide (atrazine) and a polycyclic aromatic hydrocarbon (specifically phenanthrene).

Some organic pollutants do not have established wastewater discharge regulatory limits nor accepted concentrations for drinking water, particularly in South Africa, and these compounds are collectively referred to as emerging chemical pollutants (ECPs) (Pal et al., 2014; Sima et al., 2014), and by extension this includes chemical pollutants that are not routinely monitored although they have been detected in the environment and may have adverse effects on human health and the environment (Sima et al., 2014; Bo et al., 2015). ECPs include a range of compounds, such as natural and synthetic hormones, pesticides, phytocompounds and industrial chemicals. Due to their toxic potential and increasing abundance in the environment, PAHs are also regarded as ECPs. The database of Norman Network, for example, provides a list of 1036 emerging pollutants which includes most of the PAHs including phenanthrene (Phe) (Norman-Network, 2016). The target compounds of this study, namely atrazine and phenanthrene, are thus considered as ECPs in the South African context. The development of analytical sensing and screening methods for monitoring of ECPs is therefore required to determine the potential threat they may pose to South African water bodies (Petersen et al., 2017; Odendaal et al., 2015).

A national survey that was conducted over four seasons on drinking water from South African major cities showed that the most often detected ECPs were the related pesticides atrazine and terbuthylazine, and the mood-stabilising drug, carbamazepine (Odendaal, et al., 2015). The levels of these ECPs detected were well below the maximum contaminant level (MCL) proposed by the World Health Organization (WHO) and the United States Environmental Protection Agency (US EPA). However, the range of compounds detected in drinking water, and the seasonal and geographic variability in ECP levels, warrants a more frequent screening programme, as their impact on health arising from long-term exposure is mostly unknown (Odendaal et al., 2015).

1.2. Background and motivation for the study

Pesticides are extensively used in agriculture to improve the production of food, but this may lead to severe unintended contamination of non-target areas like surface water because of surface runoff, leaching and spray drift (Nsibande et al., 2015; Nsibande & Forbes, 2016). During application, a fraction of the dosage is also lost to the atmosphere, where it may be distributed among aqueous, particle and vapor phases. Different mechanisms may return the pesticides back to the earth's surface and these include wet deposition through rain, snow and fog (Rossi, 2010). Pesticide spray drift is defined as the amount of crop protection active ingredient which comes directly from the application nozzles and is deflected out of the intended treated area by the action of air flow during the treatment process (Carlsen, 2006; Munjanja et al., 2020).

The main routes of human exposure to pesticides, including atrazine, is though air, soil, the food chain, flora and fauna (Kim et al., 2017). Upon exposure, the pesticides enter the human body through dermal, oral, eye and respiratory pathways. The pesticides are then distributed through the body via the blood stream and can lead to asthma, diabetes, Parkinson's disease, leukaemia and cancer (Kim et al., 2017).

According to the US EPA, polycyclic aromatic hydrocarbons (PAHs) are priority pollutants. A total global atmospheric emission estimation of 520,000 tons of the 16 priority PAHs were released in 2004, where Africa alone contributed 18.8% of this (Zhang & Tao, 2009). PAHs are organic pollutants present in atmospheric, aquatic and terrestrial systems (Adeniji et al., 2019). PAHs are formed mainly from the incomplete combustion of organic materials and enter the environment from various sources, which include residential heating, motor vehicle exhaust, coal-tar pitch and asphalt production, coal gasification,

liquefying plants, aluminium production, catalytic cracking towers and related activities of petroleum refineries (Abdel-Shafy & Mansour, 2016; Adeniji et al., 2019; Perez-Padilla et al., 2010).

The atmospheric partitioning of PAH compounds between the particulate and gaseous phase strongly influences their fate and transport in the atmosphere and alters the way they enter the human body. The main routes of human exposure to pollutants like PAHs are food intake, inhalation and dermal contact with the molecules, where short-and long-term effects include major respiratory and cardiovascular diseases (Perez-Padilla et al., 2010). An additional concern lies with the reactive metabolites of these compounds, such as epoxides and dihydrodiols, which can bind to cellular proteins and DNA (Zhou et al., 2017; Ewa & Danuta, 2017).

Monitoring of these ECPs is required to determine the potential threat that they may cause (Petersen et al., 2017). Until relatively recently, ECPs have not been detected in environmental samples because of their very low concentrations, which also leads to high cost of analysis (Montaseri, 2018). ECPs are generally found in the environment at concentrations below acute toxic levels, but the effect of chronic exposure to human health and development is unknown (Odendaal et al., 2015).

Organic pollutants can be detected quantitatively with conventional analytical methods, like chromatography-mass spectrometery based analyses. For routine analysis, however, this may be time consuming with very high instrumentation cost. For this reason, reliable, robust, portable, cheap and easy-to-use sensors, which do not require extensive sample preparation or processes of isolation of target analytes from matrix, need to be developed to detect the presence of these pollutants in the environment. Spectrofluorimetric methods where nanoparticles such as quantum dots (QDs) are used have gained interest in analytical chemistry for being simple and sensitive sensor-based systems (Frigerio et al., 2012; Ma & Su, 2011). Novel fluorescence sensors have the potential to allow for portable, low-cost qualitative screening of ECPs, before the positively identified compounds are quantitatively analysed with conventional methods like liquid chromatography coupled with tandem mass spectrometry detection (LC-MS/MS).

Quantum dots are semiconductor crystalline nanomaterials with electronic and optical properties that are unique, with attractive properties that make them suitable analytical sensors (Nsibande & Forbes, 2016). They have good photostability, broad excitation spectra, high quantum yields, large Strokes shifts, long fluorescence lifetimes and bright photoluminescence (Jia et al., 2017). They also have a surface which can

be modified and tailored for desired functionalities to enhance binding of analytes and decrease surface defects. However, QDs are extremely sensitive to processes like ligand removal or exchange which can either enhance, or quench the fluorescence thereof (Kalwarczyk et al., 2013). Surface defects have a negative impact on the fluorescence quantum yield, and they lead to luminescence decay and spectral shifts, with the appearance of undesirable band states which are electronic states in QDs that can have a negative impact on the performance and desired characteristics of the QDs (Chandan et al., 2018; Sotelo-Gonzalez et al., 2012). When coordinated to selected ligands, exposure to surroundings could influence the properties of QDs drastically (Giansante & Infante, 2017). Ligand exchange on the surface of QDs may also help with dispersion of the QDs in different media to form hybrid composite materials.

Quantum dots are usually synthesized from nucleation of organometallic precursors and their surfaces are protected by an organic capping ligand like trioctylphosphine (TOP) or trioctylphosphine oxide (TOPO). These can allow QDs to be tailored for specific applications (Nsibande & Forbes, 2016). They have also been confirmed as suitable fluorescence probes for analysing metal ions, small molecules and even biomacromolecules (Nsibande & Forbes, 2019). Fluorescence sensors based on QDs have been used for the detection of organophosphate pesticides, but additional research is needed on organochlorine pesticides like atrazine and terbuthylazine (Nsibande and Forbes, 2016).

Detection of organic ECPs using QDs is primarily based on surface interactions of the QD with the analyte compound which may lead to either quenching or enhancement of the fluorescence emission of QDs. For example, after an ECP binds to a QD, the electrons from the ECP can absorb energy which leads to an excited state, whereafter as the electrons return to the ground state, the energy can be transferred to the QDs resulting in the quenching of fluorescence of the donor molecule (ECP) and enhancement of the acceptor molecule (QDs) (Nsibande & Forbes, 2019).

Developing QD fluorescence sensors involves the optimization of numerous parameters in order to obtain maximal response and therefore optimal sensitivity. These parameters include contact time with target analyte, fluorescence excitation wavelength, sensor solution concentration, ratio of analyte-to-sensor in solution, type of solvent, and reaction temperature and time (Montaseri, 2018; Jorge et al., 2007).

It is also advantageous and desirable to develop a sensor that is reusable in order to decrease waste, and to ensure no time and resources are lost by making new sensors after each analysis. In this study, the proposed method involves the immobilization of QD nanomaterials into a polymer matrix solid support, for

application in the screening for the target organic pollutants in water samples. Immobilization has many advantages, as it will allow direct sensing of water samples, as well as protection of the cadmium based QDs from leaching into the sample solution. Immobilization may reduce luminescence efficiencies, however, the challenge is to retain the photoluminescent properties of the QDs after immobilization.

Polydimethylsiloxane (PDMS) is a silicone elastomer with numerous properties which make it ideal for immobilizing QDs. It is chemically inert, thermally stable, flexible, permeable to gases, is easy to manipulate and handle, non-toxic and of low cost. It is also transparent and non-fluorescent which in turn then improves optical transparency of the nanocomposites, allowing for light to pass through the material without appreciable scattering (Tao et al., 2013). Polymer PDMS films can be prepared by using a spin coater, which assists in ensuring uniform thickness of the polymer. The PDMS is also able to absorb organic non-polar analytes, allowing for their extraction and pre-concentration from water samples (Mata et al., 2005). Immobilization of QDs into PDMS may thus enable the development of a portable sensor system, enabling *in-situ* measurements to be done directly in the field.

In order to achieve this, optimization of the immobilization of QDs onto/into PDMS is required. Dispersion of QDs within the polymer is needed to ensure optical transparency and long-term stability of the nanocomposites (Tao et al., 2013). The sensor material will then have the combined advantages of QDs together with the inertness, flexibility and the ability to pre-concentrate the analytes provided by the PDMS. If fluorescence quenching or enhancement upon interaction with the target analytes correlates proportionally to the concentration thereof, the system may serve as a sensor.

Development of fluorescence QD sensors which can be used to detect organic pollutants such as pesticides have previously been performed by our research group (Nsibande & Forbes, 2019). The focus of this study was not to synthesize novel QDs, but rather to develop a suitable means to immobilize these QDs into PDMS by a reproducible method and then to conduct preliminary tests to determine whether the resulting material can be used as a sensor to detect organic pollutants in water for screening purposes.

1.3. Aim and objectives

The aim of this study was to develop a portable fluorescence sensor based on the immobilization of QDs into a PDMS thin film, which can be employed to screen for organic pollutants in surface waters at environmentally relevant concentrations. In order to achieve this aim, the objectives of this study were to:

i. Synthesize CdSeTe/ZnS QDs and characterize them with various techniques.
ii. Develop and optimize the immobilization of QDs into PDMS thin films by means of spin coating. Spin coating variables to be tested and optimized included film thickness (speed, acceleration and time used to produce thin films with the spin coater), stoichiometry (ratio of QD to PDMS), homogenous dispersion of QDs inside the films, the use of a polyacrylic acid (PAA) layer, PDMS curing temperatures, and film substrate to be used.
iii. Perform preliminary tests employing the PDMS immobilized QDs for detection of target analytes (namely atrazine and phenanthrene) in aqueous standard solutions. This included testing photostability of the prepared thin films over short and extended intervals, as well as testing different sensing variables namely, the concentration of analyte, the interaction time, the spectrometer settings including excitation wavelengths, and the method and setup to measure fluorescence of the films inside the spectrophotometer.
iv. Evaluate the performance of the QD@PDMS films in detecting analytes in a real water sample from the inlet to the Rand Water drinking water treatment plant.

1.4. Dissertation outline

In this study, QDs were synthesized and a method to reproducibly produce QDs immobilized in thin films was developed. Thereafter the films were interacted with the target organic pollutants and water samples. Chapter 2 provides a literature review on the organic water pollutants of interest in this study, namely atrazine and phenanthrene, as well as a background to QDs, thin films and their applications. Chapter 3 details the experimental methods employed regarding QD synthesis, characterization, and thin film synthesis, along with interactions of optimized low concentration quantum dot (LQD) and high concentration quantum dot (HQD) films with atrazine, phenanthrene and water samples. Methods employed to calculate thin film thickness, concentration of QDs in films, and quantum yield are described. Chapter 4 presents results obtained from the characterization of the QDs and thin film experiments described in Chapter 3. Chapter 5 provides a conclusion and highlights future work. Supporting information (chemical certificates of analysis and additional characterization results) is presented in the Appendices.

Chapter 2: Literature Review

In this chapter, literature is reviewed and discussed regarding the organic pollutants of interest in this study. Furthermore, a background is provided on the quantum dots employed, the reason for adding shell layers to the QD core, and the uses of QDs for sensing. Following that, polymer thin films are discussed, beginning with an introduction to immobilization, the polymer employed, and the method used to manufacture the thin films. Lastly, this section discusses other methods to produce thin films including the characterization thereof.

2.1. Organic water pollutants of interest in this study

2.1.1. Atrazine

The high demand for food globally has led to a need for increased food production by the agricultural sector. With the production of a broad spectrum of food crops, including maize, sorghum and sugarcane, pesticides like atrazine are needed for controlling the growth of weeds and improving food production. The chemical structure of atrazine (6-choloro-4-N-ethyl-2-N-propan-2-yl-1,3,5-triazine-2,4-diamine) is presented in Figure 2-1. Atrazine is the second most used pesticide in the world, with 70 000 - 90 000 tons being applied annually (Singh et al., 2018). The mobility and potential of atrazine to contaminate groundwater and surface freshwater sources raises concern, as both sources are used as drinking water supplies. Atrazine is one of the most frequently detected agricultural chemicals found in drinking water samples (Benotti et al., 2009; Suhl, 2016). A study in 2012 found atrazine in 32% of waterbodies in the United States of America (USA), with a mean concentration of 0.17 ppb in contaminated samples (Beaulieu et al., 2020). It has been found that atrazine is the most frequently detected pesticide in surface and ground water in the USA and Europe, respectively (Nsibande, 2015; Kim et al., 2017).

Atrazine works by inhibiting electron transport during photosynthesis of the weed, thereby destroying it, while the target crop is tolerant to atrazine because of rapid detoxification (Mohapatra et al., 2018). Atrazine can be degraded and broken down into many metabolites in the environment including desethylatrazine, deisopropylatrazine, dealkylatrazine and hydroxyatrazine (Blume et al., 2004; Singh et al., 2018).

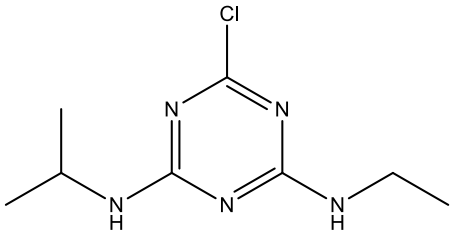

Figure 2-1: Chemical structure of atrazine.

Atrazine has a half-life of 77-101 days in soil, and over 900 days in subsurface soil (Blume et al., 2004). Transformation products of the triazine pesticides are detected most frequently in rainwater as well as in air, especially desethylatrazine (Singh et al., 2018). It is stable, mobile, and present in the environment for prolonged periods of time due to its low reactivity, slow degradation, and water solubility (Mohapatra et al., 2018), thus making it a pollutant of environmental concern.

In a study that sought to identify emerging contaminants of concern in South African water treatment plants and domestic water taps, atrazine was one of the most commonly detected pesticides (Patterton, 2013). A different study also showed that atrazine was ranked as the highest priority pesticide among 25 priority pesticides used in South Africa (Dabrowski et al., 2014). The pesticides were ranked based on weighted hazard potential (WHP), which is proportional to the toxicity potential (TP).

According to the World Health Organization (WHO), the guideline for atrazine limits in drinking water is 0.1 ppm (4.6×10^{-7} M). In postmenopausal women, atrazine has been demonstrated to have endocrine-disrupting effects (Inoue-Choi et al., 2016). HepaRG cells and human primary hepatocytes are affected by short- and long-term exposures (Nawaz et al., 2014). Atrazine may induce the following cell mutations: apoptosis of SH-SY5Y human neuroblastoma cells via the regulation of Bax/Bcl-2 ratio and caspase-3-dependent pathway (Abarikwu & Farombi, 2015); SH-SY5Y human dopaminergic neuroblastoma cells via microglial activation (Ma et al., 2015); aromatase expression is SF-1 dependent and endocrine disruptor (Fan et al., 2007) and disruption of the hypothalamic control of pituitary–ovarian function (Cooper et al., 2000).

Gas chromatography coupled with mass spectrometry (GC-MS) or a nitrogen phosphorous detector (GC-NPD), infrared (IR) spectroscopy, enzyme-linked immunosorbent assay (ELISA), liquid chromatography coupled to a mass spectrometer (LC-MS), high-performance liquid chromatography (HPLC), and ultra-performance liquid chromatography (UPLC) are conventional analytical techniques used for the quantitation of atrazine (Nsibande, 2015). HPLC/LC-MS and GC-MS are the most sensitive, with low detection limits for atrazine in the ppb range in different matrices (Singh et al., 2018). Despite the high sensitivity, selectivity, and robustness of these methods, they still suffer from severe setbacks as they require very expensive and sophisticated instruments (Mohapatra et al., 2018; Nsibande & Forbes, 2016). Therefore, there is a need for more facile methods to be developed for screening of compounds of concern in water samples. The development of an atrazine sensor could enable more frequent monitoring of water, with increased ease of use and decreased reliance on expensive, conventional instruments and resources. This would enable the routine monitoring of atrazine to ensure concentrations are below the maximum contaminant level in water, as atrazine may have adverse effects on human health and the environment.

2.1.2. Phenanthrene

Polycyclic aromatic hydrocarbons (PAHs) were selected as an important class of organic pollutants of relevance in this study. PAHs are non-polar, aromatic compounds which have a high prevalence due to pollution caused by human activity. Pyrogenic and petrogenic sources are both origins of PAHs in the environment, where pyrogenic PAHs are formed from the incomplete combustion of organic materials including fossil fuels, industrial waste and wood (Angerer et al., 1997; Lui et al., 2009), whereas petrogenic PAHs are produced from refining of petroleum products like kerosene, petrol and diesel as well as crude oils (Yunker et al., 2002; Lui et al., 2009).

PAHs can be dispersed in the environment through various pathways including long-range atmospheric transport, waste-water discharge, urban runoff and oil spills or leakages whereby they may be transported into water sources (Chen & Chen, 2011; Pies et al., 2008; Van Metre et al., 2000). Organisms in these aquatic environments can then ingest the PAHs when the molecules enter the food chain or they can accumulate when adhering to the sediment of water sources (Lui et al., 2009; Lu et al., 2012; Wang et al., 2010).

Some PAHs are recognized as carcinogens or potential carcinogens that may be harmful to the health of both humans and wildlife. They may potentially operate through the aryl hydrocarbon receptor (AhR) mechanism to cause harmful effects to detoxification, cellular homoeostasis or immune responses and may disrupt oestrogen receptor (ER)-mediated signalling (Balch et al., 1995; Larsson et al., 2012; Machala et al., 2001). The main concern regarding PAHs with respect to humans include their mutagenic and carcinogenic properties. While most toxic effect studies of PAHs have been based on other organisms, due to the similarity in biological systems, it is likely to affect all mammals including humans in the same way (Salazar-Corcia et al., 2010; Gesto et al., 2009; Bado-Nilles et al., 2009). Acute and chronic human exposure to PAHs may additionally lead to pulmonary and respiratory disorders, localized skin problems, reproductive and developmental complications, as well as behavioral and neurological problems (Davis et al., 1987).

Phenanthrene was chosen as a representative PAH in this study because of its ubiquity in the environment (Mahgoub, 2014). In Figure 2-2 the chemical structure of phenanthrene is shown: it is composed of three fused aromatic rings.

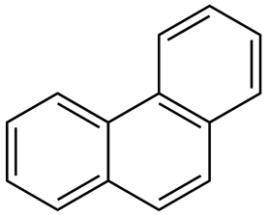

Figure 2-2: Chemical structure of phenanthrene.

The presence of PAHs in both sediment and water matrices poses a challenge in developing analytical methods for total quantification. Conventional screening procedures typically include extracting the PAHs from water and sediment using liquid-liquid or Soxhlet extraction, followed by clean up with silica gel columns, pre-concentration, and ultimately quantification using gas chromatography with flame ionization detection (Adeniji et al., 2019). Other quantification method instruments include gas chromatography-mass spectrometry (GC-MS) or gas chromatography-time of flight mass spectrometry (GC-TOFMS) which can be used to detect and quantify the PAHs and their derivatives. LC coupled with fluorescence detection and laser induced fluorescence (LIF) may also be used (Abdel-Shafy & Mansour, 2016; Pheiffer et al., 2017). All these quantification techniques require expensive equipment which are not portable, therefore this

research study aims to investigate low-cost sensing techniques which are portable for in-field monitoring purposes.

2.2. Quantum dots (QDs)

2.2.1. Background to quantum dots

Colloidal crystalline nanoparticles which exhibit quantum confinement effects and size-dependent photoluminescence (PL) properties are termed quantum dots (Hu & Zhu, 2015; Giansante & Infante, 2017). Quantum dots (QDs) are semiconductor nanoparticles/nanocrystals which are 2- 10 nm in diameter and consist of elements from periodic groups II-VI or III-V. Colloidal inorganic nanoparticles which include chalcogenide QDs (CdSe, CdSeTe etc.) have been of great interest over the past two decades due to their unique optoelectrical, magnetic and electrical properties which are between that of atoms/molecules and are different to that of the bulk material (Khan et al., 2019; Murray et al., 2000; Kudera, 2008). QDs are typically composed of hundreds to thousands of atoms, and due to recent developments are synthesized as high-quality QD ensembles with narrow size distributions. Colloidal group II-VI metal chalcogenide QDs such as CdS, CdSe, and CdTe, have undergone extensive research regarding their quantum confinement effects, including their size-dependent photoemission properties (Wang, 2009).

This interest in QDs, with a focus on metal chalcogenide QDs, is because of their quantum confinement effects and size dependent photoemission characteristics (Joo et al., 2003). Quantum confinement in QDs is possible due to their small physical diameter that is close to or smaller than the Bohr radius of the particle, which influences the absorption and emission properties of the QDs and can be altered by variation in the QD particle size, surface and structure (Brus, 1984; Zhang et al., 2003).

This quantum confinement effect is prevalent when the particle size reaches, or is smaller than the Bohr radius, and it is common for nanocrystals with diameters of 10 nm or less. Quantum confinement is observed in the optical properties, as the smallest CdSe NCs with diameters less than 2 nm show blue fluorescence but larger diameters of the same material (diameter ca. 6 nm) emit red light (Kudera, 2008). Ekimov discovered the size-dependent properties of ionic nanocrystals in a glass matrix in 1982 at the Loffe Institute in St. Petersburg, Russia (Ekimov et al., 1980; Ekimov, 1996). The bandgap is the energy between the electron filled valence band and the empty conduction band above it. When an electron (e^-) is excited by a photon with appropriate energy (when its energy exceeds the energy of the band gap) from the

valence band to the conduction band, it leaves a hole, (h^+) in the valence band. The electron and the hole form a bound state which is called the exciton. The size of this exciton is what is termed the Bohr radius. When quantum dots are very small in size, and are smaller than the Bohr radius, three-dimensional confinement of the electron and the hole arises. Thus, to "fit", the charge carriers assume a higher kinetic energy and an increase in the band gap is observed. This alters the optical and electronic properties of the nanoparticle compared to the bulk material (Tomczak et al., 2009; Kudera, 2008; Gao et al., 2005; Zhang et al., 2003). The bandgap thus increases as the size of the QD is decreased and the larger the nanocrystals are, the more the fluorescence emission wavelength is shifted towards lower energies, i.e. towards red as seen in Figure 2-3.

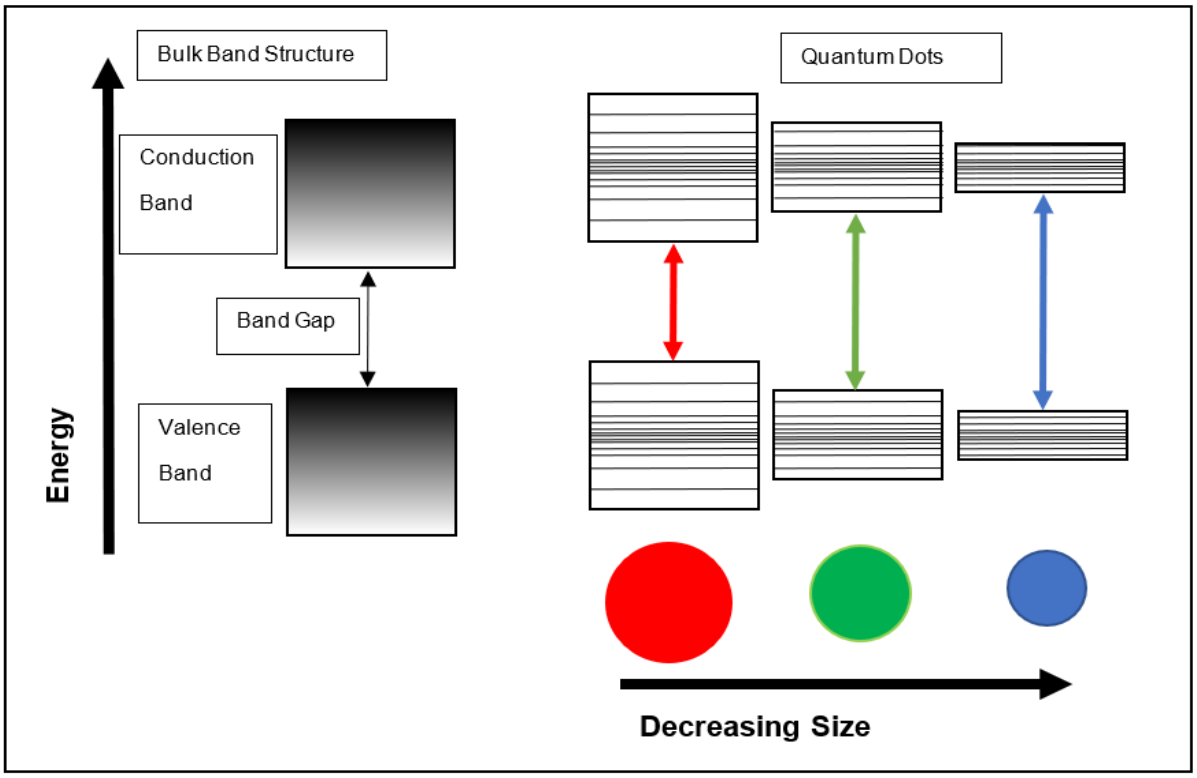

Figure 2-3: The correlation between band gap energy and the size of QDs (adapted from Kudera, 2008).

The width and form of the absorption peak is influenced by the size distribution of the QDs, as well as the shape of the QDs (Kudera, 2008). Spherical nanocrystals are considered as zero-dimensional objects, where confinement is exerted in all three dimensions (Kudera, 2008; Joo et al., 2003; Gao et al., 2005).

The emission of photons generating luminescence is categorized as fluorescence and phosphorescence. Fluorescence is a property observed when the electrons of a semiconductor absorbs photons with an energy hv_e that is larger than its band gap energy, and transitions to the conduction band, followed by a relaxation process which emits light with a longer wavelength when the electron recombines with the hole generated in the valence band. This is called a “band edge” recombination process. QDs provide a number of benefits in terms of fluorescence characteristics which include high brightness due to the extinction coefficient and quantum yield, wide absorption characteristics, a narrow band width in the emission spectra, independence of emission from the excitation wavelength, continuous and tuneable emission maxima due to quantum size effects, a longer fluorescence lifetime ranging from 10 to 40 ns, and stability under relatively harsh environments (Medintz et al., 2005; Yu et al., 2006). Controlling the size, shape, homogeneity, and surface structure of the QDs during the preparation process is critical for producing these unique properties.

As the electrons in the conduction band may become trapped by the presence of surface defects which influence the luminescence properties of the nanocrystals, careful surface handling of the QDs is essential (Tomczak et al., 2009). It is seen that the emission peak is red-shifted (is of lower energy) compared to the absorption peak and this is referred to as Stokes-shift (Kudera, 2008). Molecular orbital theory uses terms HOMO (highest occupied molecular orbital) and LUMO (lowest unoccupied molecular orbital) instead of valence and conduction bands (Kudera, 2008). Most semiconductor nanoparticles have their atoms arranged in hexagonal wurtzite or cubic zinc blende crystal structures. Both have a four-coordinate structure and differ in how the layers are stacked along the axis {111}, using an ABCABC and an ABAB sequence, respectively. There is also a wurtzite (W)-zinc blende (ZB) polytypism in the structure of some semiconductors. The same NC can exist as either structure or both concurrently depending on the experimental conditions, nucleation, and the growth of the NCs, as seen in Figure 2-4 (Ghosh et al., 2013).

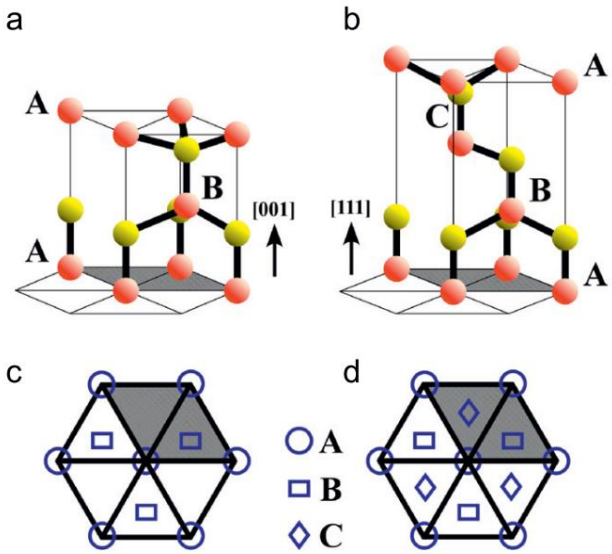

Figure 2-4: CdS crystal structure in (a) wurtzite (WZ) and (b) zinc blende (ZB) symmetries. (c) shows WZ stacking sequence of {001} and (d) the stacking sequence of ZB {111} (Image taken from Ghosh et al., 2013).

QDs have significantly evolved structurally from a fundamental mononuclear structure to more sophisticated multistructure systems. These systems, which come in a variety of configurations such as core-ligand shell, doped, alloy, core-shell, core-alloy shell, and others (Figure 2-5) each having their own characteristics. The doping of a structure is generally limited to a regional exchange of elements. It does not affect the main bandgap of QDs, but changes the band structure of local regions to improve performance regarding lower quantum dot toxicity and higher carrier transfer efficiency for example (Cheng et al., 2022). When the number of ions exchanged reaches a certain level, the alloy structure is formed, in which the different elements are evenly distributed on the surface. This can change the bandgap and other properties of QDs. The core–shell structure on the other hand, refers to a QD structure in which one or more uniform outer shells grow on the surface of the original inner core. The shell can reduce electron recombination loss (Lee et al., 2020) and enhance stability (Shapiro et al., 2016). Each of the different types of QD structures has special benefits that assist high-performance optoelectronic applications by enhancing photoelectric conversion efficiency, durability, and luminescence. Researchers have, however, also discovered some drawbacks, including difficult structural characterisation and weak control of ion location and distribution. This means that novel synthetic approaches are needed to develop such structural engineering of these materials further (Zhang et al., 2023).

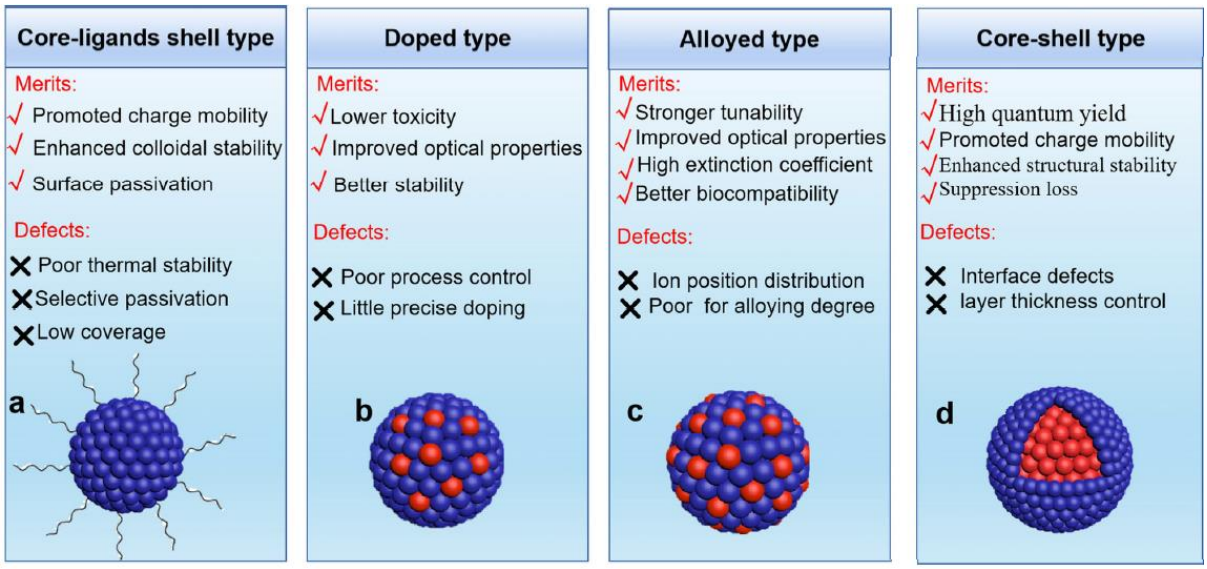

Figure 2-5: QD structures including their advantages and disadvantages a) core/ligands shell-type, b) doped-type, c) alloyed type, and d) core–shell type (Zhang et al., 2023).

2.2.2. QD synthesis

The first QDs were synthesized by precipitation of a metal-ion solution (like Ag, Hg, Pb, Zn, Cd, or In) by a hydroxide of S, Se or Te (He & Gu, 2006). Semiconductor QDs can be produced by using a variety of different reaction conditions and are synthesized in aqueous or organic solutions. The composition and temperature of the solvent have a considerable impact on the growth kinetics and structure of the produced QDs. The environment of the process may also influence the crystalline phase of the QD nanocrystals, for example CdTe nanocrystals are grown into a hexagonal wurtzite phase in organic solvents at high temperatures, but altering the reaction conditions can produce a cubic zinc blende phase (Tiwary et al., 2009; Gao et al., 2005).

The QD structure is composed of the core of the QDs, which is the centre component of the QDs that defines the optical properties of the final QD structure. Typical QDs consist of an elemental group II–IV, IV–VI, or III–V semiconductor core (e.g. CdTe, CdSe, PbSe, GaAs, GaN, InP and InAs). The central inorganic core of QDs is often overgrown by a shell of a different material. Cadmium-based QDs (CdSe, CdS, etc.) are generally coated with materials with higher/wider band gaps, such as ZnS shells (Hines & Guyot-Sionnest, 1996). The shell protects the nanoparticle from degradation and creates a more passivated surface, resulting in a reduction of surface defects/non-radiative pathways and increases the quantum yield (QY), photostability and luminescence properties of the core/shell QDs and effectively increases the

photostability thereof (Murray et al., 1993; Hines & Guyot-Sionnest, 1996; Peng & Peng, 2001; Dabbousi et al., 1997; Michalet et al., 2005; Jin et al., 2011). Passivation of the core by adding a shell layer also decreases the release of toxic cadmium ions from the core into the environment (Yu et al., 2006).

Compared to bare (core) QDs, core–shell structured QDs with a thin shell of a higher band gap element (like ZnS) are advantageous and have been shown to enhance photo-physical properties. This is attributed to the surface defects in the core acting as temporary 'traps' for the electron, hole or excitons, quenching radiative recombination and reducing the quantum yield (QY) (Giansante & Infante, 2017; Houtepen et al., 2017; Kirkwood et al., 2018). These surface traps function as local energy minima that might inhibit or delay electron-hole recombination and eliminating them is a critical step in producing bright QDs (Singh & Voznyy, 2019). It is to be noted that lattice mismatch of the core and binary shell layer could decrease QY if surface defects were induced which degrades luminescence. ZnS and AgZnSe are popular shell layers, and single or multi-shells could be covered over the core (Chung et al., 2018; Adegoke et al., 2019).

Adding shell layers affects the PLQY of the QDs as seen where water-soluble L-cysteine-capped alloyed CdSeTe core QDs (QY= 8.4%) were synthesized and deposited with three different shell layers to study the resulting changes in structural and optical properties. An overcoating of CdS shell resulted in confinement of the exciton with an improved QY of 93.5%. Addition of a ZnSe shell overcoated on the CdS shell gave an CdS/ZnSe alloy with a decreased QY of 24.7% and overcoating this with ZnS gave an CdS/ZnSe/Zns alloy with an QY of 49.5%. It was seen that the QY of the CdSeTe/CdS core/shell QDs did meet the high PLQY and stability requirements in the quality of the QDs, and that no further additional shells were needed to improve the properties. It was seen that the CdSeTe core had a slow decay (longer PL lifetime) and the CdSeTe/CdS QDs showed a fast exciton decay (shorter PL lifetime). Thus, reduced PL lifetime and enhanced PLQY was detected for the CdSeTe/CdS QDs which could be due to the removal of non-radiative recombination pathways and the exclusion of surface defects in the core/shell system (Adegoke et al., 2016). To suppress interfacial defects in the core QDs, a new alloyed ternary AgZnSe shell layer was applied to the surface of luminous CdS QDs. Alloying caused the lattice strain of the C/S QDs to relax and a smooth gradient band gap to develop. Furthermore, since the addition of the alloyed shell triggered a phase transition, the QY of the CdS/AgZnSe QDs was five times larger than that of the CdS core alone (Adegoke et al., 2019).

Organometallic synthesis is the most commonly used technique for the synthesis of these QDs since it offers precise control over their size, shape, chemical composition, and other properties. A low-temperature aqueous route can also be employed and the production of QDs with biological organisms has also gained interest (Dahl et al., 2007; Farkhani & Valizadeh, 2012).

The differences between aqueous and organometallic synthetic routes are that despite the fact that the aqueous synthesis route is inexpensive, ecologically friendly, and ideal for large-scale synthesis, it has certain major limitations which have limited the usage of these QDs (Li et al., 2003). Because of the weakly bound nature of surface ligands and their relatively low photostability, as well as the lack of crystallinity compared to QDs produced via organometallic route, QDs produced via the aqueous route are more susceptible to breakdown and aggregation in solution and frequently exhibit a broader size distribution (He & Gu, 2006; Gaponik et al, 2002). Therefore, size-selective precipitation is required to decrease the broad size distribution. CdSe-based QDs have successfully been synthesized with this method but required combinations of stabilisers before introduction to the aqueous solution (Farkhani et al., 2014).

As a result, the QDs employed in this study were synthesized using the organometallic method, as these QDs exhibit high crystallinity, a high photoluminescence quantum yield (PLQY), and smaller particle size distributions (Bakar et al., 2008; Farkhani et al., 2014; Gaponik et al., 2002; Montaseri, 2018).

The organometallic synthesis approach/high temperature preparation method of QDs was introduced in 1993 by Stiegerwald and Brus, and is an important fabrication route for monodisperse CdS, CdSe and CdTe NC QDs (Rogach, 2008). The three components that make up an organometallic system for the synthesis of QDs are precursors, organic surfactants, and solvents. In most cases, the solvent molecules—also known as surface ligands or surfactants—have a polar head group and a lengthy, non-polar alkyl chain. The strength of the polar group impacts the binding efficiency of the surface ligands, and the structure of the alkyl chain affects diffusion capabilities.

Surfactants can occasionally be used as solvents (Yin & Alivisatos, 2005). The solvent disperses and solubilizes the reactants and nanocrystals involved in the growth process (Clarke, 2008). When QDs are produced in organic solvents, the precursor molecules decompose into the monomers of the nanoparticles at high temperatures, causing nanocrystals to form. By adjusting the number of precursors and crystal growth time, metal chalcogenide-based QDs of various sizes can be produced; which is significant regarding

their fluorescence properties because their emission wavelength depends on crystal size and is therefore tuneable during synthesis (Byers & Hitchman, 2011).

The QDs synthesized in organic solvents contain hydrophobic surface ligands such as tetradecylphosphonic acid (TDPA), trioctylphosphine (TOP), trioctylphosphine oxide (TOPO), oleic acid (OA), or others. These can be replaced by hydrophilic water-soluble ligands (like thiol-based molecules) or encapsulated by hydrophilic polymers (like polyacrylic acid or polyethylene glycol) to alter the hydrophilicity nature of the QDs which increases their solubility in aqueous media if required (Yu et al., 2006).

Trioctylphosphine (TOP) and trioctylphosphine oxide (TOPO) are ligands often employed in organometallic QD synthesis, while amines and carboxylic acids are alternative types of ligands. The synthesis is carried out under inert conditions and there are several ways to include the nanocrystal monomers, but at least one of the species needs to be in the form of a liquid. Injecting the nanocrystals quickly enables a sharp nucleation event. The TOP is combined with the elemental chalcogens and is introduced as a complex (e.g. TOP-Se). CdO binds to the oleic acid-based surfactants at 300 °C, where the reaction emits steam, and the reaction mixture changes in colour from dark red to clear (Reiss, 2008). This occurs because nucleation is caused by a difference in free energy between the two phases (crystalline phase and solution phase), where nucleation is caused by a gain in chemical potential and an increase in total surface area. A gain in chemical potential is obtained when energy is released during the bond creation of the forming crystals.

In comparison to other solvents, octadecene (ODE), which was used in this study, offers a number of benefits, including good dissolving power, environmental friendliness, air stability, lower toxicity, low cost, and a low melting point (below 20° C), which makes it simple to handle at ambient temperatures. Additionally, it is inert to the Se precursor and has a high boiling point (about 360°C), which makes it an ideal solvent for the synthesis of high-quality QDs (Yu & Peng, 2002).

2.2.3. Trap states and surface defects of nanoparticles

Comprehension of the relationships between surface chemistry and quantum dot luminescence is important in understanding photoluminescence (PL) properties of QDs. The optical properties of quantum dots are influenced not only by the quantum confinement of their semiconductor core, but also, to a great extent, by their surface chemistry. Surface defects or under-passivated atoms provide sites for charge-

carrier trapping which have the potential to influence PL properties (Giansante & Infante, 2017; Houtepen et al., 2017; Kirkwood et al., 2018).

Surface engineering of QDs is used in core shell (C/S) systems to grow a second semiconductor shell over the QD core and was an early synthetic strategy developed to eliminate these trap sites, with the goal of isolating the quantum dot core and its charge carriers from the surrounding environment using a wider bandgap semiconductor layer (shell), that is structurally well-matched to minimize strain at the core/shell interface and also to confine the photoexcited electron/hole pair to the QD core. This assists in the passivation of surface defects that are primarily responsible for the loss of luminescence in these materials (Chen et al., 2008; Greytak et al., 2012; Peng et al., 1997).

Thus, with the right combination of core and shell, PLQY may be enhanced, offering stability against photo-oxidation, and allowing for the tuning of the emission wavelength across a wide spectrum range. The shell incorporated when synthesizing C/S QDs may modify both the band gap and the relative position of the electronic energy levels of the semiconductor (Chandan et al., 2018). Alloying at the CdSe/ZnS interface may improve lattice match which results in greater quantum yields, particularly when a ZnS outer shell layer is added (Bae et al., 2009).

Since the heavy metal hazardous core of QDs, which is typically cadmium, has the ability to leach into the environment during use or when the probes are discarded after usage, it is crucial to design sensors that are stable and do not leach (Montaseri, 2018; Nsibande et al., 2019; Kuzyniak et al., 2014). The encapsulation of the QDs in polymers like PDMS would also help to reduce toxicity and reduce the possibility of leaching of the toxic heavy metal QD core (Montaseri, 2018). For the development of future probes, there is also a desire for environmentally friendly, non-cadmium cores like graphene alternatives (Nsibande et al., 2019).

Another difficulty that arises with QDs is that under continuous illumination, the emission of single nanocrystals has been observed in spectroscopic studies to blink or turn on and off. Photoionization involves the trapping of charge in the nearby matrix (dangling bonds on the surface, solvent, etc.), which causes blinking. A delocalized electron or hole exists in the NC core and after further excitation, a quick, non-radiative relaxation occurs through the Auger processes. A localized charge carrier is recaptured into the core to turn "on" again, or an opposite charge carrier is captured from traps in the surrounding

environment. Both methods have the ability to rearrange the charge surrounding the NCs, which could alter the local electric field, and induce a Stark shift in the photoluminescence peak. However, the cause of the blinking behaviour in QDs is unknown (Frantsuzov et al., 2008; Kudera, 2008).

Fluorescence quantum yield (QY), which is the ratio between the number of photons absorbed and the number of photons released, is used to indicate the efficiency of QD emission. Blinking has the effect of making it challenging to detect a QY of 1, as some QDs are in the "off" state. The quenching brought on by surface trap states can also have an impact on the QY. Both variables are dependent on the quality of the QD surface (Kudera, 2008).

It has been shown that nanocrystalline semiconductors or quantum dots (QDs) have the potential to absorb UV light and selectively emit visible light (Mumin et al., 2015). Several studies revealed temporal evolution of the PL intensity of QDs under constant illumination by UV and ambient light (Wang et al, 2004 and Komaralal, et al., 2006; Cordero, et al., 2000). It has been noted that the QD emission under constant illumination underwent temporal changes over the course of 45 minutes, with a significant initial increase in PL intensity followed by a gradual decrease. This was accompanied by a blue shift in the emission, and numerous studies have supported this (Cordero et al., 2000; Wang et al., 2004; Komaralal et al., 2006). UV radiation absorbed by these polymer films causes photochemical degradation by leading to bond cleavage and depolymerization. UV stabilizers can be used to minimize degradation, although little information is available about the incorporation thereof into a polymer matrix in a manner which provides uniform distribution, long-term stability, transparency of the films, and minimising cost, which are still major concerns (Abdel-Ghany et al., 2012).

2.2.4. Applications of QDs as sensors for pesticides and PAHs

In recent years, there has been a lot of interest in the use of QDs as fluorescence sensors. Compared to other fluorophores, such as organic dyes, they exhibit superior optical properties with high fluorescence quantum yields. Because of their distinctive optical and electronic characteristics brought about by quantum confinement effects, they may be employed as alternatives to costly and time-consuming traditional analysis procedures for the detection of pesticides, for example, as they can provide low limits of detection (LODs) (Nsibande & Forbes, 2016).

Challenges involved in the quantification of trace amounts of pollutants is detection at ppm (mg/kg), ppb (µg/kg) or ppt (ng/kg) levels (Kong et al., 2016). Main strategies to enhance analytical performance of QDs are i) improving the selectivity of QD-based photoluminescent nanosensors with methods including the use of molecularly imprinted polymers (MIPs) or ion imprinted sites, ii) improving the sensitivity of the QD-based photoluminescent nanosensors including ELISA, FRET-based photoluminescent nanosensors, antibodies, sDNA etc. for signal-on intrinsic sensitivity of FRET that is associated with small changes in the distance of the donor-acceptor pair (Kong et al., 2016).

Photoluminescent nanosensors may enable on-site, dynamic, and real-time analysis. When compared to traditional analytical equipment used for monitoring, fluorescence sensors do not have the high reagent consumption, high expenses, or lengthy analysis durations and fulfil the analytical demands of miniaturization and practicality (Kong et al., 2016). The PL characteristics of colloidal semiconductor NCs/QDs have led to the development of photoluminescent nanosensors for the detection of trace levels of target analytes. Since the tunability of their PL emission bands depends on the NC size and composition, which is determined by their atomic groups II-IV, III-V, IV-VI, e.g. CdSe, CdTe, InP, PbS, CdSe/ZnS, multiplex, high throughput detection where simultaneous signals are detected from multiple QDs, is still difficult as there is co-excitation of multiple QD emission wavelengths by the use of a single excitation wavelength (Kong et al., 2016).

QD fluorescence has been shown to detect pesticide concentrations far below regulatory limits (Nsibande & Forbes, 2016). Most QD sensing involves energy transfer between the QD fluorophore and analyte, resulting in Förster resonance energy transfer (FRET). Typically, the QD absorbs the energy, which is subsequently transmitted to a neighbouring acceptor species through dipole-dipole interactions. The efficiency of this non-radiative energy transfer depends on (i) the distance between the FRET pair, (ii) the arrangement and orientations of the FRET pair, (iii) the spectral overlap of the donor emission and acceptor absorption and (iv) if the fluorescence lifetime of the donor is long enough to enable the FRET mechanism (Guo et al., 2014; Yang et al., 2010). The broad absorption spectra and high QYs of QDs make them suitable for FRET mechanism sensors, and FRET is observed where there is a decrease in the fluorescence of the QD donor molecules while the fluorescence of the acceptor molecule increases (Nsibande & Forbes, 2016). Donor-acceptor pairs of heterogenous donor QDs, such as CdSe, CdTe, and commercial QDs with specific

ligands, have been found to lessen matrix effects and increase sensitivity in signal-off mode (Kong et al., 2016).

FRET-based donors as signalling probes have been reported which consisted of thioglycolic acid-(TGA) capped CdTe QDs and cysteamine-stabilized AuNPs (CS-AuNPs) which formed electrostatic interactions leading to quenching of the fluorescence intensity of TGA-CdTe-QDs, but in the presence of the glyphosphate pesticide, the negatively charged glyphosphate binds to the positive charged CS-AuNPs, aggregating the CS-AuNPs which results in the fluorescence recovery of the quenched QDs. This provided a sensitive, selective fluorometric assay to detect glyphosphate with a linear response in the range of 0.02-2.0 ppb (µg/kg) glyphosphate with a LOD of 9.8 ppt (ng/kg), which was appropriate for on-site rapid detection of trace glyphosphate levels (Guo et al., 2014).

Organophosphate pesticides are highly toxic and have great potential to cause neurological disorders in humans. There are many conventional methods to detect them, but portable sensors are required for routine analysis. Fluorescence sensors, MIP based sensors, electrochemical sensors and biosensors are alternative techniques that have been reviewed (Kumar et al., 2015). Optical chemosensing techniques that are based on functional materials/nanomaterials have been identified as alternatives. Cyclodextrin molecules have also been used as a fluorescence sensor for parathion, malathion, atrazine, linadane, imidacloprid, and simazine pesticides (Delattre et al., 2009). The use of nanomaterials with dual transductor properties have been proposed as next generation organophosphate pesticides sensors with minimized false positives and enabling *in-situ* validation of results (Kumar et al., 2015).

The organophosphorous pesticide chlorpyrifos has been detected using surface coordinated FRET of CdTe QDs with a ligand replacement “turn-on” mechanism. When dithizone coordinates with the CdTe QDs in basic media, the green fluorescence is quenched. After the addition of organophosphorothioate pesticides like chlorpyrifos, the fluorescence is “turned-on”. This occurs because the dithizone coordinated CdTe QDs are replaced by hydrolysate of the organophosphorothioate (Zhang et al., 2010). A highly sensitive biosensor was developed for the detection of organophosphorous pesticides (OPs), using CdTe QDs integrated with acetylcholinesterase and it was assembled with the layer-by-layer (LbL) technique onto quartz or glass (using the Langmuir method). The LOD was 1.05×10^{-11} M and 4.47×10^{-12} M for paraoxon and parathion respectively, as tested in samples of vegetables and fruit (Zheng et al., 2011).

The organochlorine pesticide dicofol was selectively detected over dimethoate and was also detected in a mixture of pesticides with a fluorescent chemosensor that was developed by using glutathione-coated CdS nanoparticles. A LOD of 55 ± 11 ppb was found. Of the many pesticides that were tested, only dicofol was able to increase the fluorescence intensity of the GSH-NPs. Aggregation occurred between the NPs in the presence of dicofol (Walia & Acharya, 2014).

A class of fluorescent nanoparticles, namely carbon quantum dots (graphene quantum dots, polymer dots and carbon nanodots), are popular in fluorescence sensing. Their advantages include excellent biocompatibility, low toxicity and resistance to photobleaching, but drawbacks are lower quantum yields compared to other semiconductor QDs, however co-doping with sulphur and nitrogen atoms produces high quantum yield carbon dots (Nsibande & Forbes, 2016). These QDs show excellent potential for various applications in fields of high throughput determination of various trace contaminants (Kong et al., 2016). They have also been incorporated in polymer matrices, polymeric gels and MIPs to form polymeric nanocomposite films (Lin et al., 2014; Kausar, 2019). A novel multifunctional composite, magnetic silica beads/graphene quantum dots/molecularly imprinted polypyrrole (mSGP) was synthesized by using tributyltin, a toxic phenolic pesticide compound as the target analyte. It was able to successfully capture and signal the analyte, and the quenching of GQD photoluminescence was used to investigate the presence of the analyte. In water and seawater, the LOD was 12.78 and 42.56 ppb, respectively (Zor et al., 2015).

Graphene QDs have been used as a fluorescence sensor to determine various concentrations of phenanthrene in water, where interactions demonstrated a linear response across 1-5 × 10^{-7} mol/L with a LOD of 2.5 × 10^{-8} mol/L when the sensor solution contained 0.5 ppm (mg/L) QDs (Montaseri, 2018). QD-graphene conjugate systems for fluorescence detection of PAHs have also been produced, as have L-cysteine capped CdSeTe/ZnSe/ZnS QDs which were conjugated to graphene oxide and employed as a nanocomposite to detect PAHs in aqueous solutions. This showed linear fluorescence enhancement as PAH concentrations increased. Among the PAHs studied were phenanthrene, anthracene, pyrene, and naphthalene, with phenanthrene showing the most substantial fluorescence enhancement (Nsibande et al., 2019).

2.3. Thin films

2.3.1. Introduction to immobilization

Many fluorescence sensor systems are solution-based probes, which have the disadvantage of not being able to be recovered from the solution after sensing, thus only have a single use. Other difficulties include storage and usage for in-field sensing, as well as degradation and instablility. These limitations can be overcome by incorporating the QD probes into or onto solid materials which make them easier to handle, increases stability, portability, and may improve shelf life and reusability (Nsibande & Forbes, 2016).

Polyethylene terephthalate (PET), polyethylene naphthalate (PEN), polyimide (PI), and polydimethylsiloxane (PDMS) are examples of synthetic substrate polymers, which may be used to create flexible substrates for sensing (Xu et al., 2019; Nsibande & Forbes, 2016).The ideal composite for fluorescence-based applications would retain the original surface chemistry of the quantum dots, while also providing appropriate electronic passivation to prevent photoexcited charges from being ionized into the matrix (Todescato et al., 2012). Choosing the right matrix is crucial to achieving strong photoluminescence (PL).

Synthetic polymers are employed to create nanocomposite materials for optical applications, since the majority of these polymers are transparent in the visible electromagnetic spectrum. With the correct compatibility, the polymer material matrix increases the mechanical and chemical stability of the nanocomposite material and inhibits agglomeration of the QDs. Challenges arise from poor compatibility between nanoparticles and polymers and the apparent degradation of optical and electronical features when the particles are incorporated in the solid matrix. The ability of the QDs to maintain their PL characteristics following functionalization determines the efficiency of the combination of the polymers and NCs. Since there is no ligand exchange, the polymeric coatings that are produced on the surface of the QDs are not expected to alter the optical characteristics of the QDs (Tomczak et al., 2009). A polymer nanocomposite comprised of QDs embedded in a polymer matrix is often utilized in applications to shield QDs from harsh conditions and environments (Peng et al, 1997; Kim et al, 2012; Farmer, 2001; Yoon et al., 2020).

Silicone-based polymers are commonly used because of their excellent visible light transmittance, thermal stability and light-extraction efficacy (Jun et al, 2013; Woo et al, 2013; Xie et al, 2018). PDMS behaves like

a solvent, as molecules can easily diffuse through this sorbent material and reach the embedded QDs, enabling interactions and facilitating applications such as sensing or analysis (Mayer, 2000). Although the aggregation of QDs and the high curing temperatures make it challenging to produce highly transparent and luminescent nanocomposites when silicone-based polymers are employed as the matrix (Yoon et al., 2020).

The inclination of nanoparticles NPs to aggregate is an inherent restriction that limits their use. One method to prevent this, is to add stabilizers to the surface of the nanomaterials, which may modify their properties. QD characteristics may completely differ from those of single nanoparticles after they have been arranged into organized nanostructures. Nanoparticle assembly into ordered nanostructures can be done by utilizing polymerizable surfactants to create covalent bonds between the QD surface and matrix which will also enhance QD stability but the most simplistic solution to add QDs to polymers is to combine the polymer with already produced semiconductor QDs and utilize popular film deposition techniques including spin coating, Langmuir-Blodgett deposition, and casting (Tomczak et al., 2009; Xu et al., 2019; Wolf et al., 2018). QDs may also be immobilized by placing them on a macroscopic support surface.

When immobilizing QDs into polymers, it is important to ensure that the surface capping ligand on the QDs is compatible with the polymer it is immobilized into, as QD agglomerations which can easily be identified with the naked eye have been observed when the interaction between the two is not favorable (Tao et al., 2013). The ideal polymer is one that does not cause QDs to settle out, leaving clear resin on top, but rather where the QDs are well distributed in the matrix, as aggregation of QDs in a polymer matrix is often followed by significant loss of optical properties due to light scattering by QD aggregates and luminescence quenching via Förster resonance energy transfer (FRET) between neighbouring QDs (Fan et al., 2016; da Silva et al., 2016; Chen et al., 2018). Moreover, the high curing temperature of silicone polymers might harm the QD surface by detaching surface ligands and forming trap states, thus lowering the quantum yield (QY) of individual QDs (Wang et al., 2009; Song et al., 2014).

Numerous research studies have been performed to increase the dispersion of QDs inside the silicone matrix and to produce transparent films without QD aggregations (Hrma et al., 2017; Chitara et al., 2008; Cheng et al., 2010). Surface ligands on QDs, for example, were substituted with ligands that were more compatible with the matrix. Previously, QD dispersion in a polydimethylsiloxane (PDMS) matrix was

improved by altering the surface of the QDs with hydrophobic ligands containing a thiol anchoring group, but the improvement in quantum efficiency of the nanocomposites was not significant (Hrma et al., 2017).

A transparent QD/PDMS nanocomposite was formed utilizing bimodal PDMS-grafted QDs. Firstly, the concentration of QDs in the nanocomposite used was low (<1 wt%), and the QY of the PDMS-grafted QDs dramatically dropped (50%) following ligand exchange. The ligand exchange process had a negative effect on the surface passivation of the QDs, resulting in a decrease in QY. To address this issue, amphiphilic polymer encapsulation of QDs was developed (Cheng et al., 2010; Chen et al., 1998; Zhen et al., 2006). To change the surface, an amphiphilic polymer with both hydrophobic and hydrophilic groups was applied instead of exchanging ligands on the QD surface. The hydrophobic component of the polymer intercalated with the surface ligands of the QDs through hydrophobic contact, preserving the original surface ligands and their QY even after surface modification. However, most research on QD modification using amphiphilic polymers has concentrated on aqueous dispersion of QDs for biological purposes (Chen et al., 1998; Zhen et al, 2006).

QDs have also been modified using an amphiphilic polymer of polystyrene-co-maleic anhydride (PSMA) to encapsulate the QDs through hydrophobic interactions. The PSMA-modified QDs were then crosslinked with aminopropyl-terminated polydimethylsiloxane to form a nanocomposite film. This increased the compatibility of the QDs with the PDMS matrix as well as the dispersion of the QDs, resulting in highly luminescent and transparent QD/PDMS nanocomposite films (Yoon et al., 2020).

Using oligomer phosphine (OP) ligands functionalized with methyl methacrylate (MMA), allowed for QDs to be successfully encapsulated in polystyrene microspheres (Sheng et al., 2006). The QDs did not leach out of the beads even after being sonicated at high frequencies, undergoing solvent exchange, and being stored for long periods of time, which makes the beads ideal for use in harsh environments. Because of the protection provided by the OP ligands, the implanted QDs retained their optical properties, and nearly all QDs were integrated into the PSMS at low concentrations; however, at higher concentrations (over 0.56 nmol), free QDs were found in the supernatant (Sheng et al., 2006).Attempts to encapsulate QDs at high concentrations still results in aggregation, and as the QD concentration increases, the number of nucleation sites increases and the size of the spheres decreases until the concentration inhibits the formation of QD/PSMS (Sheng et al., 2006).

Other polymers that have been used to produce QD thin films include polymethyl methacrylate (PMMA), polyvinyl alcohol (PVA), polyvinylpyrrolidone (PVP) (Suriyaprakash & Qiao, 2018; Moura et al., 2016). Semi-transparent nanocomposites films made of nanocrystals of different sizes in PMMA were created using a film deposition approach similar to the Langmuir-Blodgett technique. To begin, the PMMA chunks were sonicated in 5 wt% toluene. Following that, CdSe nanocrystals of a certain size (2.8 nm) were placed in the PMMA solution and sonicated for a short time to ensure uniform dispersion of the nanocrystals in the PMMA solution. A continuous layer of the composite was formed by drop casting the sonicated solution of nanocrystals in PMMA over the water surface (Suriyaprakash & Qiao, 2018).

The use of tailored hydrogels has been evaluated for use as biosensors. Emerging conductive hydrogels were produced with conducting additives like graphene, conducting polymers and NCs that were added for sensor performance. Numerous materials including polymers, biocompatible materials, inorganic and conductive materials can be used as hydrogels. Polyacrylamide, polyacrylic acid (PAA), polyethylene glycol (PEG) and polyhydroxyethylmethacrylate have been used for the production of hydrogels (Bae et al., 2020).

To detect cyanide, polydisubstituted acetylene (PDSA) was employed as a "turn-on" fluorescence sensor with intense fluorescence because of the dissolution of gold nanoparticles, where Au nanoparticles were used to hybridize imidazole-functionalized PDSAs. The coordination of these resulted in the fluorescence being quenched. The addition of cyanide reduced the coordination and activated the fluorescence sensor, causing enhancement (Lou et al., 2012; Wang et al., 2018). In another case, pyridine moieties could coordinate with Cu^{2+} cations, suppressing fluorescence emission, and when S^{2-} anion was introduced, fluorescence emission was "turned on" due to S^{2-} anion interacting with Cu^{2+} cations. With a sensitivity of 5×10^{-7} mol/L, this sensor detects either cation or anion (Zhang et al., 2011; Wang et al., 2018).

Carbon dots (CDs) have been used in polymer films where they were imbedded into non-luminescent, transparent agarose gel or polymer films. CDs were embedded into five different polymers, polystyrene, PMMA, polyvinyl pyrrolidone, PEG, and PVA. This fabricated solid CD/polymer composite films that converted UV light to green, yellow, orange, and red colours, respectively. This showed the same CDs emitted different colours when mixed with different polymers under the same excitation wavelength. It is also shown that by varying the thickness of gels with the same CDs, the emission wavelength can be altered (from blue to red) under a single excitation (Wang et al., 2014; Shamsipur et al., 2017).

Requirements for perfect optical properties such as a broad absorption spectrum, narrow emission spectra and large Stokes shift are still some remaining challenges with CDs. Thus, they are not yet applicable for multiple fluorescence studies that allow simultaneous detection of dissimilar photoluminescent labels with narrow and non-overlapping emission peaks with use of a single excitation wavelength that is a shorter wavelength than the emission peak wavelength. Most reported CDs were obtained by chance and not by design (Shamsipur et al., 2017).

Sulphur-doped graphene quantum dots (S-GQD) with green fluorescence properties were produced and integrated into PVA. Sulphur doping increased the intensity, lifespan, and QY of the QDs. This allowed for the development of a versatile solid-state fluorescence system. The LOD of carbofuran pesticide in solution and immobilized into the thin film was 0.45 ppb and 60 ppb respectively, while thiram in solution and immobilized into the thin film was 1.6 ppb and 210 ppb respectively. The film effectively detected carbofuran in actual samples with a sensitivity in the ppb range. The introduction of a flexible PVA polymer improves the mechanical and chemical stabilities of the GQDs. By minimizing agglomeration, the polymer may also help GQDs maintain their emission characteristics (Nair et al., 2020).

2.3.2. Immobilization of QDs in polydimethylsiloxane

Polydimethylsiloxane (PDMS) is a transparent, biocompatible, thermally stable, non-toxic, chemically inert, oxygen permeable and hydrophobic elastomer that has a lower cost than silicon, and is easy to handle. It is formed by the crosslinking of long chain monomers that contain a siloxane backbone (Krishnan, 2007; Mata et al., 2005).

The elasticity of the PDMS can be adjusted by altering the curing agent ratio or temperature, and by adding filler materials, the hydrophobicity of PDMS can be varied. Other materials and particles can also be incorporated into PDMS (Xu et al., 2019; Wolf et al., 2018). The chemical formula for PDMS is showed in Figure 2-6.

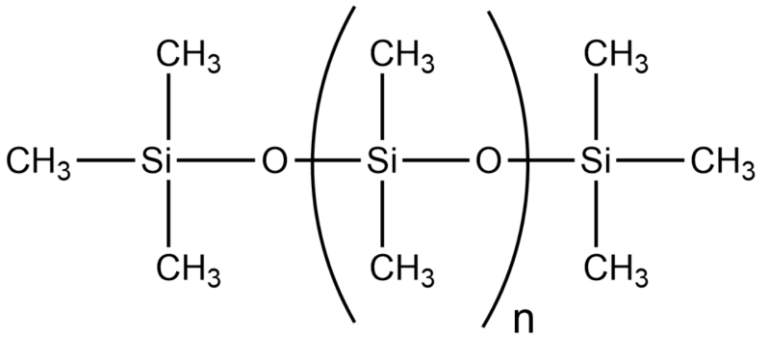

Figure 2-6: Chemical formula of PDMS.

Several of the unique properties of PDMS may be due to the heteroatom backbone, which is partially ionic, has a high Si-O bond energy, a low intermolecular force between the methyl groups, and has a highly flexible backbone (Kim et al., 2008).

2.3.3. Spin coating methods to produce thin films

Spin coating is a process that has been used for several decades for the preparation of uniform thin and ultrathin films on flat substrates. A spin coater is used for this technique, where the process starts with a deposit of a fluid resin to the middle of a substrate which is secured onto the platform of a spin coater by a vacuum. The spinning involves centrifugal forces which leads to the spreading of the resin over the substrate, leaving a thin film on the substrate after the excess is spread over the substrate edge. The thin film properties and thickness depends on the nature of the resin used (drying rate, surface tension, viscosity, percent solids, etc.) as well as the spin process parameters (acceleration, final rotational speed, etc.). A very important factor in spin coating is repeatability, where small changes in the spin process could lead to drastic variations in the films produced. The process is easy to control and has fast production rates (Tyona, 2013).

To dispense the resin, it is either deposited onto the substrate before spinning (static dispensing) or while it is already spinning at a slow speed (dynamic dispensing). The spin speed and time of spinning will ultimately define the thickness of the film (Krishnan, 2007). Edge effects can also be seen where droplets form around the edge of the substrate. After spinning the resin, heating of the film is required (Tyona,

2013; Sahu et al., 2009). This cures the polymer into a solid elastomeric film and after the PDMS film is cured with heat onto the substrate, it can be removed from the substrate by peeling, but tearing of the film during this step is common (Krishnan, 2007).

Film thickness is ultimately a balance between the force that is applied to shear the fluid resin radially outward to the edge of the substrate and the drying rate of the resin which influences its viscosity (Tyona, 2013). Acceleration towards the final spin speed is also very important as it can affect the film properties. Sometimes, up to 50% of solvents which are present in the resin could be lost within the first few seconds due to evaporation. The acceleration provides a twisting force in the resin which helps with dispersion of the fluid.

The rate at which the film dries is also influenced by temperature and humidity (Tyona, 2013). During the spin process, airflow and turbulence should be minimized or maintained at a comparable rate. Therefore, it is advantageous that spin coaters are designed in the form of a “closed bowl”, with an exhaust top that only permits very little exhaust throughout the procedure. As a result, the design helps to slow down the drying of the resin, reduces the effects of changes in ambient humidity, and reduces fluctuations in air flow around the substrate. It is possible to maintain a consistent resin viscosity across the substrate by delaying the drying process. In order to avail a suitable PDMS thin film production method, it must provide a precise and homogeneous thickness throughout the thin film, and repeatability across several production runs (Krishnan, 2007).

There are a few spin coating-related common issues that should be eliminated and looked out for. Comets are rather substantial solid particles which alter the typical flow patterns of the fluid resin. Working in more hygienic settings and filtering the coating solutions which contain a range of different particles used might lessen this effect. Striations are radially oriented lines in the film that are believed to be the result of evaporation-driven surface tension effects (Tyona, 2013).

Water molecules may play a role in the chemistry of the film, which can affect the sensitivity of the film to the environment and induce excessive striation formation or induce microcracking after drying. When the fluid resin creates a small "bead" that remains attached to the edge of the substrate due to surface tension, the edges of the film will be thicker as a consequence. As the substrate size increases, these disadvantages of spin coating become increasingly significant (Tyona, 2013; Sahu et al., 2009). An advantage of spin

coating of films is the flexibility in the preparation of different thickness films, with a quick turnaround time (Krishnan, 2007).

Polydimethylsiloxane pre-polymer was mixed with different amounts of cross-linker and was spin coated to produce films with thicknesses ranging from 171 to 308 µm at 200 revolutions per min (rpm) (Mata et al., 2005). The surface and structural properties of the different PDMS films were analysed to quantify the effect of different amounts of cross-linker used, and long-term surface hydrophobicity was also tested. The PDMS was analysed with gravimetry, tensile testing, scanning electron microscopy, X-ray photoelectron spectroscopy, as well as Fourier transform infrared spectroscopy, and it was shown that increased amounts of cross-linker agent in the PDMS formulas decreased the thickness of the films (Mata et al., 2005).

To see whether mechanical properties can be altered without surface chemistry variations, PDMS films were immersed in buffered hydrofluoric and nitric acids (Mata et al., 2005). This created micro-texture distortion, where sulfuric and unbuffered hydrofluoric acid caused a total destruction in the micro-textures. These chemical immersions did not alter the PDMS surface hydrophobicity significantly. The recommended formulation was resistant to the majority of the tested chemicals and this study concluded that mechanical properties can be altered without surface chemistry variations (Mata et al., 2005).

In our research group, CdSeTe/ZnS and graphene QDs were immobilized into PDMS by means of a spin coater, producing red and blue fluorescing films (Montaseri et al., 2018). A de-gassing setup was used to prevent air bubble defects. It was found that the emission peak of CdSeTe/ZnS QDs at 580 nm was redshifted slightly (to 594 nm) when the QDs were embedded into the PDMS. It could be that the PDMS had a passivating effect on the QDs thus affecting their surface states. The QD@PDMS film had a strong fluorescence as observed under a UV light, which showed the potential use of the material as a fluorescence sensor, which was explored further in this study.

2.3.4. Other methods to produce thin films

There are other approaches for manufacturing QD thin films. ZnCdSe QDs films were used to detect pesticides in water, after drop-casting a colloidal ZnCdSe QD solution (synthesized via wet-chemistry) onto the glass probe surface of a spectrometer as seen in Figure 2-7, and was allowed to dry and form a ZnCdSe QD film. An excitation light source (laser diode) produced light emission from the probe surface. It was seen

that the PL intensity was quenched by the presence of three pesticides namely bacillus thuringiensis, carbaryl and acibenzolar, respectively. The degree of quenching was directly proportional to the concentration of the pesticide molecules (Bakar et al., 2011).

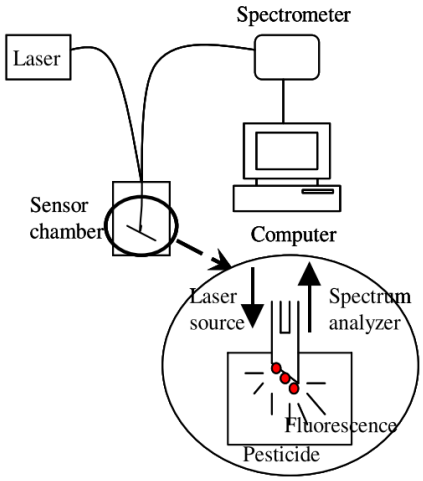

Figure 2-7: Optical sensing system and setup for the detection of pesticides (Bakar et al., 2011).

Fluorescence sensors have also been developed by integrating QDs into chemically inert and optically transparent silica nanoparticles, with reverse microemulsion being the most popular technique. This method improved chemical stability and decreased leaching, thereby lowering the potential toxicity of the QDs (Hu & Gao, 2010). Photobleaching effects were also reduced and silica nanoparticles are susceptible to surface modifications enabling functionalization with receptors for selective detection of many pesticide analytes.

Various other techniques are used to produce thin films including self-assembled monolayers (SAMs) for single layered films, and Langmuir-Blodgett (LB) techniques for multilayers. SAMs require hydrophilic particles where the LB technique can be used for hydrophobic or hydrophilic particles. Hydrophobic particles in organic solvents can typically be directly spread at the air-water (A/W) interface where lamellar and uniform multilayers can be formed (Gole et al., 2008). The appealing feature of these Langmuir films is exact control over film thickness and intrinsic control of the internal layer structure on a molecular level (Hussain & Bhattacharjee, 2009). To form a Langmuir monolayer, the substance needs to be water insoluble and soluble in organic solvents such as chloroform or benzene to ensure it does not mix with the subphase

but rather spreads across its surface. Materials that are compatible need to be amphiphiles, which consist of a hydrophilic "head" part as well as a hydrophobic "tail" part. The head will typically have a strong dipole moment with chemical groups that are capable of hydrogen bonding like -OOH, -COOH, $-NH_2$, etc. These groups will bind to the water surface and the tail will typically be a long aliphatic chain which will point away from the water surface (Figure 2-8). Once these molecules arrive at the surface, the high energy interface is lowered by hydrophilic-hydrophilic and hydrophobic-hydrophobic interfaces as all hydrophobic tails point towards the air. This ensures the molecules are anchored, with no tendency to form a layer thicker than one molecule (Hussain & Bhattacharjee, 2009).

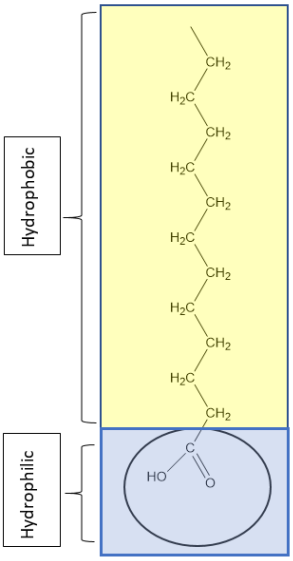

Figure 2-8: General chemical structure of LB thin film with carboxylic acid head and arbitrary tail (modified from Hussain & Bhattacharjee, 2009).

In Figure 2-9 the general schematic for a LB trough can be seen, the first requirement is a water subphase container called a Langmuir trough. All materials in contact with the water subphase should be inert and unaffected by organic solvents (Petty, 1996). The Wilhelmy plate monitors and measures the surface pressure through a microbalance that is interfaced with a computer. The barrier movement is controlled by the computer which controls the surface pressure (π), allowing the A/W interface to expand and

compress the surface film. The Langmuir approach may be used to produce a membrane by collecting molecules that are scattered on the surface of the water as the barrier moves. If the area per molecule is sufficiently large, the surfactant molecules do not interact, and as the monolayer is compressed, the pressure increases and the surface film behaves like a liquid. If the area is compressed further, the film is close-packed, has a low compressibility, and behaves like a 2D solid. If the compression is too severe, the surface layer collapses and the surface pressure falls (Hussain & Bhattacharjee, 2009).

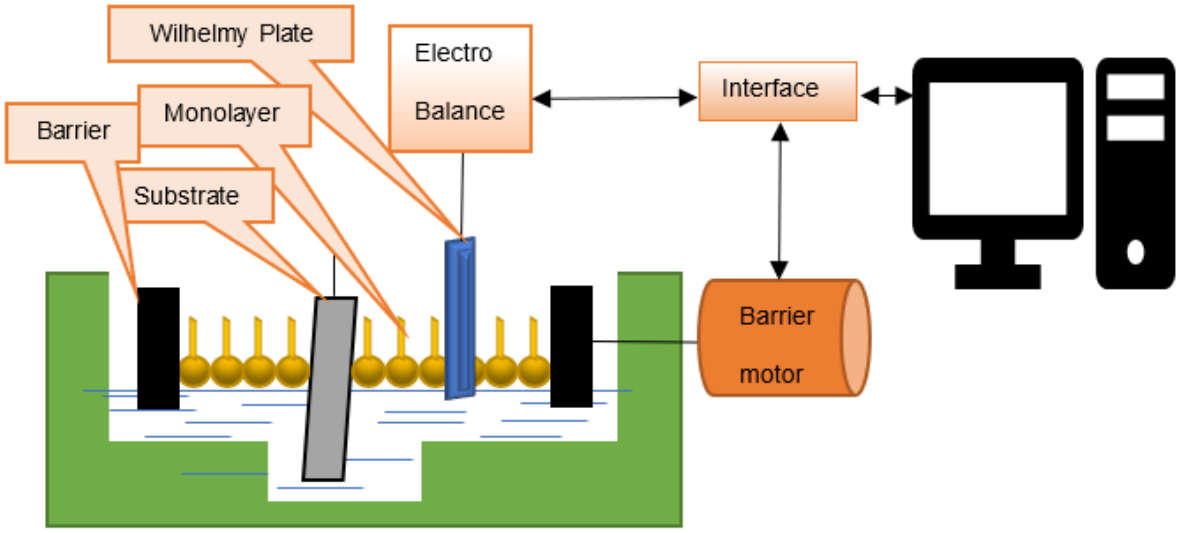

Figure 2-9: Schematic Langmuir-Blodgett trough (modified from Hussain & Bhattacharjee, 2009).

It is most common when the substrate is hydrophilic that the first monolayer is transferred to the substrate when it is raised out of the water subphase with the hydrophilic heads pointing towards the substrate, this is called the Y-type deposition and can be seen in Figure 2-10 where (a) a Langmuir monolayer formed on top of the water subphase, (b) the first monolayer is deposited onto the hydrophilic substrate as it rises through the subphase, (c) a new monolayer is deposited in a tail-to-tail pattern and (d) a new monolayer is deposited on the substrate in a head-to-head pattern.

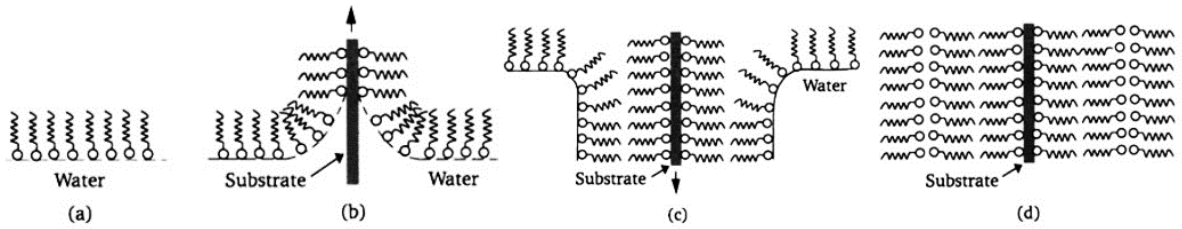

Figure 2-10: Y-type Langmuir-Blodgett film deposition (Petty, 1996).

A monolayer is deposited on top of this layer with each monolayer-air interface crossing. X-type deposition is when the monolayer is deposited on the downstroke only and Z-type deposition is when the transfer is on the upstroke only (Petty, 1996). Examples of these are shown in Figure 2-11.

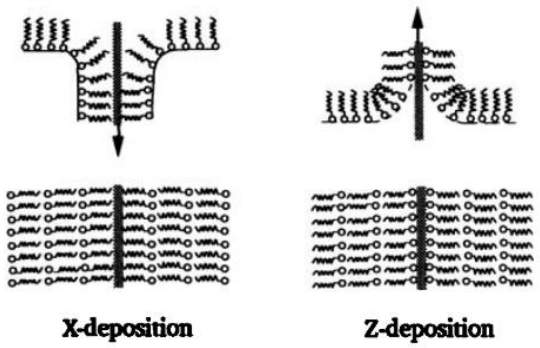

Figure 2-11: X-and-Z type deposition of monolayers onto the substrates (Petty, 1996). On the left, X-type monolayer deposition onto the hydrophobic substrate is shown with deposition only on the downstroke. On the right, Z-type monolayer deposition onto the hydrophilic substrate is shown with deposition only on the upstroke.

LB techniques can assemble a close-packed nanoparticle monolayer on an arbitrarily chosen substrate that gives a surface free of microscopic defects spanning over macroscopic dimensions (Santhanam et al., 2003). CdSe/ZnS QDs were prepared and capped with TOPO ligands, which have hydrophobic long-chain moieties. The Langmuir film method was used to create a stable CdSe/ZnS QD monolayer at the A/W interface (Ji et al., 2005). The substrates utilized were quartz slides, made hydrophobic by immersion in a cyclohexane solution of octadecyltrichlorosilane (OTS) (Ji et al., 2005).

The photoluminescence of CdSe/ZnS QDs in different configurations on substrates have also been studied by using the LbL Langmuir film method. The first, where QDs were directly prepared on solid surfaces (glass, silicon, PDMS and metals) on conductive metal surfaces (copper and gold), complete suppression of photoluminescence was observed indicating a strong quenching effect. Fluorophores located within 5-10 nm from the metal surface are thus affected by the presence of conducting and semiconducting surfaces in close proximity (Duijs et al., 2001; Wang et al., 2004; Borges et al., 2005). It was seen that there was a lower emission when the QD-LbL film was on silicon and PDMS substrates, compared to a glass substrate and was presumably caused by different reflective properties (Zimnitsky et al., 2007). What was interesting to see was that when a LbL film was placed on top of the silicon surface beneath the QDs, as the thickness of the polymer increased, the PL intensity increased. When there was a polymer coated above the QD layer, wrapping the QDs, it was seen that there was an increased photo-emission intensity, which was not expected as the distance between the silicon surface and the QD remained the same, which suggests that the interaction between the polymer matrix and the QDs is responsible for this effect.

A “floating on water” method has also been used to produce PDMS thin films of few micrometers thick without the use of special equipment. Films of <10 µm were produced by placing a liquid PDMS solution on the surface of water by thinly spreading the solution using a casting knife (this can be carried out manually or with a membrane-casting machine). The water solution was inside a petri dish which was placed on a hot plate and then heated for the film to anneal. There was no risk of tearing or breaking of the films as the membrane floated on the water and could be removed easily (Kim et al., 2019).

Physical vapor deposition (PVD) is a technique where material goes from a condensed solid phase (as a precursor), to a vapor phase and then back to the condensed phase (deposited as thin films). Common techniques include sputtering, laser surface alloying, ion plating and ion implantation. An example of this is pulsed laser deposition, which is a thin film deposition technique inside a vacuum chamber that uses high-energy laser pulses to vaporize the surface of a solid target and condense the vapor onto a substrate to form thin films. This has the advantage of being able to produce films in an ultra-high vacuum chamber, under a wide range of ambient temperatures (Selvakumar, 2012). The biggest advantage is the stoichiometric removal of atoms (without discrimination) from the target material, resulting in the evaporation and ablation of atoms which are collected on the substrate. This is done because of the fast, transient nature of the ablation process and the high laser fluence, creating surface temperatures of

approximately 5000 K within few nanoseconds. Film uniformity is one of the biggest challenges with this method and another challenge is the deposition of larger particles up to 10 µm in size as they form molten droplets being ejected during the ablation process (Selvakumar, 2012).

Vaporized material is deposited and coats a substate atom by atom inside a vacuum chamber. The thickness varies from atomically thin to a few millimeters. Alternate layers of different materials can be deposited using this technique. Vapors for deposition can be produced by thermal evaporation, sputtering or arc vaporization (Alf et al., 2010).

Chemical vapor deposition (CVD) has been used as a polymer thin-film deposition technique. With CVD, a precursor gas (or gases) is introduced inside an enclosed chamber with preheated substrates. The chemical reactions take place close to the heated substrates leading to thin film deposition of the desired material on the surface of the substrate. Although, ink-jet printing, and dip-coating are methods used to produce thin films which are employed because of ease of scaling up, and low costs of the overall process, these alternative methods which can be used for the deposition of polymers only achieves partial retention of functional groups (Scheltjens et al., 2017; Ozaydin-Ince et al., 2012).

2.4. Techniques to characterize QDs and thin films

To study processes involved at molecular level, spectroscopic methods, thermal methods, gravimetry, microscopy, mechanical tests and chemical analysis can be utilized to provide valuable information. Structural characterization of films can be done by using SEM, TEM and X-Ray diffraction, scanning-probe microscopes, and AFM (Ohring, 2002). Chemical characterization can be done with Auger electron spectroscopy (AES), X-ray photoelectron spectroscopy (XPS), secondary ion mass spectrometry (SIMS) and energy-dispersive X-ray spectroscopy (EDS) for surface and near surface atoms and compounds in the films (Ohring, 2002).

Ultraviolet-visible absorption spectroscopy (UV-Vis) may be used to measure how much a chemical substance absorbs light, allowing for rapid and simple analysis. To avoid interfering with the quantitative analysis of the sample, the ideal UV-Vis solvents should be transparent and have no absorption at the measurement wavelength of the substance

Absorption spectra of quantum dots reveal bands at specific wavelengths, indicating where the sample absorbed radiation within the UV light range. The wavelength range where the radiation is absorbed corresponds to various colors within the visible light spectrum. Zhang et al. (2016) demonstrated that the size distribution of QDs is a determining factor in the position and intensities of these distinctive peaks. While the synthetic route plays a role in determining the size distribution of QDs, it is not the only factor influencing it, as other variables may also come into play. According to Ye et al. (2008), the spectroscopic characterization of core/shell particles revealed that as the shell thickness increased, the intensity of UV absorbance also increased, and the reflectance shifted towards the higher wavelength region (Ye et al., 2008). UV–vis spectrophotometry has been used to examine the relationship between precursor concentrations and the average size of QDs (Dilag et al., 2009).

UV-Vis was thus used in this study to observe the absorption wavelength of the core and C/S QDs. It was also used in combination with fluorescence spectroscopy to determine the PLQY of the C/S QDs by dispersing the C/S QDs in chloroform and using rhodamine 6G as a reference standard which was dissolved in ethanol.

High resolution scanning electron microscopy analysis (HRSEM) can offer information on the morphology, topography and crystallographic nature of the materials being studied. Sample preparation is the most important step for accurate analysis, and the sample must be electrically conductive. In non-conducting samples, this is achieved by applying a very thin layer of carbon or gold to the sample surface (Girão et al., 2017). SEM is employed in cases where the thickness of a film is too small to be analyzed using an optical microscope or when the layers have low contrast, which makes it difficult to obtain adequate results through optical microscopy (Giurlani, 2020).

Energy-dispersive X-ray spectroscopy (EDS) allows for qualitative and semi-quantitative examination of samples, allowing for the identification of components. The thickness of silicon dioxide and silicon nitride thin films were measured in 2016 by Sokolov using EDS. This was achieved by varying the penetration depth of the analysis, adjusting the acceleration voltage of the beam, and correlating the thickness of the film with the substrate element signal to noise (Sokolov, 2016). Transmission electron microscopy (HRTEM) techniques provide very powerful tools to investigate nanometer scale structures in solids, especially by using high resolution transmission electron microscopy (HRTEM) (Scheerschmidt & Werner, 2002).

Fluorescence spectroscopy has been found to be a quick and accurate method to determine the size of quantum dots. The link between the fluorescence maximum position and the quantum dot size for a particular QD solution is correlated with the uniformity of the quantum dot size (Mutavdžić et al., 2011). Properties of semiconductor QDs are extremely sensitive to the processes taking place on their surface, such as ligand exchange or removal. In particular, such processes can enhance, weaken or quench the fluorescence of QDs (Galian & Scaiano, 2009; Chan & Rosenzweig, 2002).

In this study fluorescence spectroscopy was the main method of characterization. The measured fluorescence of the QDs dispersed in chloroform/immobilized in a PDMS polymer was obtained before and after interactions with organic analytes (atrazine and phenanthrene), with different solvents, as well as with an inlet river water sample to observe their effects on the fluorescence emission of the QDs.

Further, quantum dots were used in this study due to their unique optical and electronic properties, which make them attractive for a wide range of applications, including fluorescence sensing. They are stable and have excellent optical properties such as high quantum yields, narrow emission bandwidths, and tunable emission wavelengths. QDs were synthesized via the organometallic route because this method has been shown to produce more stable quantum dots with better optical properties compared to the aqueous method. The organometallic route involves the use of metal organic precursors, which are reacted in the presence of a coordinating solvent to form a colloidal solution of quantum dots. This method allows for precise control over the size and shape of the quantum dots, resulting in more uniform and reproducible samples. A ZnS shell layer was coated over the CdSeTe core to protect it from oxidation and other chemical reactions that can degrade its stability and optical properties. Additionally, the ZnS shell layer can improve the optical properties of the quantum dots by reducing surface defects and increasing their photoluminescence efficiency, as well as reducing their potential toxicity.

PDMS was used as the polymer to immobilize the quantum dots, where the PDMS film served as a matrix that held the quantum dots in place and provided mechanical stability, while also allowing for optical access to the quantum dots. The use of PDMS as the polymer for immobilizing the quantum dots is a good choice because it offers several advantages such as biocompatibility, optical transparency, and mechanical stability. These properties make it suitable for sensing applications. Spin coating was used to produce the QD@PDMS thin films as it is a cost-effective method that can produce consistent and uniform films with

controlled thicknesses. It is also a facile technique that can be implemented in a variety of laboratory settings.

Previous studies have shown that atrazine can interact with quantum dots in solution and cause quenching of the QD fluorescence, and the interaction was therefore tested with the PDMS films. However, atrazine is a polar molecule, and the PDMS polymer used in the study is hydrophobic and non-polar, which may limit the interaction between atrazine and the PDMS surface. Phenanthrene has been shown to also interact with QDs and enhancement in the QD fluorescence has been observed. Further it is a non-polar polycyclic aromatic hydrocarbon that is known to interact strongly with hydrophobic surfaces, making it a suitable molecule for testing its sensitivity towards the QD@PDMS films.

The detailed experimental methodology followed is provided in Chapter 3, followed by the presentation and discussion of the results obtained in Chapter 4.

Chapter 3: Experimental Methods

For this study, a ternary alloyed CdSeTe QD core, covered with a ZnS shell to form CdSeTe/ZnS QDs were made by hot-injection organometallic synthesis. These QDs were characterized, and QD@PDMS films were made for the stabilization and ease of use as a sensor for organic molecules in water. Films were spin coated and the spin coating parameters were optimized to yield the best reproducible thin films in terms of uniform thickness, with a good thin film preparation yield and repeatability over different production runs. The films were then tested as possible atrazine and phenanthrene fluorescence sensors. The films were also tested with an inlet water sample obtained from Rand Water and changes in fluorescence were observed for non-targeted testing. The experiments performed and the methods used to test target compounds in this regard, as well as the statistical analysis of the data are explained in this chapter.

3.1. Chemicals

Trioctylphosphine oxide (TOPO), 1-octadecene (ODE), oleic acid (OA), cadmium oxide, tellerium, zinc oxide, sulfur powder, rhodamine 6G, atrazine and phenanthrene were purchased from Sigma Aldrich (St. Louis, USA). Methanol, chloroform, acetone, ethylenediaminetetraacetic acid (EDTA) and selenium powder were purchased from Merck (Darmstadt, Germany). Isopropanol was purchased from VWR Chemicals (Darmstadt, Germany). An ultrapure Milli-Q Water System (Millipore, Bedford, USA) was used as water source (18.0 MΩ·cm at 25°C). A Sylgard 184 silicone elastomer kit was purchased from Dow Corning (Michigan, USA), which included a silicone elastomer base and curing agent. Polyacrylic acid (PAA) was purchased from Polysciences (Warrington, USA). All chemical reagents were used as received from the suppliers without any pre-treatment.

3.2. Characterization techniques

3.2.1. Fluorescence spectroscopy

Fluorescence spectra were measured using a Horiba Jobin Yvon FluoroMax-4 Spectrofluorometer (Horiba Scientific, New Jersey, USA). The QDs were dispersed in chloroform and placed in a quartz cuvette with a 1 cm path length and fluorescence was measured at a 90° angle to the incident beam. The fluorescence was generally measured using an excitation wavelength of 470 nm, with a recorded emission wavelength

range of 480-800 nm and slit widths of 5 nm. Where excitation and emission wavelengths varied from this, it is noted under the respective section. Spectra were normalized for comparison purposes.

The wavelengths and slit widths used to measure fluorescence spectra of QDs immobilized in the polydimethylsiloxane (PDMS) polymer films were varied for different experiments, but in general an excitation wavelength of 400 nm, with an emission wavelength range of 410-700 nm and slit widths of 2 nm were used, except when stated otherwise in the respective sections. The films were placed in a solid-state sample holder and fluorescence was also measured at a 90° angle to the incident beam.

3.2.2. Ultraviolet-visible absorption spectroscopy (UV-Vis)

UV-Vis spectra were recorded of liquid samples contained in a quartz cuvette with 1 cm path length in the range of 200 - 800 nm with a bandwidth of 1.0 nm using a Cary Eclipse spectrophotometer (Varian, Victoria, Australia). Chloroform was used as a blank and all QDs were dispersed in this solvent. All measurements were carried out at room temperature. In order to measure photoluminescence quantum yield (PLQY), the absorbance of the QDs was adjusted to within the range of 0.02-0.05 (Lakowicz, 1999).

3.2.3. Visual fluorescence imaging

Visual fluorescence imaging of synthesized QDs and PDMS polymer films which contained immobilized QDs was carried out using a UV lamp (Analytik Jena, USA) which was operated at 254 nm (short wavelength). This allowed for visual characterization of the fluorescence nature (colour and colour intensity) of the QD solutions and films.

3.2.4. High resolution transmission electron microscopy analysis (HRTEM)

HRTEM analysis was employed to determine the size and morphology of the synthesized QD core and core shell (C/S) QDs dispersed in chloroform (QD@chloroform). A drop of each QD@chloroform solution was placed on copper grids that had a holey carbon support film, followed by drying under ambient conditions. The grids were examined with a JEOL JEM 2100F TEM (Tokyo, Japan) operated at 200 kV. ImageJ software was used to determine the estimated particle size distribution from the HRTEM micrographs (Schneider et et al 2012).

3.2.5. Quantum yield

The relative PLQY of the core and C/S QDs were calculated using a standard sample (rhodamine 6G) which has a fixed and known fluorescence quantum yield value of 0.95 (Kubin, 1982), and was used to determine the unknown fluorescence quantum yield of the QDs according to Eq. (3-1).

$$\Phi_X = \Phi_{ST}\left(\frac{Grad_X}{Grad_{ST}}\right)\left(\frac{\eta_X^2}{\eta_{ST}^2}\right) \quad (3\text{-}1)$$

Where subscripts ST and X denote standard and unknown respectively, Φ is the fluorescence quantum yield, *Grad* is the gradient from the plot of integrated fluorescence intensity versus absorbance, and $\boldsymbol{\eta}$ is the refractive index of the solvent.

The slit widths used for fluorescence were 2 nm with an excitation wavelength of λ_{ex}= 470 nm and an emission wavelength range of λ_{em}= 480-800 nm. The slits were adjusted so that a satisfactory signal (strong enough but not saturated) was obtained when using the solution with the higher emission intensity rhodamine 6G (Fery-Forgues & Lavabre, 1999).

The concentrations were low enough to ensure absorbances were below 0.1 at the excitation wavelength of 470 nm used for fluorescence in order to minimize re-absorption effects (Dhami et al., 1995). The determination of PLQY of QDs was done in chloroform ($\boldsymbol{\eta}$= 1.44) and the standard was dissolved in ethanol ($\boldsymbol{\eta}$= 1.36) (Asfour & Dullien, 1981 and Wohlfarth, 2008).

3.2.6. High resolution scanning electron microscopy (HRSEM)

Film thicknesses were measured by means of high-resolution scanning electron microscopy (HRSEM) analysis of the films (Zeiss Ultra PLUS FEG SEM, Jena, Germany). The quantum dots immobilized in PDMS thin films (QD@PDMS) were cut using a diamond blade and etching pen to score the glass as shown in Figure 3-1. The films were then placed under liquid nitrogen for 10 min and hit with a blunt object causing breakage along these lines of structural weakness carved with the diamond blade and etching pen.

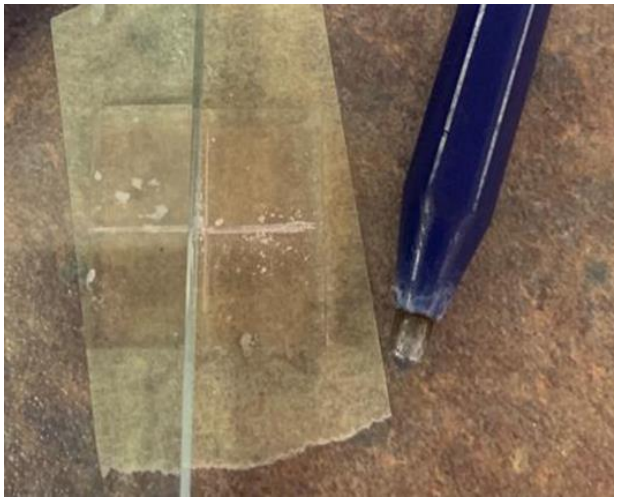

Figure 3-1: A glass ruler keeping the QD@PDMS film in place as a diamond blade pen (right) was used to make grooves across the glass surface.

The resulting pieces were then placed on a platform created by binding two metal pieces to one another with insulation tape and were then bonded to this with carbon black conductive ink as shown in Figure 3-2. It was important to rotate the films to ensure a cross section of the film was at the top where it was viewed with the SEM. The samples were coated with a very thin conductive layer of carbon that was sputtered over the sample and was then inserted into the SEM microscope in order to view the films in cross section. Analysis of the HRSEM micrographs based on magnification and instrument software in conjunction with offline analysis using ImageJ software allowed for the determination of the film thickness.

Figure 3-2: Thin films placed on a platform for viewing with a SEM microscope in cross section to determine the thickness thereof.

3.2.7. Energy-dispersive X-ray spectroscopy analysis (EDS)

To identify the elemental composition of an unknown material observed between the glass slide and the PDMS thin film, HRSEM integrated with EDS (Oxford INCAx-sight, Zeiss, Jena, Germany) was utilized (20 keV range and 150 s acquisition time).

3.3. Synthesis of quantum dots

This section describes the synthesis procedures that were followed to prepare two quantum dot batches. It also outlines the purification procedure that was followed in order to obtain crystalline hydrophobic QDs. After synthesis of the QDs, the core- and C/S QDs were characterized and compared as described in Section 3.1.

3.3.1. First batch of CdSeTe/ZnS QDs

CdSeTe/ZnS QDs were synthesized by following a method previously developed in our research group, as shown schematically in Figure 3-3 and reported in Nsibande & Forbes (2019). CdO was used as a cadmium precursor and to this, different precursors were added and reacted in a stepwise process at controlled high temperatures. Each of the precursors were separately prepared by dissolving them in TOPO and ODE as organic solvents and stirring vigorously overnight at a temperature of 40°C using a hot plate and a magnetic stirrer to ensure homogeneity. The TOPO and ODE served both as reaction solvents and surfactants to stabilize the QD nanocrystals after nucleation. To form the precursors, TOPO was added to ODE first, heated at 80°C, until it dissolved, and then Te and Se were added to form the precursors. The tellerium precursor (TOP-Te) was prepared by adding 0.46 g Te to 1.93 g TOPO in 25 mL ODE and the selenium precursor (TOP-Se) was prepared by adding 0.30 g Se to 1.94 g TOPO in 25 mL ODE. ZnO was used as a zinc precursor and was prepared by adding 0.41 g ZnO to 20 mL OA and 30 mL ODE. The sulfur precursor was prepared by adding 0.18 g S to 20 mL OA and 30 mL ODE.

The next day 1.30 g CdO was added to a 3-neck round bottom flask. The first neck of the flask contained a thermometer, which was pressed through a septum to continuously monitor the reaction temperature. A reflux condenser was attached to the second neck to prevent solvent and reactant loss at high temperatures. Argon gas was bubbled through the reaction mixture via a Pasteur pipette which was pressed through a septum in the third neck of the round bottom flask, ensuring inert reaction conditions under which all precursors were added. The thermometer and Pasteur pipette were both under the surface

of the solution but out of reach of the stirrer bar. The process was started by adding 50 mL ODE and 30 mL OA to the CdO powder to give a dark brown mixture. This mixture was stirred vigorously at a temperature of ~260-290°C, until the solution turned clear.

Thereafter, 5 mL of the TOP-Te precursor was added to the TOP-Se precursor solution while continuously purging with argon. Then, 25 mL of this TOP-Se-Te precursor mix solution was added to the clear CdO solution which immediately turned orange which indicated the initiation of the formation of the CdSeTe core through nucleation.

During synthesis, the fluorescence of the core QDs and C/S QDs were measured to indicate the growth thereof indicated by changes in the emission wavelength. The core QDs were allowed to grow and fluorescence thereof (dispersed in chloroform) was measured after 20, 40 and 60 s and at 3, 5 and 10 min of core QD growth. After 10 min, about 20 mL of the core QD solution was set aside, closed with Parafilm® M and cooled to room temperature to quench the growth of the QDs.

Then 15 mL of both the ZnO and S precursors were combined, purged with argon and poured into the remaining core QD solution. The heat was reduced to ~240°C to allow for the formation of a ZnS shell over the CdSeTe core. Fluorescence of the C/S QDs was measured at 5, 10, 20 and 40 min. When the growth slowed down and no significant additional red shifting of the fluorescence emission peak occurred, the reaction was stopped by removing it from the heat and allowing it to cool down to room temperature.

To purify the obtained QDs, the core and C/S QDs were then transferred to centrifuge tubes wherein they were washed with acetone, chloroform and methanol to remove any unreacted precursors. Chloroform was added to disperse the QDs into solution, they were then sonicated and vortexed to ensure good mixing, and the rest of the centrifuge tube was filled with a mixture of acetone and methanol to form a 1:1:1 ratio. The QDs were centrifuged and washed at 6000 rpm for 5 min and the supernatant was separated from solid QDs. This process was repeated several times until the QDs had the appearance of dispersed particles in solution, which readily settled.

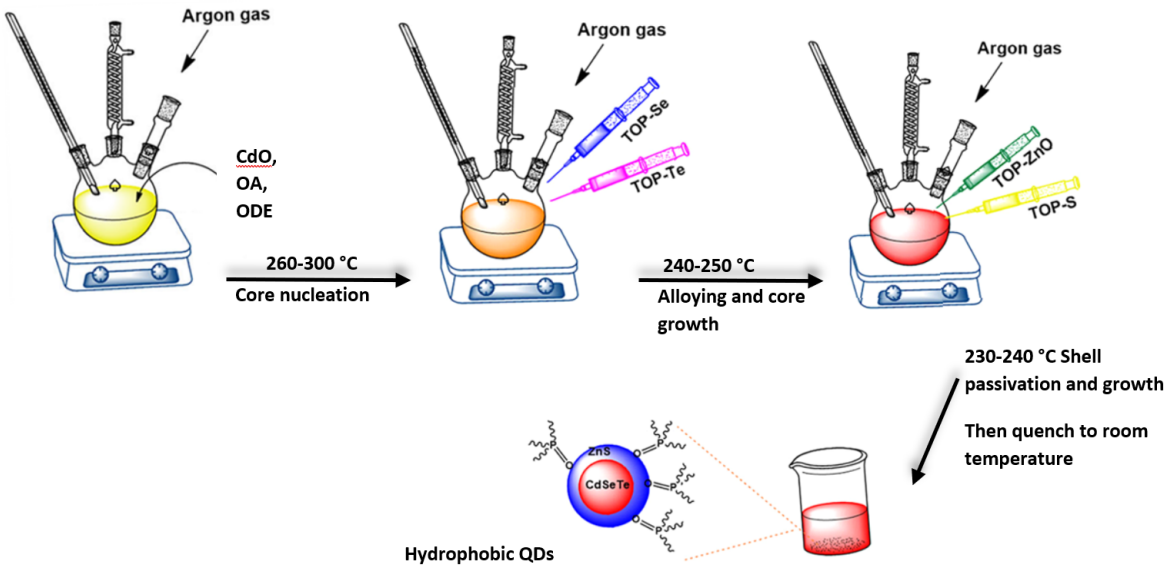

Figure 3-3: Schematic of the stepwise hot injection of organometallic precursors to synthesize CdSeTe/ZnS QDs (Nsibande & Forbes 2019).

3.3.2. Second batch of CdSeTe/ZnS QDs

The original method, as described under Section 3.3.1 was repeated but precursor quantities were reduced to decrease waste. The TOPO-Te precursor was prepared by adding 0.16 g Te to 0.68 g TOPO dissolved in 8.3 mL ODE. The TOPO-Se precursor was prepared by adding 0.30 g Se to 1.95 g TOPO dissolved in 25 mL ODE. The ZnO and S precursors were prepared separately by adding 0.137 g ZnO and 0.066 g S to both 6.6 mL OA and 10 mL ODE. For the second batch, the precursors were made during the day where they stirred at a temperature of 40^{o}C for 4 hours, as batch one had frozen during the night. Again, the TOPO was added to ODE first, heated at 80^{o}C until it dissolved, then Te and Se were added to form the precursors. After 4 hours, the method was followed as described in Section 3.3.1 until the QDs were synthesized. Then the QDs were allowed to stand in methanol overnight. The next day the QDs were transferred to centrifuge tubes and were centrifuged and washed at 6000 rpm for 5 min with chloroform: water: acetone in a 1:1:3 ratio, followed by a final wash with acetone. The QDs thus obtained were characterized as described in Section 3.1.

3.4. Sensing of atrazine using QDs in solution

Prior to immobilization of QDs in thin films, the feasibility of using the prepared QDs to detect atrazine in solution was tested. The reproducibility of the QD@chloroform solution was tested to confirm the homogeneity thereof. Thereafter, the excitation wavelength was optimized and lastly, the incubation time of atrazine with the QD@chloroform solution was optimized.

3.4.1. Optimization of reproducibility of sensing using QD@chloroform solution

A QD@chloroform solution [2×10^{-5} g/mL] was prepared and used to test the interaction of the QDs with atrazine and to investigate their reproducibility as a sensor. To three small vials, 700 µL of the prepared QD@chloroform solution was added and the fluorescence in the absence of analyte (F_0) was measured. Thereafter, 350 µL of atrazine analyte dissolved in ethanol [6×10^{-7} M] was added to each vial containing the QD@chloroform solution. The solution was mixed with a micropipette for 1 min, placed on the benchtop for 9 min to allow for interaction, and then the fluorescence after the interaction (F) was measured 11 min after the initial introduction of analyte. This was done to test the response of the QD fluorescence in the presence of atrazine and to determine whether the responses were similar in the three vials; the %RSD was required to be less than 20%. An excitation wavelength of 470 nm with an emission wavelength range of 480-800 nm was used for fluorescence measurements, with slit widths of 5 nm. Thereafter, the same sensing methodology was used for different atrazine concentrations of 2, 4, 6, 8, 10 and 12×10^{-7} M. To investigate the photostability of the QD@chloroform solution after interaction with the atrazine analyte at a concentration of 2×10^{-7} M, consecutive 1 min fluorescence measurements were done.

3.4.2. Excitation wavelength

A chloroform fluorescence blank was tested with an excitation wavelength of 470 nm, and thereafter a QD@chloroform solution [1×10^{-5} g/mL] was excited with different excitation wavelengths namely 420, 450 and 470 nm with a slit width of 4 nm to decrease the measured fluorescence intensity.

3.4.3. Interaction time

To investigate the interaction of QDs with atrazine, a 1×10^{-5} g/mL QD solution and 6×10^{-7} M atrazine dissolved in ethanol was used. First, the fluorescence of the QD@chloroform solution without atrazine was measured at 0 min to obtain the initial intensity (F_0). Then 400 µL of this QD@chloroform solution was

interacted with 300 µL atrazine dissolved in ethanol. The solution was mixed by aspiration with a micropipette for 10 s, whereafter the fluorescence was measured every 5 min up to 20 min.

This was repeated with a second sample and fluorescence was measured at 1, 2, 3 and 10 min to determine the optimal interaction time. All measurements were done with a 4 nm slit width, an excitation wavelength of 420 nm and an emission wavelength range of 430-700 nm.

3.5. Manufacture of thin films

This sub-section describes the alternative methods of film manufacture tested and thereafter films were produced by immobilizing QDs inside the PDMS films. The most consistent method of manufacture was then used to produce thin films and these were optimized to obtain a homogenous distribution of QDs inside the thin films with no central QD hole, which could be used to test analyte sensing in a reproducible manner.

3.5.1. Alternative methods for thin film manufacture

Alternative methods reported in the literature were tested to produce thin films, where QDs were deposited on top of the glass slide directly, as well as adapting the method by placing the QDs on top of the PDMS spin coated glass slide for better adherence by using hydrophobic QDs and a hydrophobic PDMS surface (Bakar et al., 2011).

All PDMS thin films were prepared via spin coating with a spin coater (model WS-650MZ-23NPPB from Laurell Technologies, North Whales, USA). To do this, 1 mL of the QD@chloroform solution (of different concentrations as mentioned in each respective section) was mixed with 10 g of PDMS and 1 g of curing agent to form an elastomer mix. This was mixed thoroughly with a glass rod and placed in a vacuum desiccator, where the PDMS was degassed for 30 min to remove air bubbles. A silicon wafer or glass slide substrates were prepared and cleaned by washing them with acetone and isopropanol followed by drying with compressed air. To prepare the film on a silicon wafer, a polyacrylic acid (PAA) layer was first spun onto the silicon substrate, before heating the substrate at 150°C for 1 min. After cooling to room temperature, the PDMS layer(s) was spun onto the PAA coated substrate. To prepare PDMS films on glass substrates, the same procedure was followed without adding the PAA layer.

A homogeneous distribution of QDs on the film surface and reproducibility was needed and were important considerations in the development of film synthesis methods. To investigate this, a solution of 0.004 g/mL QD@chloroform was used on different slides, named A, B and C. The first slide (A) was prepared by dropping 400 µL of the QD@chloroform solution directly onto the entire surface of a glass slide. This was left on the laboratory bench until the solvent had evaporated.

A second glass slide (B) was prepared by first adding a thin layer of PDMS (0.5 mL) onto the surface which was then spun using a spin coater for 15 s at a speed of 3000 rpm with an acceleration of 1000 rpm/s. Thereafter, 400 µL of the QD@chloroform solution was dropped onto the surface and allowed to dry. The third glass slide (C), coated with PDMS, was made by coating a thicker layer of PDMS on the glass slide by spin coating the PDMS solution (0.5 mL) onto the glass slide for 10 s at a lower speed of 500 rpm with an acceleration of 300 rpm/s and then dropping the QD@chloroform solution on it as done for slides A and B.

3.5.2. Preparation of PDMS films with immobilized QDs

A schematic illustration of the protocol that was followed for the preparation of QD@PDMS thin films is shown in Figure 3-4. The method ultimately used for obtaining optimal films for application followed several optimization trials, where parameters tested were glass slide size, amount of PDMS, spin speeds and curing temperatures, which were each varied and optimized.

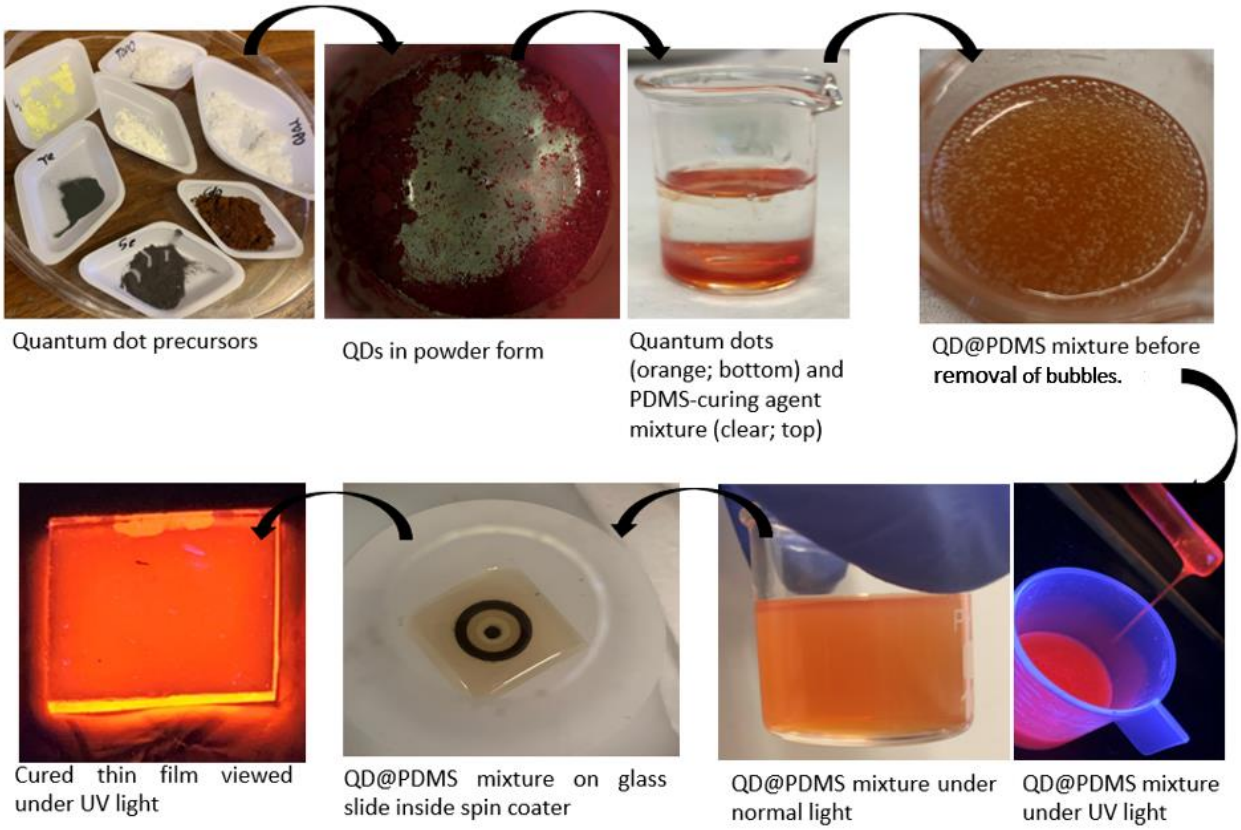

Figure 3-4: Schematic illustration of the protocol that was followed for the preparation of QD@PDMS thin films.

There were generally two different concentrations of QDs in the thin films used in this study, namely 'low concentration quantum dot' (LQD) and 'high concentration quantum dot' (HQD) films. The LQD films were prepared by weighing QDs and adding them to chloroform, forming a 0.004 g/mL QD solution, whereas the HQD films were prepared from a solution of 0.008 g/mL QD in chloroform. In each case, the QD@chloroform solution was then sonicated for 30 min to fully disperse the QDs, whereafter the curing agent and PDMS were added using a ratio of 1 mL QD@chloroform solution: 1 g curing agent: 10 g PDMS. The resulting mixture was then stirred well with a glass rod and the mixture was placed under vacuum for ~30 min to remove the air bubbles that formed during mixing. After 30 min, a cleaned glass slide (washed with acetone and isopropanol) was placed in the centre of the spin coater and the degassed QD@PDMS mixture (of varying amounts as described in respective sections) was placed in the centre of the glass slide and spin coated. The resulting films were then cured by heating on a hot plate at various temperatures and times as described in respective sections to form the cured LQD and HQD films.

3.5.3. Preparation of LQD@PDMS films: Initial optimization

All the initial films were made using the LQD film concentration. The initial testing of films was done on round 4-inch silicon wafers, which required that the films had to be removed from the wafer and cut to size prior to measuring fluorescence in the spectrophotometer. After producing the films, the edges of the films were scraped with a scalpel and the films were left overnight in deionised water so the water could infiltrate below the film and dissolve the PAA layer which would allow the film to lift from the silicon wafer substrate. The PAA layer needed to be optimized in terms of its surface homogeneity. Different amounts of PAA as well as multiple layers of PAA were experimented with, as well as different spin parameters (speed and acceleration), as described in Section 3.5.1.

Ten LQD PDMS films were then coated on the surface of small in-house cut glass microscope slides, as these were able to fit in the spectrophotometer holder directly and films did not need to be removed from the 4-inch silicon wafer substrates which caused tearing and film wastage. These films were spin coated on the in-house cut glass microscope slides using different parameters. The different parameters that were tested were the presence of a PAA layer, different curing temperatures, different curing times, different numbers of PDMS film layers, spin speeds (rpm), acceleration rates (rpm/s), and spin times (s). Films 1-10 had a PAA layer (400 µL PAA, 300 rpm, 15 s, 1000 rpm/s cured at 150°C for 1 min), while for film 11 to 23, the PAA layer was left out as films were coated directly on the glass slides and it was shown that the films could be physically removed from the glass slide without the PAA layer with tweezers, if required.

All glass slides were cleaned with acetone and isopropanol and were then dried with compressed air prior to use. All preliminary films were cured at 150 °C for 4 min on a hot plate. Films 1-14 were made on rough hand cut glass slides but were removed from the glass after curing and used without the glass support to test the fluorescence in the spectrophotometer as they adhered to the solid-state holder of the spectrophotometer. The spin coating parameters of the preliminary films (1-14) are summarized in Table 3-1.

Table 3-1: Spin coating parameters of preliminary films 1-14.

Film	Number of PDMS layers	PAA layer present	Speed (rpm)	Acceleration (rpm/s)	Spin time (s)	Curing time (min)
1	2	Yes	500	300	60	4
2	3	Yes	500	300	60	6
3	1	Yes	200	100	10	6
4	1	Yes	500	300	15	4
5	3	Yes	500	300	15	4
6	1	Yes	300	200	10	4
7	1	Yes	300	300	10	4
8	1	Yes	400	200	10	4
9	1	Yes	400	300	10	4
10	1	Yes	500	200	10	4
11	1	No	500	300	10	4
12	1	No	500	500	10	4
13 (replicate of 12)	1	No	500	500	10	4
14 (replicate of 7)	1	No	300	300	10	4

From film 15 onwards, square glass slides were used which were obtained from Listco Glassblowers (Johannesburg, South Africa) with dimensions of 20 mm x 20 mm x 2 mm, which could be inserted directly into the spectrophotometer solid sample holder. A summary of the parameters used to prepare preliminary films 15-23 is shown in Table 3-2. A few of the spin coating parameters were retested due to slight changes in the dimensions of the glass slides. From slide 15 onwards, no PAA layer was added and only one PDMS layer was spun onto the glass slides for 10 s. Different speeds and accelerations were tested. All the slides were cured on a hot plate at 150°C for 4 min.

Table 3-2: Spin coating parameters of preliminary films 15-23.

Film	15	16	17	18	19	20	21	22	23	24
Speed (rpm)	100	300	500	300	500	300	500	800	1000	1000
Acceleration (rpm/s)	100	100	199	200	200	300	300	400	600	600

3.5.4. The effect of curing temperature on thicker films

Film 16 was a thicker LQD film and it was replicated to determine the effect of different curing temperatures on thicker films. Five replicate films of film 16 were made and were cured at 80, 100, 130, 150 and 170 ^{o}C, respectively.

3.5.5. Preliminary testing of thin films with atrazine

Four films (films 19, 21, 23 and 24) were chosen to do further tests on, as these had the most homogeneous QD distribution over the films, as observed by fluorescence under the UV lamp. The different spin coating parameters from these selected films are shown in Table 3-2. Thus film 19 was the thickest due to the slower speed and acceleration, while film 24 was the thinnest film of the four due to faster spin speed and acceleration. The thinner films (23 and 24) were cured at 150^{o}C for 4 min and for the thicker films (19 and 21) the temperature was reduced to 100^{o}C for 4 min to prevent bubble formation. Films were made by spin coating 1 mL of QD@PDMS onto the glass slide with no PAA layer present. The ratio of QD: PDMS: curing agent was 1 mL QD@chloroform: 10 g: 1 g.

Replicates of film batches 24, 23, 19 and 21 were made and preliminary tests of the LQD PDMS films were done. Fluorescence was measured with a spectrophotometer according to the spatial resolution shown in Figure 3-5. This was done to account for any variation across a single film by calculating the average fluorescence measured to allow for better comparison between films. Reproducible spatial resolution measurements were achieved by making three marks at the top of the glass slide to guide measurements and indicate spot positions. Measurements were taken in a horizontal line in the middle of the film at three different positions from L (left), M (middle) to R (right) respectively, as shown in Figure 3-5.

At these positions, the fluorescence intensity of films 24, 23, 19 and 21 were measured before interaction with atrazine (F_0) and after the interaction with different concentrations of atrazine (F). For film replicates of batch 24, atrazine concentrations in the range of 4-12 × 10^{-7} M were used. After this, the concentrations were increased and atrazine concentrations in the range of 9-13 × 10^{-7} M were used for films 23, 19 and 21. In addition to these testing experiments, the film from batch 19 that had been exposed to atrazine of [8 × 10^{-7} M], was then also interacted with atrazine concentrations of [10 × 10^{-7} M] and [12 × 10^{-7} M] for 1 min each, and fluorescence (F) was measured after each consecutive interaction.

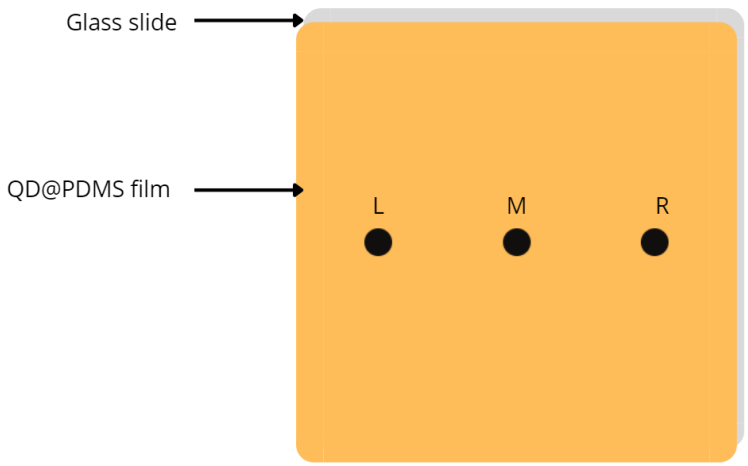

Figure 3-5: Positions where fluorescence was measured on the QD@PDMS thin films.

The atrazine interactions were achieved by placing 500 µL atrazine (in ethanol) on top of the film and allowing it to interact for 1 min and thereafter the excess droplets were blown off the surface with compressed air prior to measurements. The fluorescence excitation wavelength was 400 nm, with an emission wavelength range of 410-700 nm and slit widths of 2 nm were used for all films in subsequent experiments, except when stated otherwise. Film 24 was a very thin film and the slit width consequently had to be increased to 3 nm. Film 24 was selected and viewed through the microscope lens of a Zeiss LSM 880 CLSM confocal fluorescence microscope (Jena, Germany).

3.5.6. Fluorescence reproducibility over the thin films

To investigate the homogeneity and fluorescence reproducibility of the films, replicates of films 24, 23, 19 and 21 were made as described in Section 3.5. This was done for all four films and the slit widths were 2 nm for all reproducibility studies. Fluorescence was measured at different positions as shown in Figure 3-6 from 1 to 10 to compare fluorescence over the spots. This spatial resolution was chosen originally for testing reproducibility as it corresponded to the height at which the fluorescence would be measured with the glass slide resting in the solid-state sample holder (spots 1-5 on top), as well as the height measured when the film was lifted slightly with a piece of Prestik to measure another height on the film (lower spots 6-10).

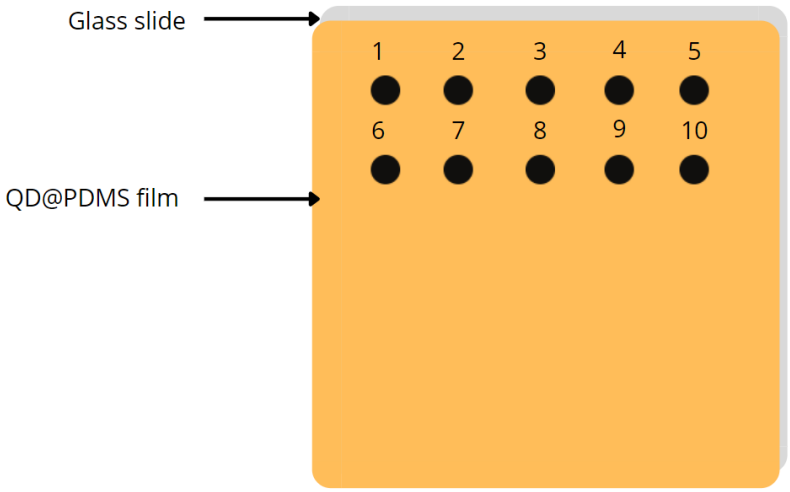

Figure 3-6: Fluorescence reproducibility tested on thin film surfaces over 10 spots.

3.5.7. Consecutive short interval (1 min) photostability tests

The effect of repeated exposure to excitation radiation on the photostability of LQD thin films was tested. To do this, films of batch 21 were selected as they had good fluorescence visible under the UV lamp, and with a homogeneous distribution of QDs over the surface. This was also the only batch for which a trend was measured after interaction with atrazine, therefore it was selected for photostability studies. Fluorescence was measured repeatedly in the middle of the film.

The fluorescence was measured every min for three replicate films from batch 21. The first film was measured consecutively for 30 min. The second film was similarly analysed, with additional measurements after 35, 40, and 50 min. The third film was similarly analysed, with additional measurements after 100 and 110 min.

To keep the QD@PDMS film flush to the solid sample spectrophotometer holder, two pieces of cardboard were cut and placed at the back of the glass slide for the first two films. The third film was placed in the solid holder with the two cardboard pieces, but after the first measurement and inspection, it was adjusted by putting an extra cardboard piece at the back of the glass slide.

3.5.8. Consecutive long interval photostability tests

Films of batch 21 were tested for photostability over different time periods. The fluorescence was measured in the middle of the film. Fluorescence was repeatedly measured on one LQD film every 30 min five times and on another LQD film every 5 and 55 min also 5 times to determine the impact of repeated short (5 min) and longer (55 min) interval measurements on the fluorescence of the films.

3.5.9. The effect of excitation wavelength on the fluorescence of QD@PDMS films

A LQD film from batch 21 was used to test the effect of different excitation wavelengths on the fluorescence emission of the QDs@PDMS film. Excitation wavelengths of 400, 380, 340 and 420 nm were tested. Slit widths of 2 nm were used as 5 nm gave too high fluorescence values.

3.6. Optimized films of varying QD concentrations

3.6.1. Methodology to produce optimized films of low and high QD concentrations

Thin films were prepared as shown in Figure 3-4. The optimized LQD films were prepared by weighing QDs and dispersing them in chloroform to form a QD@chloroform solution with concentrations of 0.004 g/mL for LQD and 0.008 g/mL for HQD, and these were each sonicated for 30 min to ensure homogenous dispersion. Then, to 1 mL of each of the QD@chloroform solutions, curing agent and PDMS were added using a ratio of 1 g curing agent: 10 g PDMS. The resulting mixture was mixed thoroughly by stirring with a glass rod and the mixture was placed under vacuum for ~30 min to remove air bubbles that formed. After 30 min the cleaned glass slide was placed in the centre of the spin coater and 0.5 mL of the degassed mixture was placed in the centre of the glass slide with the use of a pipette.

This was spin coated at a speed of 500 rpm (300 rpm/s) for 10 s to distribute the QD@PDMS solution over the glass surface. The glass slide with the QD@PDMS film was then removed from the spin coater and cured on a hot plate at a reduced temperature of 80^{o}C. The curing time was increased to 15 min as this enhanced the reproducibility of the films. The film was then removed and the excess PDMS was removed from the sides and bottom of the glass slide with a scalpel. The same protocol was followed for the preparation of HQD films.

3.6.2. Concentration of QDs in thin films

The average concentration of QDs in the thin films was calculated on a mass basis, using the individual masses of: batches of cured films; the mass of 1 mL cured PDMS (without QDs), the mass of 1 mL cured low concentration quantum dot (LQD) PDMS and the mass of 1 mL of cured high concentration quantum dot (HQD) PDMS respectively; the mass of 1 g wet curing agent; the mass of 10 g wet PDMS, in addition to the cured density of PDMS (1.03 g/mL which was obtained from the supplier). The ratio in which the QD@chloroform solution was added to the curing agent and PDMS to form the final mixture to insert in the spin coater was 1 mL QD@chloroform: 1 g: 10 g, respectively. The mass of QDs in the final solution was determined and then correlated to the volume of the films to determine the concentration of QDs in g/mL in the final film volume. The calculations are shown for LQD films and the same was done for the HQD films.

Firstly, 1 mL of PDMS was cured and weighed (N= 7) by adding the PDMS solution into a glass vial and curing it on a hot plate at 80°C for 15 min to obtain the average weight of 1 mL of cured PDMS. One result was statistically shown to be an outlier and was removed (resulting in N= 6) and the average weight for 1 mL of cured PDMS containing no QDs was obtained. This was repeated for cured 1 mL volumes of LQD and HQD PDMS solutions respectively and an average for each (N= 7) was obtained.

The mass ratio of 1 mL cured low [QD] PDMS/ 1 mL cured PDMS (no QDs) was obtained ($MassRatio_{curedLQD}$) as shown in Eq. (3-2).

$$MassRatio_{curedLQD} = \frac{Mass_{1mL(curedLQD)}}{Mass_{1mL(curedPDMS)}} \tag{3-2}$$

This was multiplied by the density of the cured PDMS to give the cured density of the LQD PDMS as shown in Eq. (3-3).

$$Density_{curedLQD} = MassRatio_{curedLQD} \times Density_{curedPDMS} \tag{3-3}$$

The volume of 10 g wet PDMS, 1 g wet curing agent and 1 mL chloroform was added together, giving the total volume of the solution prepared for spin coating. The mass of QDs in 1 mL final solution was

determined by knowing the mass of QDs in 1 mL chloroform for LQD films and dividing this by the total volume as shown in Eq. (3-4).

$$Mass_{QD\ (1\ mL\ final\ soln)} = \frac{Mass_{QD}}{Total\ vol} \tag{3-4}$$

In a vial, 1 mL of LQD PDMS solution (N= 7) was cured and weighed and the LQD films were weighed (N= 18). Both these were weighed by weighing the clean glass vial/slide without the PDMS and weighing them again post curing of the LQD@PDMS. The cured mass of the film was divided by the cured mass of 1 mL of LQD solution giving the final volume of film on the glass slide as shown in Eq. (3-5).

$$Volume_{LQD(film)in\ 1\ mL} = \frac{Mass_{curedLQD(film)}}{Mass_{1mL(curedLQD)}} \tag{3-5}$$

It was calculated using Eq (3-4) that in 1 mL final solution there was a certain mass of QDs in the LQD solution. Thus, by multiplying the mass of QDs in 1 mL final solution by the volume of the solution on the slide, the QD mass in the volume on the slide was obtained as shown in Eq. (3-6).

$$Mass_{QD(in\ film\ on\ slide)} = Mass_{QD(1mL\ final\ soln)} \times Volume_{LQD(film)in1\ mL} \tag{3-6}$$

The average film thickness was determined by SEM. The glass slide dimensions onto which the films were spin coated (20 x 20 mm) were used with the film thickness to determine the film volume. From this the final QD concentration in the film on the glass slide was calculated as shown in Eq. (3-7).

$$Concentration\ of\ QD\ in\ film = \frac{Mass_{QD(in\ film\ on\ slide)}}{Volume\ of\ film_{(l\times w\times h)}} \tag{3-7}$$

3.6.3. Very low QD concentration films

A batch of very low concentration quantum dot (VLQD) films were made to observe the fluorescence of the QDs immobilized at a lower concentration of 0.0053 mg/mL or 5.33×10^{-6} g/mL QDs per mL PDMS in

the final cured films. This was done as the concentrations of QDs in the LQD and HQD films were in the same ranges (0.28 and 0.51 mg/mL) as the QD solution concentrations previously used in our group to detect acetaminophen with 0.27 mg/mL (Montaseri et al., 2019), but the concentrations used to detect atrazine were in the range of 4.2×10^{-5} mg/mL (Nsibande & Forbes, 2019).

The fluorescence of a cardboard support only, a blank PDMS film with no QDs, as well as a VLQD, LQD and HQD film, respectively, were tested.

3.6.4. Spatially resolved fluorescence measurements

The fluorescence of the optimized QD@PDMS films spin coated onto glass slides were measured at nine spatially resolved spots over the film surface. Tip-Ex was used to make marks on two adjacent sides of the film to form a grid with nine spots over the film surface as shown Figure 3-7.

Figure 3-7: Side view of the thin film on top of a glass slide with Tip-Ex marked spots to indicate measurement points as shown in Figure 3-8.

The nine spots are shown in Figure 3-8 as the film faces forward and the glass slide is facing towards the back. This was the order in which fluorescence was measured in all subsequent experiments. The film was held in place by a solid-state fluorescence holder and three pieces of cardboard were cut out and placed behind the glass surface to ensure the QD@PDMS films stayed in place and were pressed flush against the aperture of the holder.

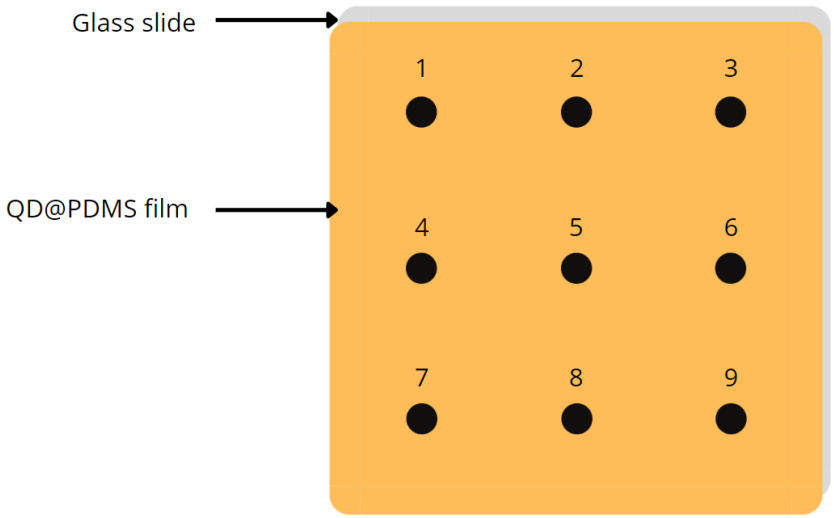

Figure 3-8: Nine spatially resolved spots over the film surface indicating where fluorescence was measured on the films.

In subsequent measurements, the fluorescence of the optimized QD@PDMS films was measured at nine spots as shown in Figure 3-8 by using an excitation wavelength of 400 nm and an emission wavelength range of 410 – 700 nm. The slit widths still had to be optimised to determine the slit width which could accommodate sensing with films of both QD concentration. The optimum slit width was found to be 2 nm after the experiments performed in Section 3.7.

3.1. Interaction of optimized films with atrazine

3.6.5. Optimization of slit widths

The first nine HQD films were made and used to test for the detection of atrazine using HQD films. The optimized HQD films were interacted with atrazine at concentrations of 2, 8 and 12 × 10^{-7} M. This was done by placing 400 µL of the atrazine solution on the film surface for 1 min. The excess droplets were then blown off with compressed air prior to measurements. Three films were tested at each atrazine concentration (N= 3) and short interaction times of 1 min each were used.

For the first nine HQD films, slit widths of 2 nm were used. The atrazine tests were then repeated with 1.2 nm slit widths as HQD films gave high fluorescence values with a 2 nm slit width. Repeated fluorescence of the HQD films was measured with a slit width of 1.2 nm. This was repeated for a LQD film with 1.2 nm

slit widths to see whether 1.2 nm could work for both LQD and HQD films. It was observed that the fluorescence intensity of the LQD films were too low with slit widths of 1.2 nm as this yielded a poor signal-to-noise ratio. Thus atrazine tests with LQD films were done using 2 nm slit widths instead.

3.6.6. Testing optimized films with atrazine

The optimized films were interacted with atrazine in a similar manner to that used to optimize the slit width (Section 3.7.1). Nine films of both LQD and HQD respectively were tested with atrazine concentrations of of 2, 8 and 12 × 10^{-7} M (N= 3), by placing 400 µL of the atrazine solution on the film surface for 1 min.

3.2. Interaction of optimized films with different solvents

Three optimized films of LQD and HQD were each immersed in 4 mL solvents of 100% deionized water, 100% ethanol, or a mixture of H_2O: ethanol (2:1) for 24 hours. Fluorescence emission was measured before and after interaction (F_0 and F) on nine spots as shown in Figure 3-8. Fluorescence was measured (F) again after 25 days of standing on the laboratory bench where films were originally covered with a plastic bag to protect them from ambient air, as well as dust which could accumulate on the film surface. The films were later transferred to a plastic box of which the top was covered with tin foil to prevent dust accumulation on the films.

3.3. Interaction of optimized films with phenanthrene

Three films of optimized LQD and HQD were each immersed in 4 mL phenanthrene solutions (the solvent was H_2O: ethanol (2:1)) at 0, 5.61 × 10^{-6} and 5.61 × 10^{-5} M for 24 hours and the fluorescence was measured before and after the interaction and again after 21 days of standing on the laboratory bench where films were originally covered with a plastic bag and were later transferred to a plastic box as previously discussed.

3.4. Testing QD thin films with water samples

Water samples were obtained from Rand Water (RW) from the inlet to a water treatment plant. The water was sampled into a 1 L glass Schott bottle on 11/03/2022. The water sampling tests were done using LQD and HQD films with (1) an unconcentrated, filtered inlet water sample and (2) a pre-concentrated inlet water sample. For (1), the water sample was filtered by passing it through a nylon syringe filter (25 mm,

0.45 µm with polypropylene prefilters) (Clarinert filter obtained from Agela Technologies, Torrance, USA) to remove large particulate matter.

For (2), 400 mL inlet water was pre-concentrated and processed through solid-phase extraction (SPE). The SPE method employed was adapted from Opriş et al. (2013) and no pH adjustment of the water sample was done. A Waters Oasis HLB cartridge (6 mL, 200 mg) was used. The sample was prepared by adding 0.2% (w/v) of EDTA to chelate any residual free metal ions that were present. The cartridge was then pre-conditioned with 10 mL ethanol to remove any impurities or bound analytes from the SPE cartridge and then tapped lightly to ensure there were no air pockets present in the sorbent bed, whereafter 10 mL ultrapure water was passed through to condition the cartridge. The sample was then loaded onto the sorbent bed by first passing it through a 22 µm nylon syringe filter. The sample was passed through the sorbent bed at a low flow rate of 1-3 mL/min. The sorbent bed was washed with 10 mL of ultrapure water remove any unretained species. The solvent was dried using vacuum for 30 min. Analytes were then eluted from the sorbent bed with 6 mL ethanol and collected in a test tube. The ethanol was blown off under vacuum at 30^{o}C. The dried sample was reconstituted in ethanol to a final volume of 100 µL.

Eight films were used and their fluorescence (F_0 and F) was measured as shown in Figure 3-8. After the interactions, the samples were allowed to dry by placing them vertically on a paper towel for 10 min. Excess water drops were blown off with compressed air prior to measurements. The F_0 values of all films used were measured beforehand.

The first film of each concentration (LQD and HQD) was interacted with an unconcentrated, filtered inlet water sample obtained from Rand Water. Of this sample, 400 µL was added to the top of the film as done previously with atrazine samples, to only cover the surface of the film. It was seen that this sample was a lot more hydrophilic than the atrazine-ethanol solution and did not spread over the hydrophobic surface as easily as the atrazine solution. Thus, to ensure the film surface was covered, a larger volume of 1.2 mL was used. This was then interacted for 1 min on both LQD and HQD films before taking fluorescence measurements.

With the second films of both concentrations, the same water sample was interacted with the films for 1 min, but the samples were immersed in 4 mL of the water sample. The third film was treated as a blank and no water was interacted with it and the F value was measured. It was seen that the fluorescence of the

films had increased during storage. These F values were measured about 35 days after the initial F_0 values, thus it was necessary to remeasure every F_0 value again before each new test. Film 3 was then immersed in the unconcentrated, filtered inlet water sample (4 mL) for 1 min, the same as for film 2.

For both concentration films, F_0 values over the nine spots were remeasured and then blank fluorescence measurements were done after 1 hour and 24 hours without introducing any solvent or analyte. A test was also done to observe the change in fluorescence when the films were immersed in a water: ethanol (2: 1) solution for 24 hours.

The fourth films of LQD and HQD were immersed in the filtered, unconcentrated water sample for 1 hour. The fifth set of films was immersed for 24 hours in the filtered, unconcentrated water sample. For the sixth set of films of both concentrations, a 1 mL concentrated SPE extract was used which was reconstituted in ethanol and was diluted with deionized water forming a total solution volume of 3 mL.

This sample extract volume was small, and a few tests needed to be done on it consecutively. It should be noted that the amount of analyte present in the sample would decrease during this process due to absorption by the PDMS thin films. The first film introduced to the sample was a LQD film, and thereafter the HQD film. The films were immersed in the 3 mL sample for 24 hours and fluorescence was measured before and after interaction.

With films from the 7th set, the concentrated extract, which had already interacted with LQD, then HQD films for 24 hours, was interacted again with a LQD then HQD film for 30 min. LQD film 8 was then also tested with this same concentrated water extract, where it was immersed for 1 min.

3.5. Statistical analysis of results

The results obtained from the fluorescence measured before and after interaction with analytes may have some differences due to slight variations in film thickness, or the way light was reflected off the sample surface between different films, as well as between different spots on a single film. For this reason, statistical methods are used to determine whether these values differed statistically significantly from each other, or not. To do this, Microsoft Excel was used as a tool for statistical analysis. General descriptive statistics were used to calculate the mean, standard error, median, mode, standard deviation and sample

variance. The 't-Test: Paired two sample for means' was used to determine statistical differences between two groups of data and this was done at a 95% confidence level. This indicated whether the mean of one group was statistically significantly different from the other group. The data range with the larger mean was used as variable 1, and the smaller for variable 2.

The null hypothesis was stated as H_0: $\mu_d = 0$, indicating that there was no significant difference between the mean values obtained for the two groups of compared data. The alternative hypothesis was stated as H_1: $\mu_d \neq 0$, indicating that there was a significant difference between the mean values obtained for the two groups of compared data.

The hypothesized mean was 0, assuming no difference between the two groups of data. An alpha value of 0.05 was used, indicating a 95% confidence interval. When the calculated t-statistic value was larger than the critical t value (one-tail value), it confirmed that there was a significant difference between the two groups and the mean of the larger group was significantly larger. At a 95% confidence interval, when the calculated t-statistical value was smaller than the critical t value (one-tail value), it confirmed that there was statistically no significant difference between the means of the two groups.

Chapter 4: Results and Discussion

In this chapter, the results obtained from the synthesis and characterization of CdSeTe/ZnS QDs are presented, as well as the results relating to progress towards the development and optimization of PDMS thin films used for immobilization of the QDs. The performance of the films when used to detect the target organic compounds present in spiked solvents as well as inlet water obtained from Rand Water is discussed. Finally, the results obtained from the statistical analysis protocol explained in Section 3.11 are presented and explained.

4.1. Synthesis and characterization of QDs

4.1.1. First batch of CdSeTe/ZnS QDs

During the synthesis process of the first batch of QDs, it was observed that the precursor solutions (which consisted of ODE and OA) were frozen by the next morning. This was attributed to the low ambient temperatures as this was in the winter season. To overcome this, the precursor solutions had to be defrosted by heating the solutions to 100^{o}C before use.

The aliquot of the CdSeTe QD core solution that was extracted during synthesis and kept aside, was found to have a maximum fluorescence emission wavelength of 570 nm (Figure 4-1), which corresponded to yellow emission when viewed under a UV-lamp. The addition of Zn and S precursors to the CdSeTe reaction mixture allowed for passivation of the core with a ZnS shell to form CdSeTe/ZnS core/shell QDs. Formation of the shell was confirmed by a red-shift in the fluorescence emission wavelength from 570 to 593 nm as shown in Figure 4-1. The ZnS QD shell was allowed to grow, and the growth was confirmed by taking fluorescence measurements at different times. The growth continued until the reaction slowed down after 50 min as observed by the insignificant change in the fluorescence emission wavelength after additional reaction time.

When comparing the fluorescence spectra of the CdSeTe QD core to that of the CdSeTe/ZnS core shell (C/S) QDs, it can be observed that the QD size increased when the ZnS shell was grown over the QD core, as shown from the normalized spectra in Figure 4-1. It is important to note that the CdSeTe core forms almost instantly as soon as the Se and Te precursors were added to the reaction mixture, suggesting that the nucleation occurred spontaneously under the reaction conditions. Thus the fluorescence measurements of

the QD core were carried out after 5 min reaction time. On the other hand, growth of the shell over the core is typically a slower process. This is confirmed by the slight red-shift in emission wavelength of C/S QDs as shown in Figure 4-1 after 5, 10, 20 and 50 min. Overall, the addition of shell precursors (Zn and S) to the CdSeTe core resulted in a shift in the maximum emission wavelengths from 570 to 602 nm. This shift is attributed to a change in size of the QDs as the shell grows over the core.

Furthermore, the fluorescence measurements show that there was a slight increase in the size distribution of the QDs, as the particle size increased slightly (as was expected) and the core and C/S QDs had full width half maximum (FWHM) values of 45.5 and 47.0 nm, respectively. The broader peak width (increased size distribution) of the C/S QDs can be attributed to several processes in the reaction mixture, including some core QDs not being capped with the shell, possible side-reactions, possible agglomeration, and general inhomogeneity of the shell coating process. The synthesized QDs were hydrophobic as they were synthesized and stabilized with the use of hydrophobic trioctylphosphine oxide (TOPO) and oleic acid (OA) capping agents. Thus, they could easily be dispersed in nonpolar organic solvents like chloroform.

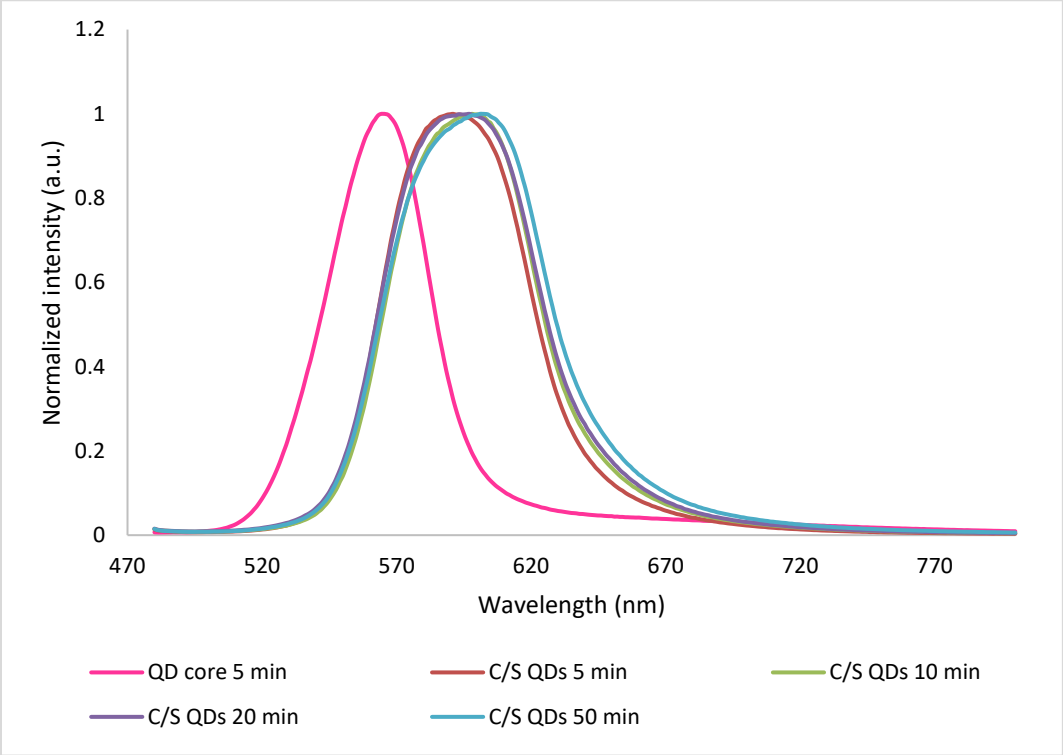

Figure 4-1: Normalized fluorescence spectra of the hydrophobic CdSeTe QD core, the addition of the ZnS shell to the core QDs and growth thereof, measured using an excitation wavelength of 470 nm.

The images in Table 4-1 show the visual differences in the first batch of synthesized CdSeTe core and CdSeTe/ZnS core/shell QDs as photographed under normal and UV light conditions. It is shown that the CdSeTe core QDs had a dark orange-brownish appearance under normal light and under UV light they had bright yellow emission. On the other hand, the CdSeTe/ZnS QDs had an dull orange appearance under normal light and a bright orange emission under UV light. This visual change in colour was used to confirm the growth of the C/S QDs during synthesis which emitted light at longer wavelengths due to red-shifting resulting from QD growth.

Table 4-1: Images showing the visual differences in the first batch of synthesized CdSeTe and CdSeTe/ZnS QDs under natural light and UV light, respectively.

	CdSeTe QDs	CdSeTe/ZnS QDs
Natural light		
UV light	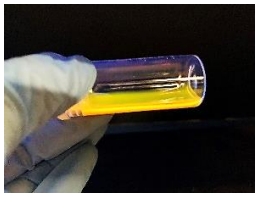	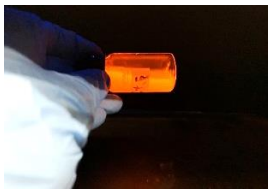
Maximum emission wavelength (nm)	570	602

The UV-vis absorption spectra for both CdSeTe core and CdSeTe/ZnS core/shell QDs are shown in Figure 4-2. It is shown that the absorbance spectra of the core and C/S QDs were generally broad, which indicated that a wide range of excitation wavelengths could be employed when using these materials as fluorescence sensors. A closer look at the CdSeTe core spectrum in the insert in Figure 4-2 shows two clear excitonic peaks that were observed at 452 and 555 nm. Upon overlaying the core with the ZnS shell it can be

observed that these exciton peaks broadened and red-shifted by ~24 nm to 476 and 573 nm, respectively. This broadening of the excitonic peaks may be due to different factors like size increase and introduction of surface defects (Adegoke et al, 2017). Therefore, the UV-vis absorption data further confirmed successful overcoating of the ZnS shell on the CdSeTe core.

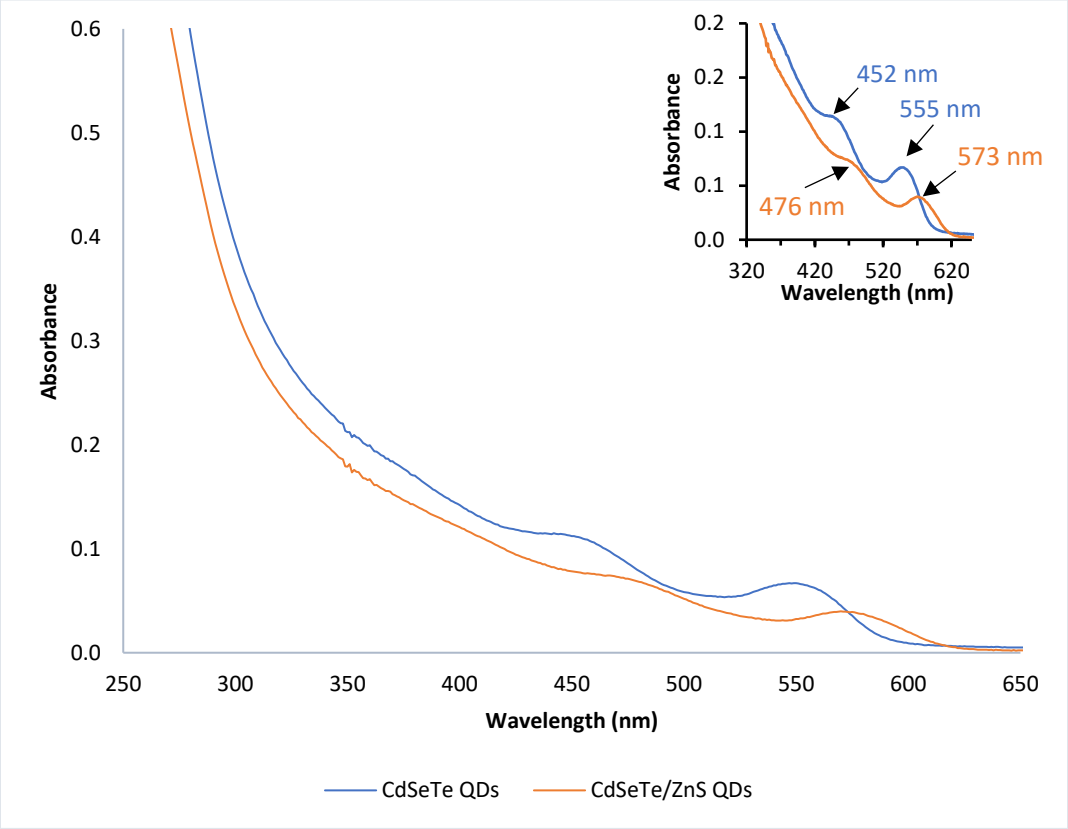

Figure 4-2: UV-Vis absorbance spectra of the first batch of CdSeTe and CdSeTe/ZnS QDs.

Figure 4-3 shows the transmission electron microscopy (TEM) micrographs of the CdSeTe QDs, viewed at a high magnification (~100 000x) with 100 - 200 nm scale bars as shown. The micrographs clearly show that the CdSeTe QDs had a quasi-spherical morphology and had a homogenous size distribution. Furthermore, it was visually observed that the nanoparticles were well dispersed in chloroform and this can be attributed to the hydrophobic ligands on their surfaces. The homogenous size distribution was to be expected since the Se and Te precursors were added simultaneously and instantly to the reaction mixture under vigorous stirring, allowing for instant nucleation and formation of a uniform core nanoparticles.

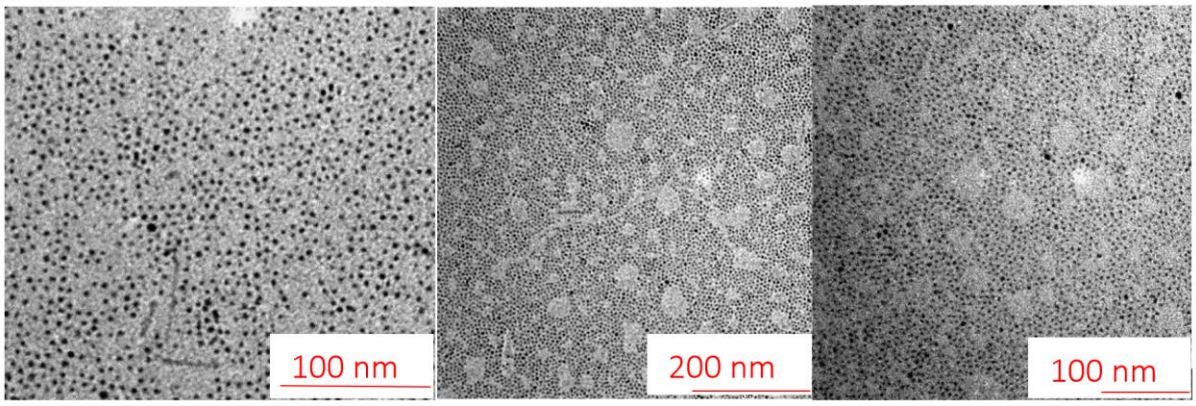

Figure 4-3: TEM micrographs of the first batch CdSeTe QDs viewed at a high magnification (~100 000x) with 100- 200 nm scale bars.

Figure 4-4 shows the TEM micrographs of the CdSeTe/ZnS QDs viewed at a high magnification (~100 000x) with 50- 100 nm scale bars as shown. The TEM micrographs from Figure 4-3 and Figure 4-4 indicate that the particles were monodispersed and were not agglomerated which was an indication of good purity of the QDs following rigorous washing.

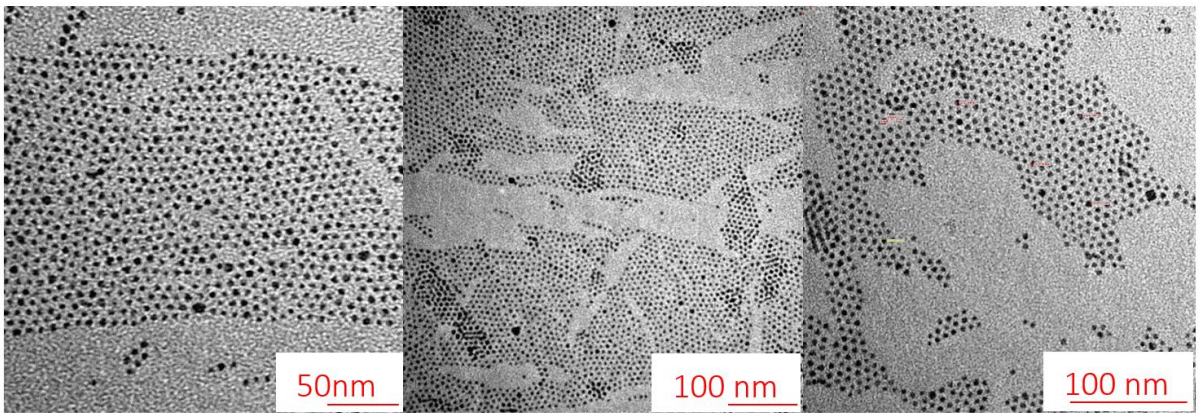

Figure 4-4: TEM micrographs of the first batch of CdSeTe/ZnS QDs viewed at a high magnification (~100 000x) with 50- 100 nm scale bars.

Figure 4-5 shows the average QD particle size distribution as determined from the TEM micrographs with ImageJ software. The average particle size for the core and C/S QDs were 2.53 and 3.40 nm, respectively. A size increase was observed for the C/S QDs as the shell layer had been coated over the QD core. There was also a slightly larger size distribution for the C/S QDs than what was observed with the core, as was expected.

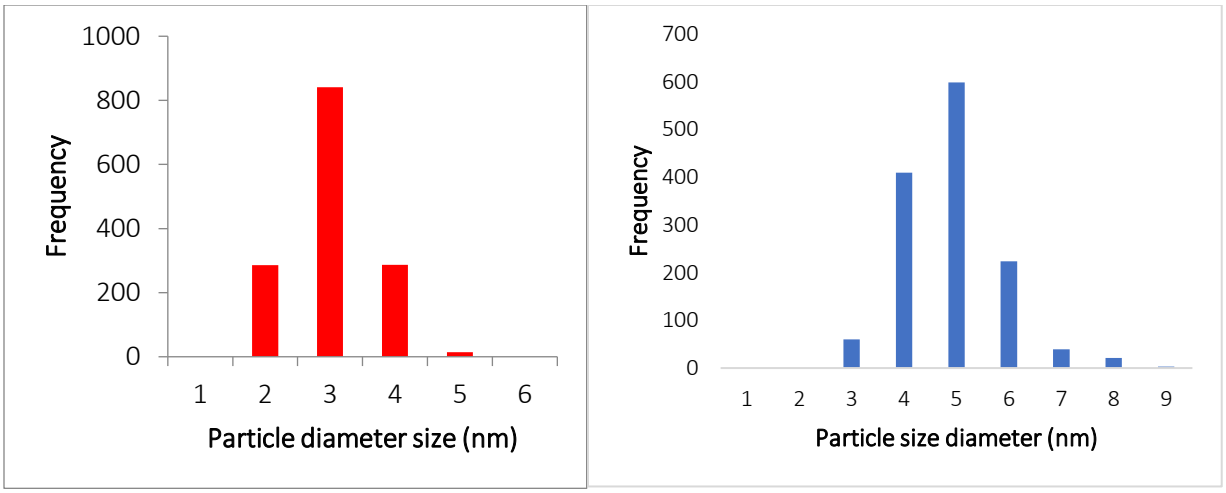

Figure 4-5: Average particle size distribution of the QD core (left) and C/S QDs (right) of the first QD batch.

4.1.2. Second batch of CdSeTe/ZnS QDs

As the first QD batch had stirred overnight for an unknown amount of time until it froze as a result of low temperatures, a second batch of QDs were synthesized. When the second batch was synthesized, the ambient temperature was warmer, and the solution was stirred vigorously at a temperature of 40°C for 4 hours during the day. For the second batch, the quantities of precursors were also reduced to decrease waste. From the normalized fluorescence emission spectra shown in Figure 4-6, the growth of the QD core is observed, as well as the subsequent growth of the C/S QDs until 60 min after adding the shell precursors. A broadening in the spectra, indicating an increase in QD size distribution, started to occur and the reaction was quenched by allowing it to cool down. The maximum emission wavelength of the QD core red-shifted from 552 nm after 20 s to 573 nm after 5 min. The maximum emission wavelength was 588 nm when the shell was added to the QD core which then red-shifted to 598 nm after 40 min and after 60 min the maximum emission wavelength had blue-shifted to 594 nm and the peak started to broaden indicating a larger distribution of QD sizes. This can be due to QD particles being reduced in size to free monomers which are supplied to increase the growth of the larger crystals (Reiss, 2008). The core and C/S QDs had FWHM values of 31.0 and 49.5 nm, respectively.

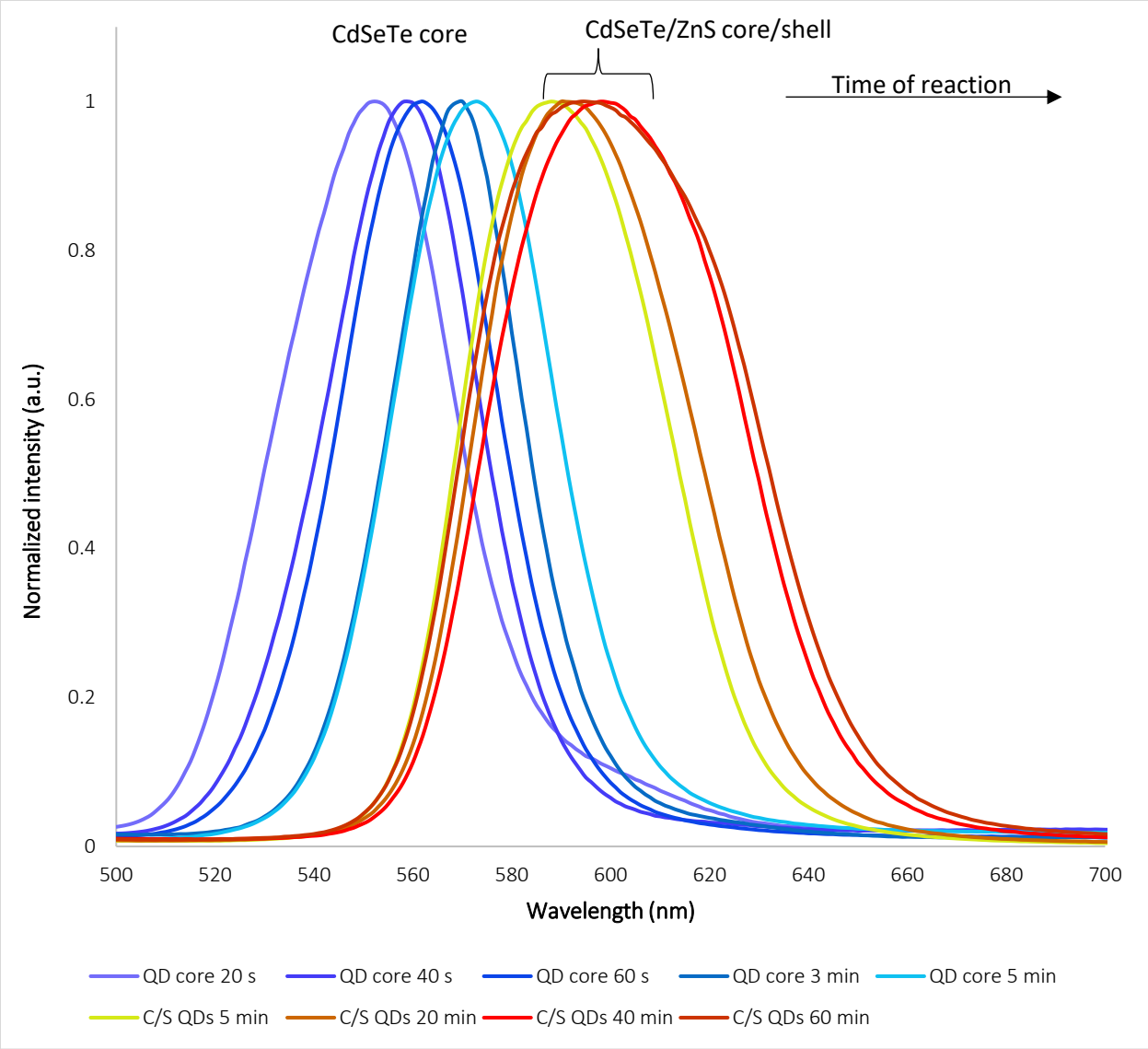

Figure 4-6: Normalized fluorescence spectra of the second batch of hydrophobic CdSeTe QDs, and the addition of the ZnS shell to the core QDs showing the growth thereof using an excitation wavelength of 470 nm.

From the normalized emission spectra shown in Figure 4-7, the fluorescence emission maximum was red-shifted from 573 nm (QD core) to a longer wavelength of 594 nm when the QD ZnS shell was added, confirming the growth of the QDs.

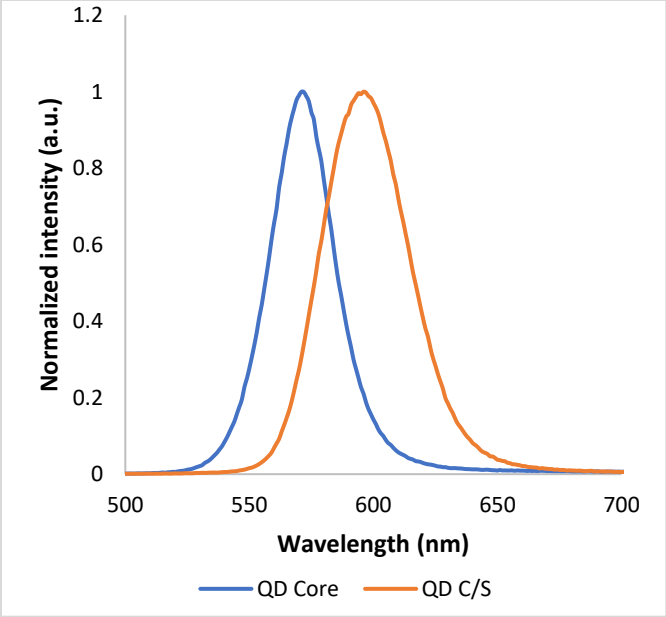

Figure 4-7: Normalized fluorescence spectra of the second batch of hydrophobic core and C/S QDs after washing, at an excitation wavelength of 470 nm.

In Table 4-2 the visual differences in the second batch of synthesized QDs under normal and UV light conditions are presented; it was shown under UV light that the QD core fluorescence emission was bright yellow, and that of the C/S QDs was bright orange, confirming the growth of the C/S QDs which emitted light at longer wavelengths due to red-shifting with the QD growth.

Table 4-2: Images showing the visual differences in the second batch of synthesized CdSeTe and CdSeTe/ZnS QDs under UV light.

	CdSeTe QDs	CdSeTe/ZnS QDs
UV light	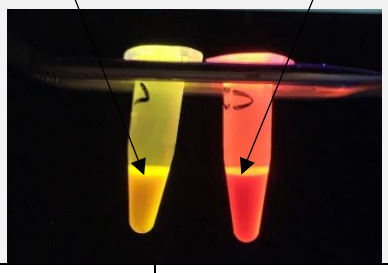	
Maximum emission wavelength (nm)	573	594

It can be seen from the UV-Vis spectra in Figure 4-8, that the absorbance spectra of the CdSeTe QDs and CdSeTe/ZnS QDs in chloroform solution contain broad peaks, which indicated that a wide range of excitation wavelengths could be employed when using these materials as fluorescence sensors. The excitation wavelength that was employed for QDs dispersed in chloroform was 470 nm.

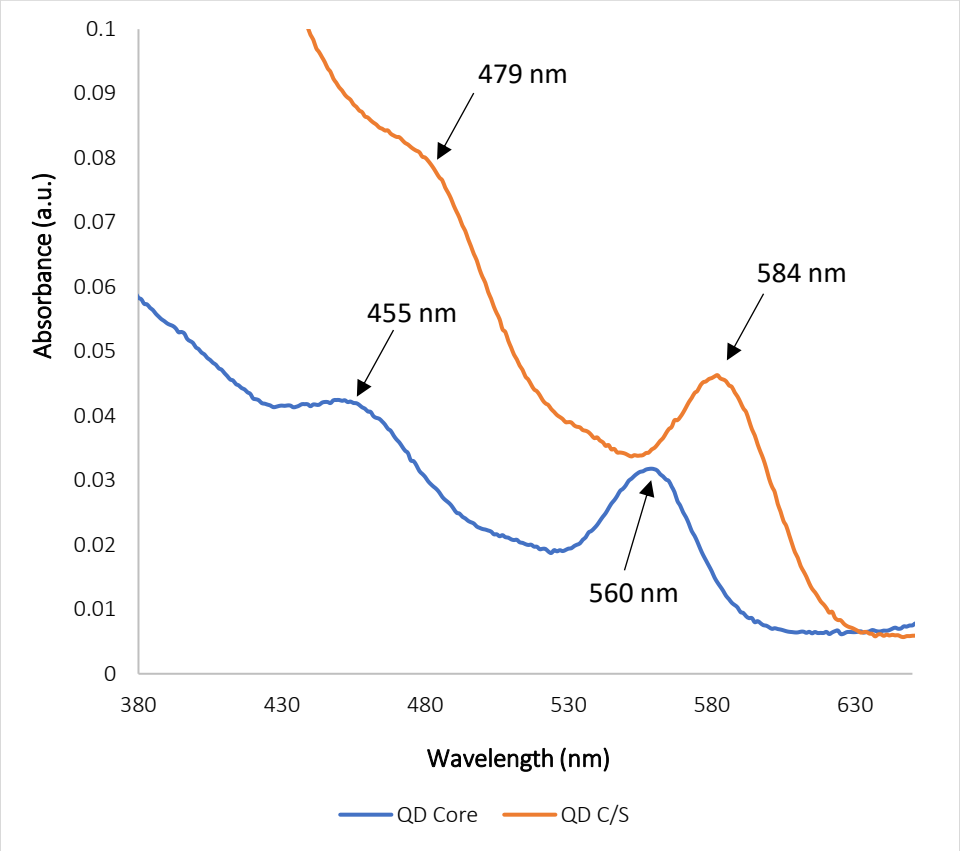

Figure 4-8: UV-Vis absorbance spectra of the second batch of CdSeTe and CdSeTe/ZnS QDs.

The results obtained when the core and C/S QDs were examined with a HRTEM microscope at a high magnification (~100 000x) with 100 nm scale bars are shown in Figure 4-9. The QD particles were monodispersed and not agglomerated which was an indication of good QD dispersion and that the QDs were washed well.

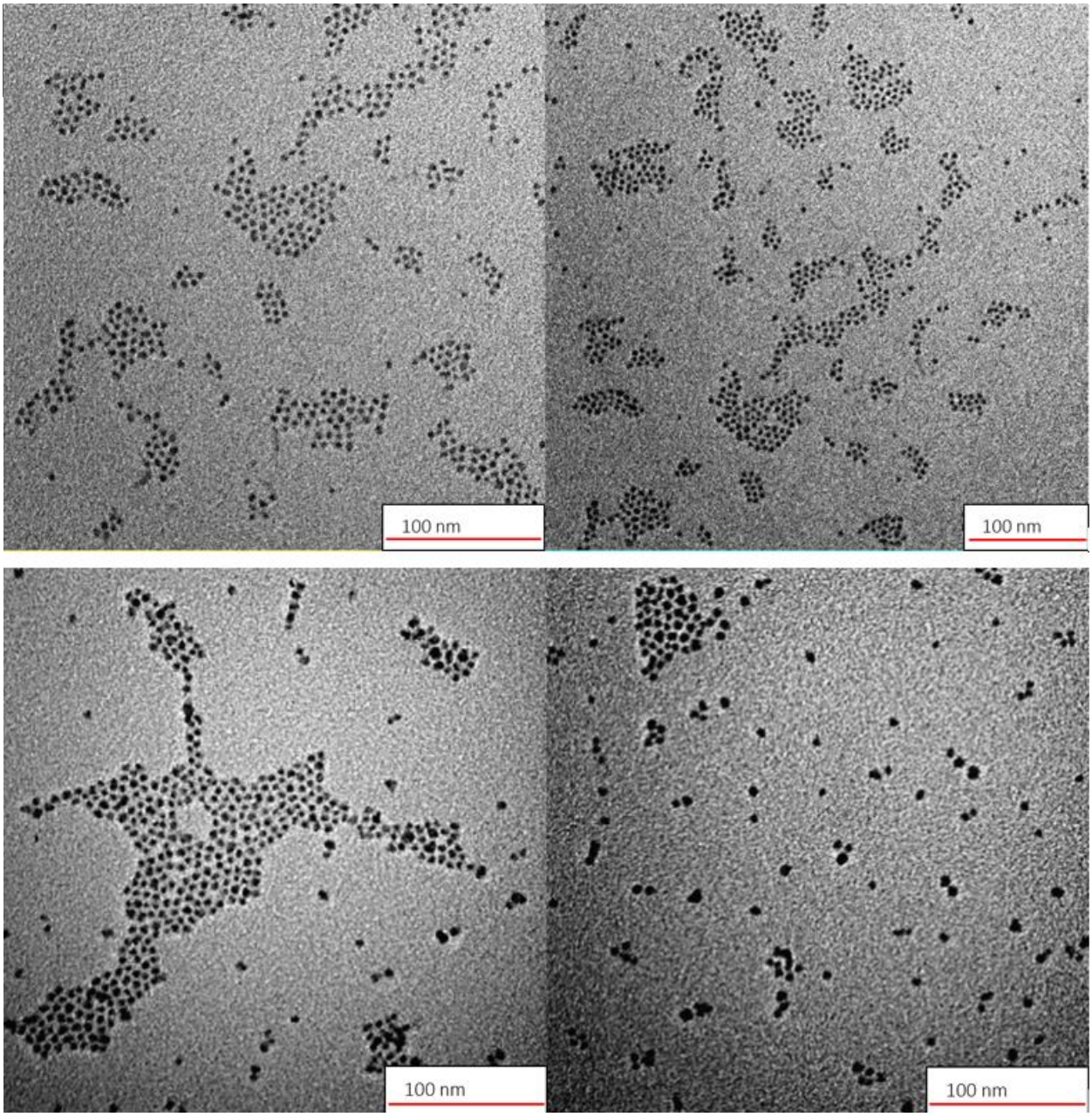

Figure 4-9: TEM micrographs of the second batch of CdSeTe QDs (top) and CdSeTe/ZnS QDs (bottom) examined at a high magnification (~100 000x) with 100 nm scale bars.

In Figure 4-10 the particle size diameter distributions are shown with the average particle size for the core and C/S QDs being 3.06 and 4.02 nm, respectively, as determined from the TEM micrographs with ImageJ software (Schneider, 2012). A size increase was observed for the C/S QDs as the shell layer had been coated over the QD core. There is also a slightly larger size distribution for the C/S QDs than what was observed with the QD core.

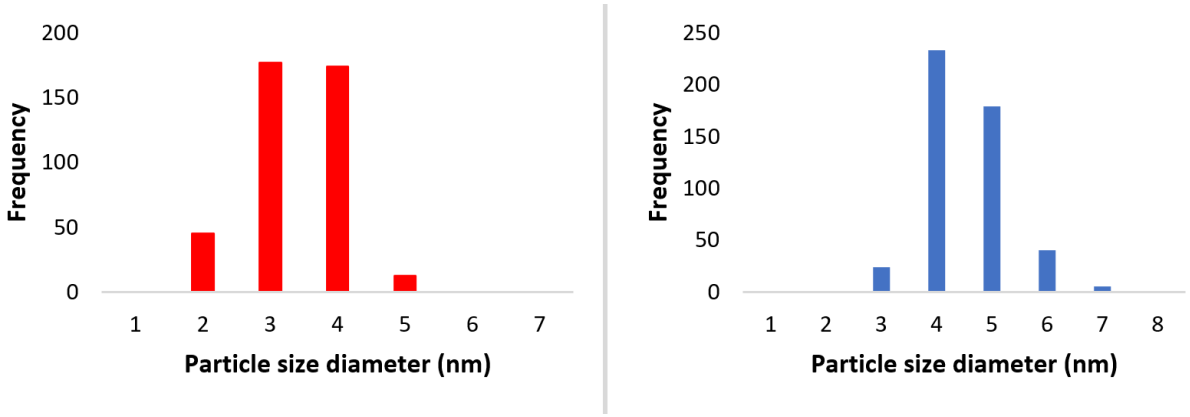

Figure 4-10: Average particle size distribution of the second batch QDs of CdSeTe QDs (left) and CdSeTe/ZnS QDs (right).

4.1.3. Quantum yield of the second batch of QDs dispersed in solution

The photoluminescence quantum yield (PLQY) of the C/S QDs was determined by using the method described in Section 3.2.5. It is important to note that this is a comparative/relative method against a fluorophore (Rhodamine 6G) that has a known PLQY. The fluorescence spectra of the C/S QDs was obtained by exciting three different concentrations of the C/S QDs dispersed in chloroform solution with an excitation wavelength of 470 nm, and the fluorescence counts per second (CPS) values ranging from 480-800 nm were obtained and integrated. This was plotted against the respective absorbance value obtained at 470 nm for each concentration to obtain the gradient of integrated fluorescence versus absorbance.

The QY was determined by using the refractive indices of chloroform ($\boldsymbol{\eta}$= 1.44) and ethanol ($\boldsymbol{\eta}$= 1.36) in which the C/S QDs and rhodamine 6G (R6G) were dispersed or dissolved in, respectively. The known PLQY of the R6G standard of Φ_{ST} was 0.95 according to literature (Fishcher and Georges, 1996; Magde et al., 2007).

The PLQY of the C/S QDs was calculated to be 47%. The calculated PLQY of the QDs was lower than expected as the fluorescence of the C/S QDs was very bright as shown in Table 4-2 and the fluorescence of these QDs was very bright even when later immobilized in the thin films (Sections 4.3.4 and 4.4). Other similar QDs like CdSeZnS/ZnS, CdSe@Zn/ZnS and CdSe/ZnS alloyed QDs have exhibited strong fluorescence of 98, 88 and 75% respectively (Kim et al., 2022; Fu et al., 2017; Hao et al., 2019). Consideration needs to be taken that a relative method was used to determine the PLQY, and this may have inherent errors. To overcome

this, absolute PLQY determination which is more accurate should be considered for future work, as this method directly measures PLQY by using scattering agents combined with accurate instruments employing integrating spheres or actinometers to calibrate the measurements. It is essential to know with precision how much excitation light the sample has received (Demas & Crosby, 1971). Absolute PLQY can also be determined with the use of calorimetry (Fischer & Georges, 1996).

4.2. Sensing of atrazine using QDs dispersed in solution

In this section, the results of the interaction of CdSeTe/ZnS QDs in chloroform (abbreviated as QD@chloroform) with atrazine are presented. To recap, this started with the testing of the reproducibility of the QD@chloroform solution, which was then followed by optimization of the excitation wavelength and the interaction time. Atrazine sensing was then performed using the optimal parameters. The QD concentration was kept low to ensure saturation of the spectrofluorometer detector did not occur whilst performing fluorescence measurements as the QDs were highly fluorescent. The atrazine concentration range used in this study [2-13 × 10^{-7} M] was relatable to the maximum contaminant limit for atrazine in water according to the World Health Organization (WHO) (Sima et al., 2014; Bo et al., 2015).

4.2.1. Optimization of reproducibility of sensing using QD@chloroform

The average fluorescence emission maximum wavelength from three replicate vials each containing 2 × 10^{-5} g/mL of QDs dispersed in chloroform (QD@chloroform) solution was found to be 597 nm. These replicate tests were essential as they showed that the QDs were homogenously dispersed in the chloroform solution.

Interaction of three QD@chloroform solutions (2 × 10^{-5} g/mL) each with atrazine (6 x 10^{-7} M) for 11 min resulted in a decrease (quenching) of the fluorescence intensity of the QDs. That is, the fluorescence intensity after adding atrazine (F) was lower than that of the QD@chloroform solution (F_0). The F/F_0 ratio, which indicates the quenching efficiency, for all three samples are shown in Table 4-3.

An average fluorescence quenching of F/F_0 = 0.80 was obtained and the calculated %RSD for the three measurements was 11%. These results showed that all three samples were quenched after the interaction and that the QD solutions reacted similarly to the introduction of atrazine.

Table 4-3: Fluorescence quenching of QD@chloroform solutions [2 × 10^{-5} g/mL] interacted with atrazine [6 × 10^{-7} M].

Trial	1	2	3
F/F_0	0.89	0.81	0.70

After this, different atrazine concentrations were tested using the same QD@chloroform stock solution (2 × 10^{-5} g/mL) by following the same methodology. Atrazine concentrations of 2, 4, 6, 8, 10 and 12 × 10^{-7} M were tested, and the results are shown in Figure 4-11. From these results it was evident that there were minimal changes in fluorescence response (F/F_0 ratio) of the QDs as a function of atrazine concentration over this small atrazine concentration range. It was also observed from these results that there was no clear linear trend in the F/F_0 response as indicated by the regression value (R^2) of 0.3767. Thus, these results prompted further investigations to better understand the interaction of atrazine with the QDs.

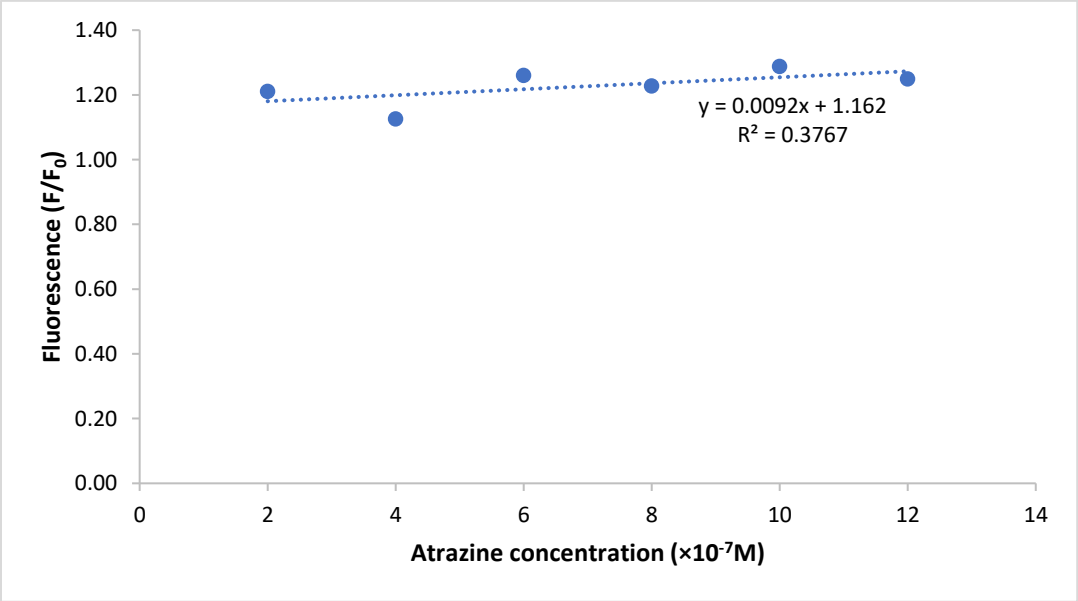

Figure 4-11: Measured fluorescence response of the QD@chloroform solution as a function of different atrazine concentrations after interaction for 11 min (λ_{ex}= 470 nm, λ_{em}= 597 nm). F_0 is the fluorescence intensity of the QD@chloroform without atrazine and F is the fluorescence intensity after interaction with atrazine.

The sample that was interacted with atrazine [2 × 10^{-7} M] then underwent repeated fluorescence measurements after interaction with atrazine, where the measurements were taken over 10 consecutive minutes. A general upward trend of the fluorescence (F/F_0) values was seen, indicating that repeated excitation led to fluorescence enhancement of the QDs, as shown in Figure 4-12. This observed trend is discussed further in Section 4.3, where literature shows that the initial fluorescence emission is enhanced under constant illumination (Zimnitsky et al., 2007), where the surface traps and dangling bonds on the surface of the QDs are reduced, which enhances the quantum yield of the QDs as surface defects in the core act as temporary 'traps' for the electron, hole or excitons, thus quenching the radiative recombination and reducing the quantum yield (QY) (Giansante & Infante, 2017; Houtepen et al., 2017; Kirkwood et al., 2018). With the study reported in the literature, the illumination was constant and not consecutive and repeated every minute as in this study, however the effect of the light would be expected to have the same impact on the QDs in this study. This implies that the QDs are stable under illumination, but that repeated fluorescence measurements should not be performed on the QDs, especially not for prolonged periods, as the surface of the QDs could be altered with each repeated measurement which may impact results. The effect of interaction time of the QDs with atrazine was investigated further, as discussed in Section 4.2.3.

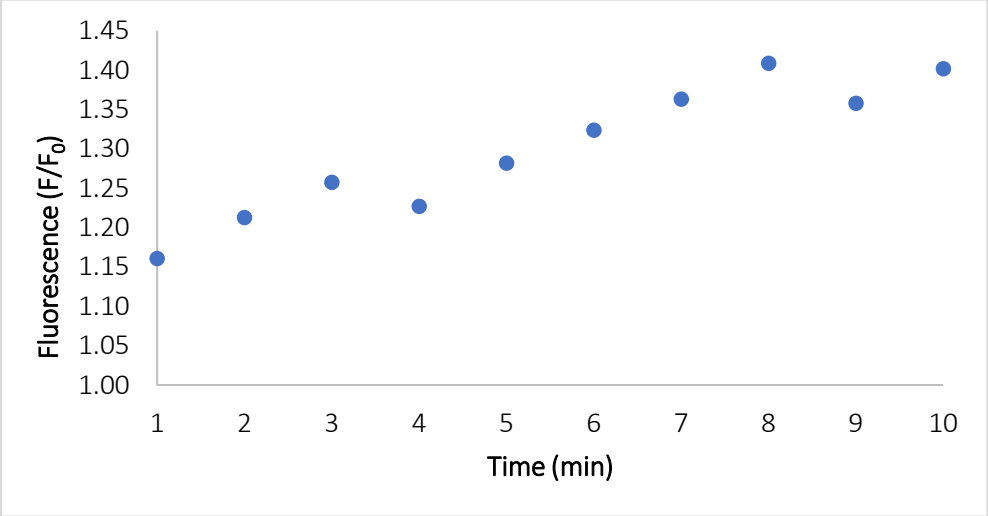

Figure 4-12: Fluorescence response of a QD@chloroform sample interacted with atrazine [2 × 10^{-7} M] over 10 min where fluorescence was measured consecutively every min for 10 min. F_0 is the fluorescence intensity of the of the QD@chloroform without atrazine and F is the fluorescence intensity after interaction with atrazine.

4.2.2. Excitation wavelength

The effect of using different excitation wavelengths on the emission spectra of the CdSeTe/ZnS QDs was investigated. The results shown in Figure 4-13 indicate that a change in excitation wavelength did not affect the maximum fluorescence emission wavelength of the C/S QDs. This result shows that the product was pure and contained QDs of a narrow size distribution, i.e. the product was of good quality. It was found that an excitation wavelength of 420 nm gave the greatest fluorescence intensity.

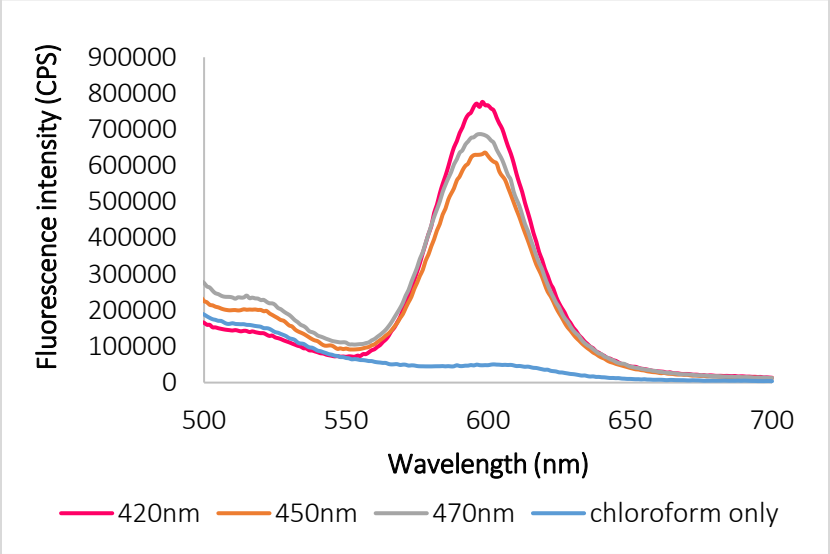

Figure 4-13: The effect of different excitation wavelengths on the measured fluorescence of the QD@chloroform solution [1 × 10^{-5} g/mL].

4.2.3. Interaction time

Figure 4-14 shows the fluorescence intensity of the QD@chloroform [1×10^{-5} g/mL] at 0 min before interaction with atrazine and the intensity at different times (5-20 min) after interaction with atrazine. The atrazine was prepared in ethanol [6×10^{-7} M], and the results show that there was fluorescence quenching upon interaction.

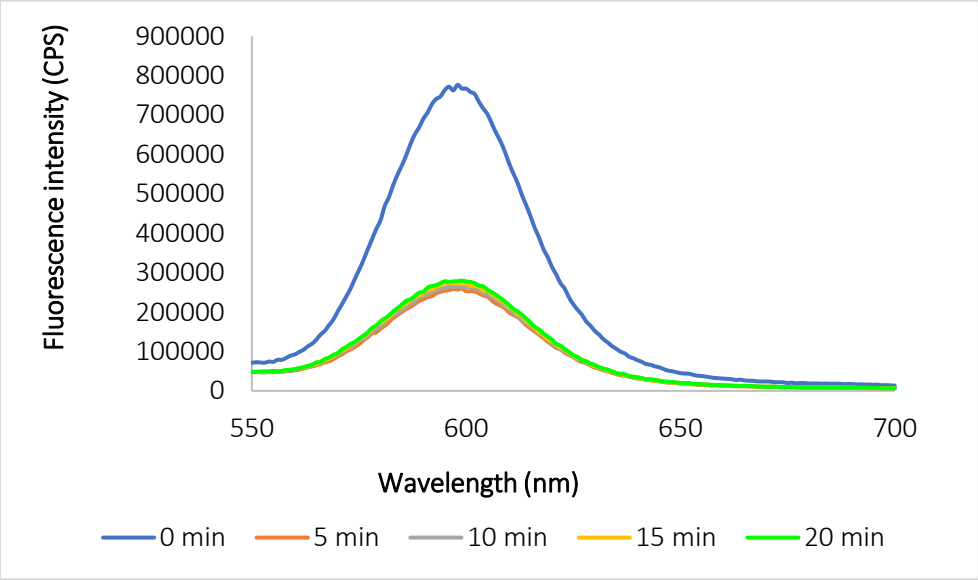

Figure 4-14: Fluorescence spectra measured of QD@chloroform [1×10^{-5} g/mL] without (0 min) and with atrazine measured over different time intervals (λ_{ex}= 470 nm, λ_{em}= 597 nm).

Figure 4-14 and Figure 4-15 show that the original fluorescence measured had an intensity of 762 690 CPS and after a 5 min interaction with atrazine the fluorescence had quenched to 258 550 CPS. Significant quenching was thus seen after 5 min interaction, with no further quenching observed with additional interaction time. It was therefore concluded that long interaction times with atrazine were not needed and that a 5 min interaction time was sufficient. After this, as shown in Figure 4-15 (on the right), for shorter interaction times of 1, 2, 3 min sufficient quenching was observed.

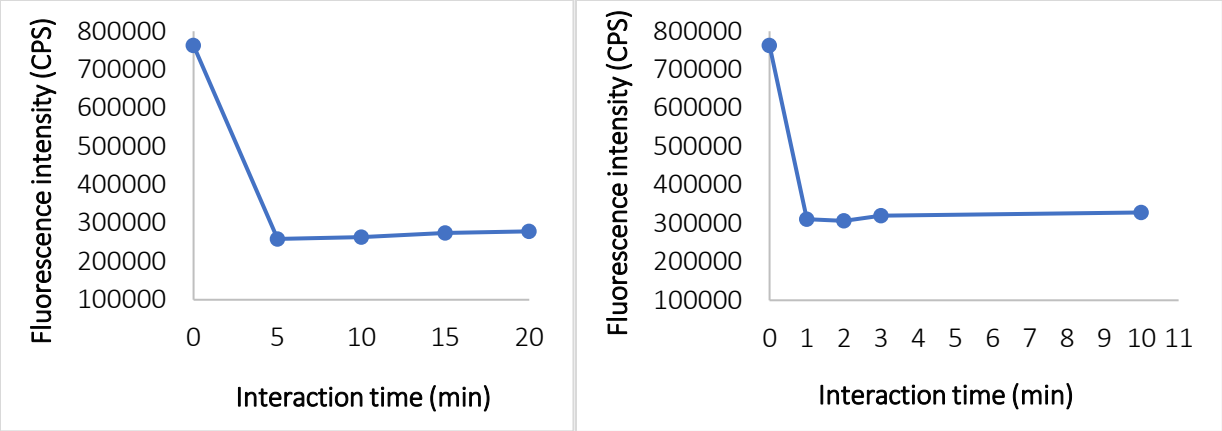

Figure 4-15: The fluorescence intensity measured versus interaction time (min) for interactions of QD@chloroform [1 × 10^{-5} g/mL] with atrazine dissolved in ethanol [6 × 10^{-7} M] after 5-20 min (left) and where the fluorescence was measured after shorter interaction times starting after 1 min (right) (λ_{ex}= 420 nm, λ_{em}= 597 nm).

From Figure 4-15 it is evident that an interaction time of 1 min was sufficient for the interaction of atrazine with the QD@chloroform solution [1 × 10^{-5} g/mL]. These results thus show proof of concept, where quenching was observed as had been previously found when these QDs overcoated with molecularly imprinted polymers (MIPs) were interacted with atrazine (Nsibande & Forbes, 2016).

4.3. Manufacture of thin films

4.3.1. Alternative methods for thin film manufacture

Depositing QDs directly on the surface of glass slides was investigated as a possible method of producing QD thin films. The film produced by this method was named “Film A”, and it was produced by completely covering a glass slide with the QD@chloroform solution [0.004 g/mL]. The idea was that as the chloroform evaporated, a thin layer (film) of QDs would remain bound or deposited on the glass slide.

The results from this method showed that, while there was a film of deposited QDs, it was not uniform as shown in Figure 4-16. This is because the so-called “coffee-ring effect” took place, which is commonly seen with drop-casting of solutions. This happens due to solvent evaporation during the film assembly that stimulates capillary flow within the drop that in turn displaces particles to the three-phase contact line (Deegan, et. Al., 1997). As a result, particle accumulation at the dry film boundaries was accelerated, and a coffee-ring was formed and observed.

It was also observed that the QDs did not have good adherence to the glass surface as the solvent evaporation forces displacing the particles were stronger than the interaction between the QDs and the glass surface. The disadvantages of this method include an inhomogeneous and non-reproducible distribution of the QDs on the glass slide surface. The "coffee-ring effect" also alters the concentration of the QDs as it is dependent on the rate of evaporation which could differ depending on external factors like ambient temperature. This could affect the concentration of QDs per area deposited on the glass slide and will alter the amount of fluorescence reaching the detector between different sensing tests. This thin film preparation method was thus deemed not fit for purpose and was not pursued any further in this study.

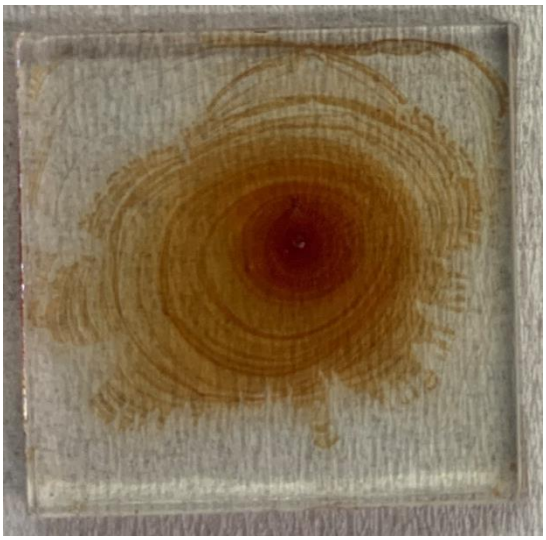

Figure 4-16: Film A on a glass slide formed from the deposition of CdSeTe/ZnS QDs solution directly onto the surface of the glass slide followed by evaporation of the solvent.

A second approach was explored where, instead of directly depositing the QDs on the glass slide, a layer of PDMS (0.5 mL) was first deposited on the slide via spin coating, followed by depositing a layer of QDs (using 400 µL of solution) on top of the PDMS layer and allowing it to dry. The slide produced this way was name "Film B". The results in Figure 4-17 (i) shows how the QD@chloroform solution covered the entire PDMS spin coated glass substrate. However, and as shown in Figure 4-17 (ii), it was observed that the QD@chloroform solution entered below the PDMS film at the edges of the glass substrate. The solution then accumulated beneath the film shown in Figure 4-17 (iii), which resulted in lifting of the PDMS from the glass slide almost entirely as the chloroform evaporated. As the film was lifted from the glass substrate, shrinkage of the film was observed. Furthermore, some of the QD@chloroform solution was still trapped

beneath the PDMS surface in patches after the film had lifted from the surface. Thus, this thin film preparation method was also deemed not fit for purpose and was not pursued further.

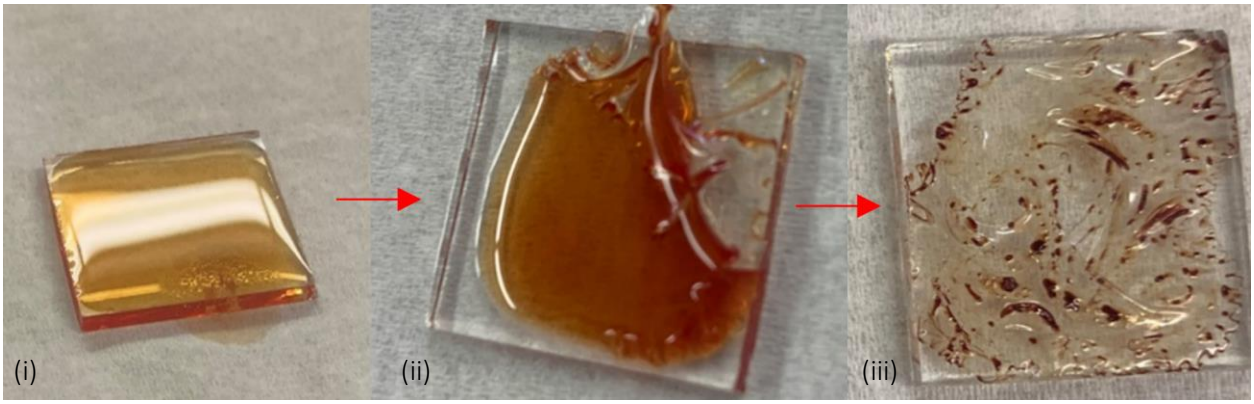

Figure 4-17: (i) QD@chloroform solution deposited over a thinly coated PDMS glass slide, (ii) where the QD@chloroform solution entered beneath the PDMS, (iii) until it had evaporated and shrinked and lifted the film from the glass substrate over ~15 min.

The third approach which was attempted to produce films was similar to the one used to obtain Film B, except that a lower spin speed (500 rpm) was used in order to obtain a thicker PDM layer on the glass substrate. The film that was obtained was labelled Film C and is shown in Figure 4-18. It was observed that when depositing QD@chloroform onto a thicker PDMS film, the distribution of QDs across the surface was not homogenous. The QDs agglomerated on top of the hydrophobic film, resulting in uneven distribution across the film surface. Furthermore, it was observed that the QD@chloroform solution started to penetrate beneath the PDMS film at the edge of the film but at a much slower rate than what was observed with film B. Therefore, this method was also deemed not appropriate for the intended application.

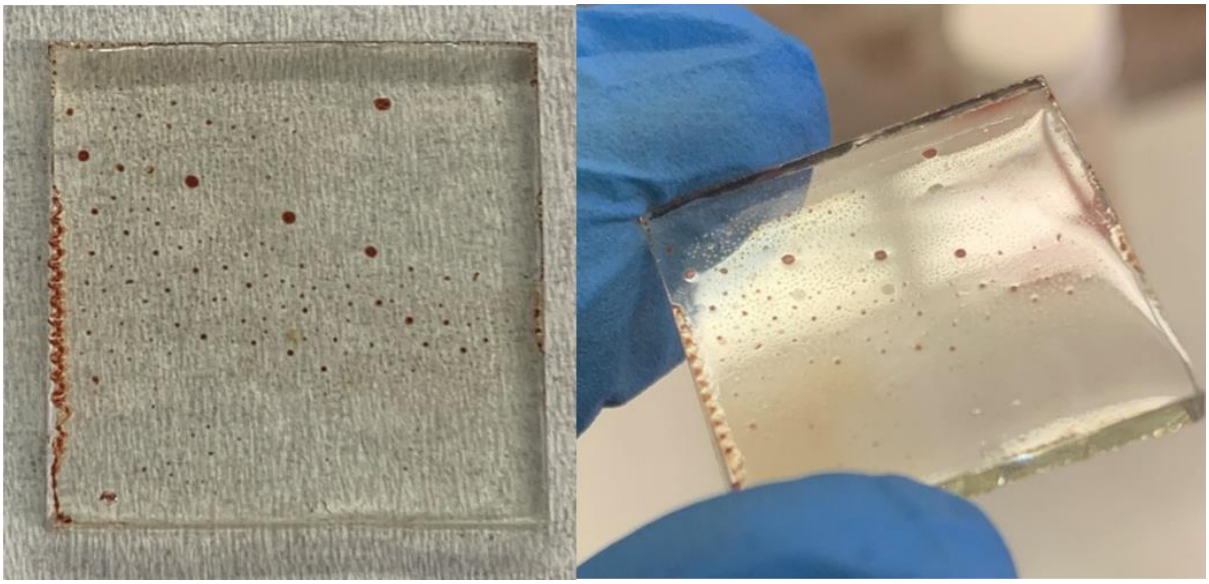

Figure 4-18: Film C prepared by drop casting QD@chloroform solution directly onto the surface of a clear PDMS covered glass slide after being allowed to dry.

These three preliminary methods for producing films resulted in inconsistent films with inhomogeneous distributions of QDs over the surface. As a result, it was decided to rather immobilize QDs inside the PDMS using spin coating, as this is a facile means of thin film preparation which should also assist in ensuring good homogeneity of QDs within the manufactured films.

4.3.2. Initial immobilization of QDs in PDMS thin films

Following the unsatisfactory outcomes as described in Section 4.3.1, a different approach (described in Section 3.5.2) was attempted, which involved mixing the QDs into the PDMS matrix before spin coating it onto a silicon wafer substrate. Polyacrylic acid (PAA) was to be used as a sacrificial layer on the silicon wafer before spin coating the QD@PDMS mixture. However, as seen in Figure 4-19, it was evident that the distribution of the polyacrylic acid (PAA) layer over the 4-inch silicon wafer was not homogenous, which meant that the PDMS would be directly in contact with the substrate rather than the PAA layer. Thus, the removal of the PDMS film from the substrate after spin coating was compromised as it caused the film to tear and not lift from the silicon wafer as expected.

Figure 4-19: Inhomogeneous, cured PAA layer on top of a 4-inch silicon wafer.

Therefore, the use of silicon wafers as substrates for producing the films was eliminated due to the described challenges with PAA. Instead, microscope glass slides (initially cut by hand in laboratory, no specific dimensions) were used as substrates onto which the PDMs films were prepared. These proved to be suitable as they fitted directly into the fluorescence spectrophotometer solid-state sample holder. The films were thus made directly on top of the glass microscope slides and it was observed that the films could be easily removed without tearing using a scalpel and tweezers. Another advantage of this approach was that the size of the films produced on the glass slides was small and could be used directly for sensing applications. Moreover, removing the films from the glass substrate was deemed not necessary as it increased the difficulty in handling the films, whereas the glass substrate provided a good support and could be used inside the solid-state sample holder of the spectrophotometer.

A number of trials were carried out to optimize the spin coating deposition of thin films on the glass slides and the following discussion focusses on the outcomes of those trials. It is important to note that while the first 10 films (films 1 – 10) were made on glass slides, PAA was still used in an attempt to have the films lift off the glass slide. None of the films in Table 4-4 were of a sufficiently good standard for sensing applications.

Table 4-4 shows the first five films where films 1, 2 and 5 consisted of multiple layers of PDMS. Film 3 was produced using a lower spin speed (200 rpm) which produced a film that was thicker resulting in big bubbles forming in the film whilst curing on the hot plate. Film 4 was the thinnest (lowest number of layers, had one layer of PDMS and was produced using a high spin speed of 500 rpm) and was cured at 150^{o}C for 4 min. However, it also had a big area in the middle of the film which did not contain an appreciable amount of

QDs, thus the film was inhomogeneous. None of the films in Table 4-4 were of a sufficiently good standard for sensing applications.

Table 4-4: QD thin films 1-5 upon visual inspection under UV light.

Film number	1	2	3	4	5
Image	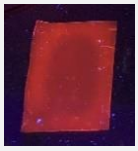	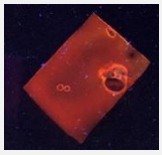	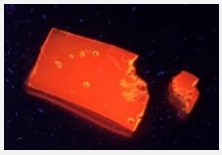	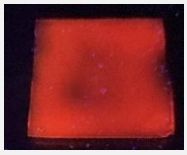	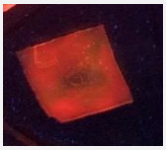
Number of PDMS layers	2	3	1	1	3
Spin coating speed (rpm)	500	500	200	500	500

Table 4-5 shows films 6 to 10 which were prepared on glass slides that were pre-coated with a PAA layer followed by one layer of PDMS as previously described. These films were also cured on a hot plate which was covered with aluminium foil to protect it from chemical spills in the laboratory. It was observed, however, that the use of aluminium foil caused the films to cure at a slight angle, therefore the aluminium foil was removed to improve homogeneity in thickness of the films. Film 10 cured slightly better with the least number of bubbles. A lower acceleration was used for film 10 which resulted in a more homogeneous distribution of QDs in the middle of the film. None of these films were, however, of a sufficiently good standard for sensing applications.

Table 4-5: QD thin films 6-10 upon visual inspection under UV light.

Film number	6	7	8	9	10
Image	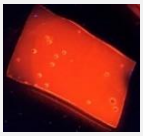	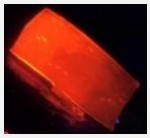	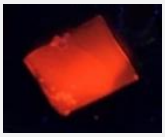	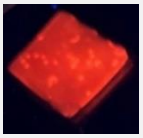	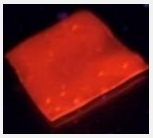
Spin coating speed (rpm)	300	300	400	400	500
Spin acceleration (rpm/s)	200	300	200	300	200

In a bid to improve the method, films 11 to 14 were prepared following the same procedure but without the use of PAA. Films 11 to 14 were thinner, but the higher spin speeds and accelerations led to uneven QD distribution over the films as shown in Table 4-6. Film 14 had the best QD distribution inside the film, although it had a significant amount of bubbles, which was not ideal, therefore this was optimized by adjusting the curing temperature and time.

Table 4-6: QD thin films 11-14 upon visual inspection under UV light.

Film number	11	12	13	14
Image	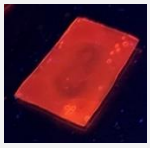	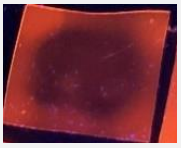	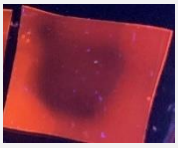	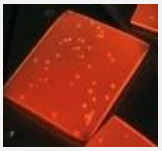

From these initial experiments it was observed that films that were thicker produced more bubbles than thinner films while curing on the hot plate. It was also found that when the acceleration rate was too high

(500 rpm/s), it increased the absence of QDs in the middle of the film. The ideal film should not have entrained bubbles, and it should have a QD distribution that is homogeneous throughout the film.

Following these unsatisfactory results, new glass slides with more precise dimensions (20 mm x 20 mm x 2 mm) were used to make films 15 to 24 based on the spin coating parameters indicated in Table 3-2. As shown in Table 4-7, it was observed that as spin speed was increased, from film 15 to 17, the film thickness decreased and the number of bubbles formed in the films during curing reduced. The same was observed with films 18 and 19. These films were not removed from the glass slides and were used with the glass substrate as support. It was found that this worked well in taking measurements with the spectrophotometer, as the films attached to the glass had increased robustness and were easier to handle.

Table 4-7: QD thin films 15-19 upon visual inspection under UV light.

Film number	15	16	17	18	19
Image	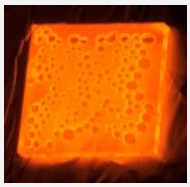	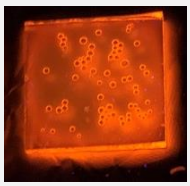	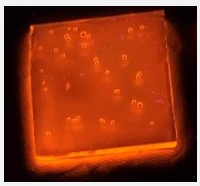	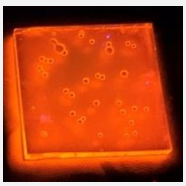	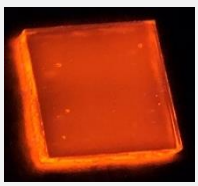
Spin coating speed (rpm) for 10 s	100	300	500	300	500
Spin acceleration (rpm/s)	100	100	100	200	200

Bubbles present in different films were observed and compared under UV light, where neither small or large bubbles observed with the eye were desired. The same trend regarding bubble formation was seen when films 20-21 and 21-24 were compared as shown in Table 4-8.

Table 4-8: QD thin films 20-24 upon visual inspection under UV light.

Film number	20	21	22	23	24
Image	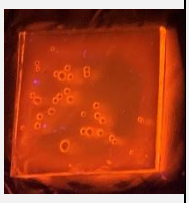	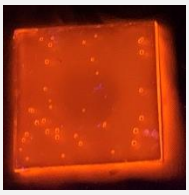	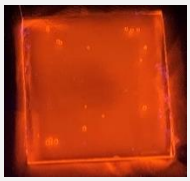	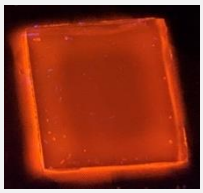	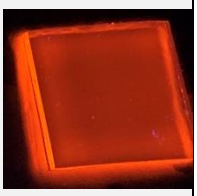
Spin speed (rpm) for 10 s	300	500	500	800	1000
Spin acceleration (rpm/s)	300	300	400	400	600

From all these films, four films (namely films 19, 21, 23 and 24) were chosen for further testing because these films had a good, homogeneous distribution of QDs. Replicates of each of these films were thus produced. Good reproducibility was noted upon visual comparison of the films from each batch under UV light, with homogenous QD dispersions throughout the films, as observed from the even fluorescence emission throughout the material when illuminated under a UV lamp.

4.3.3. The effect of curing temperature on thicker films

Replicates of film 16 were prepared and used to investigate the effect of curing temperature on films, as seen from the images captured under normal and UV light in Figure 4-20. There was a visible trend in that more bubbles formed with an increase in curing temperature for the thicker films. It should be noted that the films cured at lower temperatures may not have cured completely, especially after 4 min of curing. This does not apply to thinner films, as it was seen that thinner films cured without bubble formation even at higher temperatures of 150^{o}C.

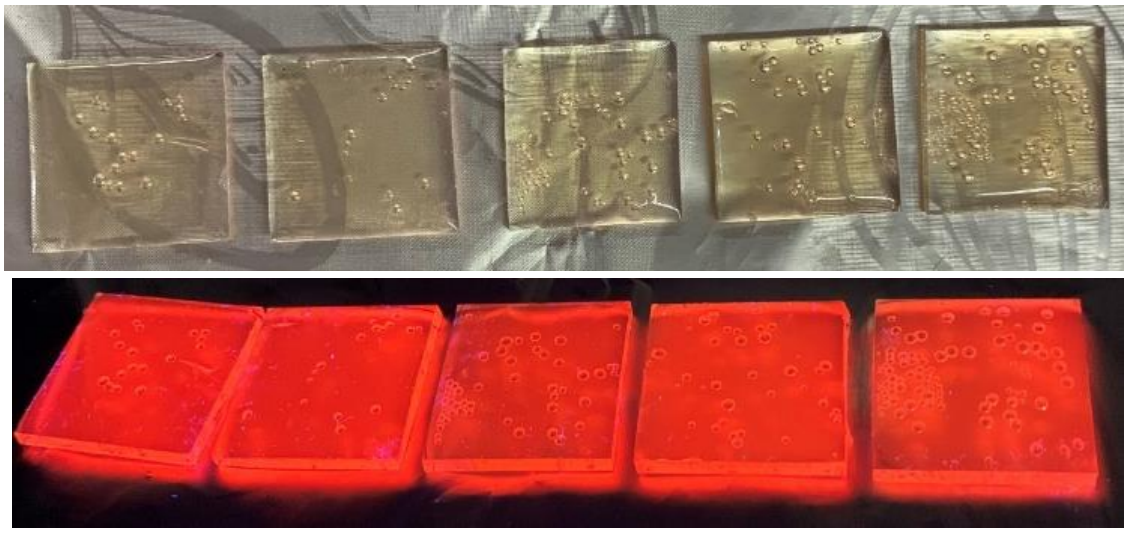

Figure 4-20: The effect of curing temperatures on a thicker film (batch of film 16) upon visual inspection under normal light (top) and UV light (bottom). From left to right the curing temperatures were 80, 100, 130, 150 and 170°C. These films have approximately 17, 17, 54, 47 and 91 bubbles, respectively.

From Figure 4-21 it is seen that there was a clear correlation between the curing temperature of a thicker film, and the amount of bubbles that had formed (R^2= 0.85). This is opposed to the behaviour of the thinner films (batch 21), where there were no bubbles present after curing.

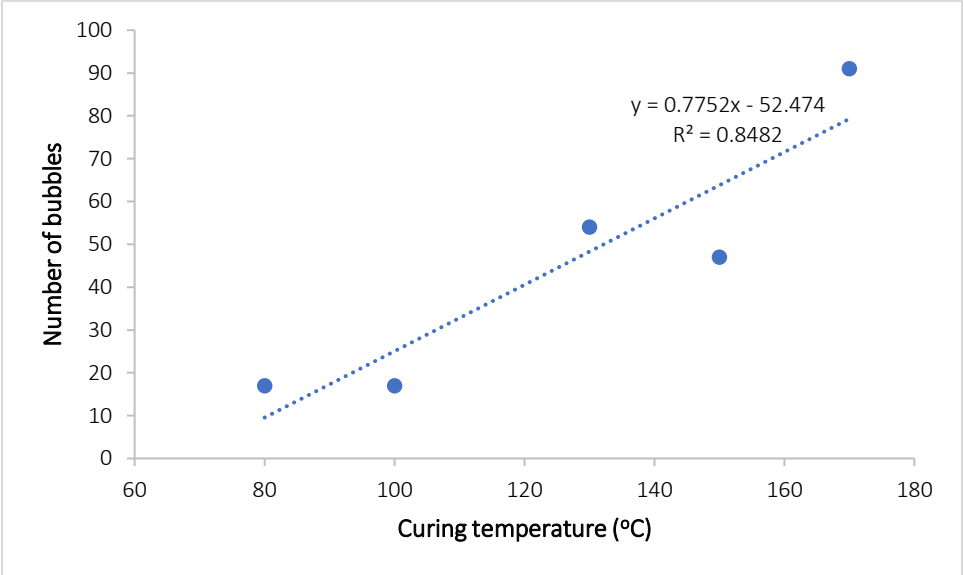

Figure 4-21: The curing temperature versus the number of bubbles formed in a thicker film (batch of film 16).

4.3.4. Preliminary testing of thin films with atrazine

The four films (films 19, 21, 23 and 24) that were showing promising results in terms of homogeneity of the QD distribution after spin coating were used to conduct preliminary atrazine detection (sensing) tests. To conduct the tests, replicates of each of these films were produced using the spin coating parameters shown in Table 4-9. Films 19, 21 were tested using atrazine concentrations in the $9 - 13 \times 10^{-7}$ M range, while film 24 was tested using atrazine concentration in the $4 - 12 \times 10^{-7}$ range. The wider concentration range for film 24 was investigated since it was substantially thinner than the rest of the films due to the high spinning speeds (1000 rpm) that were used during its production.

The excitation wavelength for all the films was 400 nm. When the QDs were in solution, the maximum emission wavelength was ~597 nm, whilst when they were immobilized in PDMS, the maximum emission wavelength red-shifted to ~603- 607 nm for films of batch 24. Other film batches had maximum emission wavelengths up to 610 nm, and it was decided to work with a maximum emission wavelength of 610 nm for all films for simplicity and standardization reasons. The films of batch 24 cannot be directly compared to batch 19, 21 and 23 (for which slit widths of 2 nm were used) because film 24 was a lot thinner, therefore a slit width of 3 nm was employed to enhance fluorescence detection.

Table 4-9: Parameters used for films 19, 21, 23, and 24. All the films were prepared using 1 mL QD@PDMS solution and curing was done for 4 min.

Film number	19	21	23	24
Spin speed (rpm) for 10 s	500	500	800	1000
Spin acceleration (rpm/s)	200	300	400	600
Curing temperature ^{o}C	100	100	150	150
PL max	λ_{em}= 610 nm	λ_{em}= 610 nm	λ_{em}= 610 nm	λ_{em}= 605 nm

The fluorescence response results for the different film batches are shown in Figure 4-22**.** For illustrative purposes, the x-axis is presented as atrazine concentrations of ($\times 10^{-6}$ M). For film 24, there was an initial increase in fluorescence as the atrazine concentration was increased from 4 to 8 × 10^{-7} M. However, this was followed by an almost linear decrease from 8 to 12 × 10^{-7} M. Film 19 showed no clear correlation of the fluorescence response to change in atrazine concentration.

Films 21 and 23 showed a clear downward trend (quenching) of fluorescence of the immobilized QDs in the films as the concentration of atrazine increased. It can be noted, however, that for film 23 the data point at 10 × 10^{-7} could be a possible outlier. It can be observed for film 21 that there was a linear response with an R^2 value of 0.87. It is important to note that this is a similar response (quenching) that was observed when the QDs were used directly to detect atrazine (i.e., before mixing with PDMS) as shown in Section 4.2 – albeit with different sensitivity (slope)). This result is therefore a "proof of concept" and shows the potential of immobilized QDs to function as a sensor that responds to changes in atrazine concentrations. The different responses in the films (19, 21, 23 and 24) may be attributed to the different parameters used to prepare the films. This, therefore, highlights the importance of optimizing and standardising film manufacturing parameters.

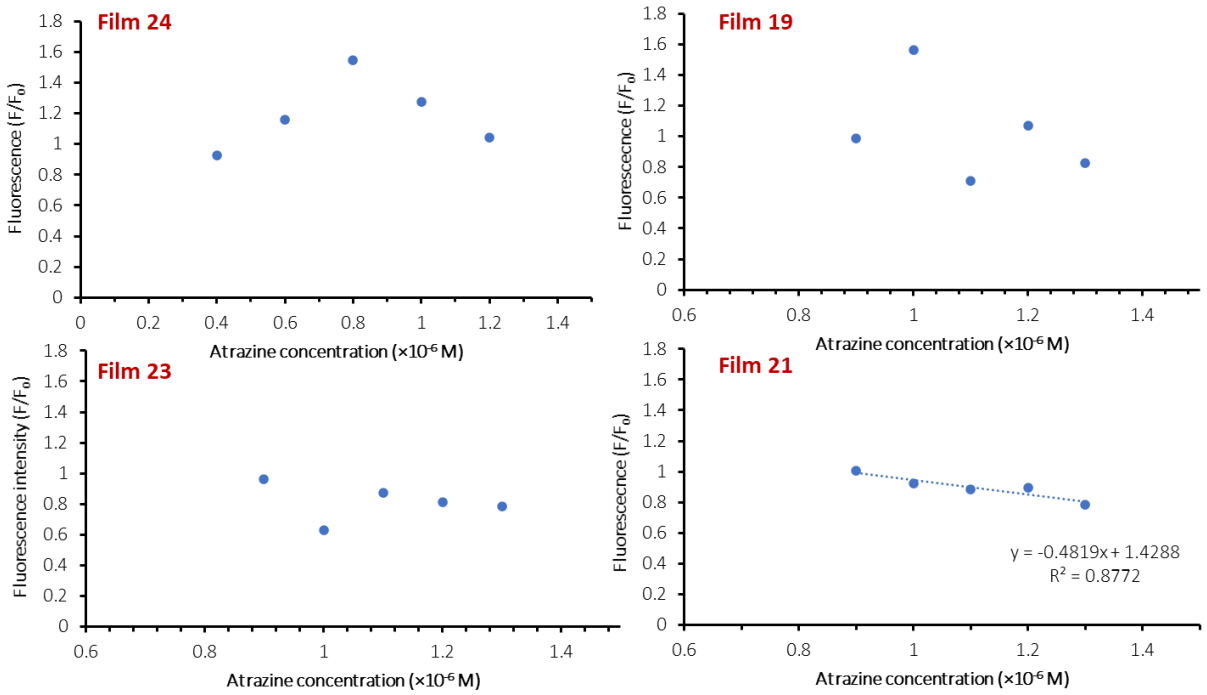

Figure 4-22: Fluorescence response (F/F_0) of the different batches of films 19, 21, 23 and 24 to atrazine concentrations 4 to 12 × 10^{-7} M (0.4 to 1.3 × 10^{-6} M).

Figure 4-23 shows that all the films had a homogenous distribution of QDs across the glass substrates. A closer look at film 24, which is the thinnest, shows QD accumulation at the edge of the film as it spun at high speeds and removing the material from the centre, and was then cured in this position (at the edge of the film). It was also observed that film batch 21 had the best distribution of QDs over the surface and did not have a greater accumulation of QDs at the edge of the film which was desired.

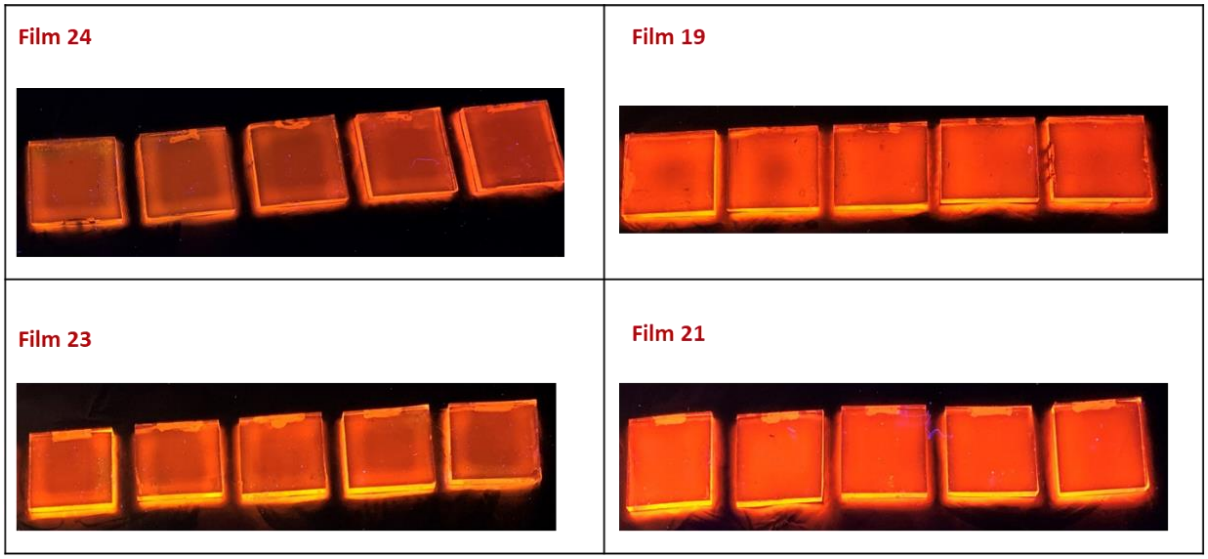

Figure 4-23: Photographs of the fluorescent film batches as viewed under UV light.

Figure 4-24 shows the film 21 batch under normal and UV light. The spin coating parameters that were used to produce film 21 were used to manufacture the rest of the films tested in this study. Under normal light, the films appear transparent, with a very slight orange tint, whilst under UV light bright fluorescent films were observed with a very good even distribution of QDs over the surface of the glass.

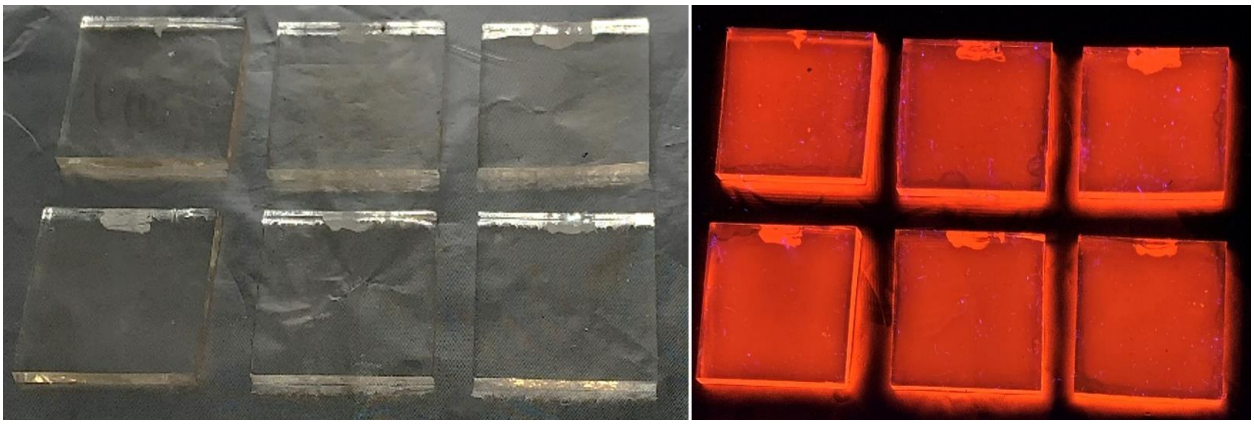

Figure 4-24: Film batch 21 upon visual inspection under normal light (left) and under UV light (right), respectively.

4.3.5. Fluorescence reproducibility over the thin films

To more accurately compare the four films for reproducibility, the average maximum emission wavelength of each film was used, and the fluorescence emission was measured over 10 different spots over each film

surface as shown in Section 3.5.6. It was observed from Table 4-25 that film 19, which had the lowest spin speeds and acceleration, produced a film which was thicker and contained more QDs, as the fluorescence response was the highest. It was also noted that an increase in spin speed and acceleration produced thinner films with lower fluorescence emission intensities over the ten spots. It was observed that there was variation between the measured fluorescence over the 10 spots (within each film) which could indicate that the films had differences in QD concentration due to variations in QD distribution. It was observed that the thickest film (film 19) had the largest range of values in QD concentration over the 10 spots, as observed from the differences in the measured fluorescence emission intensities. This could also be because the thicker film had more QD@PDMS on the glass slide, and it took longer to dry thus the QDs were able to spread over the glass slide during the drying process. Spot numbers 1-5 (which were on the edge of the glass slide) had on average higher fluorescence than 6-10 which were located more centrally on the film for the thicker film (batch 19). It was also observed that film batch 21 had the most stable fluorescence measured over the 10 spots with a %RSD of 8%.

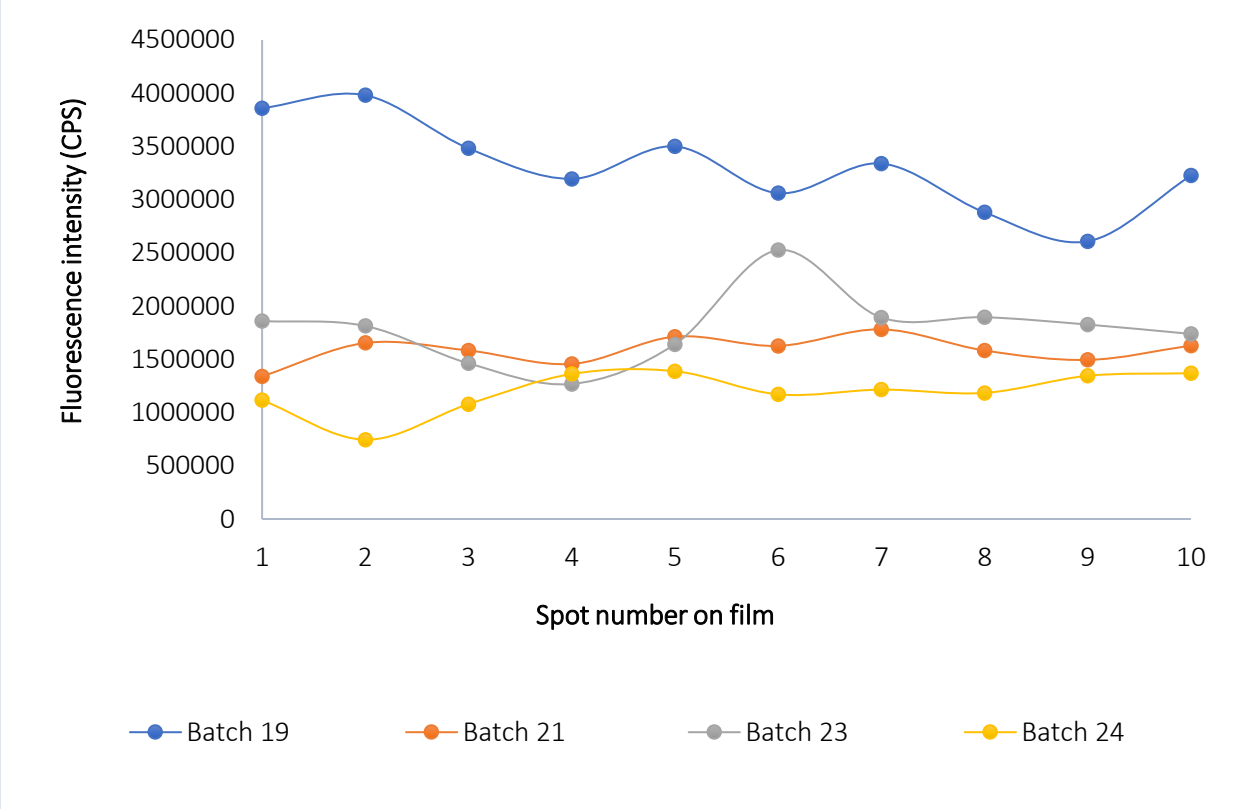

Figure 4-25: Comparison of the fluorescence emission (CPS) from films of different batches 19, 21, 23 and 24 over ten different spots on each film.

4.3.6. Consecutive short interval (1 min) photostability tests

The photostability experiment was done to observe the effect of repeated exposure to radiation on the fluorescence intensity of three identical films, namely LQD films from batch 21. Consecutive photoradiation (400 nm) was done over a 30 min period and then over extended time intervals for each film as shown in Figure 4-26. The results show that the film had great photostability with minimum fluctuations in the first 30 min followed by a slight decrease over an extended irradiation time – this trend was observed for all three films as shown in Figure 4-26.

The relatively high fluorescence intensity for film 3 was due to a slight modification in the positioning of the film in the spectrofluorometer instrument. After measuring the fluorescence of films 1 and 2 (which only had two cardboard supports behind the glass slides in the spectrophotometer), the fluorescence was further optimized by placing a third cardboard piece behind the film 3, and a dramatic increase in fluorescence was observed with the same trend as for films 1 and 2. This could be that more radiation was able to reach the detector with the additional cardboard piece added behind film 3 and that the big variation observed between the fluorescence measurements of films 1 and 2 as compared to film 3, as shown in Figure 4-26, was because it resulted in a better angle of incidence and detection inside the instrument, with less reflection losses. It was thus important to always keep all films flush with the sample holder to avoid variation in light scattering and reflection.

The trend observed was that in the first 20-25 min of irradiation, there was a slight increase in fluorescence observed after every consecutive measurement and thereafter the increase stabilised. At 30 min, the time between consecutive measurements was increased to 5 min which caused a decrease in fluorescence. The biggest decrease in fluorescence was observed with film 3 where the fluorescence decreased by 12% from 50 min (PL intensity = 1 592 330 CPS) to 100 min (PL intensity = 1 393 830 CPS) with 50 min between the two measurements. This showed a significant amount of relaxation after an increased amount of time between measurements. The additional measurements of film 3 are shown in the graph inserted in the right corner of Figure 4-26 for clarity.

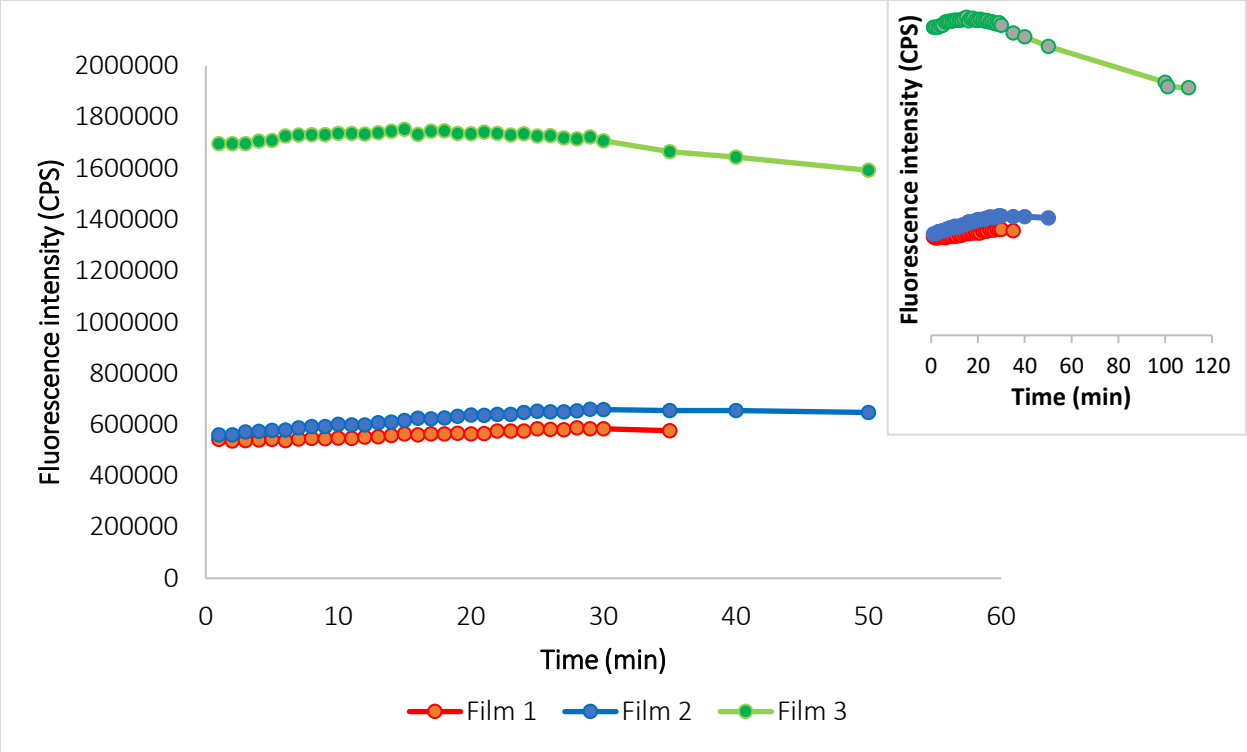

Figure 4-26: The effect of repeated exposure to excitation radiation on the photostability of LQD thin films when measuring the fluorescence every consecutive minute (λ_{ex}= 400 nm, λ_{em}= 610 nm, 2 nm slit widths). The inserted graph in the right corner shows the additional measurements taken at 100, 101 and 110 min for film 3.

It was observed in Figure 4-26 that repeated fluorescence exposure did not cause an immediate degradation of the QDs and that photobleaching did not immediately occur within the QD film structure. There were differences obtained when measurements were consecutively measured, but it is known that QD fluorescence emission under constant excitation may constantly change and turn on and off intermittently, due to the blinking effect of QDs and the differences in excited states between electrons of different QDs and therefore in the emission of energy during the process. The charge can also be trapped in the adjacent matrix, which would be the polymer in this case, which can alter the duration of the blinking effect (Kudera, 2008). With every fluorescence measurement taken, the light emitted from the QDs is able to scatter in different directions and this can also affect the amount of light reaching the fluorescence detector. It was thus of interest to determine after what period of time the repeated radiation exposure generated the most constant fluorescence emission (first 20- 30 min) in order to use that as a guideline when choosing the optimal interaction time to observe changes in fluorescence when attempting to detect

organic pollutants in water using the thin films. This also showed that the films are potentially reusable as they are photostable.

4.3.7. Consecutive long interval photostability tests

Figure 4-27 shows the measured fluorescence emission every 30 min from a LQD thin film from batch 21. It was evident that there was a repeated decrease in fluorescence emission intensity.

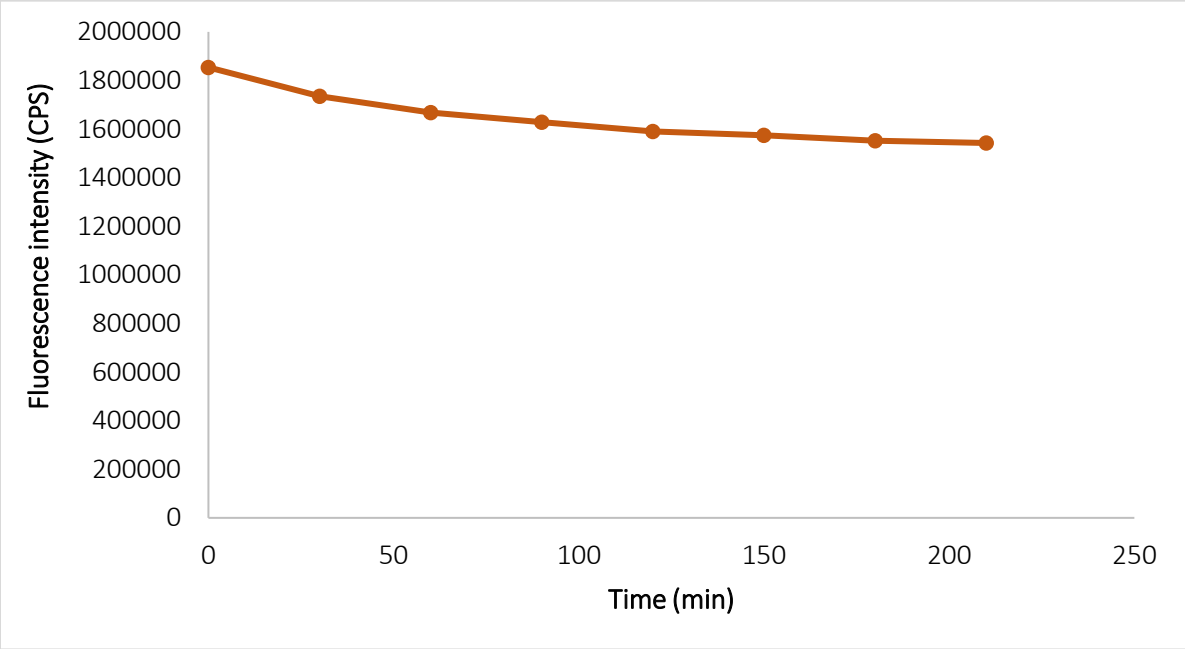

Figure 4-27: The effect of repeated exposure to excitation radiation on the photostability of LQD thin films when measuring the fluorescence every consecutive 30 min (λ_{ex}= 400 nm, λ_{em}= 610 nm, 2 nm slit widths).

Figure 4-28 shows the measured fluorescence repeatedly on one film every 55 min, with a 5 min waiting period after each measurement to determine the impact of repeated short (5 min) and longer (55 min) interval measurements. From 0-5, 120-125, 180-185 and 300-305 min, an increase in fluorescence emission intensity was observed and at 60-65 and 240-245 min a decrease in fluorescence was observed in the short-term (5 min) fluorescence. These differences were however less than 1% of the measured decrease in hourly fluorescence intensities (CPS). When considering fluorescence measurements over each hour, it was seen that from 0-60 min there was a 9% decrease and from 60-120 min there was a further 11% decrease. From 120-180, 180-240, and 240-300 min additional decreases of 5, 2, 3 and 7% were seen, respectively.

Thereafter another decrease of 6% was found after four days and 30 min (a total of 5 790 min) which indicated a somewhat reduced effect over longer time periods.

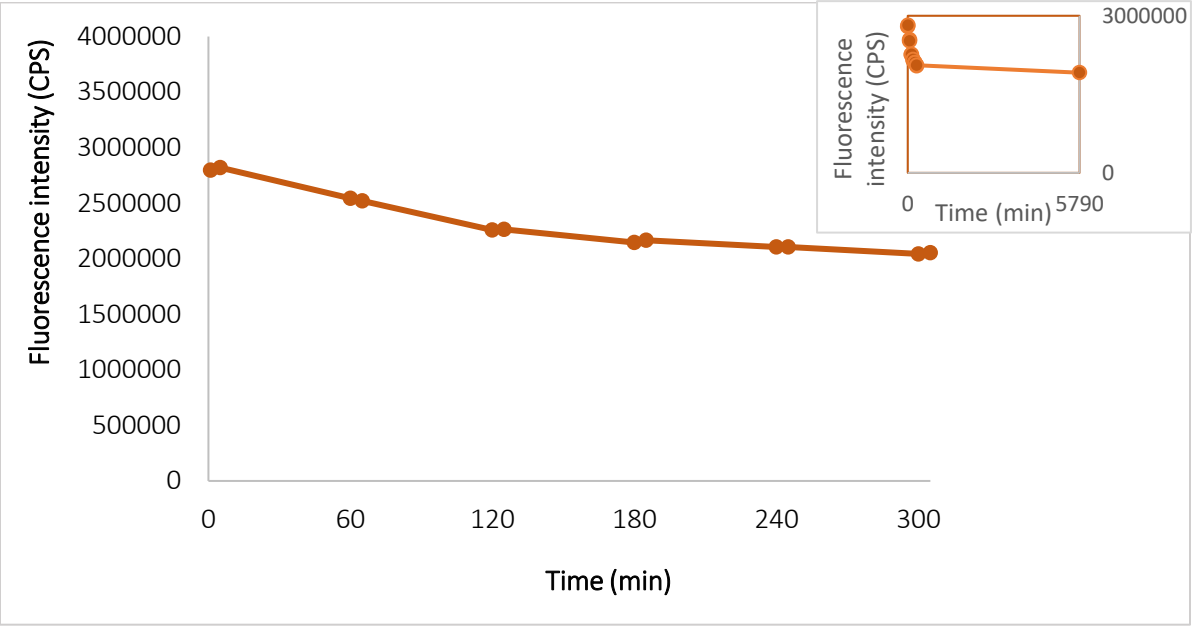

Figure 4-28: The effect of repeated exposure to excitation radiation over time on the photostability of LQD thin films when measuring the fluorescence every 55 min, with a 5 min waiting period after each measurement to determine the impact of repeated short (5 min) and longer (55 min) interval measurements (λ_{ex}= 400 nm, λ_{em}= 610 nm, 2 nm slit widths). The inserted graph in the right corner shows an additional fluorescence measurement after 5790 min.

These results can be linked to literature, where continuous UV illumination of water soluble thioacetic acid (TAA) covered CdSe/ZnS QDs resulted in a first stage during which the number of surface defects and roughness decreases, resulting in a photoemission increase. Then in the second stage, the QD size decreases due to photobleaching after continuous illumination, resulting in a decrease in intensity (Zimnitsky et al., 2007). Several recent studies revealed temporal evolution of the PL intensity of QDs under constant illumination by UV and ambient light (Wang et al, 2004 and Komaralal, et al., 2006 and Cordero, et al., 2000). With repeated excitation radiation exposure, it was seen that when the fluorescence was measured every min, there was an increase observed in the fluorescence intensity for ~20 min, whereafter there was a decline for the short interval photostability tests (Figure 4-27).

The longer interval photostability tests (Figure 4-28) showed a decrease when fluorescence was measured at intervals longer than ~20 min, which could mean that after each single illumination, there is an increase

in fluorescence as electrons are excited, whilst after 20-30 min the electrons relaxed and non-radiative emission of energy to the QD environment resulted in a decrease in measured fluorescence. From these results it was shown that the fluorescence was the most stable between consecutive short interval measurements of 1 min and that larger differences in fluorescence were obtained when fluorescence was measured over intervals longer than ~20 min. This indicates that it is crucial to measure the initial fluorescence F_0 before each sample interaction and measurement of F, and not just directly after film manufacture.

4.3.8. The effect of excitation wavelength on the fluorescence of QD@PDMS films

Figure 4-29 shows the different excitation wavelengths tested (340, 380, 400 and 420 nm) and the measured fluorescence intensity values obtained for QD@PDMS films at each of these wavelengths. The maximum emission wavelength was observed at 610 nm for the excitation wavelengths of 400, 380 and 340 nm and a maximum emission wavelength 611 nm was observed when a 420 nm excitation wavelength was used. This showed that 400 nm was the optimum wavelength to excite the QD@PDMS film with, as it resulted in the greatest fluorescence emission intensity.

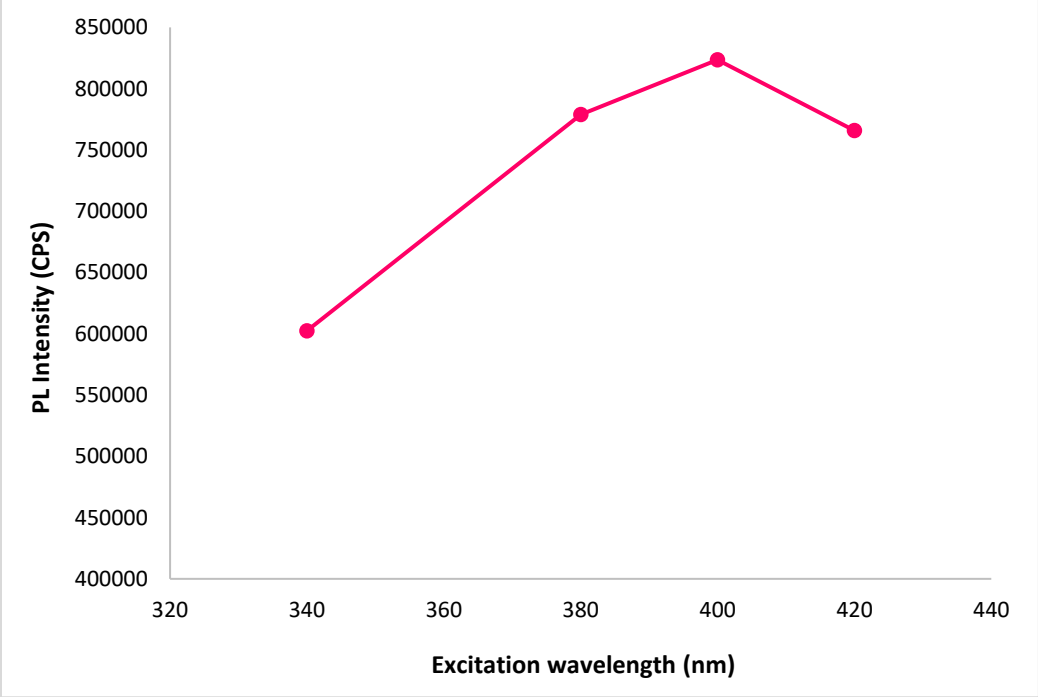

Figure 4-29: Excitation wavelength and fluorescence intensity values of QD@PDMS films obtained at that excitation wavelength.

4.4. Optimized films of varying QD concentrations

4.4.1. LQD and HQD films

A comparison of the LQD films and HQD films is shown in Figure 4-30. It can be observed that both films were transparent under normal light and the HQD film was slightly more orange than the LQD film. Both films had a strong fluorescence emission under UV light but the HQD film had a brighter fluorescence as observed with the eye and gave a higher fluorescence intensity when measured with the spectrophotometer. This high fluorescence intensity of the HQD films was to be expected due to the higher quantum dot loading (0.008 g/mL). The slit widths used to measure fluorescence still needed optimization to determine a single slit width which could be used to detect organic pollutants and to compare films. The spectral comparison of the relative fluorescence is shown later in the discussion of Figure 4-35.

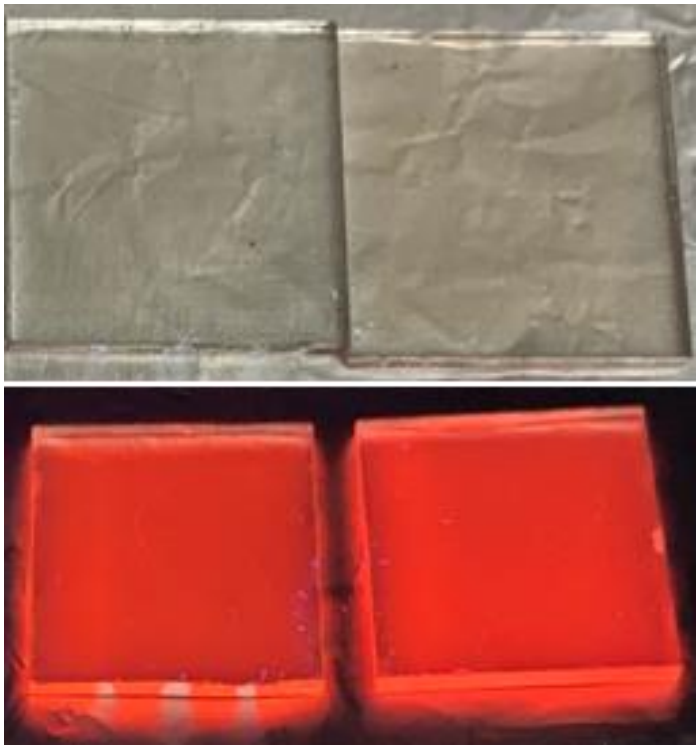

Figure 4-30: Optimized QD thin films upon visual inspection under normal light (top) and UV light (bottom) with LQD and HQD films on the left and right respectively.

4.4.2. Film thickness

The thickness of some optimized films was measured, where the only difference in the films was the QD concentration therein. Film A, B and C were HQD films which were characterized by HRSEM to determine

their thickness as described in Section 3.2.6. and shown in Figure 4-31. For these films, a diamond blade was used to score the glass substrate before breaking the films under nitrogen and this worked very effectively. Films A, B and C broke better than films D-H for which a diamond etching pen was used. Films A-C therefore had a greater number of suitable cross section regions available from which to determine the thickness using ImageJ (N= 200), whereas the measurements taken for films D-H, as shown in Figure 4-32, had fewer suitable regions (N= 19-54).

Films A, B and C were HQD replicates of each other and had average thicknesses of 297.3, 256.5 and 263.7 µm with %RSDs in thickness across the films of 3.3, 3.3 and 3.6%, respectively. The average film thickness for these HQD films was 272.5 µm (N= 3, %RSD= 3.4%) All measurements were taken randomly over the cross sections of the films and had very low %RSD over the cross sections, which shows that spin coating was an effective method to produce films with reproducible and equivalent thicknesses.

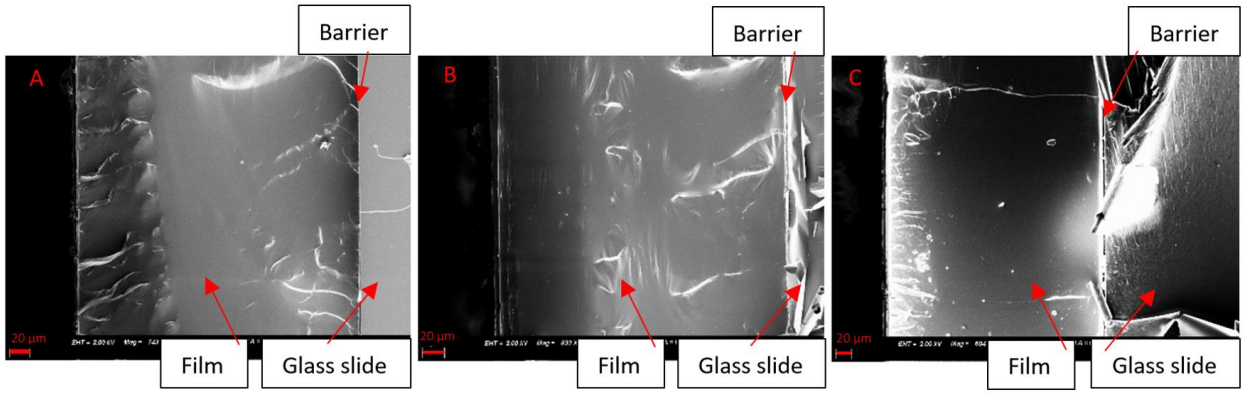

Figure 4-31: The cross sections of HQD film A, B and C as viewed under a HRSEM microscope to measure the thickness of the films examined at a magnification of ~1000x with 20 µm scale bars.

Of the five films shown in Figure 4-32, D-F were three HQD films with thicknesses of 307.4, 251.8 and 309.6 µm. The average film thickness for the HQD films was 281.0 µm (N= 6, %RSD= 9.5%) which indicated a small %RSD over different films produced with the same method. The thickness of the LQD film was 250.4 µm which was similar to the thickness obtained for two of the HQD films (256.5 and 251.8 µm), whilst the film which contained no QDs had a thickness of 437.7 µm. The thicknesses measured over each film had little variation with all %RSDs under 4.5%, which shows that these films were also produced with consistent thicknesses. As there was variability in the HQD films ranging from 251.8 to 309.6 µm, the

average of all HQD and the LQD (250.4 µm) was obtained, and this was used to determine the concentration of the QDs inside the thin films as described in Section 4.4.3.

It was seen that the film which contained no QDs had a substantially increased film thickness compared to the other films which contained QDs. This verifies that when adding QDs to the PDMS solution, the viscosity thereof was reduced, therefore the solution flowed more easily when spin coating the QD@PMDS over the glass slide leading to a thinner film produced when QDs were added to the PDMS and curing agent mixture. This effect was also observed when working in the laboratory where the PDMS solution which contained no QDs had more resistance to flow than solutions which contained QDs.

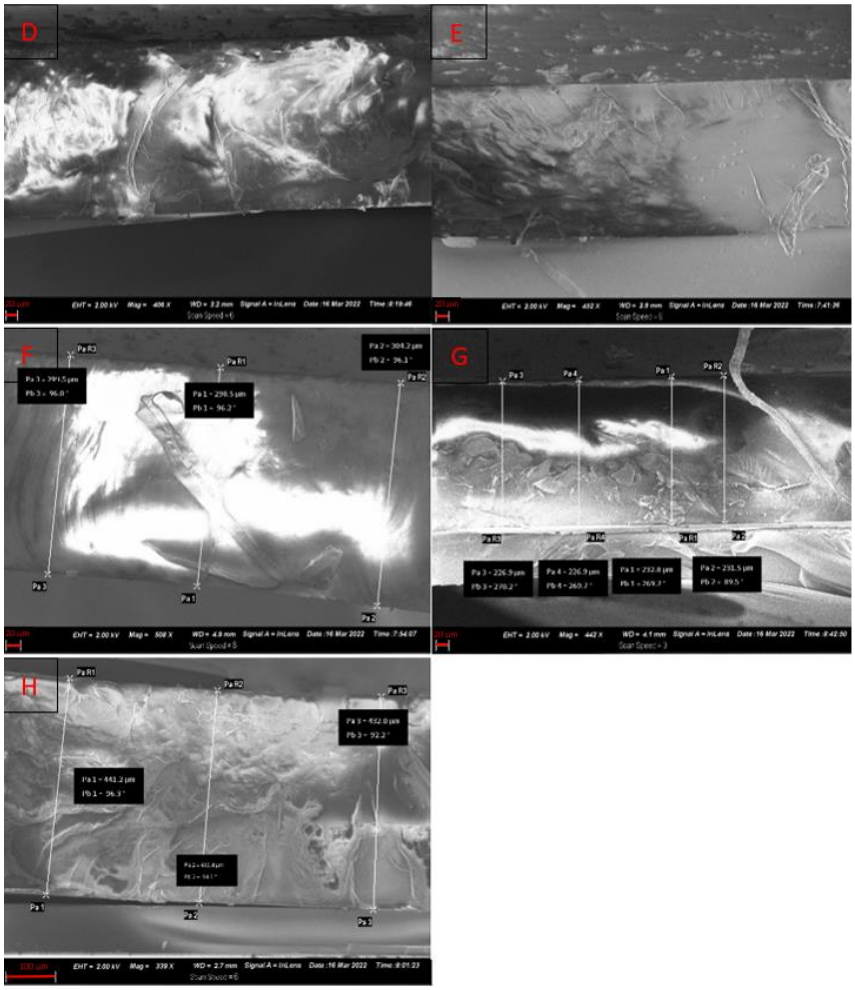

Figure 4-32: The cross sections of films D-H as viewed under a HRSEM microscope to measure the thickness of the films examined at a magnification of ~1000x with 20 µm (D-G) and 100 µm (H) scale bars. Cross sections of films were viewed with an HRSEM microscope to determine the film thickness.

In some cases, it was observed under HRSEM that the PMDS had lifted from the glass substrate and there was an unknown material stuck in the air pocket as indicated in Figure 4-33, which was suspected to be glass shards that had broken off while cutting the PDMS under nitrogen. HRSEM micrographs of the two films (D and E) were obtained as shown in Figure 4-33 where qualitative EDS was combined with HRSEM to assist with material identification and the EDS images are shown in Appendix B. The shards in the air pocket were confirmed to have the same elemental composition as the glass, which mainly consisted of silicon and oxygen and although the same was seen for PDMS, the glass contained sodium, calcium and magnesium whereas the PDMS thin film did not.

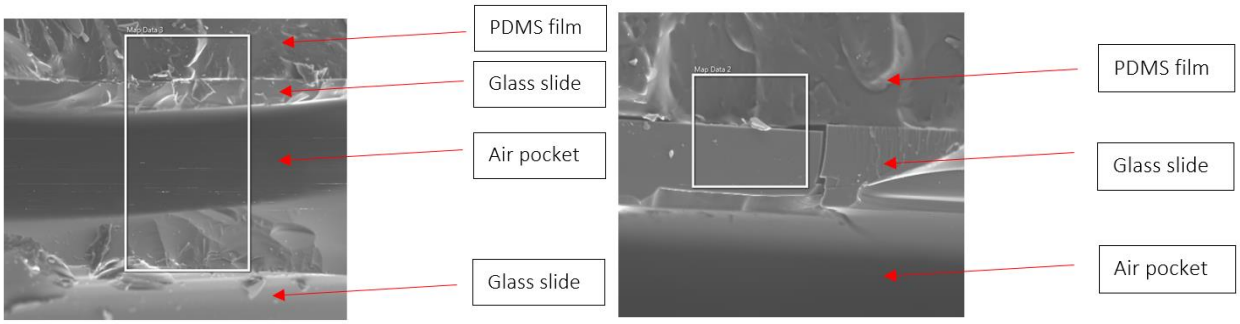

Figure 4-33: HRSEM micrographs of films D and E.

4.4.3. Concentration of QDs in thin films

Due to the fact that not all the QD@PDMS mixture added to the spin coater actually remains on the glass slide and produces the final thin film, the concentrations of QDs in the thin films were calculated by using equations shown in Section 3.2.8. The average concentrations of QDs in the thin films were calculated on a mass basis. The calculation shown here as an example was for the LQD films and the same was done for the HQD films.

Firstly, 1 mL of PDMS was cured and weighed (N= 7) by adding the PDMS solution into a glass vial and curing it on a hot plate at 80°C for 15 min to obtain the average weight of 1 mL of cured PDMS which was 0.91 g. One result was statistically shown to be an outlier and was removed (N= 6) and the corrected average weight for 1 mL of cured PDMS containing no QDs was obtained (0.94 g). This was repeated for cured 1 mL volumes of LQD and HQD PDMS solutions, respectively and an average for each (N= 7) was obtained of 0.92 g and 0.97 g, respectively. The mass ratio of 1 mL cured low [QD] PDMS/ 1 mL cured PDMS (no QDs) was obtained as shown in Eq. (4-2).

$$\boldsymbol{MassRatio_{curedLQD} = \frac{Mass_{1mL(curedLQD)}}{Mass_{1mL(curedPDMS)}} = \frac{0.92}{0.94} = 0.99} \quad (4\text{-}2)$$

The mass ratio of 1 mL cured low [QD] PDMS/ 1 mL cured PDMS (no QDs) was 0.99. This was multiplied by the density of the cured PDMS (1.03 g/mL supplied from the supplier) to give the cured density of the QD PDMS that was 1.01 g/mL as shown in Eq. (4-3).

$$\boldsymbol{Density_{curedLQD} = MassRatio_{curedLQD} \times Density_{curedPDMS} = 0.99 \times 1.03 \frac{g}{mL}} \quad (4\text{-}3)$$
$$\boldsymbol{= 1.01 \frac{g}{mL}}$$

The mass of QDs in 1 mL final solution was determined by knowing the mass of QDs in 1 mL chloroform (0.004 g) which was used to make LQD films and dividing this by the total volume of the solution which was the volume of the chloroform, curing agent and PDMS added together (12.04 mL) as shown in Eq. (4-4).

$$\boldsymbol{Mass_{QD\ (1\ mL\ final\ soln)} = \frac{Mass_{QD}}{Total\ vol} = \frac{0.004\ g\ in\ 1\ mL}{12.04\ mL} = 0.0003\ g\ QDs} \quad (4\text{-}4)$$

In a vial, 1 mL of LQD PDMS solution (N= 7) was cured and weighed, where the average was 0.92 g, whilst the LQD films had an average weight of 0.09 g (N= 18). The cured mass of the film was divided by the cured mass of 1 mL of LQD solution giving a final volume of film on the glass slide which was 0.09 mL as shown in Eq. (4-5).

$$\boldsymbol{Volume_{LQD(film)in\ 1\ mL} = \frac{Mass_{curedLQD(film)}}{Mass_{1mL(curedLQD)}} = \frac{0.09\ g}{0.92\ g} = 0.09\ in\ 1\ mL} \quad (4\text{-}5)$$

It was calculated in Eq. (4-3) that in 1 mL final solution there was 0.0003 g QDs in the LQD solution. Thus, by multiplying the mass of QDs in 1 mL final solution (0.0003 g) by the volume on the slide (0.09 mL) as

calculated in Eq. 4-4, the QD mass in the volume on the slide was obtained (3.1×10^{-5} g) as shown in Eq. (4-6).

$$\boldsymbol{Mass_{QD(in\ film\ on\ slide)} = Mass_{QD(1mL\ final\ soln)} \times Volume_{LQD(film)\ in\ 1\ mL}} \\ \boldsymbol{= 0.0003\ g(in\ 1mL) \times 0.09\ mL = 3.1 \times 10^{-5} g} \quad (4\text{-}6)$$

The average film thickness of LQD and HQD film were determined to be 0.27 mm and was used for all calculations of concentrations of QDs in films, with glass slide dimensions of 20 x 20 mm, therefore the volume of the film was calculated to be 0.11 mL. The QD mass in the volume on the slide was divided by the volume of the film as shown in Eq. (4-7).

$$\boldsymbol{Concentration\ of\ QD\ in\ film = \frac{Mass_{QD(in\ film\ on\ slide)}}{Volume\ of\ film_{(l \times w \times h)}} = \frac{3.1 \times 10^{-5} g}{0.11\ mL}} \quad (4\text{-}7)$$

$$\boldsymbol{= 2.85 \times 10^{-4} \frac{g}{mL}}$$

The average concentration of QDs in the optimized LQD films was thus 2.85×10^{-4} g/mL (0.28 mg/mL) and was similarly calculated to be 5.05×10^{-4} g/mL (0.51 mg/mL) for the HQD films.

4.4.4. Very low QD concentration thin films

After determining the concentrations of QDs in the LQD (0.28 mg/mL) and HQD (0.50 mg/mL) films, it was noted that these were in the same ranges as the concentrations of QDs dispersed in solution previously used by our research group to detect organic analytes. Specifically, acetaminophen was detected using 0.27 mg/mL water soluble CdSe/ZnS QDs (Montaseri et al., 2019), however the concentration of CdSeTe/ZnS@MIP QDs used to detect atrazine was in the range of 4.2×10^{-5} mg/mL (Nsibande & Forbes, 2019). Therefore, a batch of very low concentration quantum dot (VLQD) films was made to observe the fluorescence of the QDs immobilized at a lower concentration of 0.0053 mg/mL or 5.3×10^{-6} g/mL QDs in the final cured PDMS films. Although this concentration was still higher than the concentration used to detect atrazine in solution with CdSeTe/ZnS@MIP QDs as done by Nsibande & Forbes (2019), the films were made at these concentrations to observe the intensity of fluorescence at the lower QD concentration.

It is evident in Figure 4-34 that there was a big difference between the fluorescence emission of VLQD and the LQD and HQD films, where the latter two films had a significantly greater fluorescence intensity observed by visual inspection, whilst no fluorescence emission was visually observed with the VLQD under UV light.

Figure 4-34: Optimized QD thin films viewed under normal light (top) and UV light (bottom). The films were arranged from left to right as (i) VLQD (ii) LQD and (iii) HQD films respectively.

In Figure 4-35 it is observed that there was no fluorescence detected by the spectrophotometer and the measured fluorescence spectrum was similar to that of a blank PDMS film which contained no QDs. The fluorescence of the cardboard that was used behind the VLQD film on the transparent glass was also measured as a blank and its fluorescence was again similar to that of the VLQD film. It could be that the few QDs present in the VLQD film were not close to the surface of the film where they could be readily excited or that the fluorescence emitted was too low to be detected as not enough QDs were emitting light in the direction of the detector. In order to enhance detection limits, the slit widths were increased to 5 or 6 nm, and no increase in fluorescence emission was detected. As these films did not show a fluorescence response, they were discarded and not used for further testing.

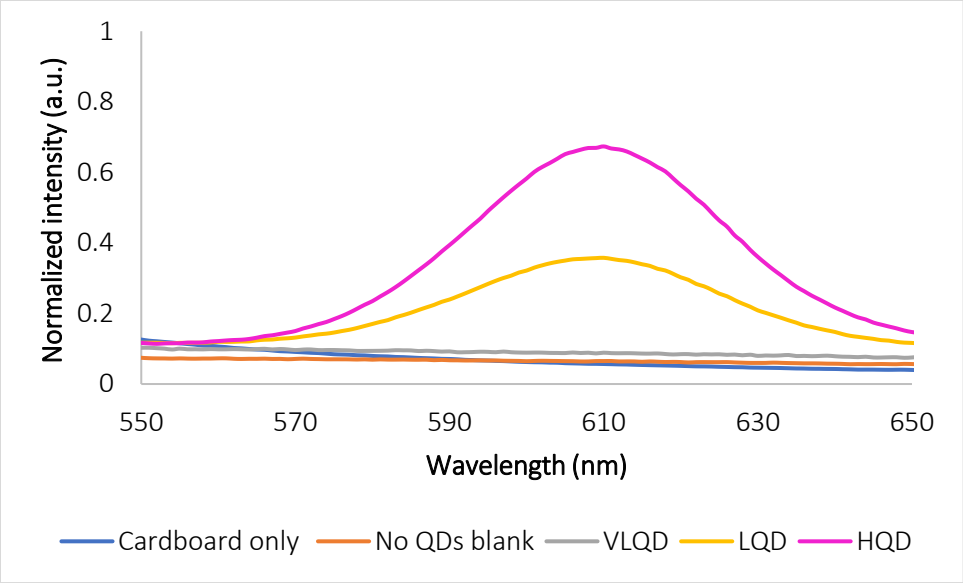

Figure 4-35: Normalized spectra showing the fluorescence emission of the cardboard support only, no QD PDMS film blank, and VLQD, LQD and HQD films (λ_{ex}= 400 nm, λ_{em}= 610 nm, 2 nm slit widths).

4.5. Interaction of optimized films with atrazine

4.5.1. Optimizing slit widths for atrazine sensing

Nine HQD films were tested with three different atrazine concentrations (N= 3 for each of the three atrazine concentrations) over the spatially resolved spots as shown in Figure 3-8. It was observed that the HQD film fluorescence values were high when using 2 nm slit widths and the atrazine sensing was thus repeated at slit widths of 1.2 nm.

Figure 4-36 shows a HQD film that was repeatedly excited in the middle of the film which relates to spot number five. The fluorescence was measured with slit widths of 1.2 nm and a decrease in fluorescence was observed as measurements were repeated on the HQD film. Over the entire repeated fluorescence illumination of the HQD film as shown in Figure 4-36, the maximum emission wavelength varied between 607 nm and 610 nm. This shows that the QDs were not photo-oxidized by the repeated illumination. The total percentage decrease in the first 60 min was 8%.

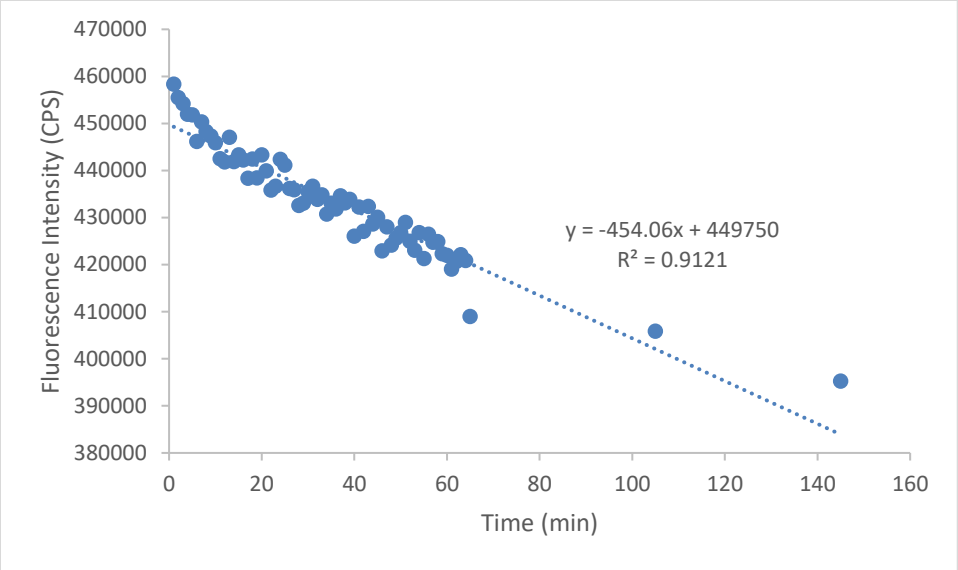

Figure 4-36: Repeated measured fluorescence of a HQD film every minute consecutively for 60 min and thereafter at 40 min intervals (λ_{ex}= 400 nm, λ_{em}= 610 nm, 1.2 nm slit widths).

Thereafter, the repeated exposure of a LQD film was measured for 60 min using 1.2 nm slit widths and a general trend of a slight decrease in fluorescence emission intensity was observed as shown in Figure 4-37. Throughout the repeated illumination of the LQD film with slits of 1.2 nm, the maximum emission wavelength varied from 608 to 611 nm. The difference between the maximum and minimum fluorescence emission intensity obtained over the 60 min was 8%.

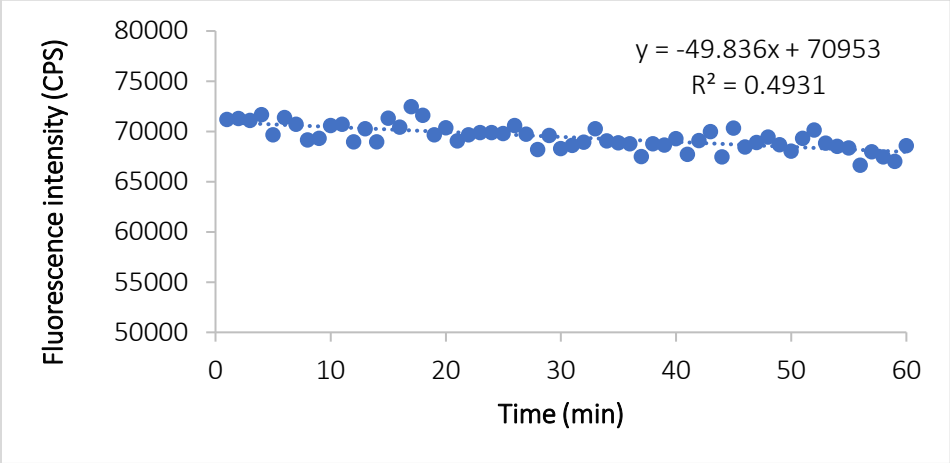

Figure 4-37: Repeated measured fluorescence emission of a LQD film every min consecutively for 60 min (λ_{ex}= 400 nm, λ_{em}= 610 nm, 1.2 nm slit widths).

When the fluorescence spectrum of the LQD film was measured with 1.2 nm slit widths as shown in Figure 4-38, the fluorescence spectrum was not smooth and the fluorescence was very low and had a poor signal-to-noise ratio, where the maximum fluorescence peak had a very low intensity (71 790 CPS, λ_{em}= 610 nm). The LQD films were therefore not tested with atrazine using slit widths of 1.2 nm, and only 2 nm slit widths were used in all subsequent experiments to obtain smoother peaks and better signal-to-noise ratios.

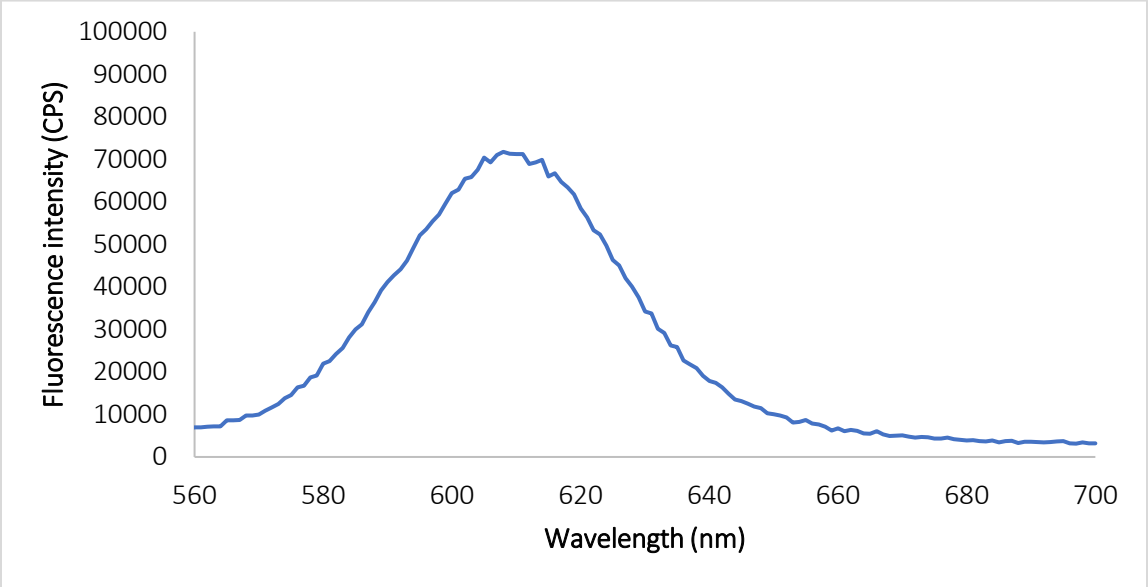

Figure 4-38: The fluorescence emission intensity (CPS) of a LQD film (λ_{ex}= 400 nm, λ_{em}= 610 nm, 1.2 nm slit widths).

The photostability was tested by measuring the impact of repeated excitation of a LQD film. The fluorescence was measured every consecutive minute, and this was done with 2 nm slit widths to obtain smoother spectra with a better signal-to-noise ratio by utilising more light to illuminate the film. The results are shown in Figure 4-39 where an increase in fluorescence emission was observed for the first 20 min whereafter it stabilised. The maximum emission wavelength of the LQD films for which fluorescence was measured using a 2 nm slit widths varied from 609 to 611 nm which was a 7% increase.

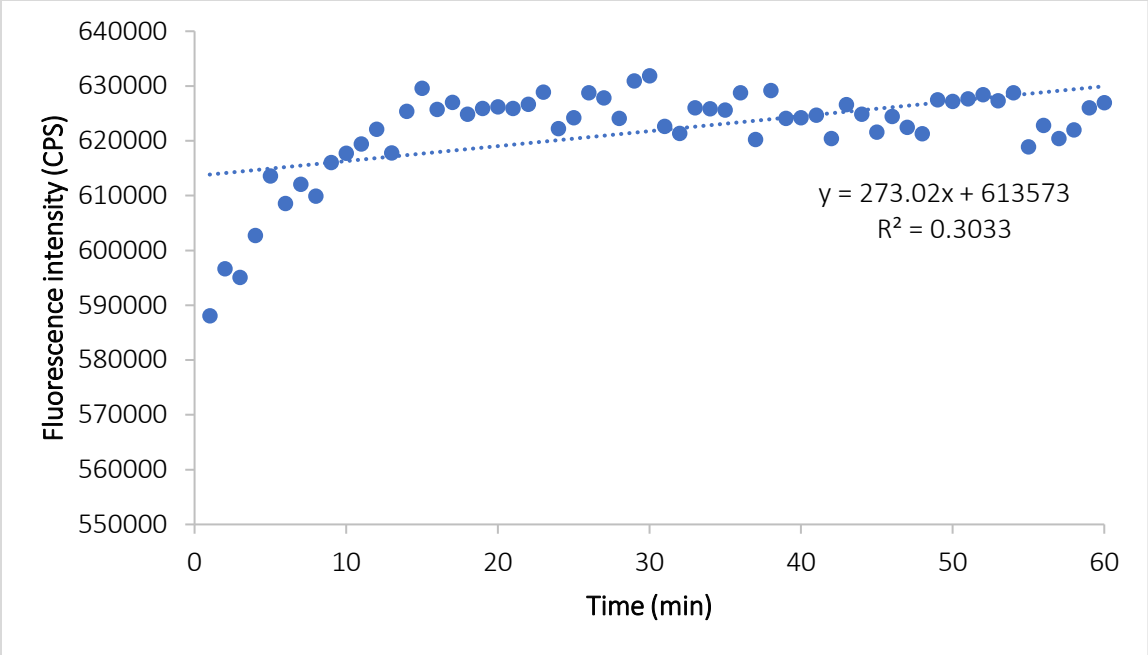

Figure 4-39: Repeated fluorescence of a LQD film measured every min consecutively for 60 min (λ_{ex}= 400 nm, λ_{em}= 610 nm, 2 nm slit widths).

It was interesting to note that when smaller slit widths (1.2 nm) were used and less light excited the sample, there was a slight decrease in fluorescence from the start of the illumination whilst larger slit widths of 2 nm showed an increase in fluorescence with repeated exposure for the first ~20 min, and then stabilized, which correlated to literature as stated in Section 4.3.

Figure 4-40 shows the graph of a single spectrum of a LQD film obtained with slit widths of 2 nm; this was a lot smoother when compared to fluorescence emission measured with 1.2 nm slit widths. A maximum fluorescence peak intensity of 592 020 CPS was obtained, which was almost a ten-fold increase from the fluorescence intensity (71 790 CPS) measured using 1.2 nm slit widths. Therefore, 2 nm slit widths were used when testing the impact of different atrazine concentrations on the fluorescence emission of LQD films.

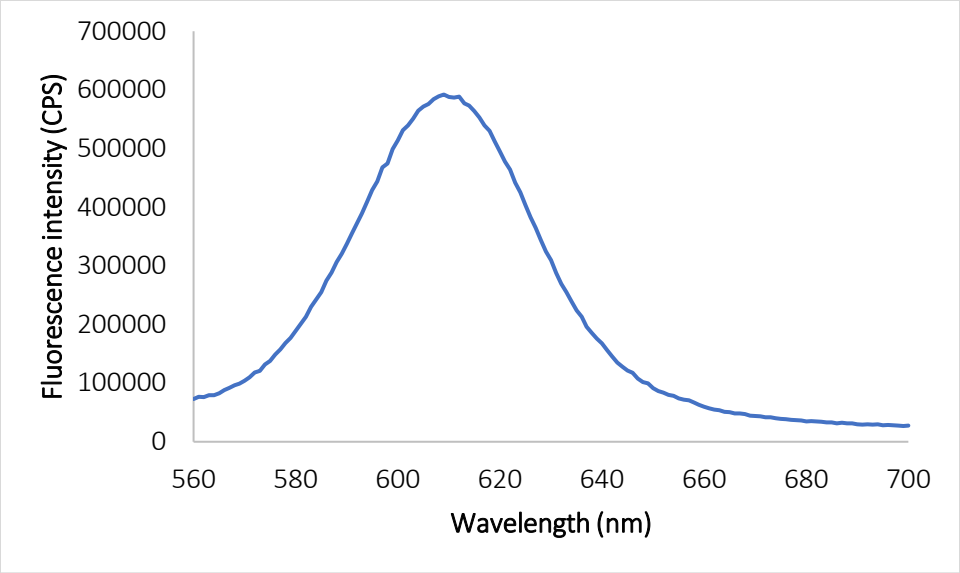

Figure 4-40: The fluorescence spectrum of a LQD film with a maximum emission wavelength of 609 nm measured with 2 nm slit widths.

When comparing the measured fluorescence responses (F/F_0) of the HQD thin films, which were tested with the same atrazine concentrations using 1.2 and 2 nm slit widths, it was observed that with 2 nm slit widths the fluorescence response (F/F_0) generally enhanced, and with 1.2 nm slit widths the fluorescence response (F/F_0) generally quenched, with F/F_0 averages of 1.26 and 0.71, respectively. In all subsequent experiments, only slit widths of 2 nm were used to keep the slit width constant. These results indicate that the amount of light (energy) that illuminates the QDs at a higher concentration inside the film may induce different opto-electronical relaxation pathways.

Nsibande & Forbes (2019) previously showed that the interaction of atrazine with CdSeTe/ZnS@MIP QDs quenched the fluorescence of the QD sensor (Nsibande & Forbes, 2019). From this, it could be concluded that 1.2 nm might be a better slit width to use for HQD films, as this produced consistent quenching for the films which agreed with literature. In the following experiments however, 2 nm was used as not enough light reached the detector when measuring the fluorescence of the LQD films using 1.2 nm slit widths, which consequently produced low quality spectra.

4.5.2. Interaction of atrazine with optimized films

Figure 4-41 shows the fluorescence spectra of each LQD film obtained from the average of the nine spatially resolved spots (as indicated in Figure 3-8), where fluorescence was measured before and after the

interaction of the film with each atrazine concentration. From the LQD films it was seen that after interaction with different atrazine concentrations, quenching was observed.

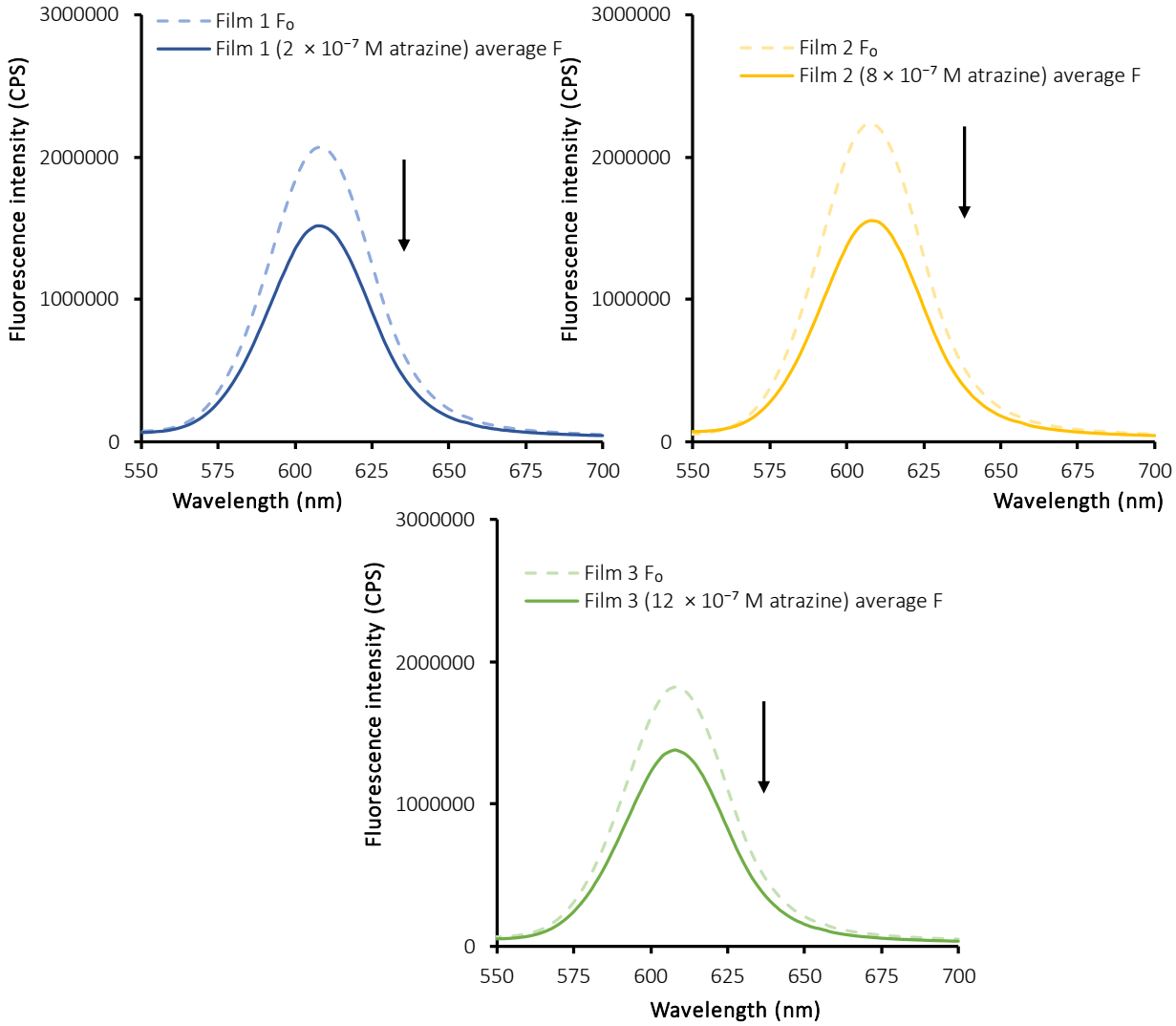

Figure 4-41: Measured fluorescence of LQD films before and after (F_0 and F) testing the films with atrazine concentrations of 2, 8 and 12 × 10^{-7} M (λ_{ex}= 400 nm, λ_{em}= 610 nm, 2 nm slit widths).

Figure 4-42 shows the fluorescence spectra of each HQD film obtained from the average of the nine spatially resolved spots where fluorescence was measured before and after the interaction of the film with each atrazine concentration.

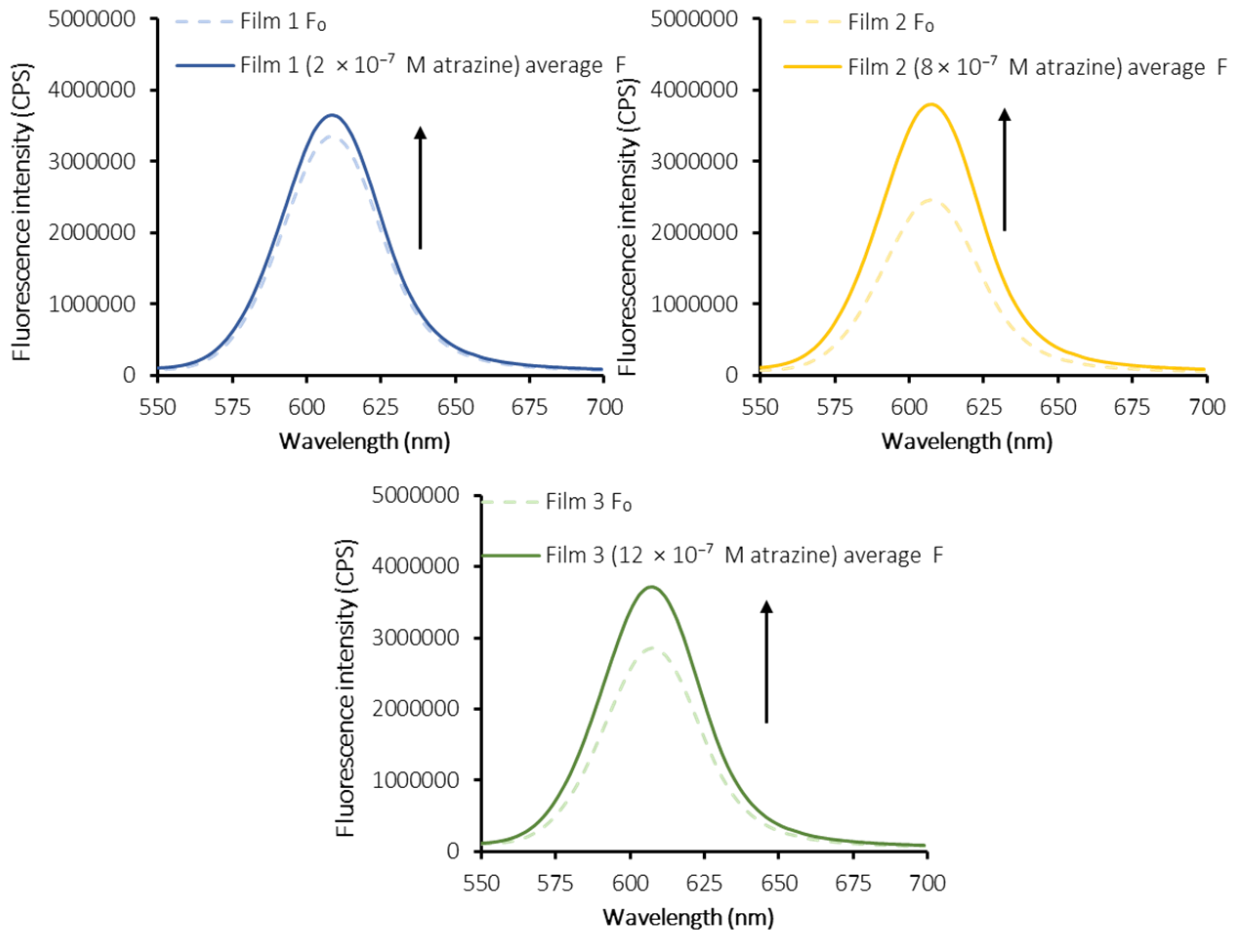

Figure 4-42: Measured fluorescence of HQD films before and after (F_0 and F) testing the films with atrazine concentrations of 2, 8 and 12 × 10^{-7} M (λ_{ex}= 400 nm, λ_{em}= 610 nm, 2 nm slit widths).

For HQD films, it was seen that after interaction thereof with different atrazine concentrations, enhancement of fluorescence was observed for atrazine concentrations of 8 and 12 × 10^{-7} M, although the %RSDs of the HQD films were larger and fluorescence was more consistent with the LQD films.

The statistical analysis of the data presented in Figure 4-41 and Figure 4-42 is discussed in Section 4.5.3. (shown in Table 4-14, Table 4-15, Table 4-16 and Table 4-17) where a t-test was done to determine whether there was a significant difference between measured fluorescence before and after interaction with atrazine (F_0 and F). The ratio of fluorescence F/F_0 measured before and after the interaction was also compared to the value one, as shown in Table 4-18.

The fluorescence of three films was measured at nine spatially resolved spots as shown in Figure 3-8 before and after the interaction with atrazine and the F/F_0 values were calculated to determine the impact of atrazine on the fluorescence emission measured at each spot on the film. These values were then averaged and F/F_0 was calculated for the entire film. The three F/F_0 values for every atrazine concentration tested were also averaged to obtain a single F/F_0 value per atrazine concentration tested as shown in Table 4-10. From this it was seen that the most quenching for all three films occurred with an atrazine concentration of 8×10^{-7} M for LQD films. Here, quenching was seen for all LQD films.

Table 4-10: Three LQD films tested per atrazine concentration with F/F_0 values averaged over the film (N= 9 spots) (λ_{ex}= 400 nm, λ_{em}= 610 nm, 2 nm slit widths) (including outliers).

[Atrazine]	2×10^{-7} M	8×10^{-7} M	12×10^{-7} M
Film 1	0.74	0.70	0.77
Film 2	0.83	0.65	0.97
Film 3	0.89	0.66	1.12
Average	**0.82**	**0.67**	**0.95**
%RSD	8.91	12.31	8.91

From Table 4-11 it is observed that when the same was done for HQD films, enhancement took place with all HQD films, as 2 nm slit widths were used. The greatest averaged enhancement for the three films was also with an atrazine concentration of 8×10^{-7} M.

Table 4-11: Three HQD films tested per atrazine concentration with F/F_0 values averaged over the film (N= 9 spots) (λ_{ex}= 400 nm, λ_{em}= 610 nm, 2 nm slit widths) (including outliers).

[Atrazine]	2×10^{-7} M	8×10^{-7} M	12×10^{-7} M
Film 1	1.08	1.59	1.36
Film 2	1.16	1.19	1.23
Film 3	0.76	1.01	0.93
Average	**1.00**	**1.26**	**1.18**
%RSD	6.20	18.89	13.88

From Table 4-12 it is observed that when only looking at one spot in the middle of the LQD film, the most quenching was still observed for the atrazine concentration of 8×10^{-7} M.

Table 4-12: Three LQD films tested per atrazine concentration with F/F_0 values obtained from the spot in the middle of the film (N= 1), (λ_{ex}= 400 nm, λ_{em}= 610 nm, 2 nm slit widths).

[Atrazine]	2×10^{-7} M	8×10^{-7} M	12×10^{-7} M
Film 1	0.96	0.74	0.68
Film 2	1.01	0.61	0.74
Film 3	0.84	0.76	1.10
Average	**0.94**	**0.70**	**0.84**

From Table 4-13 it was observed that when only looking at one spot in the middle of the HQD film the most enhancement was still seen for an atrazine concentration of 8×10^{-7} M.

Table 4-13: Three HQD films tested per atrazine concentration with F/F_0 values obtained from the spot in the middle of the film (N= 1), (λ_{ex}= 400 nm, λ_{em}= 610 nm, 2 nm slit widths).

[Atrazine]	2×10^{-7} M	8×10^{-7} M	12×10^{-7} M
Film 1	1.08	1.76	1.08
Film 2	1.17	1.33	1.00
Film 3	0.81	0.91	1.09
Average	**1.02**	**1.33**	**1.06**

When comparing the results presented in Table 4-12 and Table 4-13, it can be noted that it is important to measure the fluorescence of the films over nine spots, and not just in the middle of the film, as there was a difference in the results obtained, and by taking the average over nine spots, the results are more representative of the effect that atrazine had on the fluorescence of the thin film.

4.5.3. Statistical analysis

Nine F_0 values were measured over the spatially resolved spots as shown in Figure 3-8 for a LQD film at each atrazine concentration tested and were compared as these three films were replicates and should have had similar F_0 values; this was measured before the sensing interactions were done to confirm low %RSDs over the films. One of the three LQD films that were used to test each atrazine concentration was tested for reproducibility over the nine spots. The same was done for HQD films. The %RSD over the nine spots in the three LQD films were 13.5, 11.9 and 16.8% and 10.2, 15.7 and 15.4% for the HQD films. This was an average of 14.1, and 13.8% respectively over the nine spatially resolved spots for LQD and HQD films.

The fluorescence of three films per atrazine concentration of 2, 8 and 12 × 10^{-7} M respectively were measured before and after the interaction with atrazine and the fluorescence response (F/F_0) results are shown in Figure 4-43. These fluorescence response (F/F_0) values are represented as box-and-whisker plots as the fluorescence was measured over the nine spatially resolved spots. The abbreviation LQD (2 Atz) F1 indicates the low QD concentration film tested with an atrazine concentration of 2 × 10^{-7} M, film 1. Of the nine films, three had outliers when looking at the fluorescence for each of the nine spatially resolved spots.

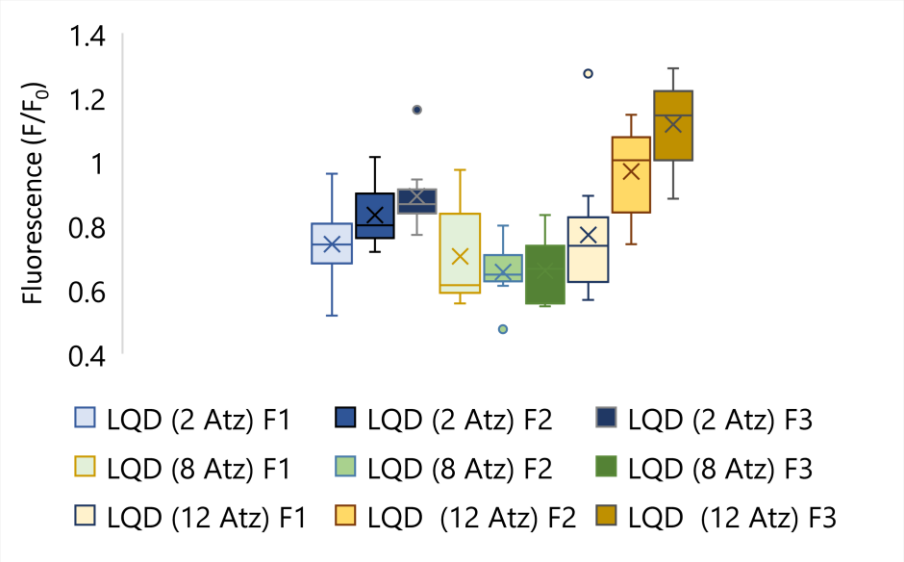

Figure 4-43: Fluorescence response (F/F_0) values (over nine spatially resolved spots) for LQD after 1 min interaction with different atrazine concentrations (λ_{ex}= 400 nm, λ_{em}= 610 nm, 2 nm slit widths).

In Figure 4-44 the fluorescence response (F/F_0) of nine HQD films are shown, three films per atrazine concentration of 2, 8 and 12 × 10^{-7} M. This is shown over the spread of nine spatially resolved spots measured on each film after a 1 min interaction with atrazine. Of the nine films, two had outliers when looking at the fluorescence over nine spatially resolved spots.

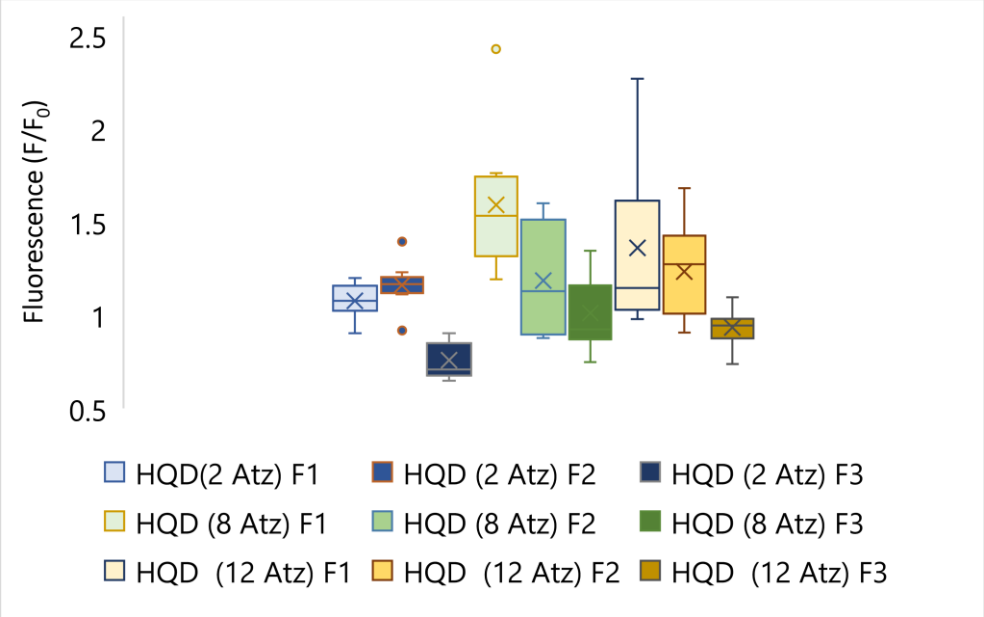

Figure 4-44: F/F_0 values (over nine spatially resolved spots) for HQD after 1 min interaction with different atrazine interactions (λ_{ex}= 400 nm, λ_{em}= 610 nm, 2 nm slit widths).

As shown in Table 4-14, when comparing the F_0 fluorescence emission values (three films, and nine spatially resolved spots on each) at 608 and 610 nm for both LQD and HQD films, it was seen that there was a significant difference for both and that the fluorescence emission at 608 nm was higher for both.

Table 4-14: Statistical data comparing the fluorescence F_0 at two emission wavelengths (608 and 610 nm) for both low and high QD concentration films.

*outliers removed	LQD		HQD	
Variable	608 nm	610 nm	608 nm	610 nm
Mean (CPS)	$1.77 \times 10^{+6}$	$1.76 \times 10^{+6}$	$3.06 \times 10^{+6}$	$3.04 \times 10^{+6}$
Observations	79		72	
df	78		71	
t Stat	12.34		12.62	
t Critical one-tail	1.66		1.67	
Significantly larger	608 nm		608 nm	

As shown in Table 4-15, at both 608 and 610 nm, the fluorescence (F_0) values of HQD films were significantly higher than the LQD values, as expected.

Table 4-15: Statistical data comparing the fluorescence emission intensity between two QD concentration films at two different wavelengths

*outliers removed	608 nm		610 nm	
Variable	HQD	LQD	HQD	LQD
Mean (CPS)	$3.06 \times 10^{+6}$	$1.80 \times 10^{+6}$	$3.04 \times 10^{+6}$	$1.79 \times 10^{+6}$
Observations	70		70	
df	69		69	
t Stat	16.43		16.22	
t Critical one-tail	1.67		1.67	
Significantly larger	HQD		HQD	

As shown in Table 4-16, quenching was observed for LQD films after a 1 min interaction with different atrazine concentrations and there was a significant difference between the fluorescence (F_0 and F) measured for atrazine concentrations of 2×10^{-7} M and 8×10^{-7} M. This indicated significant quenching at the statistical parameters chosen.

Table 4-16: Statistical data comparing the fluorescence (F_0 and F) values at three atrazine concentrations tested on LQD films.

LQD t-Test: Paired Two Sample for Means (610 nm) *outliers removed						
[Atrazine]	2×10^{-7} M		8×10^{-7} M		12×10^{-7} M	
Variable	F_0 (N= 3)	F (N= 3)	F_0 (N= 3)	F (N= 3)	F_0 (N= 3)	F (N= 3)
Mean (CPS)	$1.72 \times 10^{+6}$	$1.40 \times 10^{+6}$	$1.94 \times 10^{+6}$	$1.30 \times 10^{+6}$	$1.65 \times 10^{+6}$	$1.53 \times 10^{+6}$
Variance	$9.82 \times 10^{+10}$	$2.53 \times 10^{+10}$	$5.68 \times 10^{+10}$	$4.48 \times 10^{+10}$	$2.26 \times 10^{+10}$	$3.03 \times 10^{+10}$
Observations	3	3	3	3	3	3
df	2		2		2	
t Stat	3.32		37.47		0.65	
t Critical one-tail	2.92		2.92		2.92	
Significantly larger	F_0		F_0		None	

As shown in Table 4-17, enhancement was observed for HQD films after a 1 min interaction with different atrazine concentrations but at the statistical parameters chosen there was no statistically significant difference between the fluorescence (F_0 and F) measured before and after interaction with atrazine.

Table 4-17: Statistical data comparing the fluorescence (F_0 and F) values at three atrazine concentrations tested on HQD films.

HQD t-Test: Paired Two Sample for Means (610 nm) *outliers removed						
[Atrazine]	(2 × 10^{-7} M atrazine)		(8 × 10^{-7} M atrazine)		(12 × 10^{-7} M atrazine)	
Variable	F (N= 2)	F_0 (N= 2)	F (N= 3)	F_0 (N= 3)	F (N= 3)	F_0 (N= 3)
Mean (CPS)	3.89 × 10^{+6}	3.46 × 10^{+6}	3.38 × 10^{+6}	2.80 × 10^{+6}	3.43 × 10^{+6}	3.01 × 10^{+6}
Variance	1.29 × 10^{+11}	1.66 × 10^{+10}	1.08 × 10^{+11}	1.26 × 10^{+11}	7.91 × 10^{+10}	7.99 × 10^{+10}
Observations	2	2	3	3	3	3
df	1		2		2	
t Stat	2.60		1.50		1.29	
t Critical one-tail	6.31		2.92		2.92	
Significantly larger	None		None		None	

t-Tests were performed where the F/F_0 values were compared to the value 1, and the same results were obtained as in Table 4-14 to Table 4-17. Statistical data shown in Table 4-18, where films A, B and C were tested with atrazine concentrations of 2 x 10^{-7}, 8 x 10^{-7} and 12 x 10^{-7} M, respectively and the fluorescence response (F/F_0) values were compared to 1 to see whether quenching or enhancement was significant. As shown in this table, LQD film A and B were significantly quenched, with statistically insignificant differences for HQD films.

Table 4-18: Statistical data comparing the fluorescence response (F/F_0) values obtained from the interaction of different atrazine concentrations with the value one.

	LQD (λ_{em}= 610 nm)					
Variable	Between 1 & A		Between 1 and B		Between 1 and C	
Data entries	1.00	A	1.00	B	1.00	C
Mean (F/F_0)	1.00	0.83	1.00	0.67	1.00	0.95
Variance	0.00	0.00	0.00	0.00	0.00	0.03
Observations	3	3	3	3	3	3
df	2		2		2	
t Stat	4.53		20.67		0.49	
t Critical one-tail	2.92		2.92		2.92	
Significantly larger	1		1		None	
	HQD (λ_{em}= 610 nm)					
Variable	Between 1 & A		Between 1 and B		Between 1 and C	
Data entries	A	1	B	1	C	1
Mean (F/F_0)	1.12	1.00	1.26	1.00	1.18	1.00
Variance	0.00	0.00	0.09	0.00	0.05	0.00
Observations	2	2	2	2	3	3
df	1		1		2	
t Stat	2.80		1.52		1.39	
t Critical one-tail	6.31		2.92		2.92	
Significantly larger	None		None		None	

When comparing different fluorescence response (F/F_0) values found for different concentrations of atrazine directly to one another, as shown in Table 4-19, there was only a significant difference for the LQD films between atrazine concentrations of 2×10^{-7} M and 8×10^{-7} M, where a concentration of 8×10^{-7} M of atrazine had a significantly greater quenching. This is where the amount of inputs and the numbers of the different inputs affects the statistical comparisons made, it also affects whether the results are significant as it is clearly shown that there was a greater difference between 8×10^{-7} M and 12×10^{-7} M but the statistical data shows that this was not a significant difference between the two concentrations, but rather that a smaller difference between 2×10^{-7} M and 8×10^{-7} M was significant.

Table 4-19: Statistical data comparing the fluorescence response (F/F_0) values from different concentrations tested.

	LQD (λ_{em}= 610 nm)					
Variable	Between A and B (2&8)		Between B and C (8&12)		Between A and C (2&12)	
[Atrazine] (x 10^{-7} M)	2	8	12	8	12	2
Mean (F/F_0)	0.83	0.67	0.95	0.67	0.95	0.83
Variance	0.00	0.00	0.03	0.00	0.03	0.00
Observations	3	3	3	3	3	3
df	2		2		2	
t Stat	2.97		2.45		2.00	
t Critical one-tail	2.92		2.92		2.92	
Significantly larger	2×10^{-7} M		None		None	
	HQD (λ_{em}= 610 nm)					
Variable	Between A and B (2&8)		Between A and C (2&12)		Between B and C (8&12)	
[Atrazine] (x 10^{-7} M)	8	2	8	12	12	2
Mean (F/F_0)	1.39	1.12	1.30	1.12	1.26	1.18
Variance	0.08	0.00	0.01	0.00	0.09	0.05
Observations	2	2	2	2	3	3
df	1		1		2	
t Stat	1.10		1.69		1.07	
t Critical one-tail	6.31		6.31		2.92	
Significantly larger	None		None		None	

Looking at the chemical structure of atrazine (Figure 2-1), it contains polar groups containing chloride and nitrogen groups, thus making it quite a polar molecule. This could be preventing the interaction of atrazine with PDMS due to lack of compatibility as PDMS is nonpolar. The possibility of nonpolar PAH analytes interacting better with the PDMS was thus investigated after the impact on fluorescence of the solvent employed was investigated.

4.6. Interaction of optimized films with different solvents

Thin films were interacted with three different solvents to observe the impact thereof on the measured fluorescence emission of the films over longer periods when the films were immersed in the respective solvents for 24 hours. This shows the exaggerated effect of the solvent, as it should be noted that these interaction times were long compared to other experiments where analytes were dissolved in ethanol (atrazine) and a H_2O: ethanol (2:1) mixture (Phe) and interacted with the films. From Table 4-20 it is evident that interaction of films with different solvents led to differences in fluorescence. This could possibly impact experiments and it was important to choose solvents wisely. It was seen that 100% ethanol and 100% water resulted in substantial fluorescence enhancement for both LQD and HQD films. The greatest enhancement was seen with 100% deionised H_2O in both LQD and HQD films. The H_2O: ethanol (2:1) mixture showed slight quenching with LQD films, and more quenching with HQD films. For all experiments to test the effect of different solvents on thin film fluorescence, slit widths of 2 nm were used. For all experiments where optimized films were interacted with atrazine, the atrazine was dissolved in ethanol. These experiments were, however, of short duration (1 min) compared to the results presented in Table 4-20.

Table 4-20: F/F_0 values of LQD and HQD films after 24-hour interactions with various solvents.

Solvent	100% H_2O	100% Ethanol	H_2O: ethanol (2:1)
LQD	1.63	1.22	0.93
HQD	1.78	1.55	0.87

The statistical analysis of these results is shown in Table 4-21 and Table 4-22, where the significance of quenching and enhancement was tested. Table 4-23 indicates the maximum fluorescence intensity measured at two different emission wavelengths (608 and 610 nm) to determine whether there was a significant difference observed in the fluorescence emission of the films between the two wavelengths. Table 4-24 compares the fluorescence responses (F/F_0) between the different solvents to see whether the difference was statistically significant. Table 4-25 compares the fluorescence ratio (F/F_0) between the solvents as well, but F was measured after the samples were removed from the solvent and kept on the laboratory bench for 25 days covered with a transparent plastic bag to protect them from air and dust which could accumulate on the film surface and were later transferred to a semi-transparent plastic box of which the top was covered with aluminium foil. Table 4-26 compares the fluorescence responses (F/F_0) of

the H_2O: ethanol (2:1) interaction after 24 hours, 21 days and 25 days. As shown in Table 4-21 the F values of both 100% deionised H_2O and 100% ethanol were significantly larger than the F_0 values after the 24-hour tests.

Table 4-21: t-Test of the thin film fluorescence measured before (F_0) and after (F) 24-hour interaction with 100% H_2O and 100% ethanol solvents.

	100% H_2O				100% Ethanol			
	LQD		HQD		LQD		HQD	
Variable	F	F_0	F	F_0	F	F_0	F	F_0
Mean	$3.68 \times 10^{+6}$	$2.33 \times 10^{+6}$	$5.95 \times 10^{+6}$	$3.44 \times 10^{+6}$	$3.66 \times 10^{+6}$	$3.13 \times 10^{+6}$	$5.45 \times 10^{+6}$	$3.57 \times 10^{+6}$
df	8		8		8		8	
t Stat	6.33		11.63		2.73		7.67	
t Critical one-tail	1.86		1.86		1.86		1.86	
Significantly larger	F		F		F		F	

As shown in Table 4-22, for LQD films there were no significant differences between the fluorescence (F_0 and F) measured after interaction with H_2O: ethanol (2:1), which was good for further testing and analyte sensing applications. For HQD films there was a significant difference between the fluorescence (F_0 and F) measured, and quenching was significant.

Table 4-22: t-Test of the thin film fluorescence emission measured before (F_0) and after (F) the 24-hour interaction of H_2O: ethanol (2:1) solvent.

	LQD		HQD	
Variable	F_0	F	F_0	F
Mean	$2.48 \times 10^{+6}$	$2.18 \times 10^{+6}$	$4.98 \times 10^{+6}$	$4.31 \times 10^{+6}$
df	8		8	
t Stat	1.39		2.84	
t Critical one-tail	1.86		1.86	
Significantly larger	None		F_0	

When comparing the F_0 maximum emission values observed at 608 and 610 nm it was seen that there was a significant difference for LQD films and the null hypothesis was rejected as 608 nm was significantly larger but no significant difference was seen between the two wavelengths for HQD films as shown in Table 4-23.

Table 4-23: Statistical data comparing F_0 values at 608 and 610 nm for LQD and HQD films.

	LQD		HQD	
Variable	608 nm	610 nm	610 nm	608 nm
Mean	$2.66 \times 10^{+6}$	$2.65 \times 10^{+6}$	$4.00 \times 10^{+6}$	$3.99 \times 10^{+6}$
df	26		26	
t Stat	4.82		1.43	
t Critical one-tail	1.71		1.71	
Significantly larger	608 nm		None	

Table 4-24 shows the statistical data comparing the fluorescence ratio before and after the solvent interaction (F/F_0) between different solvents. For the LQD and HQD films there were significant differences between F/F_0 values for all the different solvents. The fluorescence of the films in 100% H_2O was significantly larger than when interacted with the 100% ethanol and the water: ethanol (2:1) mixture. The measured fluorescence response of the films tested with 100% ethanol was significantly larger than those tested with the water: ethanol (2:1) mixture. This was seen for both LQD and HQD films.

Table 4-24: Statistical data comparing the fluorescence response (F/F_0) after 24-hour interaction with the solvent for LQD and HQD films.

LQD						
Variable	100% H_2O	100% Ethanol	100% H_2O	Water: ethanol (2:1)	100% Ethanol	Water: ethanol (2:1)
Mean (F/F_0)	1.63	1.22	1.63	0.93	1.22	0.93
df	8		8		8	
t Stat	2.57		4.94		2.61	
t Critical one-tail	1.86		1.86		1.86	
Significantly larger	100% H_2O		100% H_2O		100% Ethanol	
HQD						
Variable	100% H_2O	100% Ethanol	100% H_2O	Water: ethanol (2:1)	100% Ethanol	Water: ethanol (2:1)
Mean	1.78	1.55	1.78	0.87	1.55	0.87
df	8		8		8	
t Stat	2.44		8.17		5.85	
t Critical one-tail	1.86		1.86		1.86	
Significantly larger	100% H_2O		100% H_2O		100% Ethanol	

After the interaction with different solvents, the films were removed from the solvents and left on the laboratory bench and were covered with a transparent plastic bag to protect them from air and dust which could accumulate on the film surface and was later transferred to a semi-transparent plastic box of which the top was covered with aluminium foil, whereafter the fluorescence emission was remeasured. For all of the solvents tested with LQD and HQD films, there was a significant difference between the fluorescence

(F_0 and F) measured after 25 days as shown in Table 4-25. The films in 100% H_2O showed the greatest enhancement.

Table 4-25: Measured fluorescence responses (F/F_0) of LQD and HQD films which were interacted with 100% H_2O, 100% ethanol and H_2O: ethanol (2:1) for 24 hours where fluorescence was remeasured again after 25 days after storage on a laboratory benchtop.

Solvent	100% H_2O	100% Ethanol	H_2O: ethanol (2:1)
LQD	2.77	1.71	2.07
HQD	2.98	2.61	1.68

The fluorescence of the LQD and HQD films that were immersed in H_2O: ethanol (2:1) for 24 hours was measured before (F_0) and after 24 hours as well as 21 and 25 days (after storage on the laboratory bench, removed from the solvent) on the nine spatially resolved spots and results are shown in Table 4-26. From Table 4-26 it is evident that there was quenching of both concentration films after 24 hours. Significant quenching was seen for HQD films where F was significantly smaller than F_0 whilst non-significant quenching was seen for LQD films. After 21 and 25 days, both LQD and HQD showed enhancement where the F values were significantly larger than the original F_0 values. It is uncertain whether the fluorescence enhancement observed over a prolonged period was from the effect of the solvent on the PDMS film, or whether it was because of constant illumination by ambient light during storage in the laboratory, which some studies have shown to enhance fluorescence emission over prolonged exposure (Wang et al, 2004; Komaralal, et al., 2006; Cordero, et al., 2000). These results emphasize the importance of consistent storage conditions of QD@PDMS films used for sensing, as well as careful consideration of the solvent employed.

Table 4-26: Comparison of the fluorescence response (F/F_0) of LQD and HQD films after i) 24-hour interaction with H_2O: ethanol (2:1), ii) 21 days after F_0 and iii) 25 days after F_0 measurements were measured.

F/F_0	24 hours	21 days	25 days
LQD	0.93	2.13	2.07
HQD	0.87	1.83	1.68

4.7. Interaction of optimized films with phenanthrene

For the investigation of the impact of a PAH, namely phenanthrene (Phe), on the measured fluorescence emission of the films, three LQD and HQD films were used. The initial fluorescence emission (F_0) was measured at the nine spatially resolved spots as shown in Figure 3-8, and the results are compared and represented as box-and-whisker plots in Figure 4-45. The LQD and HQD films had fluorescence intensity averages of 2 464 785 and 4 668 215, respectively, with %RSDs of 17.4 and 14.2% across the films (N= 27).

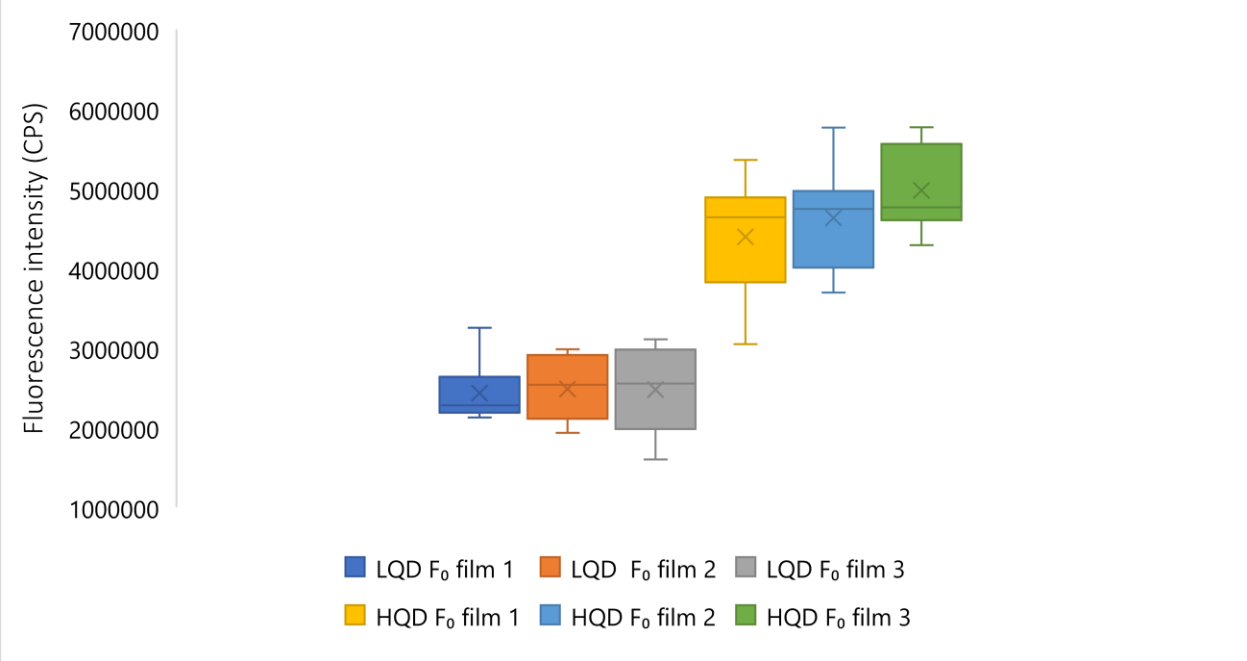

Figure 4-45: Visual representation of F_0 of three LQD and HQD films over nine spatially resolved spots on each film (λ_{ex}= 400 nm, λ_{em}= 610 nm, 2 nm slit widths).

When comparing the average F_0 values at 608 and 610 nm between LQD and HQD films, it was seen that both null hypotheses were rejected and that there was a significant difference at both wavelengths and that the F_0 values of the HQD films that were used for Phe sensing were significantly higher in both cases. The results are shown in Table 4-27.

Table 4-27: Statistical data comparing initial fluorescence (F_0) values (CPS) at different film concentrations (LQD and HQD films) at 608 and 610 nm.

	608 nm		610 nm	
Variable	HQD	LQD	HQD	LQD
Mean	$4.66 \times 10^{+6}$	$2.48 \times 10^{+6}$	$4.67 \times 10^{+6}$	$2.47 \times 10^{+6}$
df	26		26	
t Stat	14.51		14.56	
t Critical one-tail	1.71		1.71	
Significantly larger	HQD		HQD	

When looking at the F_0 values (three films, and nine spatially resolved spots on each) at wavelengths of 608 and 610 nm for both LQD and HQD films, the average F_0 values were higher at a wavelength of 608 nm for LQD films and higher at a wavelength of 610 nm for HQD films. The null hypothesis was rejected for both t-tests and there was a significant difference for both concentration films when compared at different fluorescence emission wavelengths. The statistical data is presented in
Table 4-28, and although the differences were not that large, the number of independent values was high which made it significant for the statistical parameters chosen. From this data it was shown that there were differences in the maximum emission wavelengths between the LQD and HQD films used for Phe sensing, although 610 nm was used for simplicity to interpret and compare results.

Table 4-28: Statistical data comparing F_0 fluorescence emission (CPS) at different wavelengths for LQD and HQD films.

	LQD		HQD	
Variable	608 nm	610 nm	610 nm	608 nm
Mean	$2.48 \times 10^{+6}$	$2.46 \times 10^{+6}$	$4.67 \times 10^{+6}$	$4.66 \times 10^{+6}$
df	26		26	
t Stat	6.68		2.17	
t Critical one-tail	1.71		1.71	
Significantly larger	608 nm		610 nm	

The films tested with the solvent blank (H_2O: ethanol (2:1)) showed quenching (Section 4.6) which shows that there was a clearly observed change in fluorescence emission of the films in the presence of phenanthrene in the same solvent.

Table 4 29 shows that there was an increase in fluorescence response (F/F_0) when LQD films were interacted with various Phe concentrations, and the enhancement observed was directly proportional to the Phe concentration. The same was seen for the HQD films, but no difference was observed between the 5.61×10^{-6} and 5.61×10^{-5} Phe concentrations. The films tested with the solvent blank (H_2O: ethanol (2:1)) showed quenching (Section 4.6) which shows that there was a clearly observed change in fluorescence emission of the films in the presence of phenanthrene in the same solvent.

Table 4-29: Fluorescence response (F/F_0) of three LQD and HQD films after the films were interacted with Phe concentrations of 5.61×10^{-6} and 5.61×10^{-5} M in a H_2O: ethanol (2:1) solution for 24 hours.

[Phe]	Solvent blank	5.61×10^{-6} M	5.61×10^{-5} M
LQD	0.93	1.05	1.15
HQD	0.87	1.09	1.09

When comparing the fluorescence response ratios (F/F_0) of the LQD films between the different Phe concentrations, it was seen that there was a difference between all Phe concentrations. When comparing the fluorescence response between the different concentrations it was seen that the t-stat < t-critical one-tail. Thus, for the LQD films, the null hypothesis was retained and there was statistically no difference between the variables as shown in Table 4-30, all the critical t (one-tail) values were larger than the calculated statistical t value (t-stat).

Table 4-30: Statistical data comparing the fluorescence response (F/F_0) at different Phe concentrations for LQD films.

Variable	5.61×10^{-5} M	5.61×10^{-6} M	5.61×10^{-5} M	Blank	5.61×10^{-6} M	Blank
Mean	1.15	1.05	1.15	0.93	1.05	0.93
df	8		8		8	
t Stat	0.89		1.60		0.87	
t Critical one-tail	1.86		1.86		1.86	
Significantly larger	None		None		None	

When comparing the fluorescence response (F/F_0) of the HQD films between the different Phe concentrations, as shown in Table 4-31, there was a significant difference between both 5.61×10^{-5} and 5.61×10^{-6} M Phe concentrations compared to the blank where the fluorescence emission of the solvent blank was significantly lower than the fluorescence emission of both films that were interacted with Phe. The null hypothesis was rejected for the t-tests comparing 5.61×10^{-5} M Phe and the blank, as well as 5.61×10^{-6} M Phe and the blank, as the t-stat > t-critical one-tail. Thus, it was concluded that there was a significant difference between these samples, and that the fluorescence responses (F/F_0) of the 5.61×10^{-5} M and 5.61×10^{-6} M was significantly larger than the solvent blank.

Table 4-31: Statistical data comparing the measured fluorescence response (F/F_0) of HQD films by interacting them with different Phe concentrations.

Variable	5.61×10^{-5} M	5.61×10^{-6} M	5.61×10^{-5} M	Blank	5.61×10^{-6} M	Blank
Mean	1.09	1.09	1.09	0.87	1.09	0.87
df	8		8		8	
t-Stat	0.05		4.41		3.97	
t Critical one-tail	1.86		1.86		1.86	
Significantly larger	None		5.61×10^{-5} M		5.61×10^{-6} M	

The films were then removed from the solvent and were stored on a lab bench covered with a transparent plastic bag to protect them from air and dust which could accumulate on the film surface and were later transferred to a semi-transparent plastic box for which the top was covered with aluminium foil. After 21 days from the original F_0 measurements, the fluorescence was measured again. The results shown in Table 4-32 indicates a significant increase in fluorescence and a big enhancement was seen for all films of both LQD and HQD. There was an increased fluorescence enhancement for the LQD films tested with the higher Phe concentration of 5.61×10^{-5} M.

Table 4-32: Fluorescence response (F/F_0) of three LQD and HQD films after the films were interacted with phenanthrene for 24 hours and then F was remeasured 21 days after the original F_0.

[Phe]	Solvent blank	5.61×10^{-6} M	5.61×10^{-5} M
LQD	2.13	2.12	2.45
HQD	1.83	1.50	1.87

The films which were exposed to the solvent blank had a great increase in fluorescence enhancement when their fluorescence was measured again 21 days later, as compared to the fluorescence that was quenched originally with measurement of the fluorescence emission after 24 hours.

For all the LQD and HQD films tested with different Phe concentrations (0, 1 and 5.61×10^{-5} M), a significant difference was seen between F values measured after 24 hours and 21 days after F_0, where the F values almost doubled for all the films and the F/F_0 values were significantly higher after 21 days. The statistical data is presented in Table 4-33.

Table 4-33: Statistical data comparing the fluorescence emission (F values) after 24 hours and 21 days after F_0.

LQD (610 nm)						
	Solvent blank		5.61×10^{-6} M		5.61×10^{-5} M	
Variable	F (21 days)	F (24 hours)	F (21 days)	F (24 hours)	F (21 days)	F (24 hours)
Mean	$5.09 \times 10^{+6}$	$2.18 \times 10^{+6}$	$5.13 \times 10^{+6}$	$2.57 \times 10^{+6}$	$5.84 \times 10^{+6}$	$2.75 \times 10^{+6}$
Variance	$3.29 \times 10^{+11}$	$8.58 \times 10^{+10}$	$8.06 \times 10^{+11}$	$3.58 \times 10^{+11}$	$7.15 \times 10^{+11}$	$2.33 \times 10^{+11}$
df	8		8		8	
t Stat	16.98		7.74		11.45	
t Critical one-tail	1.86		1.86		1.86	
Significantly larger	F (21 days)		F (21 days)		F (21 days)	
HQD (610 nm)						
	Solvent blank		5.61×10^{-6} M		5.61×10^{-5} M	
Variable	F (21 days)	F (24 hours)	F (21 days)	F (24 hours)	F (21 days)	F (24 hours)
Mean	$9.05 \times 10^{+6}$	$4.31 \times 10^{+6}$	$6.83 \times 10^{+6}$	$4.96 \times 10^{+6}$	$7.95 \times 10^{+6}$	$4.67 \times 10^{+6}$
Variance	$8.41 \times 10^{+11}$	$2.60 \times 10^{+11}$	$1.05 \times 10^{+12}$	$6.72 \times 10^{+11}$	$6.75 \times 10^{+11}$	$4.28 \times 10^{+11}$
df	8		8		8	
t Stat	15.16		3.62		11.94	
t Critical one-tail	1.86		1.86		1.86	
Significantly larger	F (21 days)		F (21 days)		F (21 days)	

As shown in Table 4-34, the F/F_0 values of LQD and HQD films were remeasured after 21 days. The LQD films showed a larger fluorescence enhancement (F/F_0) than HQD films after 21 days at 610 nm.

Table 4-34: The fluorescence response (F/F_0) of LQD and HQD films obtained when remeasured 21 days after their interaction with Phe.

F/F_0 values after 21 days			
[Phe]	Solvent blank	5.61×10^{-6} M Phe	5.61×10^{-5} M Phe
LQD	2.13	2.12	2.45
HQD	1.83	1.50	1.87

The films that were interacted with the solvent blank (H_2O: ethanol (2:1)) showed quenching, therefore there was an observed change in fluorescence emission of the films when they were interacted with Phe. An enhancement was observed for LQD films which was proportional to the concentration of Phe which was interacted with the films, whilst for the HQD films an enhancement was observed when films were interacted with Phe compared to the blank, but no difference between the two Phe concentrations was observed (5.61×10^{-6} M and 5.61×10^{-5} M Phe). For the results obtained from interacting LQD and HQD films with Phe, it is concluded that fluorescence should be measured directly before and after the interaction and should not be tested long after the interaction (in sensing applications measurements would be taken directly after interaction in any event).

In a previous study, L-cysteine capped CdSeTe/ZnSe/ZnS QDs were conjugated to graphene oxide (GO) which formed a QD-GO nanocomposite for the fluorescence sensing of PAHs. Fluorescence enhancement with increasing concentrations of PAHs in aqueous solution was observed, where phenanthrene showed the most significant fluorescence enhancement and could be detected down to 1.07×10^{-9} mol.L^{-1} (Adegoke & Forbes, 2016). A comparable study using CdSeTe/ZnS QDs by Adegoke et al. verified this, with a detection limit of 2.26×10^{-9} mol.L^{-1} for Phe (Adegoke et al., 2017). It is believed that the trend in the PL enhancement of the PAH samples corresponded to their adsorption affinity for the QDs-GO probe. Because PAHs are known to behave as π-electron donors owing to their high electron density, the detection mechanism may be described by the interaction between the electron-rich-π system of the PAH molecule and the π-electron system of the graphene material, as a result, the QD-GO probe exhibited an adsorption-PL enhancement effect, making it suitable for the detection of PAHs (Adegoke & Forbes, 2016).

PDMS has been employed as a passive sampler for PAHs. This approach included exposing PDMS to an aqueous solution and allowing dissolved hydrophobic PAH compounds to collect inside the polymeric sampler through equilibrium partitioning (Jonker, 2022). In this study, this effect could enhance the adsorption of the PAH into the PDMS, which could bring the analyte into close contact with the CdSeTe/ZnS QDs allowing FRET and PL enhancement to occur as was seen in the results. It should be noted that Phe itself is fluorescent, but the emission wavelengths are significantly shorter (Figure 4-46) than those of both the emission (Figure 4-7) and absorption (Figure 4-8) of the QDs. This could result in enhancement of the QDs due to them acting as an acceptor molecule when the Phe was in close contact to the QDs due to accumulation within the PDMS thin film.

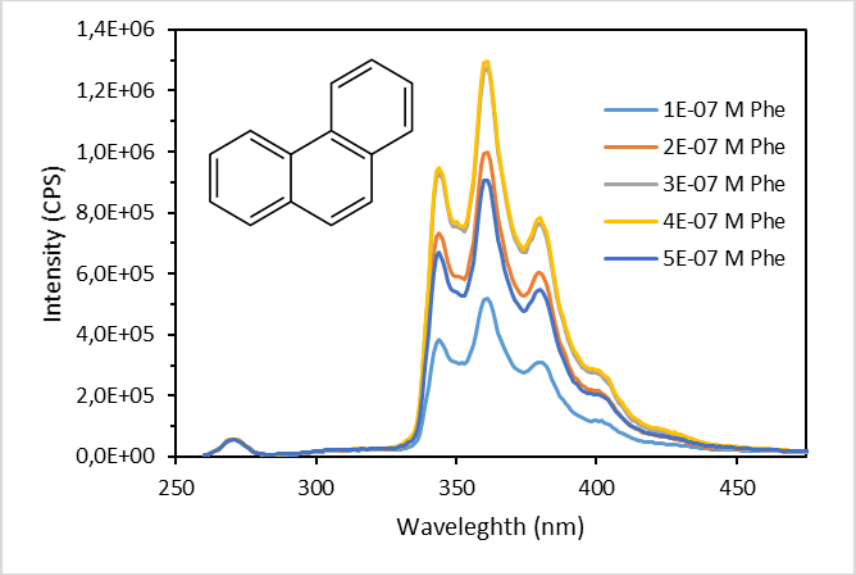

Figure 4-46: Fluorescence intensity spectra of the phenanthrene at different concentrations. The excitation wavelength was 250 nm (Adegoke et al., 2017).

4.8. Water sample sensing tests

In this series of experiments, the first film of each QD concentration (LQD and HQD) was interacted with an unconcentrated filtered inlet water sample obtained from Rand Water which was sourced from the Vaal Dam. To cover the surface of the glass slide, 1.2 mL of the sample was added on top of the films and was interacted for 1 min on both LQD and HQD films. For both LQD and HQD films it was seen that there was an enhancement in fluorescence, with F/F_0 values of 1.68 and 1.23, respectively.

With the second films of each QD concentration, the same inlet water sample was interacted with the films for 1 min, but the samples were now fully immersed in 4 mL of the inlet water sample. Fluorescence enhancement was again seen for both LQD and HQD films with F/F_0 values of 1.93 and 1.28, respectively.

The third set of films was then treated as a blank and no inlet water was interacted with them and the F value was measured. It was seen that the fluorescence of the films had increased during storage and F/F_0 values of 2.01 and 1.46 for LQD and HQD films was obtained. The F_0 value thus had to be measured directly prior to each new test. Film 3 was then immersed in the unconcentrated filtered inlet water sample (4 mL) for 1 min, the same as for film 2. This gave F/F_0 values of 1.07 and 1.03 for LQD and HQD films after the interaction. It was thus concluded that the enhancement seen with film 1 and 2 could have been due to the change in the film fluorescence over time.

The original F_0 values of the LQD and HQD films were measured (λ_{em}= 610 nm) over the nine spatially resolved spots as shown in Figure 3-8 and the fluorescence over each film was averaged. This was averaged over all films of that film concentration (N= 9 and N= 8 for LQD and HQD, respectively). These averages obtained were compared to the new fluorescence values measured after the films were left on the laboratory bench for 35 days (covered with aluminium foil). A paired t-test was done to test whether there was a significant difference between the two averages of fluorescence values measured on the different days.

The new fluorescence values measured after 35 days had significantly increased and the null hypothesis was rejected; it was thus true that there was a significant difference between the original F_0 values and the F_0 values remeasured after 35 days as shown in Table 4-35.

The fluorescence was thus remeasured before each film was interacted with the inlet water sample. It was observed that when the F_0 values measured originally on nine films (N= 9) were remeasured after the films were kept on a laboratory bench for 35 days, the fluorescence (F_0) of the LQD films (N= 9, %RSD= 9.8%) had increased by a factor of 1.76 and the fluorescence (F_0) of the HQD films (N= 8, %RSD= 10.7%) had increased by a factor of 1.36 after 35 days.

Table 4-35: Original and new fluorescence emission (F_0) measured before and after 35 days between measurements over nine spatially resolved spots of nine and eight films respectively for LQD and HQD films.

	LQD		HQD	
Variable	**New F_0**	**Original F_0**	**New F_0**	**Original F_0**
Mean	$3.98 \times 10^{+6}$	$2.26 \times 10^{+6}$	$5.64 \times 10^{+6}$	$4.14 \times 10^{+6}$
Variance	$1.51 \times 10^{+11}$	$5.04 \times 10^{+10}$	$4.16 \times 10^{+11}$	$2.30 \times 10^{+11}$
df	8		7	
t Stat	10.24		4.19	
t Critical one-tail	1.86		1.89	
Significantly larger	New F_0		New F_0	

For LQD and HQD films F_0 values over the nine spatially resolved spots were remeasured and then blank tests were done after 1 hour and 24 hours without introducing any solvent or analyte. This showed enhancement and quenching for LQD and HQD films respectively as shown in Table 4-36.

Table 4-36: LQD and HQD films for which the fluorescence was measured as blanks after 1 hour and 24 hours.

	LQD	HQD
1 hour	1.15	0.87
24 hours	1.02	1.16

For the blank test done over an hour, enhancement and quenching was seen for the LQD and HQD films respectively with F/F_0 values of 1.15 and 0.87. When the blank tests were done over 24 hours, F/F_0 values of 1.02 and 1.16 were seen as shown in Table 4-37. This indicates that almost no detectable change in fluorescence was observed for LQD and only a slight enhancement for HQD films.

Table 4-37: Comparison of the fluorescence emission of LQD and HQD films that were measured after 24 hours by using a blank test with no solvent or analyte.

	LQD	HQD
Blank	1.02	1.16

The fourth films of LQD and HQD were immersed in the filtered, unconcentrated inlet water sample for 1 hour where F/F_0 values of 0.86 and 1.05 were observed respectively (λ_{ex}= 400 nm, λ_{em}= 610 nm, 2 nm slit widths). LQD films showed visible quenching with the unconcentrated sample. Comparing this to the 1-hour blank results shown in Table 4-36, the LQD film was quenched significantly and the HQD film was enhanced significantly.

The fifth set of films were immersed for 24 hours in the filtered, unconcentrated inlet water sample. F/F_0 values of 1.00 and 1.06 were obtained which indicated that the sample had no significant effect on the fluorescence of the QD@PDMS film.

For the sixth set of films, 600 mL of the inlet water sample received from Rand Water was processed through SPE and a 1 mL concentrated SPE extract was obtained. The extract reconstituted in ethanol was diluted with deionized water forming a total solution volume of 3 mL with a water to ethanol ratio of 2:1.

This sample extract volume was small, and a few tests needed to be done on it consecutively. It should be noted that the amount of analyte present in the sample would decrease due to absorption by the PDMS thin films during each experiment. The first film introduced to the sample was a LQD film, and thereafter the HQD film. The films were immersed in the 3 mL sample for 24 hours and fluorescence was measured before and after interaction and F/F_0 values of 0.75 and 0.83 were obtained respectively. This showed that the fluorescence of the films had quenched significantly for both concentration films after the 24-hour interaction with the concentrated inlet water sample. This was also confirmed by comparing it to the 24-hour blank test as shown in Table 4-36.

For all 24-hour tests, the F/F_0 values of the LQD films were lower than the HQD films, thus more quenching was observed with the LQD films overall than with the HQD films. With films from the 7^{th} set, the concentrated extract, which had already interacted with LQD, then HQD films for 24 hours, was interacted again with a LQD then HQD film for 30 min which gave F/F_0 values of 0.87 and 1.06, respectively. It was tested once more, as LQD film 8 was tested with this concentrated inlet water extract, where it was immersed for 1 min. This gave a F/F_0 value of 1.05. With no significant quenching or enhancement, it showed that this interaction time was either not long enough or there were no more analytes present in the sample to interact with the film.

Thus, it can be concluded from the water tests that the unconcentrated filtered inlet water sample did not influence the fluorescence of the QD sensor after a 1 min interaction. When comparing the results obtained after a 1-hour interaction of the unconcentrated filtered inlet water sample with the thin films, it was observed that there was quenching, and enhancement observed of the fluorescence of the LQD and HQD films respectively. When comparing the results obtained after a 24-hour interaction of the unconcentrated filtered inlet water sample with the thin films, it was observed that the interaction had no effect on the measured fluorescence of LQD films but that quenching was observed for the measured fluorescence of HQD films.

The LQD and HQD films that were immersed in the 3 mL diluted SPE concentrated extract for 24 hours showed quenching of the fluorescence for both films, with (F/F_0) values of 0.75 and 0.83 respectively. This was also confirmed by comparing it to the 24-hour blank test as shown in Table 4-36. The fluorescence of the LQD film still quenched when it was interacted with the 3 mL diluted SPE concentrated extract for 30 min after both the previous tests.

Although these tests were non-targeted tests, it showed that the 3 mL diluted SPE concentrated extract had a similar effect on both concentration films and that by concentrating the sample with SPE and then interacting it with the films, it had a quenching effect on the fluorescence emission of the films, indicating the potential use of the thin film for non-target screening of organic pollutants in water.

4.9. Effect of ambient light on QD thin films

In the prior water testing experiments, it was noted that when fluorescence was examined again on a film after a long duration since the original fluorescence measurements, the emission had greatly increased, without the addition of an analyte or solvent. The films were stored on the laboratory benchtop immediately after the tests and were kept in a semi-transparent plastic box covered with aluminium foil to protect the films from air and dust that could build up on the film surface.

To confirm that all observed variations in fluorescence were caused by sample interaction and not by exposure of the films to light, the fluorescence was remeasured (F_0) before each water testing experiment. The emission intensity of the LQD and HQD films that were kept in a semi-transparent box increased by 1.9 and 1.4 fold, respectively, after 35 days.

Following the water experiments, the films were placed in a pitch-dark drawer and the fluorescence was measured again (F) seven months after the initial measurements (F_0), and it was found that the previously enhanced intensity had decreased back to, or was very close to, the original F_0 value.

Given that the emission of the QDs was still relatively strong after approximately 7 months, it indicated high photostability of the QDs, which raises optimism for the QD@PDMS being reused in applications over extended periods of time. Long-term photostability may suggest that the films are suitable for other applications, but the variations in fluorescence caused by ambient light make them unsuitable for sensing at trace analyte concentrations, as these variations are too large to differentiate changes brought about by the presence of a target analyte.

It was also observed that there was an increase in fluorescence emission over time when measuring fresh aliquots of QD@chlorofrom solutions, which could have been possibly impacted by the exposure of the QDs to ambient light. This is consistent with literature, which concluded that QDs require stabilization for a few days before measurement of fluorescence (Kritzinger et al., 2022).

Photochemical treatments have been found to be effective in reducing nonradiative recombination by decreasing surface defects (Bol & Meijerink, 2001) and it has been shown that the PLQY of QDs can be enhanced through illumination. Gaponik et al. irradiated diluted colloidal solutions of TGA capped CdTe QDs with 400 nm light from a 450 W xenon lamp in an oxygen-saturated solution (Gaponik et al., 2002). The PLQY steadily increased, up to 30%, and by a factor of 3 after 5 days of illumination. The enhancement effect was attributed to photochemical etching, which removed the dangling bonds associated with tellurium trap states on the QD surface, which function as hole traps (Wuister et al., 2003; Kapitonov et al., 1999).

In another study, strong fluorescence caused by the photoactivation of aqueous citrate-capped CdSe and CdSe/CdS QDs resulted from reactions of the QD surface with ambient oxygen (Wang et al., 2004; Wang et al., 2003). After several days of exposure to ambient light, the aqueous dispersions of core QDs (QY of 0.4%) and C/S QDs (with a QY below 3%), showed a dramatic increase in PLQY by up to 20% and 59%, respectively. It was again determined that the key component of photoactivation is the elimination of topological surface defects, or the smoothing of the QD surface.

Due to the asymmetrical atomic-scale topography of the QDs, charge carriers that result from the absorption of light remain trapped in the surface states which are formed. It is hypothesized that the disappearance of several midgap states results from the localization of excitons at the QD surface and the subsequent formation of a negatively charged molecular oxygen species after exciton dissociation. The trapped hole may then oxidize surface Se atoms to produce SeO_2. It is hypothesized that this causes a gradual degradation of any elevated areas on the surface, leaving behind a smooth, less trap-rich surface, resulting in a significantly enhanced PL as the nonradiative recombination sites are removed (Jing et al., 2016). This again demonstrates how ambient light and oxygen can affect results and how challenging it can be to use such QD based devices as fluorescence sensors.

Chapter 5: Conclusions and Future Work

5.1. Overall conclusions

Quantum dots (QDs) were successfully synthesized by the organometallic route, and an increase in size thereof was observed when a shell layer was grown over the QD core as observed by the red-shifting of the QD fluorescence emission peak and the QD colour change from bright yellow to bright orange when the shell was grown over the core. Broad UV-Vis absorption peaks were also observed for both core and core shell (C/S) QDs.

The PLQY of the QD C/S was 47% and from fluorescence viewed under a UV lamp, it was shown that the fluorescence of these QDs was very bright, even when they were subsequently immobilized into PDMS polymer thin films. It needs to be considered that a relative method was used to obtain the PLQY, and not a direct measurement with use of accurate instruments like an integrating sphere combined with scattering agents, which would have provided a more accurate PLQY.

Various methods to produce QD films were tested, but aside from spin coating these did not produce homogeneous QD distributions and were thus not suitable for further use. Spin coating parameters were optimized to produce QD@PDMS thin films on glass slides which could be used to screen for organic pollutants in water. Of the many different batches produced, film batch 21 had spin coating parameters which produced the best quality thin films. By visual observation of the films under a UV lamp, it was shown that the QDs were homogenously distributed with a bright fluorescence observed throughout the film replicates. Furthermore, this batch showed a trend in fluorescence response when interacted with different atrazine concentrations. LQD and HQD films were prepared by dissolving QDs in chloroform to form solutions with concentrations of 0.004 g/mL and 0.008 g/mL, respectively, and a ratio of 1 mL QD@chloroform solution: 1 g curing agent: 10 g PDMS. The optimized spin coating parameters were thus as follows for both LQD and HQD films: 0.5 mL of QD@PDMS mixture was placed in the center of the glass slide which was held in place by vacuum in the spin coater and spun at 500 rpm (300 rpm/s for 10 s). These films were then cured on a hot plate at 80^{o}C for 15 min. The fluorescence of the synthesized films was measured at nine spatially resolved spots to fully assess any variations across the film surface and to obtain an average for each film.

The overall average film thickness was determined to be 0.27 mm for both LQD and HQD films. The average concentrations of QDs in the optimized films were calculated to be 0.28 mg/mL and 0.51 mg/mL for LQD and HQD films, respectively. A batch of very LQD films was also made and had a concentration of 0.0053 mg/mL QDs in the final cured films.

When thin film fluorescence was measured before any interactions (F_0) with an excitation wavelength of 400 nm, a maximum emission wavelength of 608 nm was obtained for LQD films and the maximum emission wavelength varied between 608 and 610 nm for HQD films. The maximum emission wavelength was thus chosen as 610 nm for overall simplicity in the study. It was also seen that at both emission wavelengths (608 and 610 nm), the initial fluorescence (F_0) of the HQD films was always significantly larger than the initial fluorescence (F_0) of the LQD films which was expected as the concentration of the QDs imbedded in the films was higher.

When the LQD and HQD thin films were interacted with atrazine, it was shown that 1.2 nm slit widths were too narrow to obtain spectra of good quality for LQD films as the signal-to-noise ratio was poor, therefore all sensing experiments of optimized films was done at 2 nm slit widths for LQD and HQD films to allow for direct comparison. By interacting the LQD thin films with atrazine concentrations of 2, 8 and 12 × 10^{-7} M for 1 min, a quenching in fluorescence was observed for all three concentrations (N= 3), with the largest quenching observed for 8 × 10^{-7} M. By interacting the HQD films with atrazine concentrations of 2, 8 and 12 × 10^{-7} M for 1 min, an enhancement in fluorescence was observed for all three concentrations (N= 3), with the largest enhancement observed for 8 × 10^{-7} M. The quenching response observed with the LQD films was in agreement with the quenching observed when the QDs dispersed in solution were interacted with atrazine.

It was discovered that solvents altered the fluorescence emission of the films, which had to be taken into account when interpreting the data generated when analysing samples. When the LQD and HQD films were interacted with various solvents for 24 hours, it was observed that both deionized water and ethanol caused an increase in fluorescence emission. Thus, when sensing of atrazine in ethanol, it can be deduced that the observed quenching of LQDs was inherently due to the presence of the analyte, although the solvent would have contributed to the enhancing effect found for the HQD films.

There was quenching observed (not significant for LQD but significant for HQD) when using a water-ethanol (2:1) mixture, but the effect was lowest of the three solvents tested, which shows this is a suitable solvent

for sensing applications using the QD@PDMS material. The fluorescence ratio (F/F_0) values after testing 100% H_2O, 100% ethanol and the H_2O: ethanol (2:1) mixture respectively were 1.63, 1.22 and 0.93 for LQD, and 1.78, 1.55 and 0.87 for HQD films. The fluorescence was remeasured after leaving the films covered on a laboratory bench for 25 days and it was shown that the fluorescence measured (F/F_0) had increased to 2.77, 1.71 and 2.07 for LQD and 2.98, 2.61 and 1.68 for HQD films after immersion in the respective solvents for 24 hours. This indicates a possible stabilisation of the QD@PDMS over time, which has also been observed in QDs dispersed in solution.

LQD and HQD films were interacted with Phe which was dissolved in a H_2O: ethanol (2:1) mixture at various concentrations. An increase in fluorescence ratio (F/F_0) was found with an increased enhancement as the Phe concentration increased. This was seen for both LQD and HQD films. Because the fluorescence of the films was observed to be quenched by the H_2O: ethanol (2:1) mixture, this suggests that the overall enhancement shown in the films tested with Phe was possibly greater than what was measured owing to the influence of the solvent. However, the overall enhancement and trend detected showed the promising potential for the use of QD@PDMS as a sensor for Phe. It was thus concluded that the non-polar analyte (phenanthrene) interacted better than the polar analyte (atrazine) with the QD@PDMS films.

The influence of a Rand Water inlet water sample on the fluorescence emission of the thin films was investigated. The initial fluorescence of the films was tested 35 days before the sample testing and when the fluorescence was retested, a considerable increase in fluorescence emission from the films was detected, possibly due to stabilization of the material over time. The fluorescence (F_0) was thus measured again before each test to confirm that the fluorescence responses were due to the interaction of the film with the water sample and were not due to the time between measurements.

When LQD and HQD films were immersed in the filtered, unconcentrated Rand Water inlet water for 1-hour, fluorescence ratios (F/F_0) of 0.86 and 1.05 were observed, respectively: the LQD film was quenched and the HQD film was enhanced, which was contrary to the significant enhancement in fluorescence noted when the films were immersed in pure deionized water. When the films were immersed for 24 hours in this filtered, unconcentrated inlet water sample, F/F_0 values of 1.00 and 1.06 were obtained which indicated that the sample had no effect on the fluorescence of the QD@PDMS films. When the LQD and HQD films were consecutively interacted for 24 hours with a 1 mL concentrated extract which was obtained from SPE of a 600 mL inlet water sample received from Rand Water, and reconstituted in ethanol to a final

volume of 3 mL, F/F_0 values of 0.75 and 0.83 were obtained, respectively. This showed that the fluorescence of the films had quenched significantly for both LQD and HQD films after the 24-hour interaction with the concentrated inlet water sample. This was also confirmed by comparing it to the 24-hour blank test F/F_0 values of 1.02 and 1.16. Comparing these results to the 24-hour test in 100% deionized water which enhanced fluorescence emission, they were significantly quenched. For all 24-hour tests, the F/F_0 values of the LQD films were lower than the HQD films, thus more quenching was observed with the LQD films overall than with the HQD films. When in contact with the concentrated water sample, the fluorescence emission of both the LQD and HQD films were quenched. However, the HQD films showed less quenching, which may be due to the fact that the QDs were inherently closer to one another, and this could cause FRET between the QDs which were in close proximity to one another (Zheng et al., 2014). It has been reported in the literature that the emission of somewhat smaller QDs could be reduced while the emission of bigger QDs is enhanced, allowing for the transfer of energy from smaller to larger QDs. As a result, this effect also depends on the relative size difference between adjacent QDs in the film (Zheng et al., 2014). It should be noted that the solvent effect of water was shown to result in enhancement of the film fluorescence emission when submerged for 24-hours.

The sensing conducted in this study likely relies on fluorescence resonance energy transfer (FRET), in which energy is typically absorbed by the QD donor, and then transmitted to a neighbouring acceptor species, typically through dipole-dipole interactions. The distance between the FRET pair, the arrangement and orientation of the FRET pair, the spectral overlap of the donor emission and acceptor absorption, and the fluorescence lifetime of the donor should all be considered and optimized to enable the FRET mechanism as these all influence the effectiveness of this non-radiative energy transfer (Guo et al., 2014 and Yang et al., 2010).

Great efforts have been made to improve the dispersion of inorganic QDs inside organic polymer matrices, since it has been shown that poor compatibility between QDs and silicones may lead to loss of QD optical properties when mixed with these polymers (Sill & Emrick, 2004; Tao et al., 2011; Shen et al., 2012). QDs were coated with short-chain PDMS solutions in other studies, which could then bind well to the longer-chain commercial PDMS solutions and avoid agglomeration (Tao et al., 2013). Alternatively, grafting polymer chains containing the same chemical components as the matrix polymer onto the surface of the nanoparticles should increase particle-particle attraction between the nanoparticles and the polymer matrix and improve the inorganic QD dispersion inside the organic polymer (Akcora et al., 2009; Green,

2011). It has been demonstrated that bimodal PDMS-brush grafted QDs with excellent dispersion enhances the optical transparency and long-term stability of the PL of CdSe-silicone nanocomposites (Zvaigzne et al., 2020).

The QDs that were incorporated into the PDMS polymer in this study did not produce milky solutions and the QD@PDMS solutions were clear, which could indicate that most of the TOPO had been removed when the QDs were washed, and as a result, OA was primarily found on the surface of the QDs. This surface capping ligand and PDMS did mix well together, as there was no precipitation observed after mixing the QDs with the PDMS as was seen in another study (Tao et al., 2013). Dispersion of the QDs in the PDMS in this study was also shown to be excellent based on visual inspection under ultraviolet-visible light, where a homogeneous distribution of fluorescence over the film was observed.

It is well understood that fluorescence is a complex process and that developing sensors capable of detecting analytes and organic contaminants, particularly at low environmentally relevant concentrations, is challenging. Fluorescence emission of QDs is dependent on many factors as fluorescence properties are variable and sensitive to surface molecules (Yuan et al., 2008), local environments (Kloepter et al., 2005) and light illumination (Jones et al., 2003) owing to the high surface to volume ratio. Fluorescence may constantly change by turning on and off intermittently, due to the blinking effect of QDs and the differences in excited state between electrons of different QDs and therefore the energy of emission during the fluorescence relaxation process.

When CdSe/ZnS QD emission was observed at a single-dot level, an on/off behaviour was observed (Verberk, 2002). The fluorescence “blinking” can have off-periods of several seconds in QDs (Verberk, 2002) and can compromise QD measurements. However, when QD ensembles are observed, the blinking effect goes unnoticed because of the averaging of the luminescence emission of the bulk of the QDs (van Sark., 2002). The charge can also be trapped in the adjacent matrix, which would be the PDMS polymer in this case, which can alter the duration of the blinking effect of the QDs (Kudera, 2008). Light scattering effects should also be considered, as this affects the amount of light reaching the fluorescence detector.

Many more experiments are required to establish a repeatable sensing method, but this preliminary research sets the groundwork for future developments in this regard. Although selective sensing towards the two target organic compounds tested may not be possible, it has been demonstrated that QD@PDMS may potentially serve as a sensor for the detection of organic contamination hotspots in water sources.

An evaluation of the extent of fluorescence fluctuation of the QD@PDMS material, the determination of the intervals at which fluorescence measurements should be performed, as well as how long sensor films should be interacted with samples, have been achieved in this study.

The development of a portable fluorescence spectrometer setup would be valuable for future studies, enabling it to be utilized in the field, but since the method was not sensitive enough to detect organic analytes at trace levels with the benchtop fluorescence apparatus, it should be concluded that the portable setup will not be currently viable and sensitive enough for these sensing applications.

5.2. Future work

The fluorescence mechanism of the QD@PDMS requires further elucidation in order to better understand and predict changes in fluorescence when this material is brought into contact with various solvents and analytes. Photoinduced fluorescence enhancement (PFE) of CdSe and CdSeTe/ZnS QDs, for example, has been observed in a wide range of environments, including aggregated QD monolayers (Cordero et al., 2000), aqueous and organic solutions (Jones et al., 2003) thin polymer films (Nazzal et al., 2004), or when these QDs are exposed to ambient light (unintentional illumination by room light) (Wang et al., 2003). Upon illumination exposure, certain single QDs may exhibit a positive charge. Therefore, upon light irradiation, fluorescence emission may be suppressed rather than increased (Yuan et al., 2008), which is inconsistent with the ensemble PFE phenomena. Surface-environmental effects such as photoinduced surface passivation by water molecules (Cordero et al., 2000), and photoinduced oxidation (Wang et al., 2003), should be further investigated.

In this study, it was found that the films are very sensitive to ultraviolet–visible and ambient light, and the effect that light has on the QD fluorescence emission should thus be investigated further. It should also be investigated to what degree the fluorescence of the QD polymers can be increased by exposing them to natural light, since this might enhance the sensitivity of the sensor, although variations in this effect makes the interpretation of the sensing results difficult. It is thus recommended that the films be stored in the dark after synthesis and prior to use. The effect of ambient light, even during the brief time of sensing, should be further examined since it may alter the data obtained, and tests may need to be performed in a dark setting to avoid external impacts, which may not be practical especially for in-field measurements.

To conclude, additional research into the influence of variations in exposure to light on the fluorescence emission of QD@PDMS is crucial for future development of this material as a fluorescence sensor.

References

Abarikwu S. O., Farombi E. O. (2015). 'Atrazine induces apoptosis of SH-SY5Y human neuroblastoma cells via the regulation of Bax/Bcl- 2 ratio and caspase-3-dependent pathway.', Pesticide Biochemistry and Physiology, 118, 90–98.

Abdel-Ghany A. M., Al-Helal I. M., Alzahrani S. M., Alsadon A. A., Ali I. M. and Elleithy R. M. (2012). 'Covering materials incorporating radiation-preventing techniques to meet greenhouse cooling challenges in arid regions: a review.', Scientific World Journal, 1–11.

Abdel-Shafy, H. I. and Mansour, M. S. M. (2016). 'A review on polycyclic aromatic hydrocarbons: Source, environmental impact, effect on human health and remediation.', Egyptian Journal of Petroleum, 25, 107–123.

Adegoke, O., Dabrowski, J.M., Montaseri, H., Nsibande, S.A., Petersen, F. and Forbes, P.B.C. (2017). 'Development of novel fluorescent sensors for the screening of emerging chemical pollutants in water.', WRC report no. 2438/1/17, ISBN 978-1-4312-0936-1.

Adegoke, O. and Forbes, P.B.C. (2016). 'L-Cysteine-capped core/shell/shell quantum dot graphene oxide nanocomposite fluorescence probe for polycyclic aromatic hydrocarbon detection.', Talanta, 146, 780-788.

Adegoke, O., Montaseri, H., Nsibande, S. A. and Forbes, P. B. C. (2019). 'Passivating effect of ternary alloyed AgZnSe shell layer on the structural and luminescent properties of CdS quantum dots.', Materials Science in Semiconductor Processing, 90, 162–170.

Adegoke, O., Montaseri, H., Nsibande, S. A. and Forbes, P. B. C. (2017). 'Alloyed quaternary/binary core/shell quantum dot-graphene oxide nanocomposite: preparation, characterization and application as a fluorescence "switch ON" probe for environmental pollutants.', Journal of Alloys and Compounds, 720, 70-78.

Adegoke, O., Nyokong, T. and Forbes, P. B. C. (2016). 'Deposition of CdS, CdS/ZnSe and CdS/ZnSe/ZnS shells around CdSeTe alloyed core quantum dots: effects on optical properties.', Luminescence, 31, 694–703.

Adeniji, A. O., Okoh, O. O. and Okoh, A. I. (2019). 'Levels of polycyclic aromatic hydrocarbons in the water and sediment of buffalo river estuary, South Africa and their health risk assessment.', Archives of Environmental Contamination and Toxicology, 76(4), 657–669.

Akcora, P., Liu, H., Kumar, S. K., Moll, J., Li, Y., Benicewicz, B. C., Schadler, L. S., Acehan, D., Panagiotopoulos, A. Z., Pryamitsyn, V., Ganesan, V., Ilavsky, J., Thiyagarajan, P., Colby R. H. and Douglas, J. F. (2009). 'Anisotropic self-assembly of spherical polymer-grafted nanoparticles.', Nature Materials, 2009, 8(4), 354-359.

Alf, B. M. E., Asatekin, A., Barr, M. C., Baxamusa, S. H., Chelawat, H., Ozaydin-ince, G., Petruczok, C. D., Sreenivasan, R., Tenhaeff, W. E., Trujillo, N. J., Vaddiraju, S., Xu, J. and Gleason, K. K. (2010). 'Chemical vapor deposition of conformal, functional and responsive polymer films.', Advanced Materials, 22, 1993–2027.

Alvarez, A., Costa-Fernández, J. M., Pereiro, R., Sanz-Medel, A. and Salinas-Castillo, A. (2011). 'Fluorescent conjugated polymers for chemical and biochemical sensing.', Trends in Analytical Chemistry, 30(9), 1513–1525.

Angerer J., Mannschreck C. And Gündel J. (1997). 'Biological monitoring and biochemical effect monitoring of exposure to polycyclic aromatic hydrocarbons.', International Archives of Occupational and Environmental Health, 70, 365-377.

Asfour, A. F. A. and Dullien, F. A. L. (1981). 'Viscosities and densities of four binary liquid systems at 25.00 °C.', Journal of Chemical & Engineering Data, 26, 312–316.

Bado-Nilles, A., Quentel, C., Thomas-Guyon, H. and Le Floch, S. (2009). 'Effects of two oils and 16 pure polycyclic aromatic hydrocarbons on plasmatic immune parameters in the European sea bass, *Dicentrarchus labrax* (Linne).', Toxicology in Vitro, 23(2), 235–241.

Bae, J., Park, J., Kim, S., Cho, H., Kim, H. J., Par, S. and Shin, D. (2020). 'Tailored hydrogels for biosensor applications.', Journal of Industrial and Engineering Chemistry, 89, 1-12.

Bae, W. K., Kwak, J., Park, J. W., Char, K., Lee, C. and Lee, S. (2009). 'Highly efficient green-light-emitting diodes based on CdSe@ZnS quantum dots with a chemical-composition gradient.', Advanced Materials, 21(17), 1690–1694.

Bai, C. and Liu, M. (2012). 'Implantation of nanomaterials and nanostructures on surface and their applications.', Nano Today, 7(4), 258–281.

Bakar, N. A., Salleh, M. M., Umar, A. A. and Yahaya, M. (2011). 'The detection of pesticides in water using ZnCdSe quantum dot films.', Advances in Natural Sciences: Nanoscience and Nanotechnology, 2, 3–7.

Balch, G. C., Metcalfe, C. D. and Huestis, S. Y. (1995). 'Identification of potential fish carcinogens in sediment from Hamilton Harbour, Ontario, Canada.', Environmental Toxicology and Chemistry, 14, 79-91.

Barnham, K., Marques, J. L., Hassard, J. and O'Brien, P. (2000). 'Quantum-dot concentrator and thermodynamic model for the global redshift.', Applied Physics Letters, 76, 1197–1199.

Barrón Cuenca, J., Tirado, N., Barral, J., Ali, I., Levi, M., Stenius, U., Berglund, M. and Dreij, K. (2019). 'Increased levels of genotoxic damage in a Bolivian agricultural population exposed to mixtures of pesticides.', Science of The Total Environment, 695(133942).

Beaulieu, M., Cabana, H., Taranu, Z. and Huot, Y. (2020). 'Predicting atrazine concentrations in waterbodies across the contiguous United States: The importance of land use, hydrology, and water physicochemistry.', Limnology and Oceanography, 65(12), 2966–2983.

Benotti, M., Trenholm, R. A., Vaderford, B. J., Holady, J. C., Stanford, B. D. and Snyder, S. A. (2009). 'Pharmaceuticals and endocrine disrupting compounds in U.S. drinking water.', Environmental Science and Technology, 43(3), 597–603.

Blume, E., Bischoff, M., Moorman, T. B. and Turco, R. F. (2004). 'Degradation and binding of atrazine in surface and subsurface soils.', Journal of Agricultural and Food Chemistry, 52(24), 7382–7388.

Bo, L., Shengen, Z., Chang, C., Zhanfeng, D. and Hongxiang, L. (2015). 'Emerging pollutants – part II: treatment.', Water Environment Research, 87(10), 1873–1900.

Bol, A. A. and Meijerink, A. J. (2001). 'Luminescence quantum efficiency of nanocrystalline ZnS:Mn^{2+}. 2. Enhancement by UV irradiation.', The Journal of Physical Chemistry B, 105(42), 10203-10209.

Borges, C. A. M., Rodrigues, C. A., Faria, R. M. and Giumaraes, F. E. G. (2005). 'Strong luminescence intensity modulation near a metal-organic interface.', Synthetic Metals, 154, 133-136.

Brus, L. E. (1984). 'Electron—electron and electron-hole interactions in small semiconductor crystallites: the size dependence of the lowest excited electronic state.', The Journal of Chemical Physics, 80(9), 4403–4409.

Byers, R. J. and Hitchman, E. R. (2011). 'Quantum dots brighten biological imaging.', Progress in Histochemistry and Cytochemistry, 45(4), 201–237.

Carlsen, S. C. K. (2006). 'Drift of 10 herbicides after tractor spray application. 2. Primary drift (droplet drift).', Chemosphere, 64, 778–786.

Caruge, J. M., Halpert, J. E., Wood, V., Bulovic, V. and Bawendi, M. G. (2008). 'Colloidal quantum- dot light-emitting diodes with metal-oxide charge transport layers.', Nature Photonics, 2(4), 247–250.

Chandan, H. R., Schiffman, J. D. and Balakrishna, R. G. (2018). 'Quantum dots as fluorescent probes: synthesis, surface chemistry, energy transfer mechanisms, and applications.', Sensors and Actuators B: Chemical, 258, 1191–1214.

Chen, C. and Chen, C. (2011). 'Distribution, origin and potential toxicological significance of PAHs in sediments of Kaohsiung harbour, Taiwan.', Marine Pollution Bulletin, 63, 417-423.

Chen, M. X., Sun, R. Y., Ye, Y. C., Tang, H. J., Dong, X. Y., Yan, J. L., Wang, K. M., Zhou, Q. and Wang, Z. L. (2018). 'Application of a novel red-emitting cationic iridium(III) coordination polymer in warm white light-emitting diodes.', Optical Materials, 76, 141-146.

Chen, S. A. and Chang, E. C. (1999). 'Conjugated polymer blends as emitting layer for white light LED.', Semiconducting Polymers, 163-172.

Chen, Y., Vela, J., Htoon, H., Casson, J. L., Werder, D. J., Bussian, D. A., Klimov, V. I. and Hollingsworth, J. A. (2008). '"Giant" multishell CdSe nanocrystal quantum dots with suppressed blinking.', Journal of the American Chemical Society, 130(15), 5026–5027.

Chen, Y. and Rosenzweig, Z. (2002). 'Luminescent CdS quantum dots as selective ion probes.', Analytical Chemistry, 74, 5132.

Cheng, G., Fei, T., Zhao, Y., Ma, Y. G. and Liu, S. Y. (2010). 'White phosphorescent polymer light-emitting devices based on a wide band-gap polymer derived from 3,6-carbazole and tetraphenylsilane.', Organic Electronics, 11(3), 498-502.

Cheng, J., Mu, Y., Wu, L., Liu, Z., Su, K., Dong, G., Zhang, M. and Lu, T. (2022). 'Strongly correlated quantum dot arrays for unconventional superconductivity.', Nano Research, 15, 1845-1851.

Chitara, B., Bhat, S. V., Vivekchand, S. R. C., Gomathi, A. and Rao, C. N. R. (2008). 'White-light sources based on composites of GaN nanocrystals with conducting polymers and nanophosphors.', Solid State Communications, 147(9-10), 409-413.

Chowdhury, S., Khan, N., Kim, G.H., Harris, J., Longhurst, P. and Bolan, N. S. (2016). 'Zeolite for stripping from farm effluents.', Environmental Materials and Waste, 569-589.

Chung, Y. C., Yang, C. H., Zheng, H. W., Tsai, P. S. and Wang, T. L. (2018). 'Synthesis and characterization of CdS x Se1-x alloy quantum dots with composition-dependent band gaps and paramagnetic properties.', RSC Advances, 8(52), 30002-30011.

Clarke, S. J. (2008). 'Synthesis, biological targeting and photophysics of quantum dots.', [Doctoral dissertation, McGill University].

Cooper, R. L., Stoker, T. E., Tyrey, L., Goldman, J. M. and McElroy, W. K. (2000). 'Atrazine disrupts the hypothalamic control of pituitary-ovarian function.', Toxicological Sciences, 53(2), 297-307.

Cordero, S. R., Carson, P. J., Estabrook, R. A., Strouse, G. F. and Buratto, S. K. J. (2000). 'Photo-activated luminescence of CdSe quantum dot monolayers.', The Journal of Physical Chemistry B, 104(51), 12137–12142.

Da Silva, M. A. T., Thomazini, E. F., Albertini, M., Renzi, W., Franchello, F., Dias, I. F. L., Duarte, J. L., Pocas, L. C. and Lourenco, S. A. (2016). 'Characterization of digital textile printing and polymer blend (PFO-DMP:P3HT) for application in manufacture of organic diodes emitting white light – WOLEDS.', Optical Materials, 62, 119-131.

Dabbousi, B. O., Rodríguez-Viejo, J., Mikulec, F. V., Heine, J.R., Mattoussi, H., Ober, R., Jensen, K. F. and Bawendi, M. G. (1997). '(CdSe)ZnS core-shell quantum dots- synthesis and characterization of a size series of highly luminescent nanocrystallites.', Journal of Physical Chemistry B, 101(46), 9463-9475.

Dabrowski, J.M., Shadung, J.M. and Wepener, V. (2014). 'Prioritizing agricultural pesticides used in South Africa based on their environmental mobility and potential human health effects.', Environment International, 62, 31-40.

Dahl, J.A., Maddux, B.L. and Hutchison, J.E. (2007). 'Toward greener nanosynthesis.', Chemical Reviews, 107(6), 2228–2269.

Davis, C., Fellin, P. and Otson, R. (1987). 'A review of sampling methods for polyaromatic hydrocarbons in air.', Journal of the Air & Waste Management Association, 37, 1397–1408.

Deegan, R. D., Bakajin, O., Dupont, T. F., Huber, G., Nagel S. R. and Witten, T. A. (1997). 'Capillary flow as the cause of ring stains from dried liquid drops.', Nature, 389, 827–829.

Delattre, F., Cazier, F., Cazier, F. and Tine, A. (2009). 'Use a fluorescent molecular sensor for the detection of pesticides and herbicides in water.', Current Analytical Chemistry, 5(1), 48–52.

Demas, J. N. and Crosby, G. A. (1971). 'The Measurement of photoluminescence quantum yields. Review.', The Journal of Physical Chemistry, 75(8), 991–1024.

Dhami, S., de Mello A. J., Rumbles G., Bishop S. M., Phillips D. and Beeby A. (1995). 'Phthalocyanine fluorescence at high concentration: dimers or reabsorption effect?.', Photochemistry and Photobiology, 61, 341.

Dilag, J., Kobus, H. and Ellis, A. (2009). 'Cadmium sulfide quantum dot/chitosan nanocomposites for latent fingermark detection.', Forensic Science International, 187(1-3), 97-102.

Duijs, E. F., Findeis, F., Deutschmann, R. A., Bichler, M., Zrenner, A., Abstreiter, G., Adlkofer, K., Tanaka, M. and Sackmann, E. (2001). 'Influence of thiol coupling on photoluminescence of near surface InAs quantum dots.', Physica Status Solidi (B), 224(3), 871-875.

Ekimov, A. (1996). 'Growth and optical properties of semiconductor nanocrystals in a glass matrix.', Journal of Luminescence, 70, 1–20.

Ekimov, A. I., Onushchenko, A. A., Tsekhomskii, V. A. (1980). 'Exciton absorption by copper(I) chloride crystals in a glassy matrix.', Fizika I Khimiya Stekla, 6, 511.

Ewa, B. and Danuta, M. Š. (2017). 'Polycyclic aromatic hydrocarbons and PAH-related DNA adducts.', Journal of Applied Genetics, 58(3), 321–330.

Fan, L. M., Fan, W. L., Li, B., Zhao, X. and Zhang, X. T. (2016). 'W-shaped 1,3-di(2,4-dicarboxyphenyl)benzene based lanthanide coordination polymers with tunable white light emission.', New Journal of Chemistry, 40(12), 10440-10446.

Fan, W., Yanase, T., Morinaga, H., Gondo, S., Okabe, T., Nomura, M. and Nawata, H. (2007) 'Atrazine-induced aromatase expression is SF-1 dependent: implications for endocrine disruption in wildlife and reproductive cancers in humans.', Environmental Health Perspectives, 115(5), 720–727.

Farkhani, S. M. and Valizadeh, A. (2012). 'Review: three synthesis methods of CdX (X = Se, S or Te) quantum dots.', IET Nanobiotechnology, 8(2), 59-76.

Farmer, S. C. and Patten, T.E. (2001). 'Photoluminescent polymer/quantum dot composite nanoparticles.', Chemistry of Materials, 13, 3920–3926.

Feng, K., Yu, B. Y., Ge, D. M., Wong, M. H., Wang, X. C. and Cao, Z. H. (2003). 'Organo-chlorine pesticide (DDT and HCH) residues in the Taihu Lake Region and its movement in soil-water system I. Field survey of DDT and HCH residues in ecosystem of the region.', Chemosphere, 50(6), 683-687.

Fery-Forgues, S. and Lavabre, D. (1999). 'Are Fluorescence Quantum Yields So Tricky to Measure? A Demonstration Using Familiar Stationery Products.', Journal of Chemical Education, 76(9), 1260.

Fischer, M. and Georges, J. (1996). 'Sources of errors in the use of calorimetric references for photothermal spectroscopic methods.', Analytica Chimica Acta, 334(3), 337-344.

Frantsuzov, P., Kuno, M., Janko, B. and Marcus, R. A. (2008). 'Universal emission intermittency in quantum dots, nanorods and nanowires.', Nature Physics, 4, 519-522.

Frigerio, C., Ribeiro, D., Rodrigues, S., Abreu, V., Barbosa, J., Prior, J., Marques, K. and Santos, J. (2012). 'Application of quantum dots as analytical tools in automated chemical analysis: a review.', Analytica Chimica acta, 735, 9-22.

Fu, Y., Kim, D., Jiang, W., Yin, W., Ahn, T. K. and Chae, H. (2017). 'Excellent stability of thicker shell CdSe@ZnS/ZnS quantum dots.', RSC Advances, 7, 40866-40872.

Gao, X., Yang, L., Petros, J.A., Marshall, F.F., Simons, J.W. and Nie, S. (2005). 'In vivo molecular and cellular imaging with quantum dots.', Current Opinion in Biotechnology, 16(1), 63–72.

Galian, R.E. and Scaiano, J.C. (2009). 'Fluorescence quenching of CdSe quantum dots by tertiary amines and their surface binding effect.', Photochemical and Photobiological Sciences, 8, 70–74.

Gallagher, D., Heady, W. E., Racz, J. M. and Bhargava, R. N. J. (1995). 'Homogeneous precipitation of doped zinc sulfide nanocrystals for photonic applications.', Journal of Materials Research, 10, 870-876.

Gaponik, N. and Rogach, A. L. (2008). 'Aqueous synthesis of semiconductor nanocrystals.', In Rogach, A. (Ed.), Semiconductor Nanocrystal Quantum Dots: Synthesis, Assembly, Spectroscopy and Applications. Springer, 73–99.

Gaponik, N., Talapin, D. V., Rogach, A. L., Hoppe, K., Shevchenko, E. V., Kornowski, A., Eychmüller, A. and Weller, H. (2002). 'Thiol-capping of CdTe nanocrystals: an alternative to organometallic synthetic routes.', The Journal of Physical Chemistry B, 106(29), 7177–7185.

Gesto, M., Tintos, A., Rodriguez-ILLamola, A., Soengas, J. L. and Miguez J. M. (2009). 'Effects of naphthalene, beta-naphthoflavone and benzo(a)pyrene on the diurnal and nocturnal indoleamine metabolism and melatonin content in the pineal organ of rainbow trout, (Oncorhynchus mykiss).', Aquatic Toxicology, 92, 1–8.

Ghosh, A., Paul, S. and Raj, S. (2013). 'Structural phase transformation from wurtzite to zinc-blende in uncapped CdS nanoparticles.', Solid State Communications, 154, 25–29.

Giansante, C. and Infante, I. (2017). 'Surface traps in colloidal quantum dots: A combined experimental and theoretical perspective.', Journal of Physical Chemistry Letters, 8, 5209–5215.

Giurlani, W., Berretti, E., Innocenti, M. and Lavacchi, A. (2020) 'Measuring the thickness of metal films: A selection guide to the most suitable technique.', Materials Proceedings., 2(12), 1-30.

Girão, A.V., Caputo, G. and Ferro, M.C. (2017). 'Application of scanning electron microscopy–energy dispersive X-ray spectroscopy (SEM-EDS).', Comprehensive Analytical Chemistry, 75, 153-168.

Gole, A., Jana, N. R., Selvan, S. T. and Ying, J. Y. (2008). 'Langmuir-Blodgett thin films of quantum dots: synthesis, surface modification, and fluorescence resonance energy transfer (FRET) studies.', Langmuir, 24, 8181–8186.

Green, P. F. (2011). 'The structure of chain end-grafted nanoparticle/homopolymer nanocomposites.', Soft Matter, 7(18), 7914-7926.

Greytak, A. B., Allen, P. M., Liu, W., Zhao, J., Young, E. R., Popović, Z., Walker, B. J., Nocera, D. G. and Bawendi, M. G. (2012). 'Alternating layer addition approach to CdSe/CdS core/shell quantum dots with near-unity quantum yield and high on-time fractions.', Chemical Science, 3, 2028–2034.

Guo, J., Zhang, Y., Luo, Y., Shen, F. and Sun, C. (2014). 'Efficient fluorescence resonance energy transfer between oppositely charged CdTe quantum dots and gold nanoparticles for turn-on fluorescence detection of glyphosate.', Talanta, 125, 385–392.

Hao, J., Liu, H., Miao, J., Lu, R., Zhou, Z., Zhao, B., Xie, B., Cheng, J., Wang, K. and Delville, M.-H. (2019). 'A facile route to synthesize CdSe/ZnS thick-shell quantum dots with precisely controlled green emission properties: towards QDs based LED applications.', Scientific Reports, 9, 12048.

He, R. and Gu, H. (2006). 'Synthesis and characterization of mondispersed CdSe nanocrystals at lower temperature.', Colloids and Surfaces A: Physicochemical and Engineering Aspects, 272(1–2), 111–116.

Hines, M. A. and Guyot-Sionnest, P. (1996). 'Synthesis and characterization of strongly luminescing ZnS-capped CdSe nanocrystals.', The Journal of Physical Chemistry, 100(2), 468–471.

Houtepen, A. J., Hens, Z., Owen, J. S. and Infante, I. (2017). 'On the origin of surface traps in colloidal II–VI semiconductor nanocrystals.', Chemistry of Materials, 29(2), 752−761.

Hrma, M., Sichova, K., Svoboda, J. and Vohlidal, J. (2017). 'Assembling of bis(tpy)fluorenes with Zn^{2+} and Fe^{2+} ions into metallo-supramolecular polymers with highly efficient white-light emission.', Polymer, 122, 22-33.

Hu, M. Z. and Zhu, T. (2015). 'Semiconductor nanocrystal quantum dot synthesis approaches towards large-scale industrial production for energy applications.', Nanoscale Research Letters, 10(469), 1–15.

Hu, X. and Gao, X. (2010). 'Silica−polymer dual layer-encapsulated quantum dots with remarkable stability.' ACS Nano, 4(10), 6080–6086.

Hussain, S. A. and Bhattacharjee, D. (2009). 'Langmuir-Blodgett films and molecular electronics.', Modern Physics Letters B, 23(29), 3237-3451.

Inoue-Choi, M., Weyer, P. J., Jones, R. R., Booth, B. J., Cantor, K. P., Robien, K. and Ward, M. H. (2016). 'Atrazine in public water supplies and risk of ovarian cancer among postmenopausal women in the Iowa Women's Health Study.', Journal of Occupational and Environmental Medicine, 73(9), 582.

Jang, H. S., Yang, H., Kim, S. W., Han, J. Y., Lee, S. G. and Jeon, D. Y. (2008). 'White light-emitting diodes with excellent color rendering based on organically capped CdSe quantum dots and $Sr_3SiO_5:Ce^{3+}$, Li^+ phosphors.', Advanced Materials, 20, 2696–2702.

Ji, X., Wang, C., Xu, J., Zheng, J., Gattás-Asfura, K. M. and Leblanc, R. M. (2005). 'Surface chemistry studies of (CdSe)ZnS quantum dots at the air-water interface.', Langmuir, 21(12), 5377-5382.

Jia, M., Zhang, Z., Li, J., Shao, H., Chen, L. and Yang, X. (2017). 'A molecular imprinting fluorescence sensor based on quantum dots and a mesoporous structure for selective and sensitive detection of 2,4-dichlorophenoxyacetic acid.', Sensors and Actuators B: Chemical, 252, 934–943.

Jiang, K., Sun, S., Zhang, L., Wang, Y., Cai, C. and Lin, H. (2015). 'Bright-yellow-emissive N-doped carbon dots: preparation, cellular imaging, and bifunctional sensing.', ACS Applied Materials and Interfaces, 7(41), 23231–23238.

Jin, S., Hu, Y., Gu, Z., Liu, L. and Wu, H.-C. (2011). 'Application of quantum dots in biological imaging.', Journal of Nanomaterials, 1–13.

Jing, L., Kershaw, S. V., Li, Y., Huang, X., Li, Y., Rogach, A. L. and Gao, M. (2016). 'Aqueous based semiconductor nanocrystals.', Chemical Reviews, 116, 10623−10730.

Jones, M., Nedeljkovic, J., Ellingson, R. J. Nozik, A. J. and Rumbles, G. (2003). 'Photoenhancement of luminescence in colloidal CdSe quantum dot solutions.', The Journal of Physical Chemistry B, 107(41), 11346–11352.

Jonker, M.T.O. (2022). 'Polyethylene–water and polydimethylsiloxane–water partition coefficients for polycyclic aromatic hydrocarbons and polychlorinated biphenyls: influence of polymer source and proposed best available values.' Environmental Toxicology and Chemistry, 41, 1370-1380.

Joo, J., Na, H. B., Yu, T., Yu, J. H., Kim, Y. W., Wu, F., Zhang, J. Z. and Hyeon T. (2003). 'Generalized and facile synthesis of semiconducting metal sulfide nanocrystals.', Journal of the American Chemical Society, 125(36), 11100–11105.

Jorge, P., Martins, M. A., Trindade, T., Santos, J. L. and Farahi, F. (2007). 'Optical fiber sensing using quantum dots.', Sensors, 7, 3489–3534.

Jun, S., Lee, J. and Jang, E. (2013). 'Highly luminescent and photostable quantum dot-silica monolith and its application to light-emitting diodes.', ACS Nano, 7, 1472–1477.

Kalwarczyk, E., Ziębacz, N., Kalwarczyk, T., Hołyst, R. and Fiałkowski, M. (2013). 'A "wrap-and-wrest" mechanism of fluorescence quenching of CdSe/ZnS quantum dots by surfactant molecules.', Nanoscale, 5(20), 9908–9916.

Kapitonov, A. M., Stupak, A. P., Gaponenko, S. V., Petrov, E. P., Rogach, A. L. and Eychmüller, A. (1999). 'Luminescence properties of thiol-stabilized CdTe nanocrystals.', Journal of Physical Chemistry B, 103, 10109−10113.

Kausar, A. (2019). 'Polymer/carbon-based quantum dot nanocomposite: forthcoming materials for technical application.', Journal of Macromolecular Science, Part A, 56(4), 341–356.

Khan, I., Saeed, K. and Khan, I. (2019). 'Nanoparticles: properties, applications and toxicities.', Arabian Journal of Chemistry, 12, 908–931.

Kim, C., Gurau, M. C., Cremer, P. S. and Yu, H. (2008). 'Chain conformation of poly(dimethyl siloxane) at the air/water interface by sum frequency generation.', Langmuir, 24, 10155–10160.

Kim, D., Kim, S. H. and Park, J. Y. (2019). 'Floating-on-water fabrication method for thin polydimethylsiloxane membranes.', Polymers, 11(8).

Kim, J., Hwang, D. W., Jung, H. S., Kim, K. W., Pham, X.-H., Lee, S.-H., Byun, J. W., Kim, W., Kim, H.-M., Hahm, E., Ham, K.-M., Rho, W.-Y., Lee, D. S. and Jun, B.-H. (2022). 'High-quantum yield alloy-typed core/shell CdSeZnS/ZnS quantum dots for bio-applications.', Journal of Nanobiotechnology, 20(22).

Kim, K. H., Kabir, E. and Jahan, S. A. (2017). 'Exposure to pesticides and the associated human health effects.', Science of the Total Environment, 575, 525–535.

Kim, S., Kim, T., Kang, M., Kwak, S. K., Yoo, T. W., Park, L. S., Yang, I., Hwang, S., Lee, J. E., Kim, S. K. and Kim, S.W. (2012). 'Highly luminescent InP/GaP/ZnS nanocrystals and their application to white light-emitting diodes.', Journal of the American Chemical Society, 134, 3804–3809.

Kirkwood, N., Monchen, J. O. V., Crisp, R. W., Grimaldi, G., Bergstein, H. A. C., du Fossé, I., van der Stam, W., Infante, I. and Houtepen, A. J. (2018). 'Finding and fixing traps in II–VI and III–V colloidal quantum dots: The importance of Z-type ligand passivation.', Journal of the American Chemical Society, 140(46), 15712−15723.

Kloepter, J. A., Bradforth, S. E. and Nadean, J. L. (2005). 'Photophysical Properties of Biologically Compatible CdSe Quantum Dot Structures.', The Journal of Physical Chemistry B, 109, 9996-10003.

Komarala, V. K., Rakovich, Y. P., Bradley, A. L., Byrne, S. J., Corr, S. A. and Gun'ko, Y. K. (2006). 'Off-resonance surface plasmon enhanced spontaneous emission from CdTe quantum dots.', Applied Physics Letters, 89, 253118.

Kong, W., Yang, X., Yang, M., Zhou, H., Ouyang, Z. and Zhao, M. (2016). 'Photoluminescent nanosensors capped with quantum dots for high-throughput determination of trace contaminants: strategies for enhancing analytical performance.', Trends in Analytical Chemistry, 78, 36–47.

Krishnan, S. (2007). 'Tables of moments and deflections for a rectangular plate fixed at all edges and carrying a uniformly distributed load.', [Doctoral dissertation, Massachusetts Institute of Technology].

Kritzinger, A., Forbes, A. and Forbes, P. B. C. (2022). 'Optical trapping and fluorescence control with vectorial structured light.', Nature, Scientific Reports, 12, 17690.

Kubin, R. F. and Fletcher A. N. (1982). 'Fluorescence quantum yields of some rhodamine dyes.', Journal of Luminescence, 27, 455-462.

Kudera, S., Carbone, L., Manna, L. and Parak, W. J. (2008). 'Growth mechanism, shape and composition control of semiconductor nanocrystals.', In Rogach, A. L. (eds) Semiconductor Nanocrystal Quantum Dots, Springer, Vienna, 1-34.

Kumar, P., Kim, K. H. and Deep, A. (2015). 'Recent advancements in sensing techniques based on functional materials for organophosphate pesticides.', Biosensors and Bioelectronics, 70, 469–481.

Kuzyniak, W., Adegoke, O., Sekhosana, K., D'Souza, S., Tshangana, S. C., Hoffmann, B., Ermilov, E. A., Nyokong, T. and Höpfner, M. (2014). 'Synthesis and characterization of quantum dots designed for biomedical use.', International Journal of Pharmaceutics, 466, 382–389.

Larsson, M., Orbe, D. and Engwall, M. (2012). 'Exposure-time-dependent effects on the relative potencies and additivity of PAHs in the Ah receptor-based H4IIE-luc bioassay.', Environmental Toxicology and Chemistry, 31(5), 1149-1157.

Lee, S.-H., Han, C.-Y., Song, S.-W., Jo, D.-Y., Jo, J.-H., Yoon, S.-Y., Kim, H.-M., Hong, S., Hwang, J. Y. and Yang, H. (2020). 'Nanoporous gold films patterned with semiconductor quantum dots for plasmonic biosensing.', Chemistry of Materials, 32(16), 5768–5776.

Li, J. J., Wang, Y. A., Guo, W., Keay, J. C., Mishima, T. D., Johnson, M. B. and Peng, X. (2003). 'Large-scale synthesis of nearly monodisperse CdSe/CdS core/shell nanocrystals using air-stable reagents via successive ion layer adsorption and reaction.', Journal of the American Chemical Society, 125(41), 12567–12575.

Lin, L., Rong, M., Luo, F., Chen, D., Wang, Y. and Chen, X. (2014). 'Luminescent graphene quantum dots as new fluorescent materials for environmental and biological applications.', Trends in Analytical Chemistry, 54, 83–102.

Ling, J. and Huang, C. Z. (2010). 'Energy transfer with gold nanoparticles for analytical applications in the fields of biochemical and pharmaceutical sciences.', Analytical Methods, 2(10), 1439–1447.

Lou, X., Zeng, Q., Zhang, Y., Wan, Z., Qin, J. and Li, Z. (2012). 'Functionalized polyacetylenes with strong luminescence: "Turn-on" fluorescent detection of cyanide based on the dissolution of gold nanoparticles and its application in real samples.', Journal of Materials Chemistry, 22, 5581–5586.

Lu, M., Zeng, D. C., Liao, Y. and Tong, B. (2012). 'Distribution and characterization of organochlorine pesticides and polycyclic aromatic hydrocarbons in surface sediment from Poyang Lake, China.', Science of the Total Environment, 433, 491-497.

Lui, Y., Chen, L., Huang, Q.-H., Li, W.-Y., Tang, Y.-J. and Zhao, J.-F. (2009). 'Source apportionment of polycyclic aromatic hydrocarbons (PAHs) in surface sediments of Huangpu River, Shanghai, China.', Science of the Total Environment, 407, 2931-2938.

Ma, K., Wu, H. Y., Zhang, B., He, X. and Li, B. X. (2015). 'Neurotoxicity effects of atrazine-induced SH-SY5Y human dopaminergic neuroblastoma cells via microglial activation.', Molecular BioSystems, 11(11), 2915–2924.

Ma, Q. and Su, X. (2011). 'Recent advances and applications in QDs-based sensors.', The Analyst, 136, 4883-4893.

Machala, M., Ciganek, M., Bláha, L., Minksová, K. and Vondráček, J. (2001). 'Aryl hydrocarbon receptor-mediated and estrogenic activities of oxygenated polycyclic aromatic hydrocarbons and azaarenes originally identified in extracts of river sediments.', Environmental Toxicology and Chemistry, 20, 2736-3743.

Mahgoub, H. A. (2014). 'Extraction techniques for determination of polycyclic aromatic hydrocarbons in water samples.', International Journal of Science and Research, 5(1).

Mata, A., Fleischman, A. J. and Roy, S. (2005). 'Characterization of polydimethylsiloxane (PDMS) properties for biomedical micro/nanosystems.', Biomedical Microdevices, 7(4), 281–293.

Mayer, P., Vaes, W. H. J. and Hermens, J. L. M. (2000). 'Absorption of hydrophobic compounds into the poly(dimethylsiloxane) coating of solid-phase microextraction fibers: High partition coefficients and fluorescence microscopy images. Analytical Chemistry, 72, 459-464.

Medintz, I. L., Uyeda, H. T., Goldman, E. R. and Mattoussi, H. (2005). 'Quantum dot bioconjugates for imaging, labelling and sensing.', Nature Materials, 4(6), 435–446.

Michalet, X., Pinaud, F. F., Bentolila, L. A., Tsay, J. M., Doose, S., Li, J. J., Sundaresan, G., Wu, A. M., Gambhir, S. S. and Weiss S. (2005). 'Quantum Dots for live cells, in vivo imaging, and diagnostics.', Science, 307(5709), 538–544.

Mohapatra, S., Bera, M. K. and Das, R. K. (2018). 'Rapid "turn-on" detection of atrazine using highly luminescent N-doped carbon quantum dot.', Sensors and Actuators B: Chemical, 263, 459–468.

Montaseri, H. (2018). 'Quantum dot - molecularly imprinted polymer nanomaterials for the fluorescence sensing of selected pharmaceutical and personal care products.', [Doctoral dissertation, University of Pretoria].

Montaseri, H., Adegoke, O. and Forbes, P.B.C. (2019). 'Development of thiol-capped core/shell quantum dot sensor for acetaminophen.', South African Journal of Chemistry, 72, 108-117.

Moura, I., de Sá, A., Abreu, A. S., Oliveira, M. and Machado, A. V. (2016). 'Morphology, optical, and electric properties of polymer-quantum dots nanocomposites: effect of polymeric matrix.', Journal of Materials Science, 51, 8699–8710.

Mumin, M. A., Xu, W. Z. and Charpentier, P. A. (2015). 'Quantum dots/silica/polymer nanocomposite films with high visible light transmission and UV shielding properties.', Nanotechnology, 26(31).

Munjanja, B. K., Naudé, Y. and Forbes, P. B. C. (2020). 'A review of sampling approaches to off-target pesticide deposition.', Trends in Environmental Analytical Chemistry, 25.

Murphy, C. J. (2002). 'Peer reviewed: optical sensing with quantum dots.', Analytical Chemistry, 74(19), 520 A-526 A.

Murray, C. B., Kagan, C. R. and Bawendi, M. G. (2000). 'Synthesis and characterization of monodisperse nanocrystals and close-packed nanocrystal assemblies.', Annual Review of Materials Research, 30(1), 545–610.

Murray, C. B., Norris, D. J. and Bawendi, M. G. (1993). 'Synthesis and characterization of nearly monodisperse CdE (E = sulfur, selenium, tellurium) semiconductor nanocrystallites.', Journal of the American Chemical Society, 115, 8706-8715.

Mutavdžić, D., Xu, J., Thakur, G., Triulzi, R., Kasas, S., Jeremić, M., Leblanc, R., Radotić, K. (2011). 'Determination of the size of quantum dots by fluorescence spectroscopy.', Analyst, 136, 2391–2396.

Nair, R. V., Thomas, R. T., Mohamed, A. P. and Pillai, S. (2020). 'Fluorescent turn-off sensor based on sulphur-doped graphene quantum dots in colloidal and film forms for the ultrasensitive detection of carbamate pesticides.', Microchemical Journal, 157, 104971.

Nawaz, A., Razpotnik, A., Rouimi, P., de Sousa, G., Cravedi, J. P. and Rahmani, R. (2014). 'Cellular impact of combinations of endosulfan, atrazine, and chlorpyrifos on human primary hepatocytes and HepaRG cells after short and chronic exposures.', Cell Biology and Toxicology, 30(1), 17–29.

Nazzal, A. Y., Wang, X., Qu, L., Yu, W., Wang, Y., Peng, X. and Xiao, M. (2004). 'Environmental effects on photoluminescence of highly luminescent CdSe and CdSe/ZnS core/shell nanocrystals in polymer thin films.', The Journal of Physical Chemistry B, 108(18), 5507–5515.

Nozik, A.J. (2002). 'Quantum dot solar cells.', Physica E: Low-Dimensional Systems and Nanostructures, 14, 115–120.

Nsibande, S.A. (2015). 'Pesticide spray drift monitoring in the evaluation of air dispersion models: A South African atrazine case study.', [Masters dissertation, University of Pretoria].

Nsibande, S. A. and Forbes, P. B. C. (2016). 'Fluorescence detection of pesticides using quantum dot materials- A review.', Analytica Chimica Acta, 945, 9–22.

Nsibande, S. A. and Forbes, P. B. C. (2019). 'Development of a quantum dot molecularly imprinted polymer sensor for fluorescence detection of atrazine.', Luminescence, 34, 480-488.

Nsibande, S. A., Dabrowski, J. M., van der Walt, E., Venter, A. and Forbes, P. B. C. (2015). 'Validation of the AGDISP model for predicting airborne atrazine spray drift: A South African ground application case study.', Chemosphere, 138, 454–461.

Nsibande, S. A., Montaseri, H. and Forbes, P. B. C. (2019). 'Trends in analytical chemistry advances in the application of nanomaterial-based sensors for detection of polycyclic aromatic hydrocarbons in aquatic systems.', Trends in Analytical Chemistry, 115, 52–69.

Odendaal, C., Seaman, M. T., Kemp, G., Patterton, H. E. and Patterton, H.-G. (2015). 'An LC-MS/MS based survey of contaminants of emerging concern in drinking water in South Africa.', South African Journal of Science, 111(9), 1–6.

Ohring, M. (2002). 'Characterization of thin films and surfaces.', In Ohring, M., Materials science of thin films: Deposition and Structure, (2nd Ed.), Elsevier, 559-640.

Opriş, O., Soran, M. L., Coman, V., Copaciu, F. and Ristoiu, D. (2013). 'Determination of some frequently used antibiotics in waste waters using solid phase extraction followed by high performance liquid chromatography with diode array and mass spectrometry detection.', Central European Journal of Chemistry, 11(8), 1343–1351.

Ouyang, W., Cai, G., Huang, W. and Hao, F. (2015). 'Temporal–spatial loss of diffuse pesticide and potential risks for water quality in China.', Science of The Total Environment, 541, 551-558.

Ozaydin-Ince, G., Coclite, A. M. and Gleason, K. K. (2012). 'CVD of polymeric thin films: Applications in sensors, biotechnology, microelectronics/organic electronics, microfluidics, MEMS, composites and membranes.', Reports on Progress in Physics, 75, 1-40.

Pal, A., He, Y., Jekel, M., Reinhard, M. and Gin, K.Y. (2014). 'Emerging contaminants of public health significance as water quality indicator compounds in the urban water cycle.', Environment International, 71, 46-62.

Patterton, H. (2013). 'Scoping study and research strategy development on currently known and emerging contaminants influencing drinking water quality.', WRC Report No. 2093/1/13, W.R. Commission, Water Research Commission, https://www.wrc.org.za/wp-content/uploads/mdocs/2093-1-13.pdf.

Peng, Z. A. and Peng, X. (2001). 'Formation of high-quality CdTe, CdSe, and CdS nanocrystals using CdO as precursor.', Journal of the American Chemical Society, 123(1), 183-184.

Peng, X., Schlamp, M.C., Kadavanich, A.V. and Alivisatos, A.P. (1997). 'Epitaxial growth of highly luminescent CdSe/CdS core/shell nanocrystals with photostability and electronic accessibility.', Journal of the American Chemical Society, 119, 7019–7029.

Perez-Padilla, R., Schilmann, A. and Riojas-Rodriguez, H. (2010). 'Respiratory health effects of indoor air pollution.', The International Journal of Tuberculosis and Lung Disease, 14, 1079-1086.

Petersen, F., Dabrowski, J. M. and Forbes, P. B. C. (2017). 'Identifying potential surface water sampling sites for emerging chemical pollutants in Gauteng Province, South Africa.', Water SA, 43(1), 153–165.

Petty, M. C. (1996). 'Film deposition', in Langmuir-Blodgett films - An introduction, Cambridge University Press, 39–64.

Pheiffer, W., Smit N. J., Pieters, R., Genthe, B., Quinn, L. and Bouwman, H. (2017). 'Polycyclic aromatic hydrocarbons (PAHs) in the aquatic ecosystems of Soweto and Lenasia.', [Doctoral dissertation, North-West University (South Africa)].

Pies, C., Hoffmann, B., Petrowsky, J., Yang, Y., Ternes, T. A. and Hofmann, T. (2008). 'Characterization and source identification of polycyclic aromatic hydrocarbons (PAHs) in river bank soils.', Chemosphere, 72, 1594-1601.

Ray, S. S. and Okamoto, M. (2003). 'Polymer/layered silicate nanocomposites: a review from preparation to processing.', Progress in Polymer Science, 28(11), 1539-1641.

Reiss, P. (2008). 'Synthesis of semiconductor nanocrystals in organic solvents.', In Rogach, A. L. (eds), Semiconductor Nanocrystal Quantum Dots, Springer, Vienna, 35–72.

Rogach, A. L. (2008). 'Semiconductor nanocrystal quantum dots: Synthesis, assembly, spectroscopy, and applications.', in Ed. A. L. Rogach, Springer New York, 2008, pp. 73-100.

Rossi, D. (2010). 'Pesticides in the atmosphere. Occurrence, distribution and behaviour of selected pesticides in the vinicultural area of Trier, Germany.', [Doctoral dissertation, Universität Trier].

Roy, D., De, C.K., Ghosh, S., Mukherjee, S., Mandal, S. and Mandal, P.K. (2022). 'Electronic structure modulation of CdS quantum dots by cobalt doping for photocatalytic hydrogen evolution.', Physical Chemistry Chemical Physics, 24, 8578.

Sahu, N., Parija, B. and Panigrahi, S. (2009). 'Fundamental understanding and modeling of spin coating process: A review.', Indian Journal of Physics, 83(4), 493–502.

Salazar-Corcia, L., Schifter, I. and Gonzalez-Macias, C. (2010). 'Weighing the evidence of ecological risk from PAHs contamination in the Estuarine environment of Salina Cruz Bay, Mexico.', Environmental Monitoring and Assessment, 162, 387–406.

Samia, K., Dhouha, A., Chkirbene, A. and Mlayah, A. (2018). 'Assessment of organic pollutants (PAH and PCB) in surface water: sediments and shallow groundwater of Grombalia watershed in northeast of Tunisia.', Arabian Journal of Geosciences, 11(34).

Santhanam, V., Liu, J., Agarwal, R. and Andres, R. P. (2003). 'Self-assembly of uniform monolayer arrays of nanoparticles.', Langmuir, 19, 7881–7887.

Scheerschmidt, K. and Werner, P. (2002). 'Characterization of structure and composition of quantum dots by transmission electron microscopy.', In: Grundmann, M. (eds) Nano-Optoelectronics. NanoScience and Technology. Springer, Berlin, Heidelberg.

Scheltjens, G., Van Assche, G. and Van Mele, B. (2017). 'Effect of substrate temperature on thermal properties and deposition kinetics of atmospheric plasma deposited methyl(methacrylate) films.', Plasma Processes and Polymers, 14(3), 1–13.

Schneider, C. A., Rasband, W. S. and Eliceiri, K. W. (2012). 'NIH Image to ImageJ: 25 years of image analysis.', Nature Methods, 9(7), 671–675.

Selvakumar, N. and Barshilia, H. C. (2012). 'Review of physical vapor deposited (PVD) spectrally selective coatings for mid- and high-temperature solar thermal applications.', Solar Energy Materials and Solar Cells, 98, 1-23.

Shamsipur, M., Barati, A. and Karami, S. (2017). 'Long-wavelength, multicolor, and white-light emitting carbon-based dots: achievements made, challenges remaining, and applications.', Carbon, 124, 429–472.

Shapiro, A., Jang, Y., Rubin-Brusilovski, A., Budniak, A.K., Horani, F., Sashchiuk, A. and Lifshitz, E. (2016). 'Improved performance of quantum dot light-emitting diodes via a synergistic effect of ligand exchange and external electric field.', Chemistry of Materials, 28, 6409-6418.

Shen, Z.-R., Li, Y.-L., Liu, J.-B., Chen, M.-X., Hou, F. and Wang, L.-Q. (2012). 'Transparent luminescent bulk nanocomposites of polysiloxane embedded with CdS nanocrystallines by a direct dispersion process.', Nanoscale, 4, 1652-1657.

Sheng, W., Kim, S., Lee, J., Kim, S. W., Jensen, K. and Bawendi, M. G. (2006). '*In-situ* encapsulation of quantum dots into polymer microspheres.', Langmuir, 22(8), 3782–3790.

Sill, K. and Emrick T. (2004). 'Nitroxide-mediated radical polymerization from CdSe nanoparticles.', Chemistry of Materials, 16(7), 1240–1243.

Silvia, S. C., Magnarelli, G. and Rovedatti, M. G. (2019). 'Evaluation of endocrine disruption and gestational disorders in women residing in areas with intensive pesticide application: An exploratory study.', Environmental Toxicology and Pharmacology, 73, 103280.

Sima, L., Amador, J., da Silva, A. K., Miller, S. M., Morse, A. N., Pellegrin, M.-L., Rock, C. and Wells, M. J. M. (2014). 'Emerging pollutants – part I: occurrence, fate and transport.', Water Environment Research, 86(10), 1994–2035.

Singh, K. and Voznyy, O. (2019). 'It's a trap! Fused quantum dots are undesired defects in thin-film solar cells.', Chem, 5(7), 1692−1694.

Singh, S., Kumar, V., Chauhan, A., Datta, S., Wani, A. B., Singh, N. and Singh, J. (2018). 'Toxicity, degradation and analysis of the herbicide atrazine.', Environmental Chemistry Letters, 16(1), 211–237.

Skoog, D. A., Holler, F. J. and Crouch, S.R. (2017) Principal of Instrumental Analysis. 7th Edition, Sunder College Publisher, New York.

Sokolov, S. A., Kelm, E. A., Milovanov, R. A., Abdullaev, D. A. and Sidorov, L. N. (2016). 'Non-destructive determination of thickness of the dielectric layers using EDX.', In Society of Photo-Optical Instrumentation Engineers (SPIE) Conference Series—The International Society for Optical Engineering, Vienna, Austria Lukichev, V.F., Rudenko, K.V., Eds.; Volume 10224, 1022426.

Somaraj, G., Mathew, S., Abraham, T., Ambady, K. G., Mohan, C. and Mathew B. (2022). 'Triphenylamine-based dye-sensitized solar cells using cadmium telluride quantum dots.', ChemistrySelect, 7, 2022-2029.

Song, H. J., Shin, G. J., Choi, K. H., Lee, S. and Moon, D. K. (2014). 'White polymer light emitting diode materials introducing dendritic quinoxaline derivative: Synthesis, optical and electroluminescent properties.', Synthetic Metals, 190, 1-7.

Sotelo-Gonzalez, E., Coto-Garcia A. M., Fernandez-Argüelles, M. T., Costa-Fernandez, J. M. and Sanz-Medel A. (2012). 'Immobilization of phosphorescent quantum dots in a sol–gel matrix for acetone sensing.', Sensors and Actuators B: Chemical, 174, 102–108.

Suhl, J., Golla, V., Rinsky, J. L. and Hopenhayn, C. (2016). 'Atrazine in Kentucky Drinking Water.', Journal of Environmental Health, 79(5), E1-E6.

Suriyaprakash, J. and Qiao, T. T. (2018). 'Exploiting the optical and luminescence characteristic of quantum dots for optical device fabrication.', Applied Nanoscience, 8(4), 609–616.

Talapin, D. V., Mekis, I., Götzinger, S., Kornowski, A., Benson, O. and Weller, H. (2004). 'CdSe/CdS/ZnS and CdSe/ZnSe/ZnS core−shell−shell nanocrystals.', ACS Publications, 108(49), 18826–18831.

Tao, P., Li, Y., Siegel, R. W. and Schadler, L. S. (2013). 'Transparent luminescent silicone nanocomposites filled with bimodal PDMS-brush-grafted CdSe quantum dots.', Journal of Material Chemistry C, 1, 86–94.

Tao, P., Viswanath, A., Li, Y., Rungta, A., Benicewicz, B., Siegel, R. and Schadler, L. (2011). 'Refractive index engineering of polymer nanocomposites prepared by end-grafted polymer chains onto inorganic nanoparticles.' MRS Proceedings, 1359.

Tiwary, C., Kumbhakar, P., Mitra, A. and Chattopadhyay, K. (2009). 'Synthesis of wurtzite-phase ZnS nanocrystal and its optical properties.', Journal of Luminescence, 129(11).

Todescato, F., Chesman, A. S. R., Martucci, A., Signorini, R. and Jasieniak, J. J. (2012). 'Highly luminescent and temperature stable quantum dot thin films based on a ZnS composite.', Chemistry of Materials, 24, 2117−2126.

Tomczak, N., Jańczewski, D., Han, M. and Vancso, G. J. (2009). 'Designer polymer-quantum dot architectures.', Progress in Polymer Science, 34, 393–430.

Tyona, M. D. (2013). 'A theoritical study on spin coating technique.', Advances in Materials Research, 2(4), 195–208.

Van Metre, P. C., Mahler, B. J., Furlong, E. T. (2000). 'Urban sprawl leaves it's PAH signature.', Environmental Science and Technology, 32, 4064-4070.

Van Sark, W. G. J. H. M., Frederix, P. L. T. M., Bol A. A., Gerritsen H. C. and Meijerink A. (2002). 'Blueing, bleaching, and blinking of single CdSe/ZnS quantum dots.', ChemPhysChem, 3(10), 871-879.

Vedamalai, M., Periasamy, A. P., Wang, C. W., Tseng, Y. T., Ho, L. C., Shih, C. C. and Chang, H. T. (2014). 'Carbon nanodots prepared from o-phenylenediamine for sensing of Cu^{2+} ions in cells.', Nanoscale, 6, 13119–13125.

Verberk, R., van Oijen, A. M. and Orrit, M. (2002). 'Simple model for the power-law blinking of single semiconductor nanocrystals.', Physical Review B, 66, 233202.

Walia, S. and Acharya, A. (2014). 'Fluorescent cadmium sulfide nanoparticles for selective and sensitive detection of toxic pesticides in aqueous medium.', Journal of Nanoparticle Research, 16, 2778.

Wang, C., Jiang, Y., Chen, L., Li, S., Li, G. and Zhang, Z. (2009). 'Temperature dependence of optical properties and size tunability CdSe quantum dots via non-TOP synthesis', Materials Chemistry and Physics, 116, (2–3), 388–391.

Wang, C. F., Badolato, A., Wilson-Rae, I., Petroff, P. M. and Hu, E. (2004). 'Optical properties of single InAs quantum dots in close proximity to surfaces.', Applied Physics Letters, 85, 3423.

Wang, R., Peng, J., Qiu, F., Yang, Y. L. and Xie, Z. Y. (2009). 'Simultaneous blue, green, and red emission from diblock copolymer micellar films: A new approach to white-light emission.', Chemical Communications. (44), 6723-6725.

Wang, S., Wang, Y., He, X. and Lu, Q. (2022). 'Degradation or humification: rethinking strategies to attenuate organic pollutants.', Trends in Biotechnology, 2164, 1-12.

Wang, X., Sun, J. Z. and Tang, B. Z. (2018). 'Poly(disubstituted acetylene): Advances in polymer preparation and materials application.', Progress in Polymer Science, 79, 98–120.

Wang, Y., Kalytchuk, S., Zhang, Y., Shi, H., Kershaw, S. V. and Rogach, A. L. (2014). 'Thickness-dependent full-color emission tunability in a flexible carbon dot ionogel.', Journal of Physical Chemistry Letters, 5(8), 1412–1420.

Wang, Y., Tang, Z. Y., Correa-Duarte, M. A., Liz-Marzán, L. M. and Kotov, N. A. (2003). 'Multicolor luminescence patterning by photoactivation of semiconductor nanoparticle films.', Journal of the American Chemical Society, 125, 2830−2831.

Wang, Y., Tang, Z., Correa-Duarte, M. A., Pastoriza-Santos, I., Giersig, M., Kotov, N. A. and Liz-Marzan, L. M. (2004). 'Mechanism of strong luminescence photoactivation of citrate-stabilized water-soluble nanoparticles with CdSe cores.', The Journal of Physical Chemistry B, 108(40), 15461-15469.

Wang, Z., Li, X., Yang, Z., Li, Y., Zhang, Z. and Li, Y. (2021). 'Enhancement of the performance of a lead-free $Cs_3Bi_2I_9$ quantum dot-sensitized solar cell by optimizing the dye-loading procedure.', Journal of Materials Chemistry A, 9, 11526-11532.

Wohlfarth, C. (2008). 'Refractive index of ethanol.' M.D. Lechner (ed.), Optical constants - Refractive indices of pure liquids and binary liquid mixtures (Supplement to III/38), Condensed Matter (47).

Woo, H. Lim, J. Lee, Y. Sung, J. Shin, H. Oh, J.M. Choi, M. Yoon, H. Bae, W.K. and Char, K. (2013). 'Robust, processable, and bright quantum dot/organosilicate hybrid films with uniform QD distribution based on thiol-containing organosilicate ligands.', Journal of Materials Chemistry C, 1, 1983–1989.

Wolf, M. P., Salieb-Beugelaar, G. B. and Hunziker, P. (2018). 'PDMS with designer functionalities—properties, modifications strategies, and applications.', Progress in Polymer Science, 83, 97–134.

Wuister, S. F., van Driel, F. and Meijerink, A. (2003). 'Luminescence of CdTe Nanocrystals.', Journal of Lumininescence, 102−103, 327−332.

Xie, B., Cheng, Y., Hao, J., Yu, X., Shu, W., Wang, K. and Luo, X. (2018). 'White light-emitting diodes with enhanced efficiency and thermal stability optimized by quantum dots- silica nanoparticles.', IEEE Transactions on Electron Devices, 65, 605–609.

Xu, M., Obodo, D. and Yadavalli, V. K. (2019). 'The design, fabrication, and applications of flexible biosensing devices.', Biosensors and Bioelectronics, 124–125, 96–114.

Yang, L., Chen, B., Luo, S., Li, J., Liu, R. and Cai, Q. (2010). 'Sensitive detection of polycyclic aromatic hydrocarbons using CdTe quantum dot-modified TiO_2 nanotube array through fluorescence resonance energy transfer.', Environmental Science & Technology, 44, 7884–7889.

Ye, J., Van de Broek, B., De Palma, R., Libaers, W., Clays, K., Van Roy, W., Borghs, G. and Maes, G. (2008). 'Surface morphology changes on silica-coated gold colloids.', Colloids and Surfaces A: Physicochemical and Engineering Aspects, 322(1), 225-233.

Yin, Y. and Alivisatos, A. P. (2005). 'Colloidal nanocrystal synthesis and the organic-inorganic interface.', Nature, 437(7059), 664–670.

Yoon, C., Yang, K. P., Kim, J., Shin, K. and Lee, K. (2020). 'Fabrication of highly transparent and luminescent quantum dot/polymer nanocomposite for light emitting diode using amphiphilic polymer-modified quantum dots.', Chemical Engineering Journal, 382, 122792.

Yu, W. W., Chang, E., Drezek, R. and Colvin, V. L. (2006). 'Water-soluble quantum dots for biomedical applications.', Biochemical and Biophysical Research Communications, 348(3), 781–786.

Yu, W. W. and Peng, X. (2002). 'Formation of high-quality CdS and other II–VI semiconductor nanocrystals in noncoordinating solvents: tunable reactivity of monomers.', Angewandte Chemie International Edition, 41(13), 2368–2371.

Yuan, C. T. Chou, W. C. Chuu, D. S. Chen, Y. N. Lin, C. A. and Chang W. H. (2008). 'Photoinduced fluorescence enhancement in colloidal CdSeTe⁄ZnS core/shell quantum dots.', Applied Physics Letters, 92, 183108.

Yunker M. B., Macdonald R. W., Vingarzan R., Mitchell R. H., Goyette D. and Sylvestre S. (2002). 'PAHs in the Fraser River Basin: a critical appraisal of PAH ratios as indicators of PAH source and composition.', Organic Geochemistry, 33, 189-515.

Zhang, F., Liu, F., Wang, C., Xin, X., Liu, J., Guo, S. and Zhang, J. (2016). 'Effect of lateral size of graphene quantum dots on their properties and application.', ACS Applied Materials and Interfaces, 8(3), 2104-2110.

Zhang, H., Wang, L., Xiong, H., Hu, L., Yang, B. and Li, W. (2003). 'Hydrothermal synthesis for high-quality CdTe nanocrystals.', Advanced Materials, 15(20), 1712–1715.

Zhang, J., Zhang, S., Zhang, Y., Al-Hartomy, O. A., Wageh, S., Al-Sehemi, A. G., Hao, Y., Gao, L., Wang, H. and Zhang H. (2023). 'Colloidal quantum dots: synthesis, composition, structure, and emerging optoelectronic applications.', Laser & Photonics Reviews, 17, 2200551.

Zhang, K., Mei, Q., Guan, G., Liu, B., Wang, S. and Zhang, Z. (2010). 'Ligand replacement-induced fluorescence switch of quantum dots for ultrasensitive detection of organophosphorothioate pesticides.', Analytical Chemistry, 82, 9579–9586.

Zhang, L., Lou, X., Yu, Y., Qin, J. and Li, Z. (2011). 'A new disubstituted polyacetylene bearing pyridine moieties: Convenient synthesis and sensitive chemosensor toward sulfide anion with high selectivity.', Macromolecules, 44(13), 5186–5193.

Zhang, Y. and Tao, S. (2009). 'Global atmospheric emission inventory of polycyclic aromatic hydrocarbons (PAHs) for 2004.', Atmospheric Environment, 43, 812-819.

Zhen, H. Y., Xu, W., King, W., Chen, Q. L., Xu, Y. H., Jiang, J. X., Peng, J. B. and Cao, Y. (2006). 'White-light emission from a single polymer with singlet and triplet chromophores on the backbone.', Macromolecular Rapid Communications, 27(24), 2095-2100.

Zheng, K., Žídek, K., Abdellah, M., Zhu, N., Chabera, P., Lenngren, N., Chi, Q. and Pullerits, T. N. (2014). 'Directed energy transfer in films of CdSe quantum dots: beyond the point dipole approximation.', Journal of the American Chemical Society, 136, 6259−6268.

Zheng, Z., Zhou, Y., Li, X., Liu, S. and Tang, Z. (2011). 'Highly-sensitive organophosphorous pesticide biosensors based on nanostructured films of acetylcholinesterase and CdTe quantum dots.', Biosensors and Bioelectronics, 26(6), 3081–3085.

Zhou, R. B., Zhu, L. Z., Yang, K. and Chen, Y. Y. (2006). 'Distribution of organochlorine pesticides in surface water and sediments from Qiantang River, East China.', Journal of Hazardous Material, 137, 68-75.

Zhou, S., Yeung, L., Forbes, M., Mabury, S. and Abbatt, J. (2017). 'Epoxide formation from heterogeneous oxidation of benzo[a]pyrene with gas-phase ozone and indoor air.', Environmental Science: Processes & Impacts, 19, 1292-1299.

Zimnitsky, D., Jiang, C., Xu, J., Lin, Z. and Tsukruk, V. V. (2007). 'Substrate-and time-dependent photoluminescence of quantum dots inside the ultrathin polymer LbL film.', Langmuir, 23(8), 4509–4515.

Zor, E., Morales-narva, E., Zamora-ga, A., Bingol, H. and Ersoz, M. (2015). 'Graphene quantum dots-based photoluminescent sensor: A multifunctional composite for pesticide detection.', ACS Applied Materials & Interfaces, 7(36), 20272-20279.

Zvaigzne, M., Domanina, I., Il, D., Yakimansky, A., Nabiev, I. and Samokhvalov, P. (2020). 'Quantum dot – polyfluorene composites for white-light-emitting quantum dot-based LEDs.', Nanomaterials, 10(12), 2487.

Appendices

Appendix A: Certificates of Analysis

Atrazine

SIGMA-ALDRICH

CERTIFICATE OF ANALYSIS

Sigma-Aldrich Laborchemikalien GmbH D-30918 Seelze
Telefon: +49 5137 8238-150

Seelze, 25.06.2013/488046/13/12641

Order-No.:
Customer-No.:

Order-Code:

Quantity:

Production Date: 07.Jun.2013
Expiry Date: 07.Jun.2018

Article/Product: 45330 Batch : SZBD158XV

Atrazine PESTANAL®

Reference Material (RM)

1. General Information

Formula: C8H14ClN5 Molar mass: 215.68 g/Mole
CAS-No.: [1912-24-9] Recomm. storage temp.: roomtemp.
Usage : Herbicide

The estimated uncertainty of a single measurement of the assay can be expected to be 0.5 % relative (confidence level = 95%, n= 6) whereby the assay measurements are calculated by 100% minus found impurities.

2. Batch Analysis

Identity (NMR)	complying	
Assay (HPLC)	99.1	area %
Melting range	175.3-177.6	°C
Water (Karl Fischer)	0.19	%
Date of Analysis	24.Jun.2013	

3. Advice and Remarks

- The expiry date is based on the current knowledge and holds only for proper storage conditions in the originally closed flasks/ packages.
- Whenever the container is opened for removal of aliqout portions of the substance, the person handling the substance must assure, that the integrity of the substance is maintained and proper records of all its handlings are kept. Special care has to be taken to avoid any contamination or adulteration of the substance.
- We herewith confirm that the delivery is effected according to the technical delivery conditions agreed.
- Particular properties of the products or the suitability for a particular area of application are not assured.
- We guarantee a proper quality within our General Conditions of Sales.

Sigma-Aldrich Laborchemikalien GmbH
Quality Management SA-LC

This document was produced electronically and is valid without a signature

HPLC-Method

Article	: Atrazine
Article-No	: 45330
Batch	: SZBD158XV
Column	: L=250mm, ID=4,6mm; Supelcosil LC-18 5µm
Eluent	: 50 % Acetonitrile 50 % Water + 1mmol Ammonium acetate
Detector	: UV-226nm
Injection-Volume	: 5µl
Sample-Preparation	: 0,1mg/ml Eluent
Linearity	: checked
Evaluation	: Normalisation (uncorrected)
Operator	: Schowe

Chromatogram
Atrazin C:\LabSolutions\Data\Project1\1312641.AIA\SIGNAL01.cdf

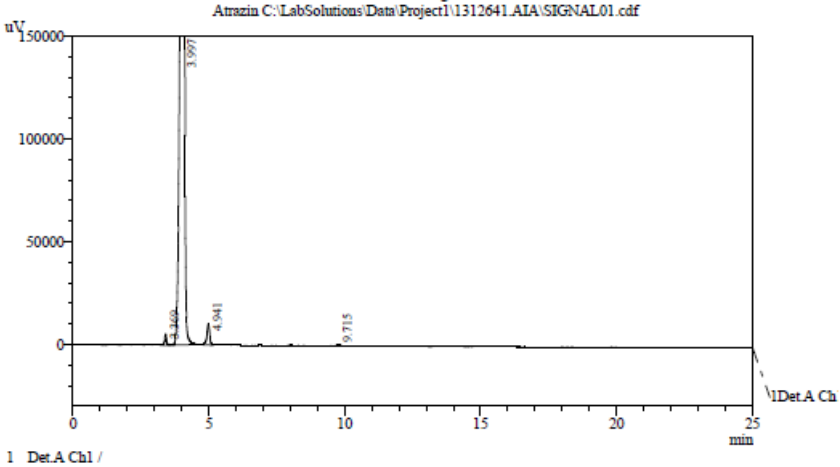

1 Det.A Ch1 /

PeakTable

Ch1

Peak#	Ret. Time	Area	Area %
1	3.369	27	0.233
2	3.997	11348	99.106
3	4.941	71	0.617
4	9.715	5	0.045
Total		11450	100.000

Phenanthrene

Certificate of Composition

DESCRIPTION: Phenanthrene
MPG. DATE: Jul 2004
CATALOG NO.: 48569 (1)
LOT NO.: LB21549
EXP. DATE: Jul 2007

CAS NUMBER: 85-01-8
MOLECULAR FORMULA: C14H10
MOLECULAR WEIGHT: 178

PHYSICAL PROPERTIES	ASSAY	
FTIR	Matches: SUPELCO	Lib. No.: QA-1 106
GC - Mass Spec	Matches: NIST	Lib. No.: 68641
Purity (2)	99.9%	
Purity (2)	99.8% (a)	
Melting point	98.0 - 99.0 deg C	

(1) This product is packaged from R430810 Lot number LB04592.
(2) Determined by GC-PID unless otherwise noted.
(a) HPLC UV-254nm

Elwood Doughty
Quality Control Supervisor

SUPELCO

Supelco warrants that its products conform to the information contained in this publication. Purchaser must determine the suitability of the product for its particular use. Please see the latest Catalog or order invoice and packing slip for additional terms and conditions of sale.

595 North Harrison Road
Bellefonte, PA 16823-0048 USA
Phone (814) 359-3441

Appendix B: Qualitative EDS analyses

As shown in Figure 4-33, the following images were used to confirm that the glass and PDMS polymer had a similar elemental composition, but that the two were in fact not the same material and that there were glass shards that broke off when the glass slide was hit and cracked in order to determine the film thickness.

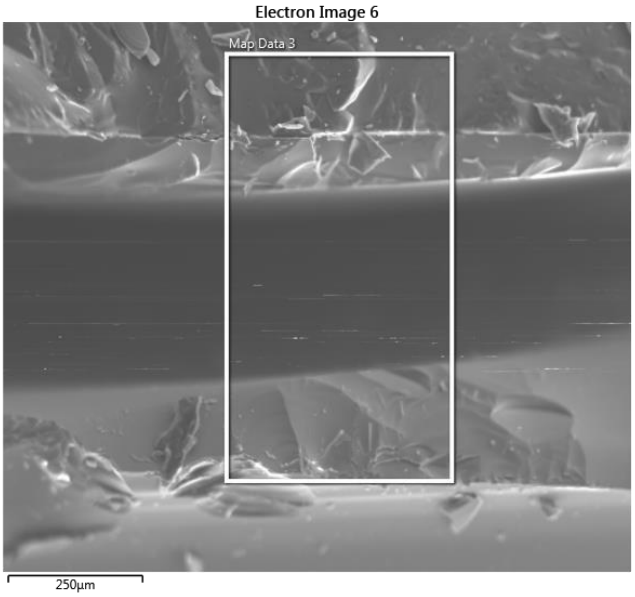

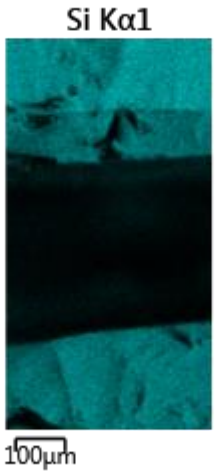

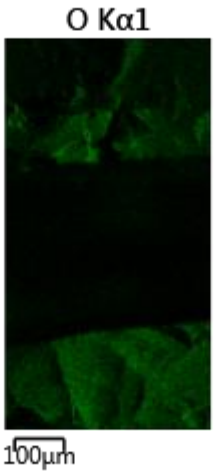

C Kα1_2

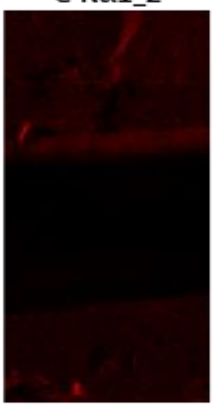

Na Kα1_2

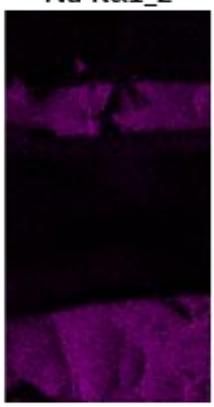

Ca Kα1

Mg Kα1_2

Al Kα1

S Kα1

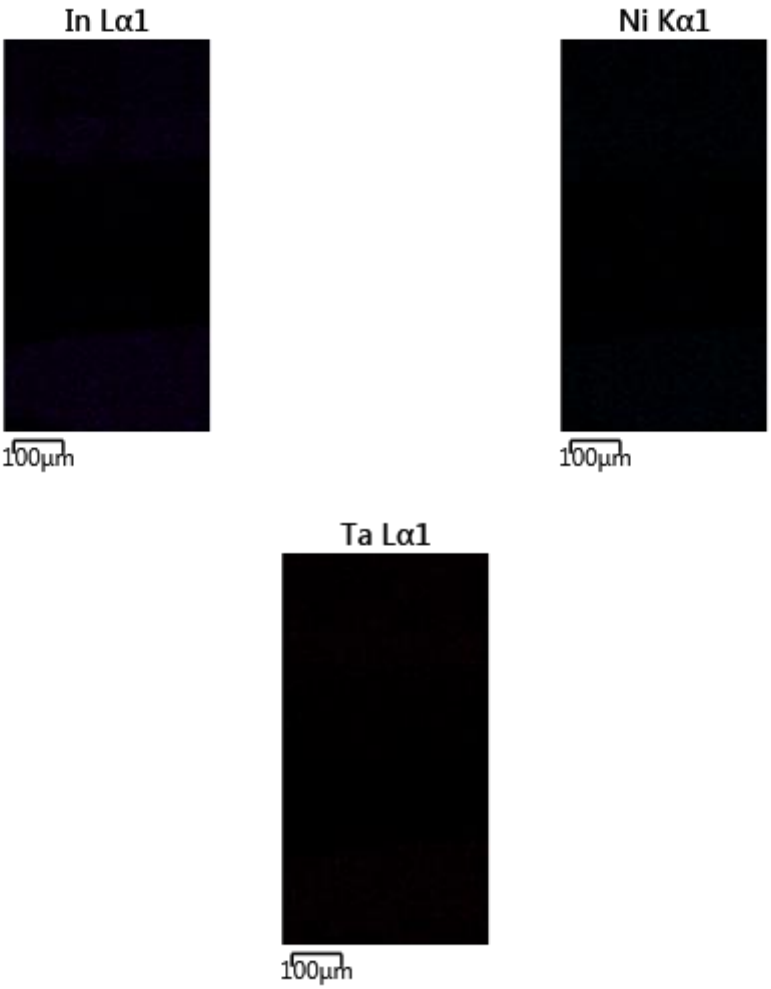

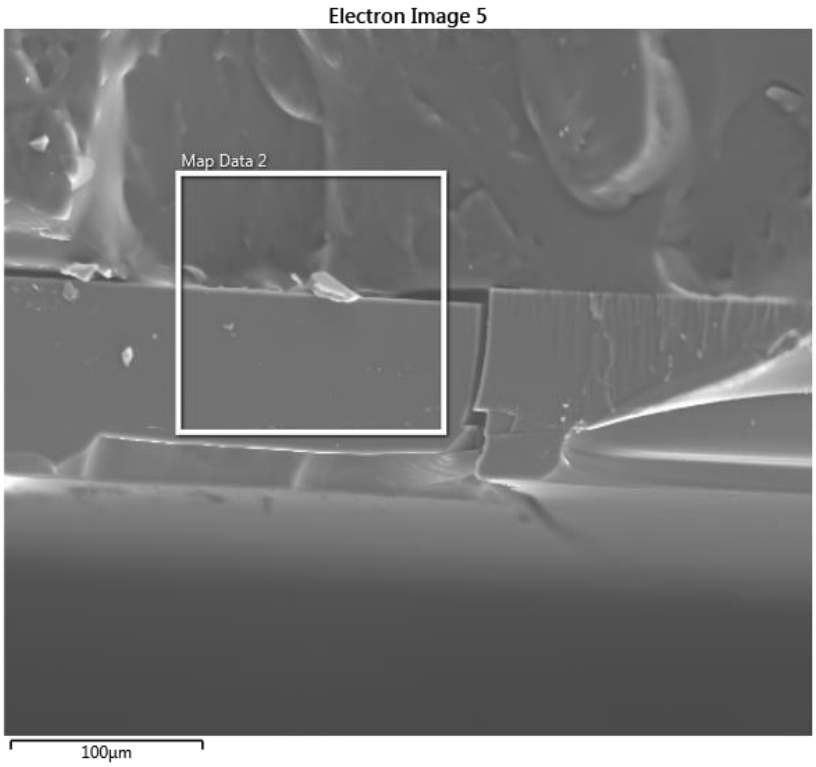

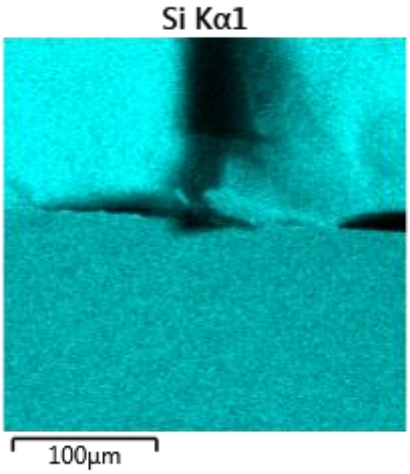

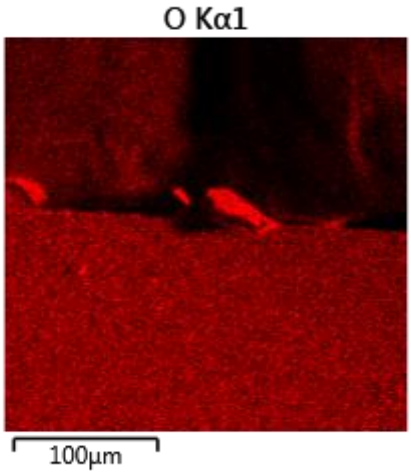

C Kα1_2

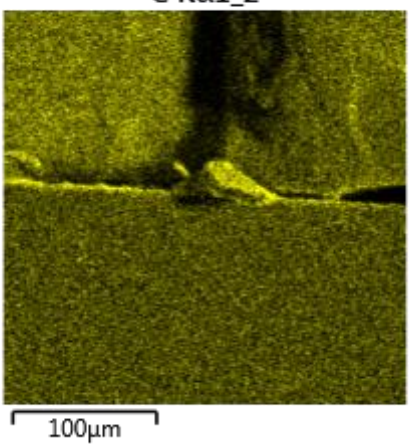

Ca Kα1

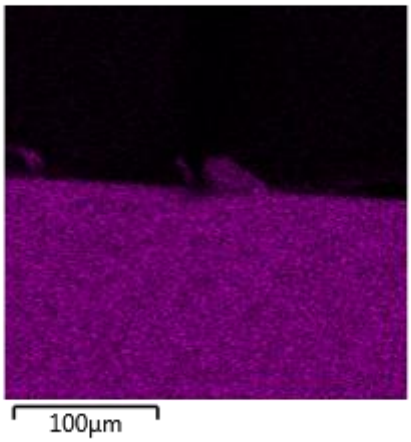

Na Kα1_2

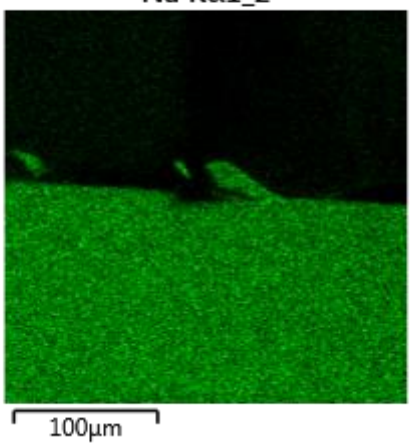

Sb Lα1

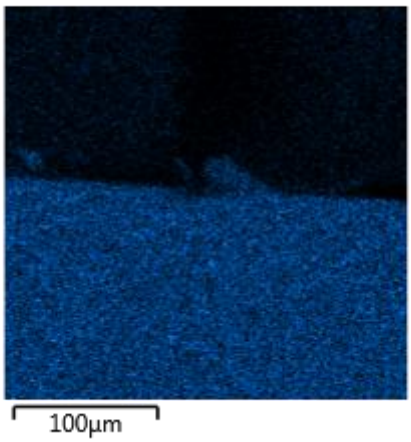

Mg Kα1_2

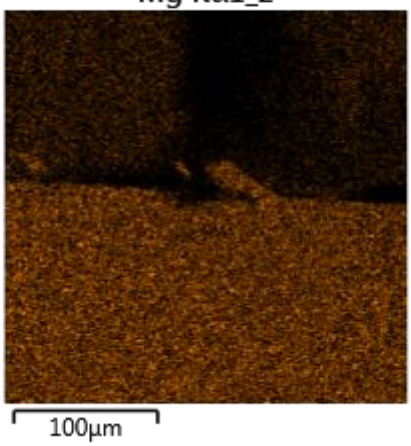

Al Kα1